Calcium channel signalling and modulation in colorectal cancer

Judith Elizabeth Valluru

Submitted in accordance with the requirements for the degree of Doctorate of Philosophy in Medicine.

The University of Leeds

School of Medicine

Leeds Institute of Cardiovascular and Metabolic Medicine

May 2019

The candidate confirms that the work submitted is her own and that appropriate credit has been given where reference has been made to the work of others.

This copy has been supplied on the understanding that it is copyright material and that no quotation from the thesis may be published without proper acknowledgement.

The right of Judith Elizabeth Valluru to be identified as Author of this work has been asserted by Judith Elizabeth Valluru in accordance with the Copyright, Designs and Patents Act 1988.

Table of Contents and List of Tables and Illustrative Material

Contents

List of Figures and Tables

Acknowledgements

"You cannot teach a man anything; you can only help him discover it in himself".

Galileo

There is no quote that better capitulates the learning experience that underlies the study for a PhD. This has been an incredible journey. It has been the hardest thing I have ever done and will forever be my biggest accomplishment in my professional life. I have learned so much over the last 4 years. I have faced and overcome a plethora of challenges, and developed tenacity and resourcefulness in order to deliver this, as is part of the PhD process. I am proud of the work that I have delivered in this thesis and the small contribution it makes to the increasing body of knowledge of calcium channel signalling in cancer.

I could not have done any of this without the input and support of so many people. I am grateful to my panel of supervisors for their advice and support throughout this programme. In particular, I would like to thank Professor Beech for his guidance, patience and support and the faith he has ultimately shown in me to deliver this. I am also grateful to the other postdoctoral research staff and fellow students of the Beech lab and associated groups for their guidance and help in the lab, in particular Dr Jing Li, Dr Baptiste Rode, Dr Nadira Yuldeshiva and Mrs Debra Evans, who took so much time to guide and support me. I am also grateful for the support of Mr Phil Warburton, Dr Rajendra Gosein, Dr Anson Cheung, Mrs Katarzyna Marzsalek, Dr Lynn McKeown, Dr Melanie Ludlow and Dr Hannah Gaunt for their help with molecular laboratory techniques. Outside of Leeds, I would also like to thank Dr Caro Staton, Dr Manoj Valluru, Dr Ali Khurram and Dr Chryso Kanthou for technical and histopathological advice. Furthermore, Dr Lucy Stead, Dr Matthew Parker, Dr Thomas Drake and Dr James Bradford for their support and guidance as I started to grapple with huge bioinformatics data files and learning coding for analysis from scratch.

I have had so much support from my wonderful friends and family throughout my time at Leeds. In particular, Corinne, Jules, Lou, Mo Gossiel and Audrey have helped to keep me going through both the best and the worst of it. Last but not least, I would like to thank my staunchest supporters who have had my back every step of the way from day 1: my son Daniel, who I think I may have inadvertently put off academia for life, and my husband Manoj. Their faith in my abilities during these

years has at times been incredibly humbling, and kept me going in order that I could meet those expectations and make them proud. I would also like to make mention of my daughter Jenny, the whirling dervish who arrived half way through the PhD to light up our lives and hearts.

I dedicate this thesis to my late parents, John and June.

Abstract

Background

Colorectal cancer (CRC) is a huge global problem, being the 3rd most common cancer worldwide. It is caused by an interplay between genetic and chromosomal aberrations as well as dietary and lifestyle factors. Calcium channel receptor signalling is important in a number of cancers, in particular calcium release-activated calcium (CRAC) channel signalling and more recently PIEZO1. The hypothesis is that modulating these channels will have physiological effects on cancer growth in CRC.

Key Results

A novel ORAI1 inhibitor, named JPIII, demonstrated better pharmacokinetic properties than existing CRAC channel inhibitors, and inhibited ORAI1 channel function in both CRC and human umbilical vein endothelial cells (HUVECs). Furthermore, JPIII suppressed cell viability, migration and invasion in both CRC and endothelial cells. ORAI1 channel inhibition inhibited cell viability without causing cell death in HUVECs. JPIII reduced cell viability and clonogenicity of CRCs. Furthermore, JPIII treatment activated autophagy whilst simultaneously inhibiting AKT phosphorylation. In addition, a role for PIEZO1 in CRC tumourigenesis is described for the first time. PIEZO1 channels are functionally expressed, and PIEZO1 siRNA knockdown inhibited CRC viability and resulted in an increase in G2/M cell cycle arrest. The Cancer Genome Atlas (TCGA) transcriptome data revealed that ORAI1 and PIEZO1 are differentially overexpressed in CRC relative to normal colon. However, calcium signalling and ion transport processes on the whole are downregulated in CRC. ORAI1 and PIEZO1 expression does not vary across disease stage or survival outcomes. However, expression of both channels was inversely associated with lymphatic invasion. Both ORAI1 and PIEZO1 expression demonstrated a tumour-specific correlation with one another that was not present in normal colon, and expression associated with IGF2R, postulating a potential oncogenic process for further research.

Conclusion

This work has demonstrated that both ORAI1 and PIEZO1 are involved in CRC molecular signalling.

Abbreviations

3D	Three dimensional
5-FU	5-fluourouracil
2-APB	2- Aminoethyl diphenylborinate
ACF	Aberrant crypt focus
AIF	Apoptosis initiating factor
AJCC	American Joint Committee on Cancer
AM	Acetoxymethyl
APC	Adenomatous polyposis coli
ASR	Age standardised rate
AUC	Area under the curve
BAPTA	1,2-bis(2-aminophenoxy) ethane-N,NV,NY',N'-tetra-acetic acid
BCP	bromochloropropane
BHQ	2,5-di-(t-butyl)-1,4-hydroquinone
BP	Biological processes
BRAF	B-Raf proto-oncogene
BSA	Bovine serum albumin
Ca^{2+}	Calcium
$CaCl_2$	Calcium chloride
CAI	Carboxyamidotriazole
CaM	Calmodulin
CAMKII	Ca2+/calmodulin-dependent protein kinase II
CC	Cellular components
cDNA	Complementary DNA
CCD	Charge-coupled device
CFP	Cyan fluorescent protein
CI	Confidence interval
CO_2	Carbon dioxide
CNV	Copy number variation
COSMIC	Catalogue of Somatic Mutations in Cancer
cpm	Counts per million

CRC	Colorectal cancer
CRAC	Calcium release-activating channel
Cryo-EM	Cryo-electron microscopy
CT	Threshold cycle
CT	Computed tomography
DEG	Differentially expressed gene
DES	Diethylstilbestrol
DGCA	Differential gene correlation analysis
DMEM	Dulbecco's Modified Eagle Medium
DMSO	Dimethyl sulphide
DNA	Deoxyribonucleic acid
dNTP	Deoxyribonucleotide triphosphate
EC	Endothelial cell
ECM	Extracellular matrix
EF	E and F helix hand
EGF	Epidermal growth factor
EGTA	Ethylene glycol bis-NN,NV',N'-tetra-acetic acid
EM	Electron microscopy
EMT	Epithelial-mesenchymal transition
ER	Endoplasmic reticulum
ERK	Extracellular signal-regulated kinase
ER-PM	Endoplasmic reticulum-plasma membrane
ERBB2	Erb-B2 Receptor Tyrosine Kinase 2
FAP	Familial adenomatous polyposis
FDA	(U.S.) Food and Drug Administration
FIT	faecal immunochemical test
FITC	Fluorescein isothiocyanate
FOBT	Faecal occult blood test
FC	Fold change
FPKM	Fragments per kilobase of transcript per million mapped reads
FRET	Förster resonance energy transfer
GBM	Glioblastoma multiforme

Gd	Gadolinium
GPRC	G protein coupled receptor
GO	Gene ontology
GSEA	Gene set enrichment analysis
H&E	Haematoxylin and eosin
HEPES	(4-(2-hydroxyethyl)-1-piperazineethanesulfonic acid)
HR	Hazard ratio
HRP	Horeradish peroxidase
HRFMA	High Resolution Fluorescent Microsatellite Analysis
HUVECs	Human umbilical vein endothelial cells
IC50	Concentration that results in 50% inhibition
I_{CRAC}	Calcium release-activated calcium current
IGF2	Insulin-like growth factor 2
InsP$_3$/IP3	Inositol 1,4,5-triphosphate
IP	Intraperitoneal
IV	Intravenous
JNK	c-Jun N-terminal kinase
kDa	Kilodalton
KCl	Potassium chloride
K-RAS	Kirsten Rat Sarcoma Viral [Oncogene] Homolog
LEF-1	Lymphoid enhancer-binding factor 1
Log	Log2
MCU	Mitochondrial calcium uniporter
MDCK	Madin-Derby canine kidney cells
MDT	Multi-disciplinary team
MF	Molecular function
MgCl$_2$	Magnesium chloride
MEK	Mitogen-activated protein kinase kinase
MEKi	Mitogen-activated protein kinase kinase inhibitor
mRNA	Messenger RNA
MSI	Microsatellite instability
MSS	Microsatellite stable

MVD	Microvessel density
NAD(P)H	Nicotinamide adenine dinucleotide phosphate
NCI	National Cancer Institute
NCX	Sodium calcium transporter
NFAT	Nuclear factor of activated T-cells
NHGRI	National Human Genome Research Institute
NS	Not significant
NSCLC	Non-small cell lung cancer
NT	Non-transfected (mock)
OR	Odds ratio
OS	Overall survival
PBMC	Peripheral blood mononuclear cells
PBS	Phosphate buffered saline
PC	Purkinje cells
PCA	Principal component analysis
PCR	Polymerase chain reaction
PDGF	Platelet derived growth factor
PDX	Patient derived xenograft
PIK3CA	Phosphatidylinositol-4,5-Bisphosphate 3-Kinase Catalytic Subunit Alpha
PIP2	Phosphatidylinositol 4,5-bisphosphate
PLC	Phospholipase C
PFI	Progression free interval
PFS	Progression free survival
PTEN	Phosphatase And Tensin Homologue
qRT-PCR	Quantitative real time polymerase chain reaction
RBL	Rat basophilic leukaemia cell line
Rel.	Relative
RPKM	Reads per kilobase of transcript per million mapped reads
RPMI 1640	Roswell Park Memorial Institute 1640 medium
RPPA	Reverse phase protein analysis
RNA	Ribonucleic acid

RO2959	2,6-Difluoro-N-(5-[4-methyl-1-(5-methyl-thiazol-2-yl)-1,2,5,6-tetrahydro-pyridin-3-yl]-pyrazin-2-yl)-benzamide
RR	Ruthenium red
RR	Relative risk
RT	Reverse transcriptase
RTK	Receptor tyrosine kinase
RWD	Relative wound density
S66	Synta66
SCA15	Spinocerebellar ataxia type 15
SBS	Salt buffered solution
SCC	Squamous cell carcinoma
SCID	Severe combined immune deficiency
SCR	Scrambled
SDS-PAGE	Sodium dodecyl sulphate polyacrylamide gel electrophoresis
SEM	Standard error of the mean
SERCA	Sarcoplasmic/endoplasmic reticulum calcium ATPase
SFM	Serum free medium
SMAD4	SMAD family member 4
SNP	Single nucleotide polymorphism
SOAR	STIM1-ORAI1-activating region
SOCE	Store operated calcium entry
SS	Serum starved
SSP	Staurosporine
STIM	Stromal interaction molecule
TBS	Tris buffered saline
TBS-T	Tris buffered saline and Tween-20
TCF	Transcription factor
TCGA	The Cancer Genome Project
Tg	Thapsigargin
TFF1	Trefoil factor family 1
TGFβ	Transforming growth factor beta
TMM	Trimmed mean of m-values

TNF	Tumour necrosis factor
TNM	Tumour node metastasis
TP53	Tumour protein p53
TRP	Transient receptor potential
USA	United States of America
VEGF	Vascular endothelial growth factor
VGCC	Voltage gated calcium channels
VSMC	Vascular smooth muscle cell
WB	Western blot
WGCNA	Weighted gene correlation network analysis
w/v	Weight per volume
YFP	Yellow fluorescent protein

Units

ng	Nanogram
nM	Nanomolar
µg	Microgram
µl	Microlitre
µM	Micromolar
U	Unit

Publications and Abstracts

Abstract

- Ritchie, JE., Young, RS., Gosein, R., Plante, J., Foster, R., Prasad, KR., Beech, DJ. Small Molecule Calcium Channel Blockade Suppresses Function of Endothelial Cells and Cancer Cell Lines. INCA 2015, Imperial College London. Poster.

Publications

- Li, J., Bruns, A. F., Hou, B., Rode, B., Webster, P. J., Bailey, M. A., Appleby, H. L., Moss, N. K., **Ritchie, J. E**., Yuldasheva, N. Y., Tumova, S., Quinney, M., McKeown, L., Taylor, H., Prasad, K. R., Burke, D., O'Regan, D., Porter, K. E., Foster, R., Kearney, M. T., and Beech, D. J. Orai3 Surface Accumulation and Calcium Entry Evoked by Vascular Endothelial Growth Factor. Atherosclerosis, Thrombosis and Vascular Biology 2015 35(9):1987-94. doi: 10.1161/ATVBAHA.115.305969. PMID 26160956

- Webster, P. J., Littlejohns, A. T., Gaunt, H. J., Young, R. S., Rode, B., **Ritchie, J. E**., Stead, L., Harrison, S., Droop, D., Martin, H. L., Tomlinson, D. C., Hyman, A. J., Appleby, H. L., Boxall, S., Bruns, A. F., Li, J., Prasad, R. K., Lodge, P. A., Burke, D. A., and Beech, D. J. Upregulated WEE1 protects endothelial cells of colorectal cancer liver metastases. Oncotarget 2017 8: 42288-42299. doi: 10.18632/oncotarget.15039. PMID 28178688

Publications in preparation

- **Valluru J.E**., Warburton P., Ludlow MJ., Boxall, S., Marszalek, K., McKeown, L., Stead, L., Beech, D.J. PIEZO1 forms mechanosensitive ion channels in colorectal cancer. Scientific Reports.

- **Valluru J**., Bailey, M.A., Gosein, R., Foster, R., Beech, D.J. ORAI1 channel is a druggable channel in colorectal cancer.

Chapter 1: Introduction

1.1. Colorectal cancer: clinical aspects

1.1.1. Epidemiology

Cancer is a significant problem worldwide. There were an estimated 18.1 million new cases of cancer worldwide in 2018, 43,800,000 prevalent cases and 9.5 million deaths(Bray et al., 2018). This is particularly endemic in Europe, which accounts for 25% of global cancer incidence and a fifth of cancer mortality despite it being home to only 9% of the global population(Bray et al., 2018).

Colon cancer is the 3th most common cancer worldwide, with 1.8 million cases in 2018, with an age-standardized incidence rate of 32.1 per 100,000 was 2018(Ferlay, 2018), one of the highest of all cancers (Figure 1.1). In 2012, there were 100,762 diagnoses of colorectal cancer in the UK, 56,369 (56%) in men and 44,393 (44%) in women(Office of National Statistics, 2016). There were 881,000 deaths in 2018 (Bray et al., 2018). The age-standardized mortality in the UK was 11.1 per 100,000. The age-standardised incidence (Figure 1.1) and mortality (Figure 1.2) rates vary across the world, but is highest in Europe, North America, Asia and Australia. These figures are presented in Table 1.1.

1.1.2. Pathophysiology

There are a number of important molecular and genetic factors at play in colorectal tumourigenesis. The most commonly described molecular processes include both somatic and hereditary genetic mutations, that encompass aberrations in the WNT/APC/β-catenin signalling pathway, the multi-hit phenomenon of the adenoma-carcinoma sequence, microsatellite instability and chromosomal instability. We shall now consider each of these in turn.
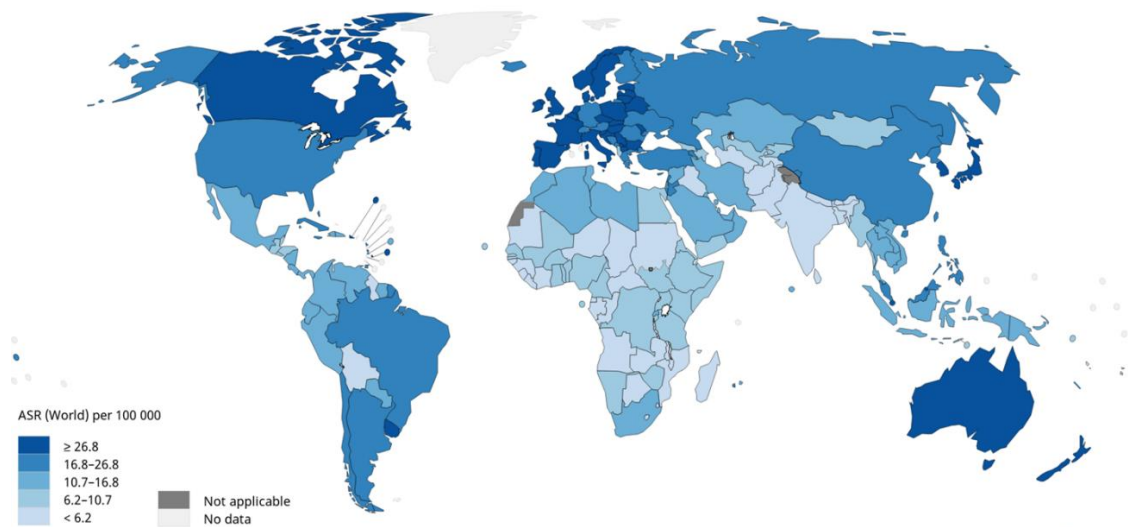
Figure 1.1. World map presenting the age-standardized rate (ASR) of incidence of CRC in 2018 by geographic region. Please refer to the key for the Presented in numbers of people per 100,000 in 2018. Exported from the International Agency for Research on Cancer's Cancer Today database(International Agency for Research on Cancer, 2019).
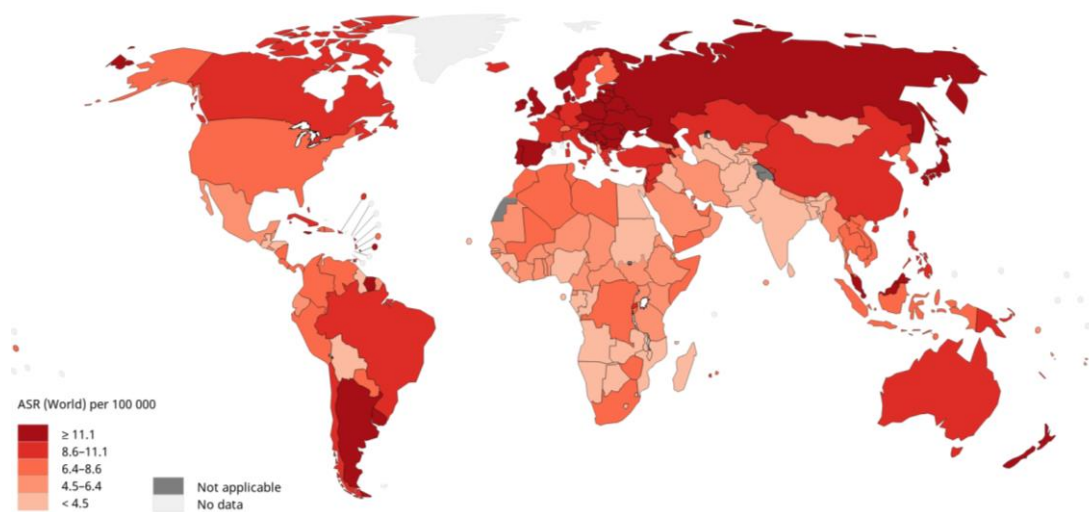
Figure 1.2. World map presenting the ASR of mortality of CRC by geographic region. Data presented in numbers of people per 100,000 in 2018. Exported from the International Agency for Research on Cancer's Cancer Today(International Agency for Research on Cancer, 2019).

	Age-standardised incidence rate (per 100,000)	Age-standardised mortality rate (per 100,000)
Australia	468	91.8
USA	352.2	91
France	344.1	109.8
Canada	334	92.8
UK	319.2	102.6
Germany	313.1	104.2
Spain	273.3	92.3
Turkey	225.1	121.5
Russia	222.1	119.2
South Africa	213.5	117
Brazil	217.2	91.3
China	201.7	130.1
Libya	120.3	69.1
India	89.4	61.4

Table 1.1. Table with age-standardised incidence and mortality rates per 100,000 of the population for CRC in different countries around the world. Data obtained from the International Agency for Research on Cancer's Cancer Today(International Agency for Research on Cancer, 2019).

1.1.2.1. Somatic mutations

A number of genetic and epigenetic changes can be either germline or sporadic *de novo* mutations that result in neoplasia, genomic instability and subsequent progression onto colorectal cancer.

1.1.2.1.1. The adenoma-carcinoma sequence

The adenoma-carcinoma sequence (Figure 1.3) describes a sequence of genotypic and phenotypic changes that underlie transformation of normal tissue into colorectal cancer.

The first microscopic histological changes are aberrant crypt foci (ACF). These microscopic lesions are histologically recognised as large, thick crypts upon methylene blue staining. ACF are thought to precede the development of adenomas. Adenomas can either be dysplastic or hyperplastic, and can undergo malignant transformation. Dysplastic ACF are more prevalent in patients with the syndrome familial adenomatous polyposis (FAP) than in non-FAP patients(Takayama et al., 2001). There is a positive correlation between the size of ACF and the number of adenomas, and they are significantly more prevalent in dysplastic polyps and 100% prevalent in cancer(Takayama et al., 1998). Vogelstein *et al* reported further genotypic differences between adenomas and carcinomas. They found that 73% of tumours had increasing numbers of allelic losses of chromosomes 5 and 18 across class I to III adenomas and carcinoma and increasing numbers of allelic loss in chromosome 17 across adenomas and cancer (Vogelstein et al., 1988). Further study has identified a number of important genetic mutations that develop with increasing frequency across increasingly dysplastic and malignant tissue types, in particular APC, K-Ras, SMAD4 and p53.

APC is classed as a tumour suppressor gene located on chromosome 5 in band 5 q21. The coding region spreads over 15 exons and encodes a 309kDa protein consisting of 2,843 amino acids. APC has been shown to bind to β-catenin(Rubinfeld et al., 1993) at the cytoplasmic surface of the cell membrane to facilitate adhesion and cytoskeletal organisation, in a complex with axin, β-catenin and GSK-3β. APC mutations have been demonstrated to result in a truncated protein product(Smith et al., 1993) that impairs the binding activity of the central pore with β-catenin(Munemitsu et al., 1995), resulting in stabilisation and subsequent accumulation of β-catenin. Beta-catenin has been shown to translocate to the nucleus and form a transcriptional activating complex with T-cell specific

transcription factor Tcf/LEF-1 family of transcription factors (Graham et al., 2000), binding to the promoter regions of Wnt target genes and activating transcription. APC mutations occur early in human tumourigenesis, being present in 78% of aberrant crypt foci(Takayama et al., 2001), 60% of adenomas and 60% human tumours(Powell et al., 1992). The consistent mutation rates seen through these tissues suggest that this mutation may play a key role in driving tumourigenesis.

The RAS genes encode GTPase proteins consisting of 188-189 amino acids. There are 3 types in humans: H-RAS, K-RAS and N-RAS. They are considered to be oncogenes because activating mutations of these genes drive tumourigenesis independent of upstream growth factor signalling, a key example being K-RAS mutations resulting in cellular insensitivity to inhibition of the EGF receptor upstream of the K-RAS. Of these genes, K-RAS constitutes 80% of the RAS mutations seen in adenomas and carcinomas(Vogelstein et al., 1988). K-RAS mutations have not been found in normal colon tissue(Yan et al., 2015) but have been reported in 13% of ACF samples (Smith et al., 1994), 67% of adenomas(Takayama et al., 2001) and about a 33-50% of colorectal tumours(Benvenuti et al., 2007, Vogelstein et al., 1988, Yan et al., 2015).

Similarly, p53 mutations are not found in normal colon(Yan et al., 2015) or aberrant foci(Shivapurkar et al., 1997) but have been reported in 44% of adenomas(Yan et al., 2015) and 42-76% of sequenced colonic tumours(Yan et al., 2015, Shivapurkar et al., 1997). These findings suggest that p53 mutations occur in cancer progression rather than during the process of tumour initiation.

SMAD4 is encoded on chromosome 18q. Expression is inherent in colonic mucosa but is lost in up to 33% of cancers(Salovaara et al., 2002). SMAD4 is not mutated in normal colonic tissue, but mutations occur with increasing frequency in cancerous tissue: 10% of intramucosal tumour and 7% of invasive carcinomas.

Furthermore, BRAF mutations are present in about 12% of tumours(Benvenuti et al., 2007). The most negative prognostic mutation is valine to glutamic change at codon 600, BRAF^{V600E}, that is present in almost half of all hypermutated compared to 3% of non-hypermutated tumours(The Cancer Genome Atlas Network et al., 2012). It is associated with worse outcome, with a reported median overall survival of 13.4 months compared to 37.1 months in BRAF-naïve patients in patients with metastatic CRC(Cremolini et al., 2015a).
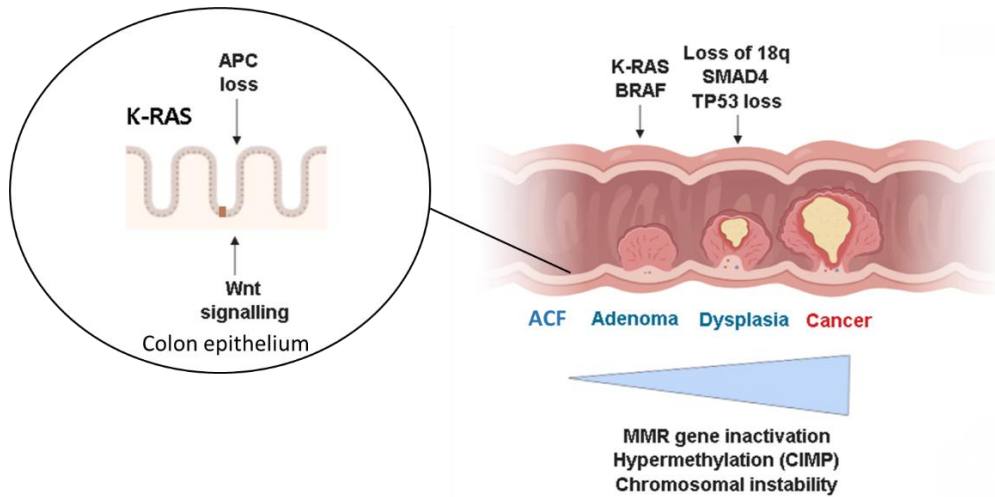
Figure 1.3. A-B: Illustration of the stepwise sequence of genetic changes in the adenoma carcinoma sequence that result in the development of adenoma and subsequently carcinoma.

APC mutation results in truncated protein that is unable to regulate Wnt signalling resulting in accumulation of beta-catenin, which has been associated with aberrant crypt formation (ACF), depicted in brown on the colon epithelium figure. K-RAS activating mutation also occurs, these changes drive adenomatosis. Activating K-RAS mutations and BRAF mutation have also been associated with subsequent dysplastic change. Tumour-specific genotypic changes include loss of p53 (TP53) and SMAD4 as well as chromosome 18q, inactivation of mismatch repair (MMR) genes with subsequent chromosomal instability as well as hypermethylation.

Image created using Biorender at https://app.biorender.com.

1.1.2.1.2 Microsatellite instability

Microsatellites consist of short tandem repeats of 1-6 base pairs found throughout all genomic sequences, both coding and non-coding. These account for 3% of the genome. Microsatellite instability (MSI) is defined as alternate sized short tandem (or dinucleotide) repeats in tumour tissue that are not present in genomic DNA. Western blot analysis and High Resolution Fluorescent Microsatellite Analysis (HRFMA) have shown that cell lines that do not express the mismatch repair proteins hMSH6 and hMLH1 have marked microsatellite instability(Oki et al., 1999), suggesting that these genes are important in repairing and preventing MSI. Loss of mismatch repair proteins can be via point mutations making a dysfunctional protein or by transcriptional silencing by hypermethylation of the promoter sites of these genes (CpG island methylator phenotype). It occurs in 10% of cases of CRC(The Cancer Genome Atlas Network et al., 2012)

1.1.2.1.3. Chromosomal instability

Chromosomal instability is defined as an accelerated rate of loss or gain of whole or parts of chromosomes, and has been demonstrated in 60-70% of colorectal cancer. Resultant loss or gain of part or all of part of chromosomal alleles results in aneuploidy, loss of heterozygosity and sub-chromosomal genomic amplifications. Karyotype analysis has demonstrated losses in the chromosome arms 1p, 5q, 8p, 17p in 52%, 36%, 48%, 42% of sequenced tumours and complete loss of chromosomes 17 and 18 in 31% and 64% respectively(Thiagalingam et al., 2001). A meta-analysis of comparative genomic hybridisation (CGH) studies found incremental increases in the frequency of loss of chromosome arms 4p, 4q, 8p and 18q over progressive disease stages (Diep et al., 2006). Equally, gains have been reported at 1q, 7p, 8q and 20q(Diep et al., 2006).

In a study looking at the mechanism of chromosomal loss, fluorescent in situ hybridization (FISH) analysis of colon cancer cells found that partial allelic loss was due to interchromosomal recombinations and deletions associated with DNA double-strand breaks. However, total chromosomal loss was concluded to be due to mitotic nondisjunction, with some segregation of both chromatids to one daughter cell that in some cases was subsequently duplicated, generating aneuploidy(Thiagalingam et al., 2001). Important genes involved in colorectal

cancer development are encoded on these chromosomes: the APC gene on chromosome 5q, p53 on chromosome 17p and SMAD4 on 18q.

Interestingly, the APC protein has been shown to bind to and stabilise microtubules, preserving their length and protecting them against depolymerization following nocodazole treatment(Zumbrunn et al., 2001). Karotype analysis has revealed chromosomal instability in embryonic stem cells with APC mutants generating truncated APC proteins, and mutants with truncation of the C terminal region that interacts with EB1 generated chromosomal instability(Fodde et al., 2001). Therefore, as tumourigenesis progresses, loss of heterozygosity and somatic mutations of the remaining allele can be seen to further generate chromosomal instability and tumour development.

1.1.3. Aetiology of colorectal cancer

There are a number of hereditary conditions and inflammatory conditions that predispose sufferers to a higher risk of colorectal cancer than the background population. These are thought to constitute approximately 25% of cases. The remaining cancers are deemed to be sporadic. Lifestyle factors have been shown to contribute to carcinogenesis.

1.1.3.1. Dietary factors

The highly processed, fibre-poor diet of the western world has been associated with a higher risk of colorectal cancer, in particular processed and red meats, as well as alcohol and a sedentary lifestyle(World Cancer Research Fund International and American Institute for Cancer Research, 2016).

The World Cancer Research Fund reported in 2016 that consumption of wholegrain, dietary fibre, dairy and calcium supplements is associated with a lower risk of colorectal cancer. On the other hand, red meat, processed meat, alcoholic drinks and obesity is associated with an increased risk(World Cancer Research Fund International and American Institute for Cancer Research, 2016).

1.1.3.2. Hereditary conditions

There are a number of hereditary colon cancer syndromes that have been described, attributable to genetic mutations.

1.1.3.2.1. Familial adenomatous polyposis

Familial adenomatous polyposis (FAP) is autosomal dominantly transmitted, and accounts for 1% of all colorectal cancers. There are two phenotypic variants. The classical condition results in the development of hundreds or thousands of adenomatous polyps in the colon. The attenuated condition results in a milder phenotype, with less than 100 polyps and a later disease onset(Nielsen et al., 2007). Pathogenic mutations of APC are prevalent in 80% of cases with polyposis, mostly by single base substitutions or deletions. Biallelic mutations in the DNA base excision repair gene MUTYH are prevalent in 2% of cases(Grover et al., 2012), causing MUTYH-associated polyposis (MAP), transmitted in an autosomal recessive manner. The majority are germline, however 30% of cases develop from de novo mutations. Both germline and sporadic cancers resulting from APC mutation develop following loss of heterozygosity of chromosome 5q21-22(Miyaki et al., 1994). The condition also has extracolonic manifestations, including polyposis of the upper gastrointestinal tract, desmoid tumours and congenital hypertrophy of the retinal pigment epithelium(Caspari et al., 1995). Furthermore, a base substitution T>A at APC nucleotide 3920 (I1307K) has been described in Ashkenazi Jews with attenuated polyposis and carcinoma that makes the region hypermutatable with no truncation of the protein(Laken et al., 1997). There is 100% penetrance of cancer in FAP by the age of 40 years(Bisgaard et al., 1994), but disease is delayed by 15 years in AFAP(Knudsen et al., 2010).

1.1.3.2.2. Hereditary non-polyposis colorectal cancer

Hereditary non-polyposis colorectal cancer, or Lynch syndrome, constitutes 1-3% of all colorectal cancers. It is autosomal dominantly inherited, comprising inactivating deletions to the sequence of mismatch repair genes MLH1(Papadopoulos et al., 1994), MSH2(Leach et al., 1993), MSH6(Akiyama et al., 1997), PMS1 and PMS2(Nicolaides et al., 1994). Phenotypically this disease results in the development of large adenomas with villous histological components(De Jong et al., 2004). Lynch syndrome is also associated with extracolonic cancers including uterine, pancreatic and stomach tumours. There is a combined penetrance of all cancers of 32% before the age of 50 and 42% before 70(Jenkins et al., 2006).

1.1.3.3. Inflammatory bowel disease

Meta-analysis of studies reporting on the risk of colorectal cancer in ulcerative colitis has reported an increasing incidence over the length of the disease, from 0.91 per 100,000 per year in the first decade to 4.07 and 4.55 in the second and third decades respectively(Castano-Milla et al., 2014). Incidence rates are higher in those with extensive colitis, reported 44.4 per 100,000 per year. Meta-analysis of clinical studies also reported a similar increasing risk of neoplasia over time for Crohns, with cumulative risk of 2.9%, 5.6% and 8.3% at 10, 20 and 30 years post-diagnosis with significantly higher cumulative risks in both UC and Crohns than in the general population (Canavan et al., 2006),.

Meta-analysis also reported lower incidence rates for ulcerative colitis in papers stratified by date of publication into the last decade (1.21/100,000/y) versus those published in the 1950s (4.29/100,000/y)(Castano-Milla et al., 2014), which may reflect an improvement of primary treatment, earlier detection via endoscopic surveillance and earlier surgical resection.

1.1.3.4. Screening

The UK bowel cancer screening programme is a population screening programme that aims to detect asymptomatic cancers in the UK population. It is offered to people in the UK between 60-74 years of age. It tests human stool samples for blood that is often secreted by colonic tumours. Traditionally this has been done using a faecal occult test that detects the presence of haemoglobin in the stool. This test is completed at home and returned to the laboratory in the post by the patient. Patients with positive stool tests are then invited for further investigation, usually a colonoscopy.

Long-term follow-up of a randomised controlled trial of faecal occult blood testing in asymptomatic patients proposed a 13% reduction in mortality from colorectal cancer(Scholefield et al., 2002). This was the clinical rationale behind the introduction of the UK bowel cancer screening programme. The screening programme was started in 2006 and rolled out nationwide by 2009. Initial results appeared promising, as positive faecal occult blood tests were found to be cancer in 11.6% of men and 7.8% of women; high risk adenomatous polyps in 12% of men and 6.2% of women, and; intermediate risk adenomatous polyps in 19.3% of men and 14.6% of women(Logan et al., 2012b). In 2018, ministers voted on lowering the age of eligibility to this screening programme to 50 years of age. Further

developments include the introduction of a one-off bowel endoscopy for all patients at 55 years of age.

The clear advantage of the NHS bowel screening programme is detection of cancerous and pre-cancerous lesions in asymptomatic people that can be removed prior to cancer development. Furthermore, it has proven to be a cost-effective measure in detecting cancers at an earlier stage. Retrospective analysis of health systems data has revealed incidence costs of £17,241 in patients under 65 and £14,776 in those over 65 years of age, with 5-year prevalence costs for total healthcare of £216,549 in those under 65 and £458,688 in those over 65 years old. This analysis revealed that these costs are lower in early stage (Stage 1-2) disease than advanced stages (Stages 3-4): £14,911 versus £19,187 for those under 65 and; £14,196 versus £15,411 in over 65(Laudicella et al., 2016), demonstrating a cost advantage to early diagnosis. In addition, there is benefit to instituting surveillance measures in those patients who are diagnosed with a hereditary colorectal cancer syndrome.   However, only 1 in 10 cancers are diagnosed through the UK bowel screening programme(Office of National Statistics, 2016). The main disadvantage of the screening programme is the high proportion of false positive screening tests, which require injection of healthcare resource and cost to investigate. The original guaiac faecal occult blood test has recently been replaced with a faecal immunochemical test (FIT)(National Institute of Health and Clinical Excellence, 2017). Advantages of FIT include specificity to human haemoglobin rather than any haemoglobin that may have been ingested. Furthermore, the sample undergoes automated analysis with more quantitation in micrograms per gram of faeces, rather than subjective operator-dependent interpretation of colour change. A health technology assessment systematic review reported sensitivities of 92.1-100% and specificities of 85.8-76.6% have been reported and the test was deemed cost effective for use within the NHS(Westwood et al., 2017). This may help to reduce the proportion of false positive tests.

Another issue with the screening programme has been low population uptake of the test. Of the first 2 million tests, only half were returned (49.5% of men, 54.4% of women), with lower uptake in lower socio-economic and ethnic groups (Logan et al., 2012a). Interventions such as face-to-face invitation/discussion and telephone invitation have been shown to increase uptake in these groups(Shankleman et al., 2014).

1.1.3.5. Surveillance endoscopy

Certain patient groups should undergo surveillance endoscopy as they are at greater risk of developing colorectal cancer. These include:

1. Patients who have had adenomas removed at diagnostic endoscopy.
2. Patients with inflammatory bowel disease.
3. Patients with genetic conditions that predispose to colorectal cancer.

Adenomas discovered at endoscopy should be removed where this is technically feasible and safe to do so and sent for histology. Patients should be stratified into the risk of progression onto colorectal cancer to determine follow-up. UK endoscopic guidelines currently do this based on the size and number of adenomas (Figure 1.4). The benefits of endoscopic follow-up have been reported. Follow-up surveillance of intermediate-risk patients is associated with a significant reduction in the incidence rate of colorectal cancer, with a hazard ratios at 1, 2 or 3+ follow-ups of 0.57, 0.51 and 0.54 respectively(Atkin et al., 2017). More comprehensive results will hopefully be released from the All Adenoma Study that was funded by the Health Technology Assessment Programme UK, that ceased recruitment in February 2019.

Patients with Crohns and ulcerative colitis should undergo surveillance endoscopy. The frequency of endoscopy is determined by both macro-   and   microscopic changes on biopsies and are outlined in Figure 1.5.

Baseline colonoscopy

Low risk	Intermediate risk	High risk
1-2 adenomas <1cm in size	3-4 adenomas <1cm size At least 1 >1cm in size	≥5 small adenomas <1cm OR ≥3 with at least 1cm in size

Low risk:
No surveillance
OR 5 years depending on age, comorbidity, family history, procedural success

Findings at Follow-Up
1 negative exam → 3 years
2 negative exams → No FU
Low/intermediate risk → 3 years
High risk adenomas → 1 year

Intermediate risk: 3 years

Findings at Follow-Up
1 negative exam → 3 years
2 negative exams → No FU
Low/intermediate risk → 3 years
High risk adenomas → 1 year

High risk: 1 year

Findings at Follow-Up
Negative, low or intermediate adenomas → 3 years
High risk adenomas → 1 year

Figure 1.4. Guidelines for subsequent surveillance after endoscopic adenoma removal. Modified from (Cairns et al., 2010).

Screening colonoscopy

Lower risk
Extensive colitis with no active endoscopic/histological inflammation
OR
Left sided colitis
OR
Crohns colitis of <50% colon
→ 5 years

Intermediate risk
Extensive colitis with MILD ACTIVE endoscopic/histological inflammation
OR
Post-inflammatory polyps
OR
Family history of CRC in FDR <50
→ 3 years

Higher risk
Extensive colitis with moderate/severe active endoscopic/histological inflammation OR stricture in past 5 years OR dysplasia in past 5 years declining surgery
OR PSC/transplant for PSC OR family history of CRC in FDR < 50 years
→ 1 year

Figure 1.5. Guidelines for surveillance for patients with inflammatory bowel disease. Biopsies should be taken from macroscopically abnormal tissue, otherwise 2-4 random biopsies from every 10cm of colorectum. Modified from (Cairns et al., 2010).

1.1.3.6. Symptomatic patients

Clinical suspicion of a lower gastrointestinal tract tumour warrants urgent 2 week wait referral to secondary care for appropriate investigation. This is the most common route by which patients are diagnosed with colorectal cancer(Cancer Research UK, 2019a). The referral criteria are set out within the NICE guidance *Suspected cancer: recognition and referral*(National Institute for Health and Care Excellence, 2015) for patients:

- Aged 40 years or more with unexplained weight loss and abdominal pain.
- Aged 50 years or more with unexplained rectal bleeding.
- Aged 60 years or more with either iron deficiency anaemia or changes in their bowel habit.
- Positive faecal occult blood test.
- A rectal or abdominal mass.
- Aged 50 or more with rectal bleeding plus any of the following:
  - Abdominal pain
  - Change in bowel habit
  - Weight loss
  - Iron deficiency anaemia.

Patients present as an emergency in approximately 20% of cases with obstruction or perforation(Kyllönen, 1987).

The referring clinician will perform a digital rectal examination, particularly in patients presenting with bleeding, to look for pathology that can cause bleeding, such as haemorrhoids or anal fissure. Patients presenting with these features will be referred on the 2-week wait pathway for assessment at colorectal clinic. The most common first-line investigation is either:

- Colonoscopy.

  This is the gold standard for investigation. It has high reported global sensitivity of 92.5% and specificity of 73.2% for diagnosis of pathology including adenomas and cancer(Martin-Lopez et al., 2014), as it allows clearer visualisation of the bowel lumen and the ability to take tissue biopsies for histology. Limiting factors include inadequate bowel preparation, poor patient tolerance and inability to pass the scope all the

way to the terminal ileum, which prevent a thorough and complete examination.

- CT colonoscopy.

  CT colonoscopy has been reported to have similar detection rates to colonoscopy for colorectal lesions, with 10.7% via CT colonography versus 12% via colonoscopy(Atkin et al., 2013). This makes this test more acceptable as a first line investigation in older patients for whom preparation for colonoscopy may be more challenging, e.g. patients on anticoagulation. It also has a higher detection rate than barium enema(Halligan et al., 2013). However, this is balanced against a higher requirement for further investigations, reported at 30% versus 8% for those undergoing colonoscopy(Atkin et al., 2013), predominantly for lesions under 10mm in size.

  CT would be used for patients presenting as an emergency with clinical concern of obstruction or peritonitis from perforated bowel.

1.1.4. Staging

Approximately 95% of all colorectal cancers are adenocarcinoma. Other rarer subtypes include adeno-squamous carcinoma and high-grade neuroendocrine carcinoma. Diagnosis via endoscopy or CT colonoscopy then requires staging of the disease.

1.1.4.1. Imaging

Patients diagnosed by endoscopy and/or pathological biopsy should then undergo appropriate imaging in order to determine local and distant metastatic spread. This is important in planning the course of treatment for the patient.

First line imaging of colorectal cancer is usually a contrast CT scan of the chest, abdomen and pelvis. PET-CT can also be used. Patients with rectal cancer should undergo magnetic resonance imaging (MRI), then patients with potentially resectable disease on MRI should be offered endorectal ultrasound to further assess resection margins(National Institute of Health and Clinical Excellence, 2014). Results from imaging is used to determine metastases as part of the TNM staging.

1.1.4.2. AJCC TNM Staging

Clinicians use the TNM staging system. This comprises information regarding Tumour, regional lymph Nodes and Metastases that are used to decide whether adjuvant treatment is indicated. TNM staging can be provisionally interpreted from imaging, where multi-disciplinary team assessment of biopsies and imaging seek to determine the feasibility of an R0 surgical resection of primary and metastatic disease. However, the ultimate TNM staging is derived from pathological analysis of resection specimens.

T staging is summarised in Table 1.2, N staging in Table 1.3 and M staging in Table 1.4. Pathologists do not assign the M stage. Carcinoma found within a polyp warrants resection if there is high grade invasive carcinoma, cancer less than 1mm of the resection margin or lymphovascular invasion present. Lymph node staging requires a complete histological resection of the mesorectum containing no less than 12 lymph nodes in order for accurate staging.

The TNM classification can also be summarised into Stages 0 to 4 (Table 1.5). These staging systems have superseded the Dukes classification system.

The Office of National Statistics report on cancer diagnosis by stage in the UK in 2012 demonstrate a fairly even proportion of diagnoses by different cancer stages (Table 1.6).

T	Definition
TX	Primary tumour cannot be assessed
T0	No evidence of primary tumour
Tis	Carcinoma in situ: intramucosal carcinoma involving lamina propria that does not extend through the muscularis mucosae
T1	Tumour invades submucosa (through muscularis mucosa but not into the muscularis propria)
T2	Tumour invades muscularis propria
T3	Tumour invades through muscularis propria into pericolorectal tissues
T4	
T4a	Tumour invades through visceral peritoneum (including gross perforation of the bowel through tumour and continuous invasion of tumour through areas of inflammation to the surface of the visceral peritoneum)
T4b	Tumour directly invades or adheres to other adjacent organs or structures

Table 1.2. Summary of the T staging classifications.

N	Definition
NX	Regional lymph nodes cannot be assessed
N0	No regional lymph node metastasis
N1	Metastasis in 1-3 regional lymph nodes
N1a	Metastasis in 1 regional lymph node
N1b	Metastasis in 2-3 regional lymph nodes
N1c	No positive regional lymph nodes but there are tumour deposits in the subserosa, mesentery or non-peritonealized pericolic or perirectal/mesorectal tissues
N2	Metastasis in 4 or more regional lymph nodes
N2a	Metastasis in 4-6 regional lymph nodes
N2b	Metastasis in 7 or more regional lymph nodes

Table 1.3. Summary of the N classification system.

M	Definition
M0	No distant metastasis by imaging and no evidence of tumour in other sites or organs
M1	Distant metastasis
M1a	Metastasis confined to 1 organ or site without peritoneal metastasis
M1b	Metastasis to 2 or more sites or organs without peritoneal metastasis
M1c	Metastasis to the peritoneal surface, alone or with other site or organ metastasis

Table 1.4. Summary of the M classification.

Stage	T	N	M
0	Tis	N0	M0
I	T1-T2	N0	M0
IIA	T3	N0	M0
IIB	T4a	N0	M0
IIC	T4b	N0	M0
IIIA	T1-T2	N1N1c	M0
	T1	N2a	M0
IIIB	T3-T4a	N1/N1c	M0
	T2-T3	N2a	M0
	T1-T2	N2b	M0
IIIC	T4a	N2a	M0
	T3-T4a	N2b	M0
	T4b	N1-N2	M0
Stage IVA	Any T	Any N	M1a
Stage IVB	Any T	Any N	M1b
Stage IVC	Any T	Any N	M1c

Table 1.5. Summary of the Staging classification

Sex	Number of diagnoses	Stage 1 (%)	Stage 2 (%)	Stage 3 (%)	Stage 4 (%)	Unknown (%)
Male	56,329	16	22	25	22	15
Female	44,393	14	23	24	22	18

Table 1.6. Adults in England diagnosed 2012-2014. Source National Cancer Registration and Analysis Service Public Health England(Office of National Statistics, 2016).

Serum carcinoembryonic antigen (CEA) is routinely taken at diagnosis and measured as part of follow-ups. It is used in combination with clinical assessment and imaging where appropriate, as it is a poor marker alone for assessing for recurrence, with a Cochrane review reporting a pooled sensitivity of 82% (95% confidence interval (CI) of 78-86%) and pooled specificity of 80% (95% CI 59-92%)(Nicholson et al., 2015). However, there is some evidence that CEA trends during palliative chemotherapy can be useful as the rate of increase of CEA levels correlates poorly with prognosis(Yu et al., 2018).

There is evidence emerging for the use of mutational analysis for prognostication in modern pathological tumour tissue analysis. BRAF V600E mutation and K-RAS mutations have both been shown to negatively impact on overall survival and progression-free survival of both metastatic (Cremolini et al., 2015b) and non-metastatic(Taieb et al., 2016) tumours. Determination of microsatellite status may prove helpful in this respect, as BRAF V600E mutation has been shown to negatively impact on overall survival and disease-free survival in microsatellite stable (MSS) tumours, whereas it has been associated with longer disease-free survival in patients with tumours with microsatellite instability (MSI) (Cremolini et al., 2015b).

Mutational analysis can also direct appropriate adjuvant therapies. The monoclonal antibodies cetuximab and panitumumab target the extracellular domain of the epidermal growth factor (EGF) receptor. Tumours with activating K-RAS mutations have been shown *in vitro* to be more resistant to anti-EGFR antibody cetuximab(Benvenuti et al., 2007). Subsequent clinical trials have also shown similar resistance. A meta-analysis of 9 randomised controlled trials testing for mutations in exons 2, 3, and 4 of K-RAS and exons 2, 3 and 4 of N-RAS demonstrated significantly improved overall survival and progression-free survival in metastatic colorectal cancer with wild-type RAS genes, but no survival benefit for those with K- and N-RAS mutations(Sorich et al., 2014). Consequently, joint guidelines from the American Society of Clinical Pathology, College of American Pathologists, Association for Molecular Pathology and the American Society of Clinical Oncology recommend RAS mutational testing to determine eligibility for anti-EGFR monoclonal therapy in metastatic CRC (Sepulveda et al., 2017).

1.1.5. Treatment

1.1.5.1. Surgical resection

Treatment of colorectal cancer is primarily surgical resection. The decision regarding the feasibility of surgical resection is made at the multidisciplinary team (MDT) meeting where the patient's imaging, histopathology from biopsies and assessment of patient co-morbidities and physical fitness is made by surgeons, histopathologists and radiologists, and involving the patient in the decision-making process after this meeting at clinic. About 4% of patients present with synchronous disease(Mulder et al., 2011), i.e. metastasis at the time of or within 6 months of the diagnosis of the primary colorectal cancer. Presentation with synchronous metastases to the liver and/or lungs that are deemed technically resectable are resected where this is feasible, and the decision is made at MDT regarding whether metastases should be removed simultaneously or by separate operations. Patients presenting as an emergency are assessed by the on call surgical team with emergency imaging and prompt decision is made regarding proceeding to surgical resection.

1.1.5.2. Left sided colonic stenting

Patients undergoing emergency surgery have been shown to have more advanced disease, a 4-fold higher mortality rate and lower 5 year survival rates than those presenting electively(Kyllönen, 1987). Stenting of left sided obstructing tumours is an alternative, allowing decompression of the bowel and allowing pre-operative staging and preparation. A meta-analysis of 7 randomised controlled trials has shown that compared to proceeding to immediate emergency surgery, this procedure has a lower risk of complications to emergency surgery (relative risk 0.6, confidence interval (CI) 0.38-0.958, p=0.032) with a comparable 3 year progression free survival rate, with odds ratio of 1.429 (95% CI 0.8-2.55, =0.087) (Foo et al., 2019).

1.1.5.3. Chemotherapy

Chemotherapy can be used in a number of scenarios:

1. Adjuvant chemotherapy for high risk stage II and for all stage III rectal or colon cancer.

   This is with the aim of reducing the risk of local or systemic recurrence.

2. Advanced or metastatic colorectal cancer.

   This can be used for unresectable disease for palliation but can also be used with the aim of downsizing tumour burden. Where this is successful, patients may undergo follow-up imaging and be deemed resectable and be treated with surgery.

Adjuvant chemotherapy regimes commonly used for high risk stage II or stage III colorectal cancer include:

- Capecitabine monotherapy.
- Oxaliplatin, 5-fluorouracil and folinic acid (FOLFOX).

Chemotherapy regimes used in advanced or metastatic colorectal cancers include:

- FOLFOX as first-line treatment followed by irinotecan as second-line treatment, or;
- FOLFOX as first-line treatment followed by 5-fluorouracil, irinotecan and folinic acid (FOLFIRI) as second-line treatment, or;
- Oxaliplatin and capecitabine as first-line treatment then FOLFIRI as second line treatment.

Meta-analysis has found benefit for palliative chemotherapy in inoperable disease, with a median improvement in survival of 3.7 months, but reporting of symptom control and quality of life is inconsistent across studies and generally poor(Colorectal Cancer Collaborative Group, 2000).

Chemotherapy treatment regimes are limited by the patient's fitness and medical comorbidities, and are commonly limited by anaphylaxis and pharmacological side effects. XELOX, FOLFOX and FOLFIRI regimes have been associated with neutropenia, thrombocytopenia, vomiting, diarrhoea, mucositis, skin changes, alopecia, fatigue and peripheral neuropathy (Kosugi et al., 2018, Tournigand et al., 2004). Adverse effects are not reported in a standardised manner across studies,

making conclusions difficult to draw by meta-analysis(Colorectal Cancer Collaborative Group, 2000).

1.1.5.4. Radiotherapy

Radiotherapy plays an important role in neoadjuvant treatment in rectal carcinoma. Patients should undergo MRI plus/minus endoscopic ultrasound (EUS) to determine the extent of disease and to stratify their risk of recurrence before a decision is made regarding chemoradiotherapy. NICE guidance recommends that a short-course of chemoradiotherapy should be offered immediately prior to resection to those of moderate risk of recurrence(National Institute of Health and Clinical Excellence, 2014), i.e. any of the following features on MRI or EUS:

- Any tumour staged at pT3b or greater and no threatened surgical resection margin.
- Any suspicious lymph node disease that threatens the resection margin
- Extramural vascular invasion

NICE guidance also recommends that a longer course of chemoradiotherapy should be offered to those who are deemed high risk of recurrence(National Institute of Health and Clinical Excellence, 2014), i.e.:

- A threatened (<1mm) or breached resection margin
- Low rectal tumours encroaching onto the inter-sphincteric plane or with levator involvement.

1.1.6. Prognosis

Recent statistics report a 77.3% and 79.6% 1 year survival and 59.2% and 59% 5 year survival in women and men respectively (Office for National Statistics, 2019). There has been a steady increase in clinical outcomes for patients diagnosed with colorectal cancer in the UK over the last few decades, with an increase in 1- and 10-year age-standardised survival of 46.2% and 21.8% for those diagnosed between 1971-1972 to 72.6% and 50.8% for those diagnosed between 2005-2006(Cancer Research UK, 2019b). This is likely related to a combination of factors, including the use of the UK bowel screening programme, more aggressive surgical management of extracolonic metastases and the routine use of chemoradiotherapy to downsize unresectable disease and proceeding on to surgical resection. Multivariate analysis

reports no difference in relative survival risks in patients who have synchronous or metachronous disease (hazards ratio 1.02), but higher risks identified in patients with synchronous disease and disease on the right side of the colon (ascending colon), increasing age (>70 years old) and distant metastases (HR 9.6) (Mulder et al., 2011).

Poor 1 year survival has been reported in those presenting over 75 years old, emergent presentation and with more advanced and inoperable disease(Network, 2012a).

This introduction shall now move on to discuss calcium signalling and the calcium signalling receptors that have been studied in this thesis, namely ORAI1 and PIEZO1.

1.2. Calcium

Calcium is ubiquitous in all eukaryotic cells. Its first physiological role was identified by accident by Sydney Ringer who noted that rat hearts suspended in tap water continued to contract whereas they didn't in distilled water, later identifying that this was mediated by calcium salts(Ringer, 1883). It plays a crucial role as a signalling molecule in a number of signal transduction pathways, for a diverse range of cellular processes, including muscle contraction, secretion, cell proliferation and cell death. Calcium initiates muscle contraction by binding to troponin C in both cardiac(Putkey et al., 1989) and skeletal(Babu et al., 1993) muscle fibres, generating a conformational change in the tropomyosin complex to allow actomyosin fibres to bind in a rolling fashion to generate muscle fibre shortening and contraction(Holthauzen et al., 2004). Cellular proliferation and cell death. Calcium is implicated in various signalling processes that stimulate in proliferation(Pinto et al., 2015), including NFAT activation(Kar et al., 2014), NFkB(Theatre et al., 2009), Akt(Dugourd et al., 2003) and MAPK pathways including JNK(Tfelt-Hansen et al., 2004) and ERK(Pintus et al., 2003, Huang et al., 2001), which are summarised in Figure 1.6. Conversely, calcium signalling has been implicated in various cell death mechanisms including anoikis(Khaw-On et al., 2019) and necrosis(Baek et al., 2017) as well as apoptosis and autophagy. Apoptosis can be initiated by either ligand-gated death receptor activation at the cell surface (the extrinsic pathway) or within the cell at the mitochondria (the intrinsic pathway)(Elmore, 2007), activating the caspase cascade to initiate cell death (Figure 1.7). Pro-apoptotic members of the

Bcl-2 family such as tcBID have been shown to propagate ER store calcium release and mitochondrial uptake(Csordas et al., 2002). Increased intracellular calcium has been reported to initiate apoptosis, as this calcium can be taken up through the mitochondrial calcium uniporter (MCU) and result in apoptosis(Brisac et al., 2010), but the MCU has also been activated by oxidative stress(Dong et al., 2017). Apoptosis can also occur through caspase-independent signalling by the release of apoptosis initiating factor (AIF), and calcium can mediate this. The calcium-dependent protease calpain has been found to induce AIF release from the mitochondria(Polster et al., 2005). Autophagy is a multi-step process that degrades and recycles cytoplasmic components during conditions of stress. It can be cytoprotective during conditions of cell stress or initiate cell death(Orrenius et al., 2015). Calcium has been shown to both trigger and inhibit autophagy via different pathways (Figure 1.8), for instance activating autophagy via calcium/calmodulin-dependent kinase kinase β (CaMKKβ)(Hoyer-Hansen, 2007) activating AMPK1 and ULK1 phosphorylation(Vingtdeux, 2010).

The cytosolic concentration of calcium in an unexcited cell is maintained to approximately 100nM versus 1.5mM in the extracellular environment. In order to do this, the cell maintains intracellular calcium stores, mainly within the sarcoplasmic (SR) or endoplasmic reticulum (ER). This was first discovered using electron microscopy and calcium ion binding assays in muscle (sarcoplasmic reticulum)(Ebashi and Lipmann, 1962). Studies using genetic targeting of the calcium-sensitive photoprotein aequorin and strontium have estimated stores to be 2mM in concentration(Montero et al., 1995). A small amount is also taken up by the mitochondria(Rizzuto et al., 1992) but the predominant store is the ER(Brini et al., 1997). Furthermore, a range of channels mediate calcium flux into and out of the cell, which are controlled by a number of processes including calcium ATPases and sodium-calcium exchanger pumps. These are summarised in Figure 1.9.

Calcium signalling is generated by two principal mechanisms, importing calcium from the extracellular environment or by release from internal stores, termed store operated calcium release. There is a wide range of intracellular calcium signalling components that are used in order to generate calcium signalling. Store release is a universal mechanism for generating calcium signalling in non-excitable cells.
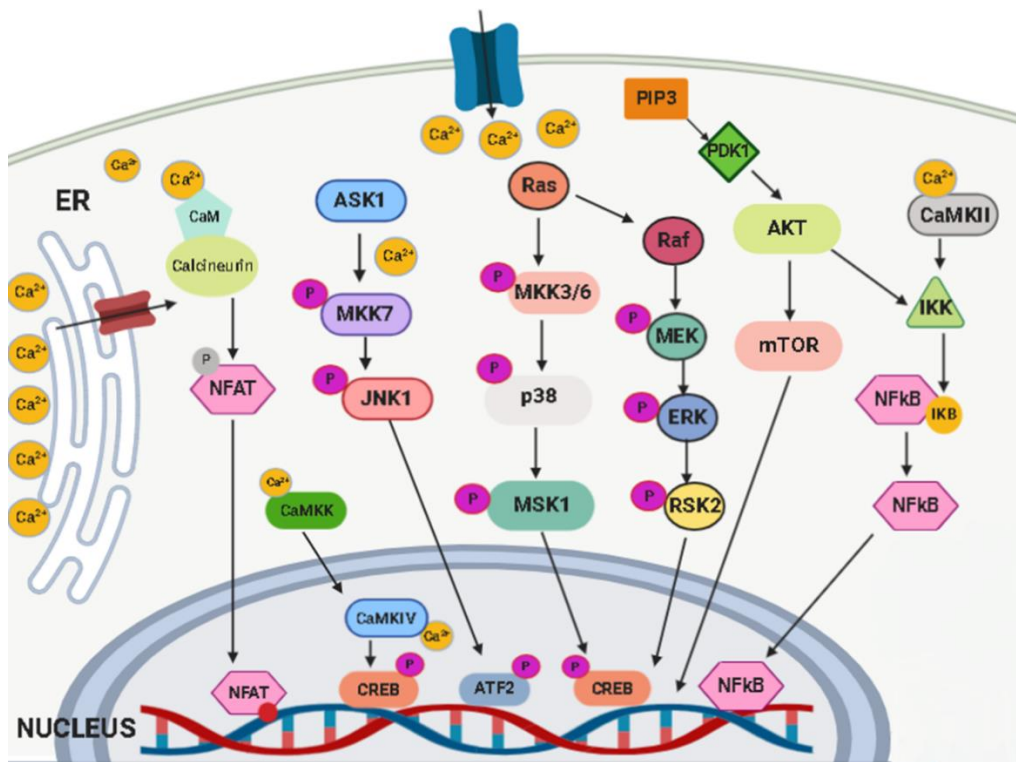
Figure 1.6. Illustrative figure summarising the intracellular molecular signalling processes involved in cell proliferation. Modified from (Pinto et al., 2015).
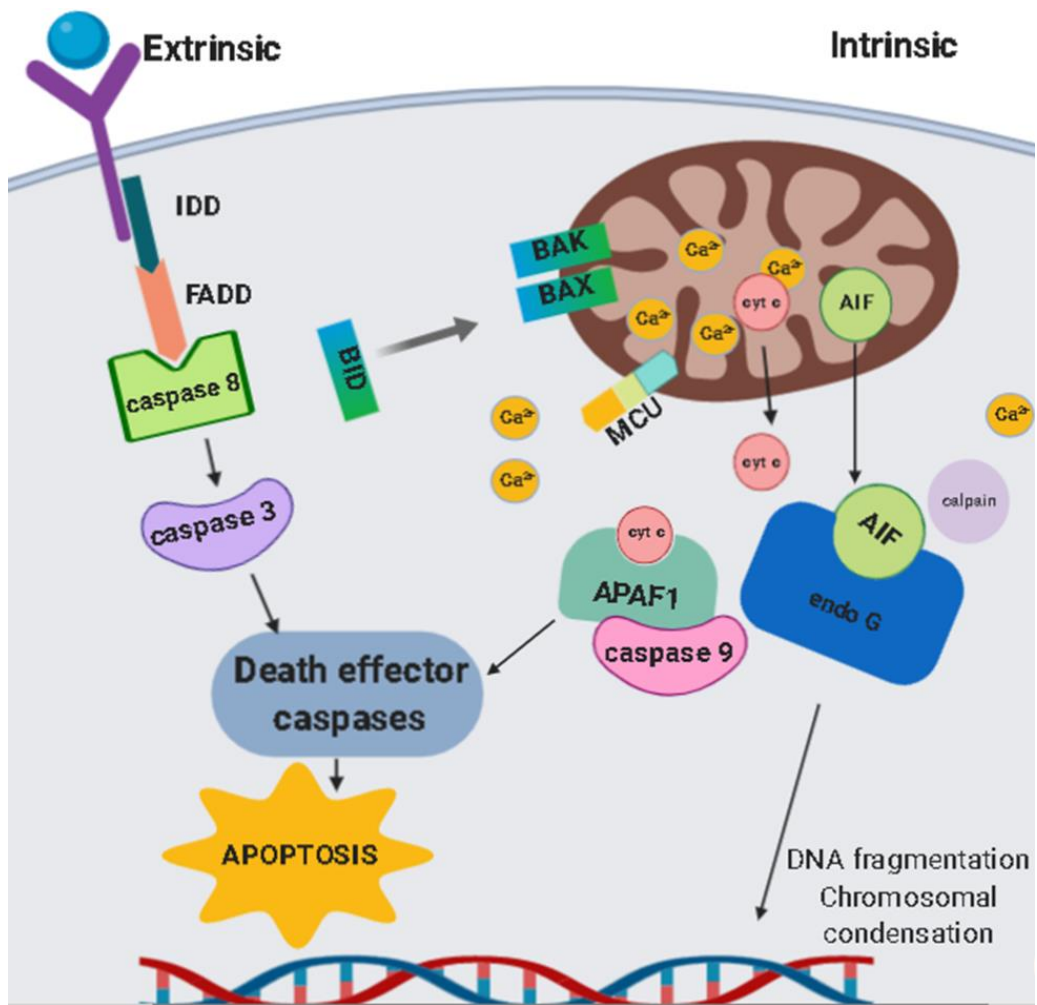
Figure 1.7. Illustrative figure summarising the intracellular molecular signalling processes involved in apoptosis. Modified from (Chen et al., 2018a)
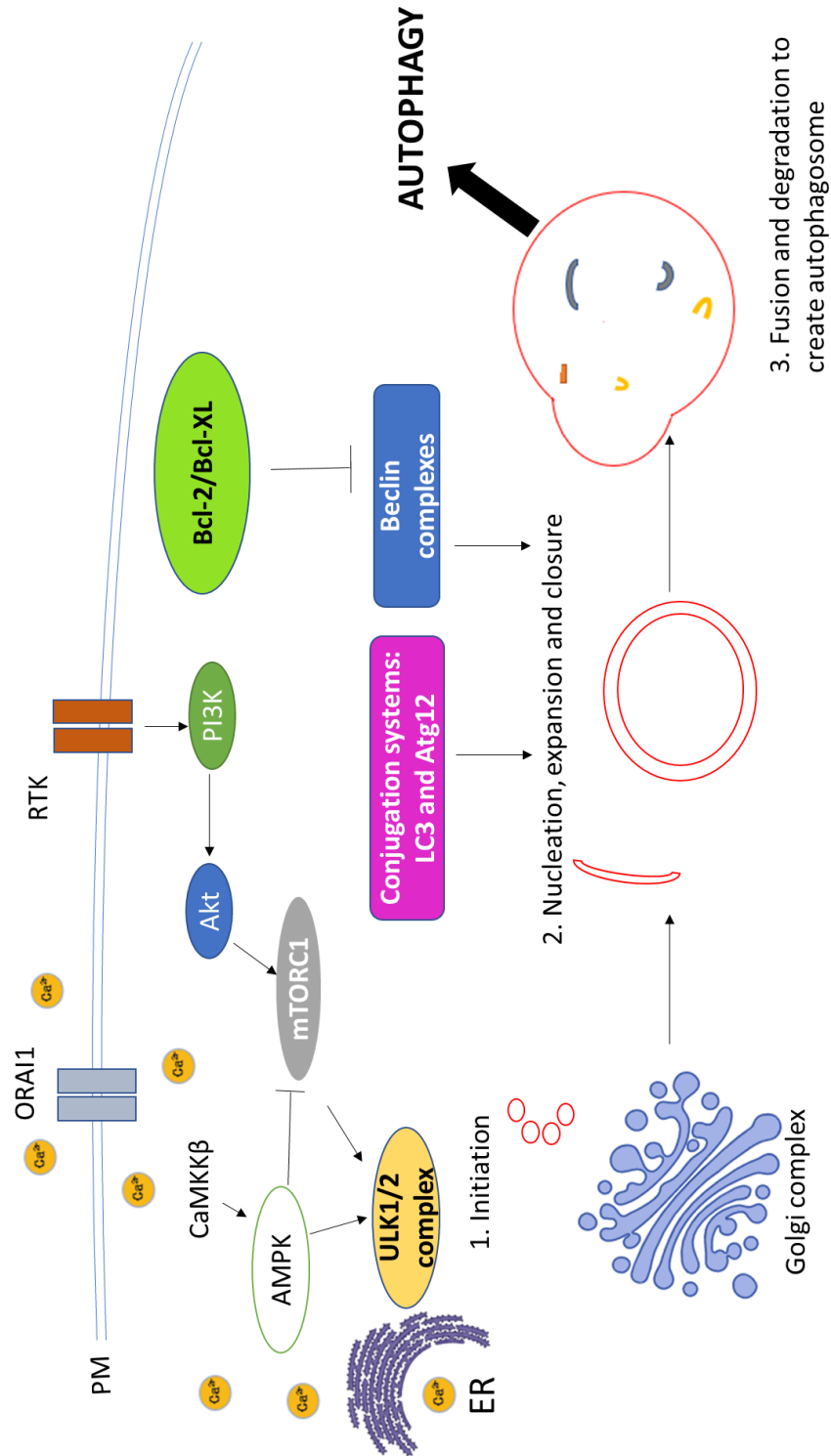
Figure 1.8. Illustrative figure summarising the intracellular molecular signalling processes involved in autophagy. Modified from (Chen et al., 2018a) and (Bootman et al., 2018)

1.2.1. Store operated calcium release

CRAC channel signalling begins at the cell surface via binding of extracellular ligands such as hormones and neurotransmitters to G protein coupled receptors. The Gαq/G11 activates phospholipase Cβ, which catalyses cytosolic 1, 4, 5-inositol triphosphate (IP$_3$) generation from phosphatidylinositol 4, 5-bisphosphate (PIP$_2$)(Berstein et al., 1992). Endoplasmic reticulum store release is stimulated by InsP$_3$(Button and Eidsath, 1996) to the InsP$_3$ receptor on the endoplasmic reticulum membrane. The large cytosolic component of the channel consists of an N-terminal β- trefoil suppressor domain, an IP3 binding domain (IBC) and 3 α-helical domains, with the channel domain at the C terminus(Hamada et al., 2017). The channel is tetrameric, forming homo- and heterodimers with different isoforms. Three isoforms of the InsP3 channels have been identified and have been found to be tissue-specific. The large cytosolic domain consists of an IP3 binding core that results in a conformational change resulting in rotation the alpha helical domains that activates the calcium channel domain(Hamada et al., 2017), resulting in an outward current.

Store operated calcium release can be activated experimentally using thapsigargin, calcium chelators such as EGTA and BAPTA and ionomycin(Hoth and Penner, 1993), as well as the reversible SERCA pump inhibitor cyclopiazonic acid.

1.2.2. The CRAC channel

Calcium release-activated calcium (CRAC) channels are calcium-selective channels that are relatively insensitive to monovalent ions and potently blocked by lanthium, and are activated by store operated calcium release(Hoth and Penner, 1993). The concept of CRAC channel signalling was first hypothesized by Putney in a paper proposing the capacitative model in 1986(Putney, 1986b). The term CRAC channel was devised as the process of CRAC channel signalling was identified before the genes responsible for the actual channel were identified.

The search for the gene responsible for the CRAC channel was solved in 2006, when genome-wide RNAi screen and subsequent patch-clamp studies of Drosophila S2R+ cells identified CRACM1 and CRACM2 as modulators of the current (the M standing for modulator), but with no observed effects from genetic overexpression(Vig et al., 2006b). Human CRACM1 was identified in an RNAi screen of HEK293 cells by the same group in the same study(Vig et al., 2006b). Around the same time, the same channel was identified by Feske and colleagues using modified linkage analysis and

SNP arrays of families suffering from severe combined immune deficiency (SCID) alongside functional studies using an RNAi screen of Drosophila cells and named ORAI1(Feske et al., 2006). ORAI has largely superseded the term CRAC although many authors use these interchangeably.
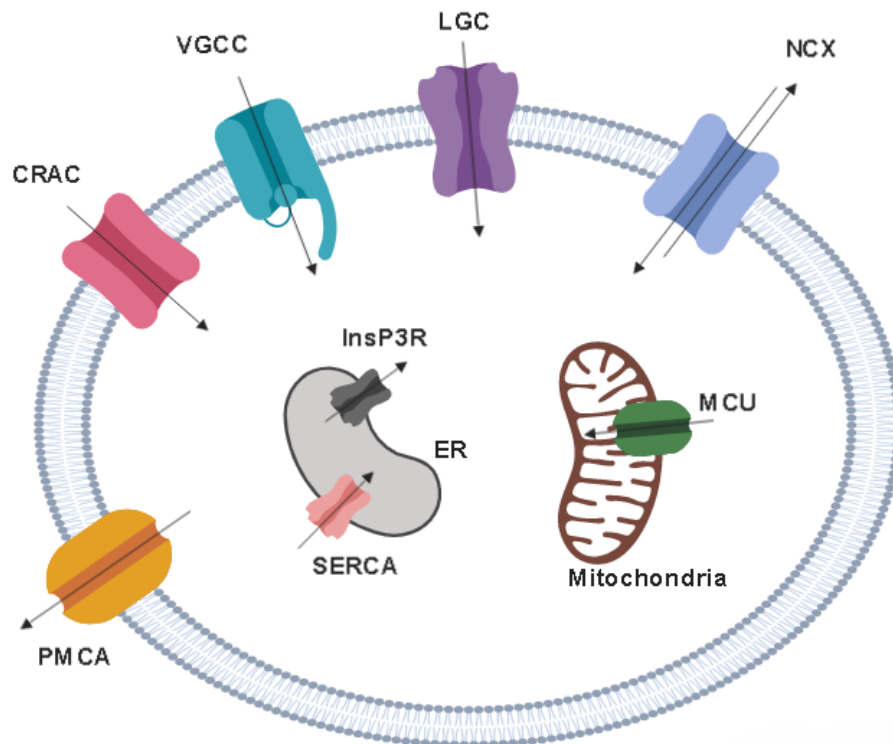
Figure 1.9. Summative illustration of key calcium transporters in the cell. Plasma membrane channels importing calcium into the cell include CRAC channel (CRAC, pink), voltage gated calcium channel (VGCC, blue), ligand-gated calcium channel (LGC, purple). Plasma membrane calcium exporter channels include plasma membrane calcium ATPase pumps (PMCA, yellow) and sodium-calcium exchanger (NCX, lilac). Organelle calcium importers include mitochondrial calcium unit (MCU, green) and SERCA pumps (SERCA, pink). Organelle calcium exporter channels include InsP3R channels (InsP3R, grey). Modified from (Parekh, 2005) and the KEGG calcium channel pathway downloaded from the KEGG pathway database (https://www.genome.jp/kegg/pathway.html). Image created by Biorender at https://app.biorender.com.

Subsequent to this, CRACM1, CRACM2 and CRACM3 have subsequently become known as ORAI1, ORAI2 and ORAI3.

1.2.2.1. CRAC channel activation by STIM

CRAC channel activation is instigated following store depletion by the stromal interaction molecule (STIM). This is a single-pass ER membrane protein, with a NH2 terminus in the ER lumen and a cytoplasmic COOH terminus.

Endoplasmic reticulum store depletion is sensed by the EF-rich calcium-sensing motif in the N terminus of the STIM1 molecule(Zhang SL, 2005), a 685 amino acid, highly conserved ER transmembrane protein consisting of a single membrane spanning domain that is essential to CRAC channel signalling(Roos et al., 2005) (Figure 1.10). Dissociation of calcium from the EF hand induces a conformational change, resulting in oligomerisation and translocation to puncta at endoplasmic reticulum-plasma membrane (ER-PM) junctions(Liou et al., 2007) where it can associate with and activate channels to generate calcium influx. FRET co-localisation studies of CFP- and YFP-conjugated STIM1 molecules in the tumour mast cell line RBL and HeLa cervical cancer cell line using both physiological and experimental stimulation of IP3-mediated store depletion demonstrated STIM1 oligomerisation and aggregation into puncta at the plasma membrane-endoplasmic reticulum junctions (Liou et al., 2007). In addition, ionomycin treatment demonstrated oligomerisation at the ER membrane prior to sequential translocation to the PM-ER junctions(Liou et al., 2007). STIM1 oligomer translocation is reversible. Reversible ER calcium ATPase inhibitor 2,5-di-(t-butyl)-1,4-hydroquinone (BHQ) administration with histamine-induced store depletion in HeLa cells resulted in STIM1 punctae formation and translocation that then dissipated following wash-out and calcium refilling(Liou et al., 2007). Mutational studies in HeLa cells have shown that a polybasic sequence motif in the C terminal sequence of the STIM1 molecule is important for translocation of puncta to the ER-PM membrane, but CFP and YFP tagging of this STIM1 mutant showed that mutation did not affect oligomerisation(Liou et al., 2007).

The channel is constitutively inactive. When calcium stores are depleted, the resultant STIM1 punctae associate directly with the ORAI pore at both the 107 amino acid CRAC-channel activation domain (CAD) of the C terminus and the coiled-coil element of the N-terminus(McNally et al., 2013), a process that is required to

activate the channel(McNally et al., 2012) and resulting calcium influx into the cell. Its calcium selectivity is conferred from acidic residues in the transmembrane and extracellular domains(Vig et al., 2006a). A rise in cytosolic calcium entry then inactivates the channel through changes to the charge of pore residues Y80 and W76, resulting in a conformational change of the channel(Mullins et al., 2016), resulting in a transient and self-regulating calcium current.

There is some recent evidence that CRAC channel signalling requires other molecules to support it. Experiments in Hela and Jurkat cells that the ER resident molecule TMEM110 is required to support STIM1 clustering and STIM-ORAI association at the plasma membrane-endoplasmic reticulum junction(Quintana et al., 2015).

Store operated calcium release and CRAC channel signalling is summarised in Figure 1.6.
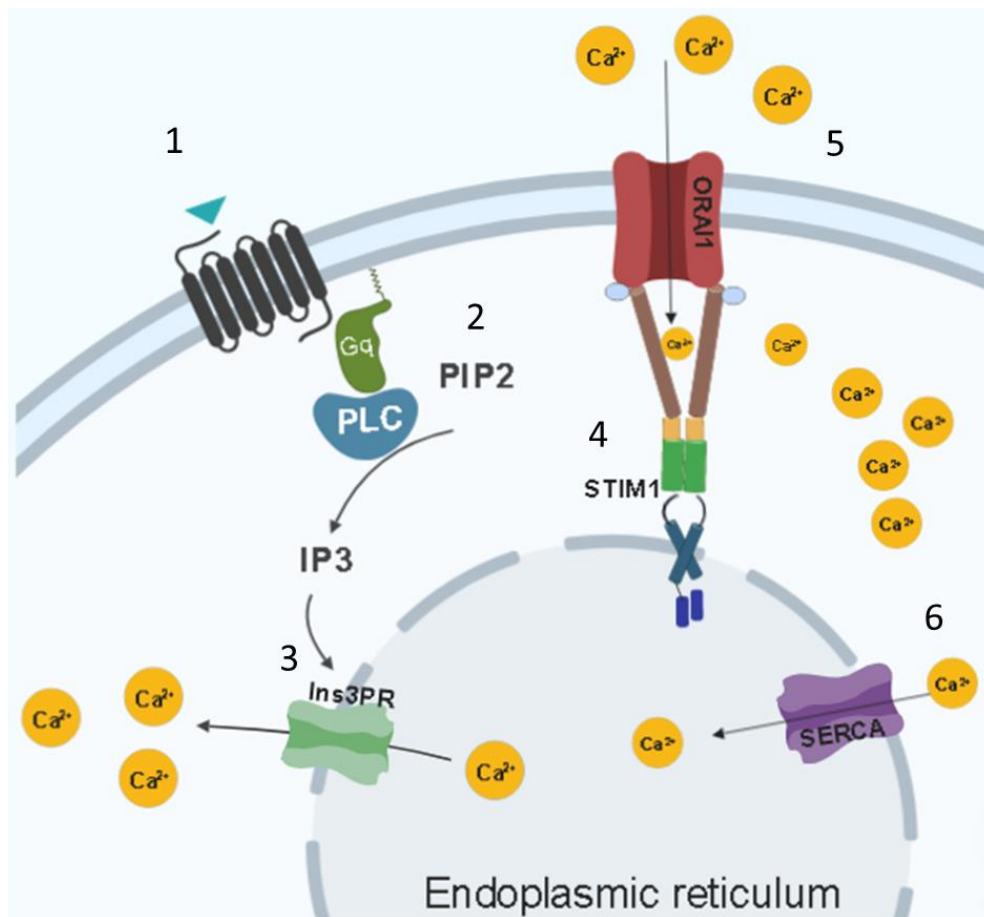
Figure 1.10. Illustrative depiction of store operated calcium release and subsequent CRAC channel signalling. 1. Extracellular binding of a ligand to its receptor coupled with a GPCR, activating the Gq/11 subunit which activates PLCβ. 2. Activated PLCβ catalyses conversion of PIP2 to IP3. 3. IP3 then binds to the IP3R receptor within the ER membrane, resulting in calcium release and store depletion. 4. Calcium depletion results in calcium dissociation from the EF hand domain of the STIM1 molecule (purple subunits). Dimerisation and oligomerisation is not depicted. However, the interaction of the STIM1 molecule with the ORAI1 receptor through the STIM1-ORAI1-activating region (SOAR) is illustrated (brown subunits), which generates a conformational change in the ORAI1 pore that opens the channel. 5. Calcium enters through the ORAI1 channel into the cytosol. 6. Calcium is taken up into the ER by the SERCA pump. Modified from (Soboloff et al., 2018). Image created by Biorender at https://app.biorender.com.

1.2.2.2. The ORAI family

Three ORAI channels have been described to date: ORAI1, 2 and 3. All 3 ORAI channels displayed typical CRAC channel responses to store depletion and instillation of BAPTA. Patch clamp experiments showed that they can generate inwardly rectifying current in a store dependent manner (Lis et al., 2007). However, the current amplitudes of ORAI2 and ORAI3 were seen to be lower than that of ORAI1 in both endogenous channels of HEK293 or overexpression using vectors transfected with ORAI2 and ORAI3(Lis et al., 2007).

1.2.2.2.1. ORAI1

The functional significance of the ORAI1 channel was first discovered in T cells. It is the most characterised of the 3 ORAI channels.

The ORAI1 channel is well conserved across species. It is formed from transmembrane domains around a central pore. ORAI1 has been shown to be able to multimerise with itself(Vig et al., 2006a). It was initially reported to be able to form homotetramers of ORAI1 subunits in STIM1-overexpressing HEK293 cells(Mignen et al., 2008b). However, it was subsequently shown that the channel can form tetramers with other ORAI subunits such as ORAI3(Mignen et al., 2009). Furthermore, subsequent crystal structure studies of the Drosophila ORAI1 (dORAI1) channel was shown to form a hexameric structure, with each subunit formed from 4 transmembrane helices (M1-4) and a cytosolic extension from M4 cytosolic that interact with the M4 extension sequences of other ORAI1 subunits in the channel to mediate STIM1 binding (Hou et al., 2012) (Figure 1.11). The channel pore was found to be formed from amino acids from the M1 helix from each pore(Hou et al., 2012). The Drosophila channel shares 73% sequence homology to the human channel.

1.2.2.2.2. ORAI3

To date, ORAI3 has been well described as an important component of the arachidonic acid-regulated calcium (ARC) channel, which is regulated by STIM1 in a store independent manner(Mignen et al., 2008a). It has been shown to cluster with ORAI1 to generate a pentameric channel(Mignen et al., 2009). Arachidonic acid activates ORAI3 through a cytosolic N-terminal domain of
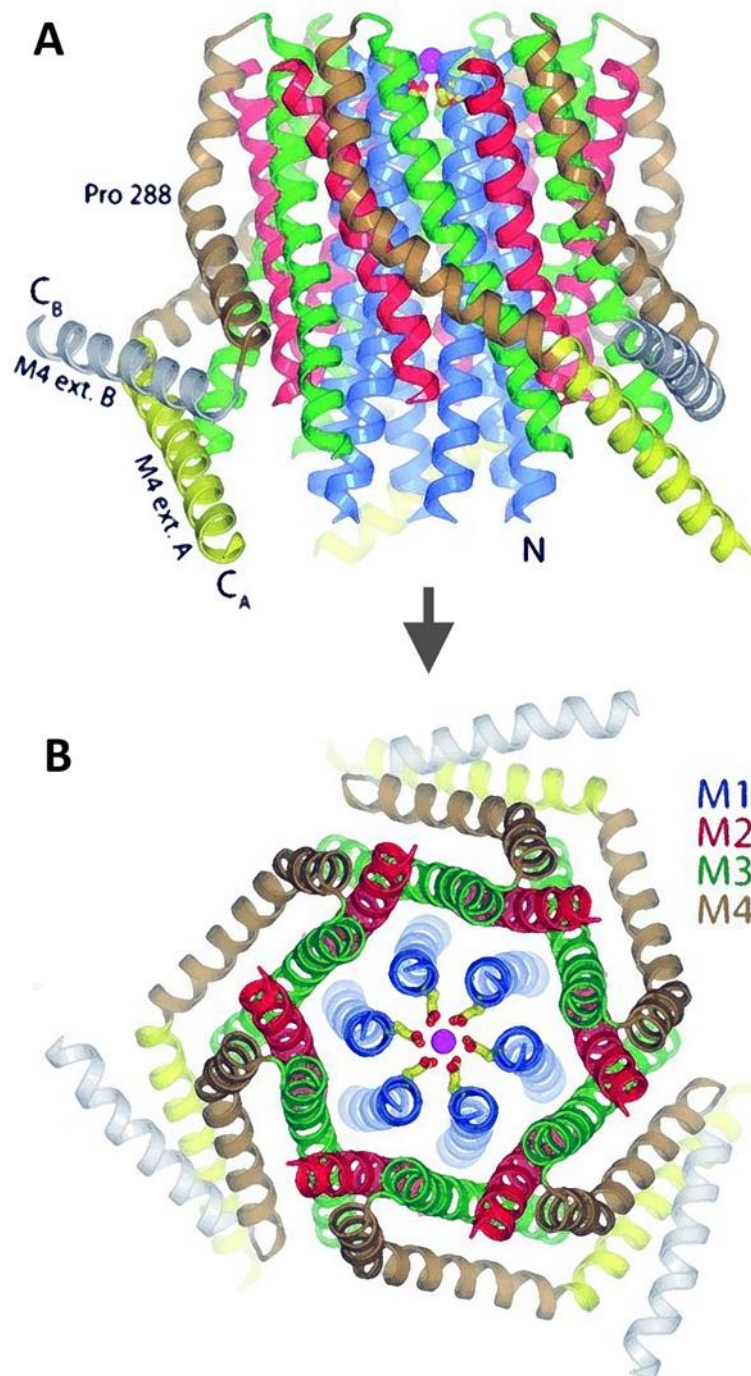
Figure 1.11. A-B: Ribbon topography of the tertiary structure of the Drosophila ORAI1 channel.

A. Side view of the ORAI1 channel. B. Extracellular view of the channel.

The 4 helices (or M) of the ORAI1 channel are colour coded for ease of visual interpretation. M1 (blue), M2 (red); M3 (green); M4 (brown); yellow and grey represent extension of M4. Calcium ions are depicted as magenta spheres.

Modified from (Hou et al., 2012).

ORAI3(Thompson et al., 2010). However, ORAI3 is dependent upon the presence of ORAI1 to generate the current(Mignen et al., 2009).

1.2.3. Calcium removal from the cytoplasm

This rapid increase in cytosolic calcium is transient as it is then removed from the cell. The sarcoplasmic/endoplasmic reticulum calcium ATPase (SERCA) pump takes up calcium from the cytosol into the ER. It is a 100kDa P-type ATPase composed of 10 transmembrane helices that span the ER membrane. Amino acid mutagenesis studies identified crucial sequences in the 4th, 5th, 6th and 8th helices responsible for calcium-dependent phosphorylation and subsequent calcium transport(Clarke et al., 1989). They are encoded by 3 genes, SERCA1, SERCA2 and SERCA 3.

1.2.4. CRAC channel signalling in health and disease

1.2.4.1. InsP3R

InsP3R1 predominates in brain tissue and has an important role in maintaining normal morphology of Purkinje cells (PC). Using inducible knockouts of this channel, InsP3R1-knockout mice have denser and longer PC spines, and develop severe ataxia(Sugawara et al., 2013). Clinical deletion has been identified in families suffering from spinocerebellar ataxia type 15 (SCA15)(Di Gregorio et al., 2010, Hara et al., 2008). Mutated presenilin 1 has been shown *in vitro* to interact with InsP3R to generate higher levels of calcium release, stimulating processing of amyloid β that is pathognomonic of Alzheimers(Cheung et al., 2008).

1.2.4.2. ORAI1

ORAI1 has been found to be endogenously present in a wide variety of tissues and structures. It has been shown to be present and important in the normal function of skin(Gwack et al., 2008). ORAI1 is expressed in human skin(Vandenberghe et al., 2013), and is functionally important in keratinocyte viability and migration, as ORAI1 knockdown reduced both(Vandenberghe et al., 2013). Furthermore, keratinocytes isolated from ORAI1 null transgenic mice had markedly lower CRAC channel signalling, proliferation and migration(Vandenberghe et al., 2013).

ORAI1 has also been shown to be important *in vitro* in endothelial cell proliferation(Abdullaev et al., 2008) and arterial myocyte function(Baryshnikov et al., 2009). It is present in vascular smooth muscle cells (VSMC) (Li et al., 2011b, Yang

et al., 2012) and crucial for PDGF-induced vascular smooth muscle cell (VSMC) migration(Bisaillon et al., 2010). ORAI1 is upregulated and functional in the process of neointima formation following carotid artery injury(Zhang et al., 2011), as well as proliferation, migration and hypertrophy occurring in airway smooth muscle cell remodelling in asthmatic mice(Spinelli et al., 2012).

Furthermore, ORAI1 appears to be important in normal perinatal development. ORAI1 null transgenic mouse models found ORAI deficiency has been shown to generate a phenotype, consisting of blepharitis and abnormally thin keratinocytes(Gwack et al., 2008). In addition, there was a significant increase in perinatal lethality in ORAI1 null mice(Gwack et al., 2008).

There is an established role for CRAC channel signalling in immune cell function. T cell activation has been shown to result in upregulation of ORAI1 and STIM1(Lioudyno et al., 2008), with downstream calcium signalling and activation of NFκB signalling dependent on STIM and ORAI1 activation(Liu et al., 2016, Lioudyno et al., 2008). ORAI1 null mice have been shown to display significantly reduced store operated calcium entry response in both B and T cells(Gwack et al., 2008).

ORAI1 mutation has been linked to pathological immune dysfunction. A critical function of the channel in human immunity was first reported by Feske and colleagues in 2006 when patients with a heterozygous SCID phenotype had reduced rate and peak of thapsigargin-induced intracellular calcium(Feske et al., 2006). SNP mapping array of genomic DNA from patients from 2 pedigrees of SCID disease alongside a Drosophila RNAi interference screen identified an SNP in the region of chromosome 12, and subsequent genomic sequencing revealed a novel missense mutation in exon 1 of human ORAI1 coding sequence (C→T transition at position 271, R91W)(Feske et al., 2006) that was not present in SNP screening of multi-ethnic healthy controls. Furthermore, a gene-dosage effect was described between heterozygous carriers and their homozygous offspring(Feske et al., 2006). This mutation was validated *in vitro*, as transfection of wild type ORAI1 in an IRES-GFP retroviral vector into SCID T cells restored thapsigargin-induced calcium entry in GFP positive cells(Feske et al., 2006), suggesting the ORAI1 channel is essential for store operated calcium entry.

1.2.4.3. ORAI3

ORAI3 signalling has also been described in vascular smooth muscle cells and shown to be mediated by thrombin and the inflammatory mediator leukotriene C4 in a store-independent manner(Gonzalez-Cobos et al., 2013), but again requiring both STIM1 and ORAI1 to generate this signalling(Gonzalez-Cobos et al., 2013). In addition, VEGF has been shown to induce ORAI3 surface trafficking and calcium entry in endothelial cells(Li et al., 2015b).

More recently, ORAI3 has been functionally described in vascular smooth muscle remodelling, with upregulation demonstrated in neointimal neoplasia in carotid artery injury *in vivo*(Gonzalez-Cobos et al., 2013).

1.2.4.4. ORAI signalling in cancer

CRAC channel signalling has been studied in a number of human cancers. It is overexpressed in human tumour samples from non-small cell lung cancers (NSCLC)(Zhan, 2015), clear cell renal carcinoma(Kim, 2014), oesophageal carcinoma(Ranade et al., 2014) and glioblastoma multiforme(Motiani et al., 2013a) compared to neighbouring normal tissues. ORAI1 expression is abundant in human melanoma cells, with higher expression in metastatic melanoma relative to primary tumours(Umemura et al., 2014).

In vitro studies provide evidence of an important role of ORAI1 signalling in tumour development. Pharmacological blockade and siRNA of ORAI1 reduced proliferation and tumour cell migration of clear cell renal carcinoma(Kim et al., 2014), oesophageal carcinoma(Zhu et al., 2014) and melanoma(Umemura et al., 2014). STIM1/ORAI1 inhibition in human melanoma cell lines using both shRNA and pharmacological CRAC inhibitor SFK96365 resulted in a reduction in invadopodia and tumour invasion into gelatin matrix(Sun et al., 2014). Similarly, both ORAI1 siRNA and pharmacological treatment with SKF96365 inhibited breast cancer cell migration(Yang, 2009). ORAI1 and STIM1 siRNA transfection in primary human glioblastoma multiforme cell cultures markedly reduced migration and invasion but with minimal effect on cell proliferation(Motiani et al., 2013a). However, this conflicts reports from Liu and colleagues, who used glioblastoma cell lines established from rat and human, finding that siRNA and pharmacological targeting of ORAI1 with SFK96365, 2-aminoethoxydiphenyl borate (2-APB) and diethylstilbestrol (DES) inhibited proliferation of both lines, with increased apoptosis of the rat cancer cell line(Liu et al., 2011).

In vivo effects of ORAI1 blockade have also been reported. Intraperitoneal treatment with SFK96365 resulted in significantly smaller oesophageal tumour xenograft development in nude mice *in vivo*(Zhu et al., 2014). Furthermore, breast cancer metastasis using tail vein seeding of tumour cells treated with ORAI1 or control siRNA resulted in significantly less systemic metastatic burden in the ORAI1 knockdown(Yang, 2009).

Molecular studies have shown that there is convergence of ORAI1 and ERK signalling pathways in a number of tumour models, which are responsible for driving cellular proliferation. siRNA treatment in non-small cell lung cancer cell lines showed that ORAI1 is important in cell proliferation interacting with the PI3K/AKT/ERK pathway(Zhan, 2015). Furthermore, STIM1 siRNA and SOCE blockade with YM58483 in melanoma cells resulted in a reduction of ERK1/2 phosphorylation(Umemura et al., 2014) and cell migration.

There is some evidence that CRAC signalling may be implicated in chemoresistance. ORAI1 and STIM1 levels were found to be higher in cisplatin-resistant versus cisplatin-sensitive ovarian cancer cell line A2780, with an associated increase in SOCE(Schmidt et al., 2014). Furthermore, ORAI1 and STIM1 siRNA treatment in pancreatic adenocarcinoma cell line Panc1 resulted in a small but significant increase in 5-FU and gemcitabine-induced apoptosis(Kondratska et al., 2014). Conversely, ORAI1 siRNA treatment of prostate cancer conferred resistance to cisplatin-induced apoptosis(Flourakis et al., 2010). In addition, augmented CRAC in the cisplatin-resistant ovarian cancer cell line was also associated with Akt, as pharmacological inhibition of Akt reduced CRAC (Schmidt et al., 2014).

Upregulation of ORAI1 may also be associated with poorer clinical outcomes. High ORAI1 expression in patient samples of NSCLC has been correlated with poorer clinical prognosis and survival(Zhan, 2015). In cervical cancer, STIM1 overexpression was reported in three quarters of cervical cancer samples relative to normal tissue, with increasing expression associated with development of metastatic disease and outcome(Chen et al., 2011).

CRAC channel signalling has been shown to be influenced by hormones in cancer. Activation of membrane androgen receptors in breast cancer cell line MCF7 resulted in a transient increase in ORAI1 expression and CRAC signalling(Liu et al., 2015). Similarly, androgen receptor-insensitive prostate cancer cell lines have been reported to have lower ORAI1 expression levels(Flourakis et al., 2010). The

androgen receptor has been postulated as potentially controlling ORAI1 activity. Evidence supporting this stems from androgen receptor siRNA treatment of prostate cancer cell line LNaCP which resulted in reduced ORAI1 mRNA levels and SOCE(Flourakis et al., 2010).

There is also some evidence of ORAI3 involvement in tumourigenic processes. Both ORAI1 and ORAI3 have been implicated in prostate tumour proliferation and progression: together they mediate arachidonic acid-induced calcium entry, with subsequent tumour cell proliferation that was lost following ORAI1 and ORAI3 siRNA(Dubois et al., 2014). Further evidence of a tumourigenic role of ORAI3 stems from proliferation studies in prostate cell line stably overexpressing ORAI3, which had higher rates of proliferation and were more resistant to thapsigargin-induced apoptosis(Dubois et al., 2014). ORAI3 has also been shown to be important in oestrogen receptor-positive breast cancer development. ERα knockdown significantly reduced ORAI3-mediated SOCE(Motiani et al., 2013b). ORAI3 knockdown resulted in downstream reduction in ERK, NFAT and FAK phosphorylation and signalling without impacting on ERα expression, suggesting the channel is regulated by ERα(Motiani et al., 2013b). ORAI3 has been found to mediate both SOCE and cell survival in response to reactive oxygen species in prostate cancer and prostate epithelial cell lines(Holzmann et al., 2015b), with greater levels of ORAI3 conferring greater resistance to ROS-induced apoptosis.

1.2.5. Piezo channels

Piezo comes from the Greek piesi, which means 'pressure'. It is a mechanoreceptor. Two Piezo channels have been identified, PIEZO1 and Piezo2.

PIEZO1 and Piezo2 are two large transmembrane proteins that are highly conserved across vertebrate species. They are non-selective cation channels. Both proteins were very recently identified as important components of mechanosensation in murine neuroblastoma cells(Coste et al., 2010a) and Drosophila melanogaster(Kim et al., 2012). Analysis of a wide range of tissues from different species has revealed that the two proteins are differentially expressed in different tissues, with greater levels of expression of PIEZO1 in human skin(Coste et al., 2010a). Coste and colleagues reported that PIEZO1 forms a tetrameric complex with channel properties. Its mechanosensitive current is inhibited by ruthenium red, the non-

specific cationic channel blocker that has been shown to block the pore, both in whole cell and reconstituted in lipid bilayers (Coste et al., 2012).

1.2.5.1. PIEZO1

PIEZO1 (previously known as FAM38A) is encoded on chromosome 16 at 16q24.3. It encodes a 287kDa protein. The murine PIEZO1 channel structure was largely determined in 2017 by Zhao and colleagues by cryo-electron microscopy (EM). This study identified 9 repetitive units encoding 4 transmembrane helices that form an extracellular cap with 3 blades forming a propeller distribution with a central region forming an intracellular beam structure with a hydrophobic pore (Figure 1.12) (Zhao et al., 2018).

1.2.5.2. Piezo in health and disease

PIEZO1 has been implicated in a number of physiologically relevant processes. It has been found to be present in the human bladder, where it senses urothelial stretch with consequent ATP release from the urothelial cell into the extracellular environment (Miyamoto et al., 2014). PIEZO1 knockdown in zebrafish resulted in erythrocyte swelling(Faucherre et al., 2014). The interplay between PIEZO1 function and red blood cell volume appears to have pathological implications. Mutations of the human PIEZO1 gene, which carries 54% homology to the zebrafish gene(Faucherre et al., 2014), has been associated with the clinical conditions human xerocytosis and haemolytic anaemia(Bae et al., 2013) as well as dehydrated hereditary stomatocytosis(Andolfo et al., 2013). In addition to red blood cell volume homeostasis, PIEZO1 has been shown to be important in endothelial cell alignment in response to shear stress, with PIEZO1 gene knockout resulting in disordered vascular development in utero and proves embryonic lethal in homozygous deletion(Li et al., 2014).
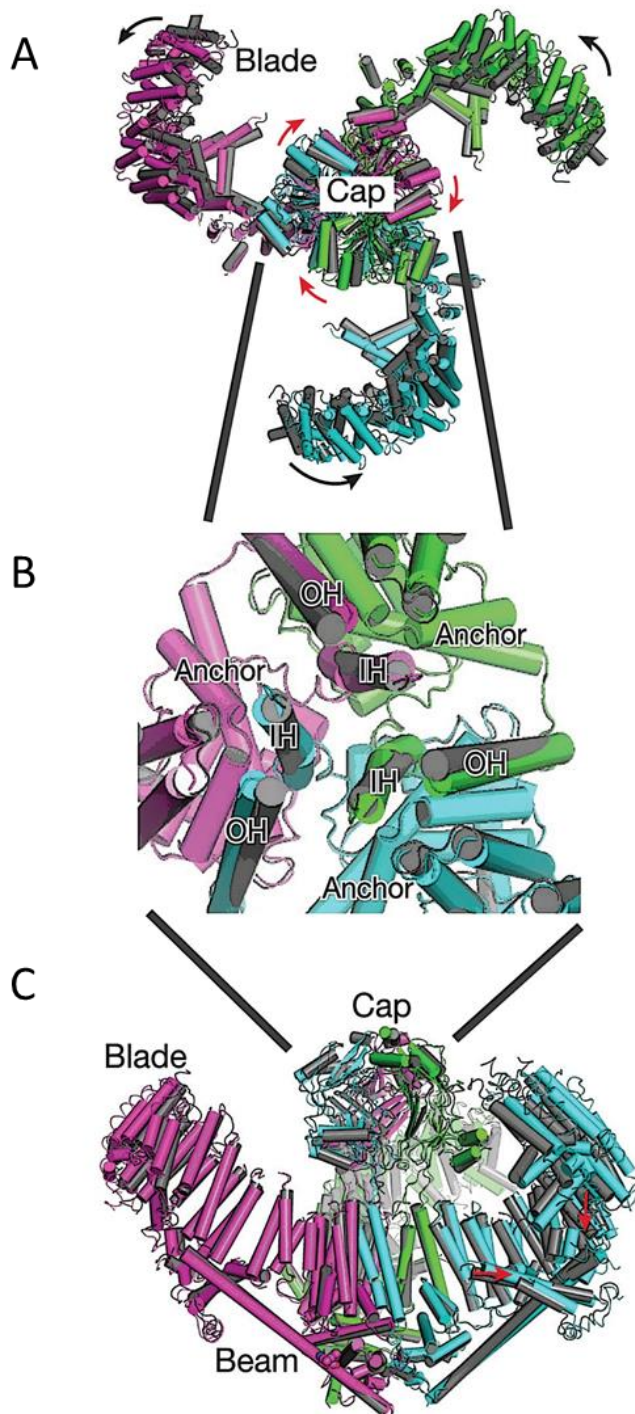
Figure 1.12. A-C: Topography of the tertiary structure of the murine PIEZO1 channel derived from cry-EM studies. A. Extracellular view of the central cap and 3 blades forming a propeller structure; B. Side sliced view of the channel showing the cap and blades above the central pore region; C. Extracellular view with the cap removed showing the pore. Images from (Zhao et al., 2018).

Furthermore, PIEZO1 appears to be important in lymphatic system formation and function. Whole-exome sequencing identified biallelic mutations in PIEZO1 in families suffering from congenital lymphatic dysplasia(Lukacs et al., 2015). Autosomal recessive inheritance of PIEZO1 nonsense and missense mutations have been associated with generalised lymphatic dysplasia which results in the fatal condition of non-immune hydrops fetalis(Datkhaeva et al., 2018).

Piezo2 expression has been noted to be relatively lower than that of PIEZO1 across different species, with lower conductance and more rapid inactivation than PIEZO1(Coste et al., 2010a). It is highly expressed in the dorsal sensory ganglia, where the channel is responsible for mechanically induced ion channel currents (Coste et al., 2010a). They have also been described as important for mechanosensation in cutaneous sensory nerve fibres through testing nerve fibres from Piezo2 knockout transgenic mouse models(Ranade et al., 2014).

1.2.5.3. Piezo in cancer

More recently, PIEZO1 has been implicated in tumour function. McHugh and colleagues found that siRNA resulted in a reduction of β1 integrin affinity and subsequent cell adhesion in HeLa cervical cancer cells(McHugh et al., 2010), which was mediated by R-Ras. They subsequently reported that PIEZO1 expression in NSCLC cell lines was significantly lower than normal lung epithelial cell lines(McHugh et al., 2012). Using siRNA treatment in these lung epithelial lines, they demonstrated that knockdown again reduced integrin affinity and promoted anchorage-independent survival and integrin-independent migration and Matrigel invasion(McHugh et al., 2012). Conversely, Li and colleagues found that PIEZO1 is important in malignant migration of breast cancer cell line MCF7 relative to the normal mammary epithelial cell line MCF10A(Li et al., 2015a). Rather than use siRNA, this group used the spider toxin GsMTX4(Li et al., 2015a), that has been previously been reported to block PIEZO1(Bae C, 2011). PIEZO1 has not been reported in colorectal cancer.

It is possible that PIEZO1 interplays with store operated calcium entry and subsequent CRAC channel signalling. PIEZO1 siRNA knockdown has been shown to reduce endoplasmic reticulum store depletion in HeLa cells with a subsequent reduction in calpain activity(McHugh et al., 2010), which may be dependent on R-Ras. However, this needs to be explored further.

1.3. Pharmacology

1.3.1. ORAI1 modulating drugs

A number of ORAI1 channel inhibitors that have been described in the literature (Table 1.7). Most are commercially available.

Most excitingly, there is one compound RP4010, that has been patented and found to be effective in reducing viability and inducing apoptosis in diffuse large B-cell lymphoma (DLBCL) *in vitro* and *in vivo(Locatelli et al., 2017)* that is now in a Phase Ia/Ib safety and efficacy clinical trial in patients with relapsed or refractory lymphomas (ClinicalTrials.gov Identifier NCT03119467). A study screening a library of FDA licensed medicines found 5 drugs that inhibited CRAC channel function in RBL cells: leflunomide and teriflunomide at clinically therapeutic doses, as well as lansoprazole, tolvaptan and roflumilast(Rahman and Rahman, 2017).

1.3.2. PIEZO1 modulating drugs

Relative to ORAI1 channel inhibitors, there are only a few PIEZO1 channel modulating compounds (Table 1.8). The spider toxin GsMTX4 has been shown to inhibit PIEZO1 function(Bae, 2011). Yoda1 is the first chemical activator to have been discovered that activates PIEZO1(Syeda et al., 2015). More recently our laboratory has characterised the first reversible Yoda1 antagonist, Dooku1(Evans et al., 2018). These compounds are important experimental tools in the study of PIEZO1.

1.4. Summary

In summary, there has been a growing body of evidence to support a role for CRAC channel signalling in most cells of the body since it was initially discovered in T cells, and a rapid increase in evidence for PIEZO1 channel function also. Furthermore, there is growing evidence that these channels play an important role in tumour development and progression, with channel function in proliferation, migration and invasion *in vitro* and *in vivo*, as well as the potential pro-angiogenic functions as both channels are active in endothelial cell function also. At the time of starting this project, there were no published studies looking at CRAC channel function and pharmacological inhibition in colorectal cancer, and no evidence of PIEZO1 function in colorectal cancer.

Name	*In vitro* cancer studies	*In vivo* cancer studies	Other biological studies	Chemical structure
RO2959	-	-	T cell function(Chen et al., 2013)	
Synta66 (S66)	-	-	Endothelial cell function(Li et al., 2011a); vascular smooth muscle cells(Li et al., 2011b)	
SFK-96365	CRC (Jing et al., 2016); melanoma(Sun et al., 2014); glioblastoma(Liu et al., 2011)	CRC(Jing et al., 2016); oesophageal (Zhu et al., 2014)	Urethral smooth muscle function(Drumm et al., 2018)	
YM-58483	Melanoma (Umemura et al., 2014)	-	Asthma(Yoshino et al., 2007); allergy(Ohga et al., 2008); T cell function (Chen et al., 2013)	
GSK-7975A	-	-	Diabetic endothelial function(Sachdeva et al., 2019); urethral smooth muscle function(Drumm et al., 2018); glomerular mesangial cells(Chaudhari et al., 2017); embryonic cortical neurones(Chauvet et al., 2016); bronchial smooth muscle(Chen and Sanderson, 2017); pancreatitis(Peng et al., 2016)	
DPB162-AE	Diffuse large B cell lymphoma (Bittremieux et al., 2018)	-	-	
2-APB	Glioblastoma(Liu et al., 2011)	-	-	
DES	Glioblastoma(Liu et al., 2011)	-	-	
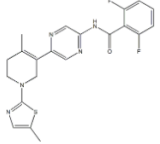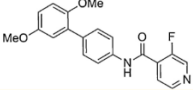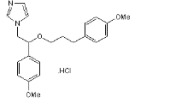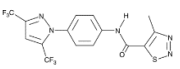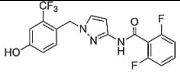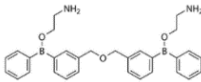
Table 1.7. Table summarising published CRAC channel inhibitors and an overview of some of the referenced biological studies that they have been used in. *In vivo* refers to murine cancer studies using tumour xenografts.

Name	*In vitro* cancer studies	*In vivo* (murine xenograft) studies	Other biological studies	Chemical structure
GsMTX4	Breast(Li et al., 2015a)	-	HEK293 cells(Bae, 2011); HUVECs(Li et al., 2014)	
Yoda1	-	-	HEK293, reconstituted mPIEZO1(Syeda et al., 2015)	
Dooku1	-	-	HEK293, HUVECs(Evans et al., 2018)	
Ruthenium red	Neuro2A murine neuroblastoma(Coste et al., 2010b)	-	HUVECs(Li et al., 2014)	
Gadolinium	Neuro2A murine neuroblastoma(Coste et al., 2010b)	-	-	
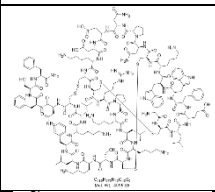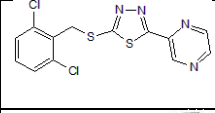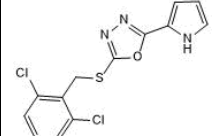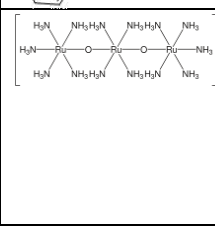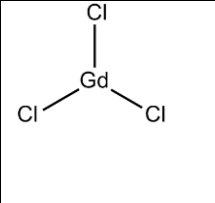
Table 1.8. Table summarising published PIEZO1 channel modulators and an overview of some of the referenced biological studies that they have been used in. *In vivo* refers to murine cancer studies using tumour xenografts.

CRC is posing a huge disease burden worldwide but particularly in developed countries. Despite increasingly aggressive surgical treatment regimes, surveillance programmes for high risk patient groups and the implementation of the UK Bowel Screening Programme, incidence and mortality remain high. Furthermore, there is a need for improved chemotherapy treatment regimes with improved anti-cancer results profiles and fewer side effect profiles.

CRAC channel inhibitors have been patented with a number being commercially available for research. These have successfully demonstrated anti-cancer effects *in vitro* and *in vivo* and one such agent is now being tested in clinical trials. The main problem of testing these compounds *in vivo* is their pharmacokinetic properties that limit their use *in vivo*. This has driven the development of novel CRAC channel inhibitors here at Leeds in the quest to find a compound with better pharmacokinetic properties. There are no such direct pharmacological inhibitors for PIEZO1 available.

1.5. Thesis Aims and Objectives

Overall Aim

The overall aim of this thesis is to gain an understanding of calcium channel physiology and modulation in colorectal cancer, focusing on PIEZO1 and ORAI1.

Hypothesis

Calcium channel signalling through ORAI1 and PIEZO1 channels plays a role in colorectal cancer cell function and metastatic potential.

Chapter Objectives

Three

- Determine whether ORAI1 channels are functionally expressed in colorectal cancer cell lines.
- Determine the effectiveness of current and novel CRAC channel inhibitors on inhibiting SOCE in both colorectal cancer and endothelial cells.
- Determine the functional effect of CRAC channel inhibition on both tumour and endothelial cell viability, cell death, migration and invasion.

- Investigate the downstream effects of CRAC channel inhibition on molecular signalling of the cancer cell.

Four

- Determine whether PIEZO1 channels are functionally expressed in colorectal cancer cell lines.
- Determine the functional effect of PIEZO1 on tumour cell viability, migration, invasion and cell cycle.

Five

Using TCGA data, the objectives of this chapter are to:

- Determine whether ORAI1 and PIEZO1 channels are differentially overexpressed in cancer relative to normal colon.
- Determine whether ORAI1 and PIEZO1 channel expression is associated with clinicopathological markers of progression, namely disease stage, lymphatic and venous invasion, overall survival and progression free survival.
- Determine whether ORAI1 and PIEZO1 channel expression correlates with genes in cancer relative to normal colon.
- Explore potential functional pathways of ORAI1 and PIEZO1 with differentially expressed genes.
- Determine whether ORAI1 and PIEZO1 channels associate with oncogenic signalling targets described in colorectal cancer.

Chapter 2. Materials and Methods

2.1. Solutions and reagents

2.1.1. Chemical reagents and antibodies

Reagent	Supplier	Catalogue Number
1-bromo-3-chloropropane (BCP)	Sigma	B62404
Biorad Protein Assay	Biorad	5000002
Bovine serum albumin	Sigma	A2153
Calcium chloride, 1M	Sigma	21115
Dimethylsulfide (DMSO)	Sigma	D8418
Dulbecco's Modified Eagle Medium high glucose GlutaMAX™	ThermoScientific	31966021
Turbo DNase kit: 10xDNAse buffer, DNase enzyme and Inactivation Enzyme (Ambion)	ThermoFisher Scientific	AM1907
Ethylene glycol-bis(2-aminoethylether)-N,N,N',N'-tetraacetic acid (EGTA)	Sigma	E3889
Ethyl alcohol	Sigma	459836
Fura-2AM	Invitrogen	F1221
FITC Annexin V Apoptosis Kit	BD Pharmingen™	556547
Gadolinium (III) chloride	Sigma	439770
Gelatin glycerol	Sigma	GG1
D-glucose	Sigma	G8270
GsMTx4 toxin from Chilean rose tarantula Grammostola spatulate	Pepta Nova	4393
HEPES	Sigma	H3375

High Capacity RNA to cDNA Kit (Applied Biosystems) 10xRT Buffer; 2xRT enzyme; 25xdNTP; 10xRT primers, Reverse Transcriptase (50U/µL)	ThermoFisher Scientific	4387406
Isopropanol/2-propanol	Sigma	I9516
Lipofectamine 2000	ThermoFisher Scientific	11668019
Lipofectamine RNAiMAX	ThermoFisher Scientific	13778030
Magnesium chloride, 1M	Sigma	M1028
Matrigel Matrix reduced growth factor	Corning	356230
Methylene blue	Sigma	M9140
Nonidet 40 lysis buffer	Sigma	11754599001
Nuclease free water	Sigma	W4502
PD98059	Cell Signalling	9900
Phosphate buffered saline (PBS) tablets	Sigma	P4417
Phosphate buffered saline (PBS) without calcium and magnesium	Lonza	17-516F
Pluronic F-127	Sigma	P2443
Potassium chloride	Sigma	P5405
Propidium iodide flow cytometry kit	Abcam	ab139418
Protease inhibitor	Sigma	P8340-1ML
Phosphatase inhibitor	Sigma	P5726

Roswell Park Memorial Institute 1640 (RPMI 1640) culture medium	ThermoScientific	A1049101
Ruthenium red	Sigma	557450
Sodium chloride	Sigma	S7653
SuperSignal WestFemto kit	ThermoScientific	34095
Synta66 (S66)	Sigma	SML 1949
SYBR Green Mastermix	ThermoScientific	4309155
Thapsigargin	Sigma	T9033
Tris buffered saline tablets	Sigma	T5030
Trizma base/Tris	Sigma	T1503
Trizol reagent	Sigma	T9424
0.4% trypan blue	Sigma	T8154
0.0525% trypsin-EDTA	ThermoFisher Scientific	25300054
Tween20	Sigma	P1379
WST1 Cell Proliferation Reagent (Roche)	Sigma	000000011644807001
Yoda-1 (2-[5-[[2,6-dichlorophenyl)methyl]thio]-1,3,4-thiadiazol-2-yl]pyrazine)	Tocris	5586

2.1.2. Antibodies

Antibody	Company	Catalogue no.	Species
p44/42 MAPK (Erk1/2)	Cell Signalling	9102	Rabbit
Phospho-p44/42 MAPK (Erk1/2) (Thr202/Tyr204)	Cell Signalling	9101	Rabbit
Phospho-Akt (Ser473)	Cell Signalling	9271	Rabbit
AKt	Cell Signalling	9272	Rabbit
Horseradish peroxidase antibody	Jacksons ImmunoResearch Europe Ltd	111-036-047	Goat anti-rabbit

2.1.3. siRNA

siRNA	Company	Catalogue no.
PIEZO1 Silencer Select siRNA (s18891)	ThermoFisher Scientific	s18891
Piezo Silencer Select siRNA (s138387)	ThermoFisher Scientific	s138387
ON-TARGETplus Human ORAI1 siRNA	Dharmacon	L-014998

2.1.4. Solution Preparations

- Fura-2AM was reconstituted in DMSO to a stock concentration of 1mM, protected from light and stored at -20°C.
- JPIII (4-(2,5-dimethoxyphenyl)-N-(pyridin-4-ylmethyl)aniline) was synthesized by the Department of Chemistry at the University of Leeds. The

compound was derived from Synta 66, which is under patent WO 2005/009954.

- Pluronic acid was made from Pluronic F-127 powder reconstituted in DMSO to a stock concentration of 10% (w/v) and used at a final concentration of 0.01% in experiments.

- Thapsigargin was reconstituted in DMSO to a stock concentration of 5mM and stored at -20°C and used at a final concentration of 1µM.

- The tris-buffered solution (TBS) was prepared from tablets reconstituted in deionized water, or alternatively made from 50mM Tris and 150mM sodium chloride, with pH adjustment to pH 7.6 using hydrochloric acid.

- Ruthenium red was reconstituted in water to a stock concentration of 30mM.

- Synta66 (S66) (Sigma) was reconstituted in DMSO to a stock concentration of 10mM, aliquoted and stored at -20°C.

- Gadolinium (III) chloride (Gd) was reconstituted in water to a stock concentration of 10mM and stored at room temperature.

- Yoda1 was reconstituted in DMSO to a stock concentration of 10mM, aliquoted and stored at -20°C.

- Methylene blue. 2% (w/v) in 70% ethanol. Stored at room temperature.

2.2. Cell Culture

Cancer cell lines were cultured in vented 75cm^3 flasks at 37°C with supplementation of 5% CO_2 to the air in a Sanyo incubator. All routine cell culture and cell culture experiments were set up and carried out in a laminar airflow hood in sterile conditions. Cell lines were maintained in antibiotic-free culture.

2.2.1. Cancer cell lines

HT29

HT-29 is an adherent epithelial colon cancer cell line isolated from a 44-year-old female in 1964. These are reported to form well-differentiated adenocarcinoma xenografts in nude mice. It was obtained from Sigma (catalogue number 91072201). Cells were grown in Dulbecco's Modified Eagle Medium (DMEM) supplemented with 10% foetal calf serum.

HCT116

HCT116 is an adherent epithelial colorectal carcinoma that was isolated from the tumour of an adult male. These were purchased from ATCC (CCL-247). Cells were cultured in Roswell Park Memorial Institute (RPMI) 1640 medium supplemented with 10% foetal calf serum.

SW480

SW480 is an adherent epithelial colon cancer cell line isolated from a Dukes B colorectal adenocarcinoma that had been removed from a 50-year-old Caucasian male. The cell line was obtained from Sigma Aldrich (catalogue number 8709201). Cells were cultured in RPMI 1640 medium supplemented with 10% foetal calf serum.

2.3. Transfections

2.3.1. Small interfering RNAs (siRNA)

Small interfering siRNA (siRNA) technology allows transient knockdown of a protein of interest. It uses double-stranded RNA (dsRNA) containing siRNAs that can target the mRNA of a particular gene of interest. This can be introduced into the cell using a lipid- or amine-based transfection reagent such as lipofectamine 2000. Once it has entered the cell, the dsRNA is spliced into 21 nucleotide fragments by the Dicer enzyme. These fragments bind to Argonaute proteins, one strand of dsRNA is removed and the remaining strand associates with the complementary DNA through base pairing. The associated Argonaute protein can then either regulate or destroy the mRNA(Wittrup and Lieberman, 2015).

In vitro siRNA transfections were carried out in Opti-MEM Reduced Serum media using Lipofectamine 2000 for the PIEZO1 s18891 siRNA sequence and using Lipofectamine RNAiMAX for the PIEZO1 s138387 siRNA sequence .

Adherent SW480 cells were transfected with 45nM of both PIEZO1 siRNAs for 8 hours in Optim-Mem medium. Following transfection, the transfection solution was removed and replaced with normal culture medium.

HT-29 cells were reverse transfected with both siRNAs: cells were plated in the presence of 45nM with lipoRNAiMax in optimum and complete growth medium for 48 hours.

2.4. Calcium measurement experiments

Intracellular calcium measurements were taken using Fura-2AM dye on the FlexStation 3 platform. Fura-2AM is a commercially available ratiometric intracellular calcium indicator dye. The cells are excited at 340nm and 380nm and has an emission wavelength of 510nm. The ratiometric nature of the dye means it is less affected by photobleaching, unequal dye loading or dye leak thereby giving a more accurate intracellular calcium measurement(Grynkiewicz et al., 1985). The acetoxymethyl ester (AM) attached to the fura-2 dye is membrane permeable and then cleaved within by the cytosolic esterases to generate a cell-impermeant fluorescent indicator. Calcium binding creates a shift in the excitation spectrum resulting in increased fluorescence emission at 340nm and a decrease at 380nm (Figure 2.1). The ratiometric intracellular calcium was calculated from the 340/380 ratio by the FlexStation SoftMaxPro capture software. An increase in this ratio (ΔCa^{2+}) correlates with an increase in cytosolic calcium.

Intracellular calcium measurements were taken on the FlexStation Multimode Microplate Reader (Molecular Devices). All cells were loaded in salt buffered solution (SBS) containing 130mM NaCl, 5mM KCl, 8mM D-glucose, 10mM HEPES, 1.2mM $MgCl_2$ and 1.5mM $CaCl_2$.

Calcium-free SBS was used for store depletion which contained 130mM NaCl, 5mM KCl, 8mM D-glucose, 10mM HEPES, 1.2mM $MgCl_2$ and 60μM EGTA.

2.4.1. Cell preparation

Cells were counted with Neubauer haemocytometer and plated into a 96 well plate (ThermoFisher, catalogue number 167008) at a seeding density that delivered a confluent monolayer on the day of the experiment and cultured in standard culture conditions.

2.4.2. Cell loading

Cells were loaded with 1μM Fura2AM in SBS containing 10% pluronic acid in the dark for 1 hour at 37°C in a CO_2-free environment.

2.4.3. Store depletion and calcium add-back

For store depletion experiments testing CRAC channel inhibitors, the treatment solution was prepared from calcium-free salt buffered solution with 1µM thapsigargin final working concentration with a range of treatment concentrations of the CRAC channel inhibitor, alongside a DMSO vehicle control (referred to as the vehicle control). Cells were incubated at room temperature for an optimised time period, which was 20 minutes for HT-29, SW480 and HCT116.

2.4.4. Inhibitor Treatments and Yoda-1

Following Fura2AM loading, loading solution was removed and replaced with SBS. Cells were treated with any PIEZO1 inhibitors (ruthenium red, GsMTX4, Gd) in SBS for 30 minutes at room temperature. Yoda-1 compound solution was prepared from SBS containing 1.5mM calcium.
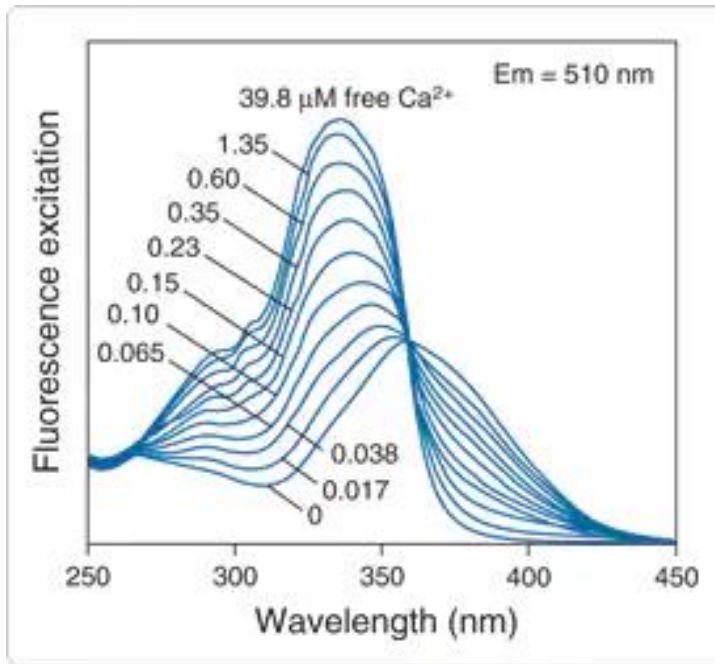
Figure 2.1. Fluorescence excitation spectra of fura-2 in different cytoplasmic calcium concentrations.

Increasing concentrations of intracellular calcium causes fura-2 fluorescence emission intensity at 510nm to increase at the excitation wavelength 340nm and decrease at 380nm. Image adapted from (ThermoFisher Scientific, 2010).

2.4.5. FlexStation recording and addition phase

Calcium add-back and intracellular fluorescence measurements were automated through SoftMax Pro software on the FlexStation PC console (Molecular Devices). This is a high throughput fluorescence plate reader that allows kinetic measurement of calcium traces in either 96-well or 384-well microplates. Compounds or solutions for addback to the cells are loaded along with a plate of Fura2-loaded cells and FlexStation tips. This is a kinetic experiment as the software is programmed by the user to add the solutions or compounds to the cells at a desired time during fluorescence readings.

Addback solutions were tailored to contain the same concentration of treatment compound to prevent dilution of the drug concentration in each well. For store depletion experiments, the compound solution was prepared from salt buffered solution containing 1.5mM calcium, such that a final concentration of 0.3mM calcium was delivered to each well.

For store depletion experiments, measurements were taken every 5 seconds over a 300 second period. For Yoda-1 experiments, measurements were taken for between 300 or 600 seconds. Experiments were carried out at room temperature.

2.4.6. FlexStation data analysis

The parameters measured for the store depletion experiments were:

- The peak calcium amplitude achieved (peak amplitude), which denoted the magnitude of calcium entry from baseline. This was calculated by determining the highest and lowest calcium measurements and subtracting the difference. This was corrected for any physiological effect seen in untreated (vehicle) cells by subtracting the mean peak amplitude of vehicle treated cells from the mean peak amplitude of treated cells prior to further calculations and are corrected unless specifically stated otherwise.
- The area under the curve (AUC), which gives a standardised numerical summary of the total amount of CRAC channel calcium entry to allow comparison across the cell lines. This was calculated using the Integrate function within Origin Pro 9.

Dose-response curves were calculated using the peak calcium amplitudes in cells treated with different concentrations of drug. Percentage calcium entry was

calculated for each concentration relative to the thapsigargin calcium response. These data points were plotted and fitted with a Hill curve, from which the IC50 concentration was extrapolated. The residual calcium entry at maximal concentration is also reported.

2.5. RNA isolation and q-RT-PCR

2.5.1. RNA isolation

Cells were lysed in Trizol (Sigma) reagent either directly from the culture vessel or immediately following trypsinisation after centrifugation and washing of the cell pellet. Trizol solution was transferred directly into a 1.5ml Eppendorf, and either stored at -80°C or processed immediately. To extract the RNA, the Trizol reagent was vortexed and incubated at room temperature for 5 minutes. Phase separation of DNA, RNA and protein within the sample was achieved by adding bromochloropropane (BCP). RNA was removed from the top (aqueous) layer and concentrated by precipitating it in isopropanol. The resultant RNA was pelleted and washed in 75% ethanol and then air-dried. The RNA pellet was then dissolved in RNase-free water at 55°C for a short period. The RNA was treated with 0.04U of DNase enzyme in buffer at 37°C for 1 hour to break down any contaminating DNA, and the reaction was stopped using Inactivation Enzyme. The RNA was collected from the supernatant into an autoclaved Eppendorf following the last centrifugation.

2.5.3. NanoDrop™ RNA quantification protocol

The NanoDrop™ 2000 (ThermoScientific) is a benchtop micro-volume UV-vis spectrophotometer that can be used to rapidly and accurately quantify RNA or DNA concentrations of samples. From each sample 2µl of RNA was loaded onto the pedestal between 2 optical surfaces to create a sample column, in which the machine measures the concentration using a xenon lamp and charge-coupled device (CCD) camera. DNA and RNA was measured at 260nm. The machine takes 2 measurements at 0.2mm and 1mm which can allow it to adjust for any concentration. The set-up and read-out takes place in the NanoDrop software provided with the machine. Prior to use, the optical surfaces were cleaned repeatedly with deionised water, and the machine was zeroed through absorbance reading of the RNA buffer (RNase free water). For each sample, 1µl was loaded onto

the machine. Each sample was read twice to ensure consistency between readings. Concentration readings were provided in ng/µl in the software.

2.5.4. Reverse transcription

Reverse transcription of the mRNA to cDNA was carried out for all samples using both enzyme-containing and enzyme-free reactions using the High Capacity RNA-to-Complementary DNA (cDNA) reverse transcription kit (Applied Biosystems), with 0.5 µg of RNA was mixed with 5 µl 2x RT buffer, 0.5 µl 20x enzyme mix and nuclease-free water to make a 10 µl total reaction volume. Non-reverse transcribed (-RT) control solutions were prepared and tested in parallel. The mix was centrifuged and incubated in the Lifecycler$^{©}$ PCR Machine (Eppendorf) for 1 hour at 37°C, 5 minutes at 95°C, followed by a 4°C hold step until use. Enzyme-free reactions detect genomic DNA contamination of samples at the time of the PCR reaction, as the reaction will use genomic DNA as a template and produce non-specific results. The resultant cDNA was then stored at -20°C until they were required for use.

2.5.5. Real-Time quantitative polymerase chain reaction (qRT-PCR)

The PCR process amplifies the cDNA to detectable levels. Heating to 95°C denatures the cDNA by breaking down hydrogen bonds between the double strands to generate single strand molecules. The primers anneal at a lower temperature optimised for the particular primer with a DNA polymerase enzyme, which begins to synthesize new DNA at 72°C and extend the fragment. Incorporation of the Applied Biosystems™ SYBR Green dye™ (ThermoScientific) into the fragments allows fluoroscopic detection, as it intercalates with double stranded DNA, fluoresces when excited at 470nm and emits at 530nm. Each reaction consisted of 0.5µl SYBR Green I mix, 0.8µl MgCl$_2$ (4mM), 0.135µl forward primer (0.5µM), 0.135µl reverse primer (0.5µM), 0.5µl cDNA and 2.93µl of nuclease-free water to make it up to 5µl of reaction product.

Levels of amplified product are normalised against a static ("housekeeping") gene such as β-actin and 18S and relative quantification across samples can be made. Melt curve analysis ensures specificity of binding of the primers to the cDNA. The threshold cycle (CT) for each gene was detected by the Lightcycler 480$^{©}$ version 1.5 software and adjusted to take values across all samples in the exponential phase of amplification.

2.5.6. Primers

ORAI1 expression was normalised against 18S gene expression. PIEZO1 expression was normalised against β-actin.

Primer sequences are given below:

Gene	Forward Sequence	Reverse Sequence	Predicted Product size (bp)
PIEZO1	AGATCTCGCACTCCAT	CTCCTTCTCACGAGTCC	180
Orai1	TGCTCATCGCCTTCAGTGCC	CTCACCGCCTCGATGTTGGG	100
B-actin	TCGAGCAATCTCAACTCGG	TGAAGGTAGTTTCGTTGGATG	194
18S5	GTAACCCGTTGAACCCCATT	CCATCCAATCGGTAGTAGCG	180

The regions amplified by the PIEZO1 and ORAI1 primers are illustrated in Figures 2.2A and 2.2B. Analysis of the gene sequence demonstrates that the primers amplify the primary protein coding transcript. The EMSEMBLE ID is included in the figure.

2.5.7. Calculation of relative abundance of target gene

The raw CT values for genes of interest were corrected against the CT values of the internal control gene to generate the ΔCT value. The ΔCT value corrects against the value against a housekeeping gene of choice. Either 18S or β-actin were used in these experiments:

$$\Delta CT = CT^{gene} - \Delta^{\beta\text{-actin}}$$

The $2\char`^(-\Delta CT)$ calculation was used to reveal the actual expression, upon which comparative statistical analysis can be performed (with t test or ANOVA testing) (Schmittgen and Livak, 2008). This was used to determine fold change following siRNA knockdown relative to an untreated or control sample:

The fold change was then calculated using the equation:

Fold change = $2\char`^\Delta\Delta CT$

A

PIEZO1 (ENST00000301015.14) - Exon 51
CATCATGGGGCTGTACGTGTCCATCGTGCTGGTCATCGGCAAGTTCGTGCGCGGATTCTTCAGCG**AGATCTCG CACTCCATTATGTTCGAGGAGCTGCCGTGCGTGGACCGCATCCTCAAGCTCTGCCAGGACATCTTCCTGG TGCGGGAGACTCGGGAGCTGGAGCTGGAGGAGGAGTTGTACGCCAAGCTCATCTTCCTCTACCGCTCA CCGGAGACCATGATCAAGTGGACTCGTGAGAAGGAG**TAG

B

ORAI1 (ENST00000617316.2) - Exon 3
GTGGCAATGGTGGAGGTGCAGCTGGACGCTGACCACGACTACCCACCGGGG**CTGCTCATCGCCTTCAGT GCCTGCACCACAGTGCTGGTGGCTGTGCACCTGTTTGCGCTCATGATCAGCACCTGCATCCTGCCCAACA TCGAGGCGGTGAG**CAACGTGCACAATCTCAACTCGGTCAAGGAGTCCCCGCATGAGCGCATGCACCGCC ACATCGAGCTGGCCTGGGCCTTCTCCACCGTCATCGGCACGCTGCTCTTCCTAGCTGAGGTGGTGCTGCTC TGCTGGGTCAAGTTCTTGCCCCTCAAGAAGCAGCCAGGCCAGCCAAGGCCACCAGCAAGCCCCCGGCCA GTGGCGCAGCAGCCAACGTCAGCACCAGCGGCATCACCCCGGGCCAGGCAGCTGCCATCGCCTCGACCA CCATCATGGTGCCCTTCGGCCTGATCTTTATCGTCTTCGCGGTCCACTTCTACCGCTCACTGGTTAGCCATA AGACTGACCGACAGTTCCAGGAGCTCAACGAGCTGGCGGAGTTTGCCCGCTTACAGGACCAGCTGGACC ACAGAGGGGACCACCCCCTGACGCCCGGCAGCCACTATGCCTAG

Figure 2.2. Illustration of the sequence amplified by the primers: A. PIEZO1; B. ORAI1. The forward primer target sequence is denoted in red and the reverse primer target sequence is denoted in blue. The amplified region is denoted in bold.

2.6. Western blotting

Sodium dodecyl sulphate polyacrylamide electrophoresis (SDS-PAGE) was used to separate proteins by mass along an applied electrical field. Prior to SDS-PAGE, samples are lysed, chemically denatured and boiled in order to break down protein-protein disulphide bonds and break down the tertiary structure of the protein to allow separation on the SDS gel. SDS assists with this and also masks the protein's intrinsic charge so that the proteins will separate by weight alone. Polyacrylamide forms a pore matrix within the gel, that can be manipulated with different concentrations to separate out heavier and lighter proteins more eloquently. The proteins are then transferred out of the gel onto a membrane that can then be stained for the desired protein using an appropriate antibody. Subsequent staining with a horseradish peroxidase (HRP)-conjugated secondary antibody can then be visualised using a chemiluminescent solution that can be detected either on X-ray film or a CCD.

2.6.1. Protein extraction and quantification

Adherent cells cultured in a 6-well plate were washed in PBS prior to addition of a lysis buffer consisting of Nonidet 40 detergent (Sigma), protease and phosphatase inhibitors (Sigma). Cells were collected into the lysis buffer by a combination of scraping and pipetting. Cells were either processed immediately or stored at -80°C. The lysate was incubated on ice for 30 minutes with vigorous vortexing every 10 minutes and then sheared through a 21G needle to help with mechanical digestion. The lysate was centrifuged for 20 minutes at 13000rpm at 4°C. The supernatant was collected as this contained the protein lysate, the pellet contained cellular debris.

Protein concentration of each lysate was determined against bovine serum albumin (BSA) standards of known protein concentrations with colorimetric Biorad Protein Assay kit (Biorad). This method is based on a modification of the Lowry method(Lowry et al., 1951), with reduction of the Folin phenol reagent in the kit by a number of amino acids on the protein. This generated a colour change that is dependent on the protein concentration, that can be interpreted against a standard curve derived from the absorbance readings of samples of known protein concentrations.

2.6.2. Sample preparation, SDS-PAGE, protein transfer and immunoblotting

Each sample was prepared to run 20μg of protein per well, along with a 1:4 volume of the denaturing agent β-mercaptoethanol that was added to break protein-protein disulphide bonds as well as a protein dye.

Samples were loaded alongside a protein molecular weight marker to orientate the user to the gel and subsequently to facilitate interpretation of the bands on the membrane. Samples were run in buffer containing SDS-containing running buffer until the proteins were suitably separated. The gel was then removed from the running tank apparatus and equilibrated in methanol for 5 minutes prior to transferring the proteins onto a nitrocellulose membrane. The semi-dry transfer system (Biorad) was used for this. The membrane was blocked for non-specific staining for 1 hour at room temperature in 5% w/v BSA in TBS 0.05% Tween-20 blocking solution on an orbital shaker, an important step to stop non-specific antibody binding. The membrane was then incubated with primary antibody at the appropriate dilution in antibody incubation solution comprising 5% w/v BSA in TBS 0.05% Tween-20 at 4°C overnight on an orbital shaker. The antibody dilutions are detailed in the table below. The next day the membrane was washed in washing solution comprised of TBS 0.05% tween-20 (TBS-T) 3 times on the orbital shaker prior to incubation with the HRP-conjugated secondary antibody reared against the species of the primary antibody diluted in antibody incubation solution for 1 hour at room temperature on the orbital shaker. The membrane was washed three times in TBS-T. The membrane was then exposed to chemiluminescent substrate from the SuperSignal WestFemto kit (ThermoScientific) and immediately imaged using the CCD camera (BioRad).

The antibody dilutions are listed below:

Antibody	Antibody Dilution
p44/42 MAPK (Erk1/2)	1:1000
Phospho-p44/42 MAPK (Erk1/2) (Thr202/Tyr204)	1:1000
Phospho-Akt (Ser473)	1:1000
AKt	1:1000
LC3	1:25
HRP secondary antibody	1:5000

2.7.2. Protein quantification

The ImageJ software(Schneider et al., 2012) was used to determine the pixel density of the bands from the CCD images. Our laboratory has previously used this method to generate relative quantification of expression and published data from this(Li et al., 2014). The CCD images were inverted to generate grayscale digital images of the western blot and the intensity of each band was determined by Image J within a rectangle that was drawn around a band to a size that was large enough to incorporate each band. Image intensity of each band of interest was normalised to the intensity of each loading control by subtracting the loading control intensity from the intensity of the band of interest.

2.7. *In vitro* functional assays

2.7.1. WST-1 cell viability assay

WST-1 (Roche) is one of several water-soluble tetrazolium dyes used to measure cytotoxicity. It is cleaved by metabolically active cells in a NAD(P)H-dependent manner to form a soluble formazan product that can be detected spectrophotometrically. Therefore, incubation of cells with WST-1 reagent can generate information regarding the viability of the cells. It is commonly used to determine response to cytotoxic agents in experiments using a microplate format. The 96 well plate was used for these experiments.

Experiments were set up for desired treatments, and relative viability was determined by comparison to appropriate controls (such as drug vehicle or scrambled transfection control). Cells were counted with a Neubauer haemocytometer, seeded and cultured in 100μl of media per well. Surrounding wells were filled with PBS to prevent evaporation of the media in peripheral wells which can impact on cell culture. WST-1 reagent was added to each cell-containing well as well as media only-containing well in a 1:10 ratio. The plate was incubated at 37°C for a time period optimised for that cell line and experiment to avoid saturation of the system with formazan, delivering a spectrophotometric reading below 1. The plate was read on a spectrophotometric plate reader at 450nm with subtraction of background reading taken at 620nm.

2.7.2. Colony formation assay

The colony formation assay is an *in vitro* model of replicative immortality(Munshi et al., 2005), as a single cell divides indefinitely to produce a large colony of cells that can be fixed and stained and subsequently counted. Cells were counted with a Neubauer haemocytometer and a single cell suspension was optimised to determine the appropriate number of cells that would give sufficient discernible colonies in one well of a 6 well plate to count under a dissection microscope. HT-29 cells were seeded in a suspension of 50 cells/ml with 1ml added to 1ml of culture media in each well then returned to the incubator. Drug treatments were added to wells 2 hours after seeding. When colonies were macroscopically visible in the control wells, media was aspirated and colonies were fixed and stained in methanol blue in 70% alcohol. Plates were washed and air dried. Colonies were counted under a dissecting microscope.

2.7.3. Growth curve

Growth curves were used to analyse growth kinetics of cell lines under basal culture conditions or following treatment such as with drugs or siRNA transfection. For each cell line, both the cell seeding density and cell culture vessel were optimised to result in exponential growth. Both HT-29 and SW480 cells were seeded at 30,000 cells per well in 12 well plates. In cytotoxicity experiments, drug-containing media was changed every other day.

For transfection growth curves, cells were trypsinised 24 hours after transfection with lipofectamine 2000 only (non-transfected cells), scrambled siRNA and PIEZO1 siRNA, counted using a Neubauer haemocytometer and plated in 12 well plates in 1ml of media. Triplicate wells were plated for each of the transfection conditions. Media was changed every other day.

At the time of cell harvest, both the media and PBS wash were transferred from the well to a 1.5ml Eppendorf tube. Following trypsinization, trypsin was neutralized with the collected media and the well washed to collect any remnant cells. Cell counts were performed in 0.2% trypan blue using a Neubauer haemocytometer. This method allowed inclusion and counting of cells that have detached following treatment. Cells that did not stain for trypan blue were counted to determine the live/viable cell fraction. Cells that stained with trypan blue were counted to determine the dead cell fraction.

2.8. Migration

2.8.1. Migration Optimisation

There are a number of steps to optimise prior to using a cellular migration model. Firstly, conditions of serum starvation and low serum culture conditions should be optimised in order to generate proliferative arrest without affecting cellular viability. This would therefore allow focused study of cellular migration.

In order to study the effect of serum conditions on cellular proliferation, 15,000 cells were plated in each well of a 24 well plate and cultured overnight to allow adherence to the culture vessel. The next day, media was removed and wells were washed with PBS. Wells were cultured in serum-free media for 24 hours alongside a control with normal serum conditions. Cells were counted following 24 hours of serum starvation. In addition, the media of the serum starved cells was changed to culture media containing 0.5% serum for 24 hours alongside cells that were serum starved for a further 24 hours and a control with normal serum conditions. All wells were counted the next day. At the time of counting, media and PBS washes from each well were kept in a labelled Eppendorf. Trypsin was neutralised in media containing 10% serum and added to the media and PBS wash solution. This method allowed counting of all detached cells as well as adherent ones. Counts were carried out with 0.2% trypan blue.

2.8.2. Scratch wound migration assay

The Essen Incucyte® Zoom (Essen Bioscience) is a fully automated live-cell imaging platform that allows both phase contrast and fluorescence imaging. It allows kinetic assessment of cell migration using an imaging unit with a 10x objective that holds small vessels and microplates within an incubator that maintains cell culture conditions of $37^{o}C$ and $5^{o}C$ CO_2. Cells were plated on 96-well plates (Essen Bioscience) to give 90-100% confluent wells the next day. Cells were serum starved prior to the assay in order to arrest proliferation but allow cell migration. The WoundMaker™ pin tool was used to scratch the wells. This is a 96-pin device that creates homogenous scratches between 700-800 microns in width without scratching the underlying plastic. The scratch is engineered using a lever on the WoundMaker™ that is pressed to move the pins homogenously across the cell layer to create horizontal scratches. Following scratching, the cell layer was washed 3 times with PBS to remove any remnant cells using a micro-channel pipette. Scratch wounds were treated with reduced serum medium following serum starvation to

minimize any proliferation. The plate was placed in the Incucyte® Zoom system within a Sanyo incubator, and kinetic imaging was programmed at desired time intervals using the Incucyte® software. The relative wound density (RWD) is the cell density within the scratch wound area expressed relative to the cell density outside the wound area and expressed as a percentage. Repeated imaging allows kinetic assessment of migration over time. Representative photomicrographs of a scratch wound are presented at baseline in Figure 2.3A and representative scratch wound masks generated by the Incucyte Zoom software analysis are presented at baseline in Figure 2.3B.
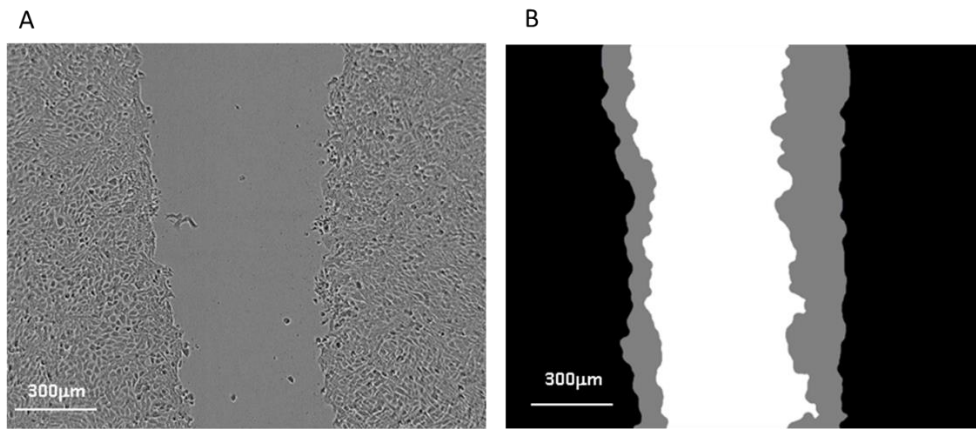
Figure 2.3. Representative images from the Essen kinetic imaging software scratch wound module. A-B. Photomicrographs of HT-29 cells that have sustained a scratch wound. A. Immediately following the scratch; B. Software interpretations of the scratch wound in A. Black represents the cell layer, white represents the region of the scratch, grey represents cells migrating into the area of the scratch:

2.8.3. Boyden chamber migration assay

The Boyden chamber assay was originally developed to study leucocyte migration via chemotaxis. It consists of 2 chambers separated by a microporous membrane that consists of pores of a defined size(Falasca et al., 2011). Cells are seeded in the upper chamber and are incubated for an appropriate length of time to allow them to migrate through the pores towards a chemoattractant, which was media containing 20% foetal bovine serum. The assay set-up is illustrated in Figure 2.4A and a representative photomicrograph of migrating cells is presented in Figure 2.4B. At the end of the assay, the wells are washed and cells fixed in 70% ethanol before staining with methylene blue. The membranes are then cut from the bottom of the chamber and mounted on a slide in gelatin-glycerol with a cover slip. The pores are imaged under a microscope and the number of cells in 6 randomly selected light fields are counted.

Boyden chambers with 8-micron pores were used for both the migration and invasion assays with the cancer cells.

2.9. Invasion
2.9.1. Boyden Chamber Invasion Assay

The Boyden chamber assay allows the study of invasive properties by coating the porous membranes with an appropriate extracellular matrix (ECM) such as Matrigel that recreates the tissue matrices that cancer cells must invade through *in vivo*(Marshall, 2011). The assay is set up in an identical manner as for the Boyden migration chamber. The Boyden chamber invasion assay is illustrated in Figure 2.4C.

Boyden chambers coated with Matrigel were first hydrated in serum free medium for 5 minutes and then medium was aspirated off. The inserts were placed in a transwell 24 well plate. The cell suspensions were prepared by trypsinization, washing, counting and diluting to the desired cell number that can be delivered in 500μl to the top chamber.

2.9.2. Essen scratch wound invasion assay

The invasive properties of the HUVEC cells were tested using the Essen Incucyte® Zoom (Essen Bioscience). Cells are set up, serum starved and scratched using the
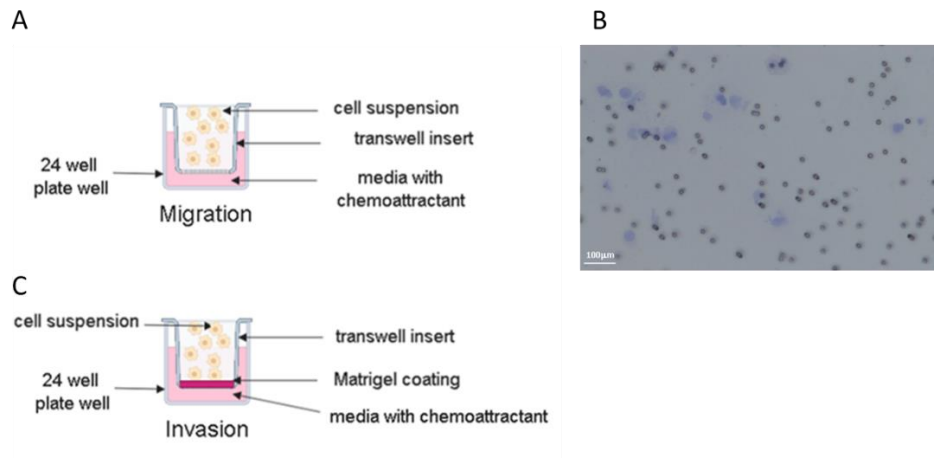
Figure 2.4. Illustrative depiction of the Boyden chamber assay. A. Migration. B. Matrigel invasion. C. Representative photomicrograph of fixed migrated SW480 cells (20x objective). Illustrative images created in Biorender. https://biorender.com/

same method as described in Section 2.8.2. Prior to the assay, Matrigel Matrix (Corning) was defrosted and prepared containing the appropriate drug concentration or vehicle control. After the cells were scratched and washed, 50μl of the appropriate Matrigel was pipetted onto the scratch wound. Media was then applied over the top of the Matrigel prior to placing the plate into the Incucyte and programming the software to image the scratch wound over the desired time points. This method has been used successfully with endothelial cells in our laboratory(Webster et al., 2017).

2.10. pH determination

Cells were cultured continuously in 2ml of media containing media only, DMSO vehicle control, 10μM and 30μM JPIII alongside 50μM 5-fluorouracil (5-FU) in 6 well plates for 72 hours. Drug containing media was also incubated in cell-free wells as a cell-free control. The media was harvested for pH reading at 24, 48 and 72 hours. Media was transferred immediately after harvesting and read on a pre-calibrated pH benchtop meter (ThermoScientific).

2.11. Analysis of Microarray Data

Raw .chp files of the microarray dataset from the study by Chen *et al*(Chen et al., 2013) was obtained from GEO Express. The open access software Transcriptome Analysis Console (TAC) software was downloaded from the Applied Biosystems. The dataset was uploaded into the TAC software. The dataset passed internal quality control that was carried out by the TAC software with the researcher's hybridisation controls.

Raw data for T cells activated by stimulation with anti- CD3/CD28 treated with both vehicle control and the CRAC channel inhibitor RO2959 was merged into one file and run through limma package in r to perform differential expression, generating mean log fold (FC) changes with Benjamini-Hochberg statistical correction.

Differentially expressed genes were filtered by significance with a false discovery rate (FDR) of 0.01 using the Benjamini-Hochberg correction. An FDR of less than 0.01 denotes higher power with lower type 1 error(Benjamini and Hochberg, 1995). Genes were then separated into 2 sets relative to the untreated control: upregulated genes (those with a fold change of 0.5 or above) and downregulated genes (those with a fold change of 0.5 or below). The two gene lists were uploaded

into Cytoscape 3.7.0. STRING network and gene ontology (GO) enrichment analyses were carried out for both upregulated and downregulated genes within Cytoscape.

2.12. Flow cytometry

2.12.1. Annexin V Propidium iodide flow cytometry assay

The flow cytometer uses laser-based technology to detect fluorophore-stained cells in a single cell suspension, as these will be excited by certain lasers and the intensity of their emission energy can then be detected (Figure 2.5A). This system allows co-staining with multiple fluorescent probes, such as propidium iodide (PI) and annexin V. Annexin V is a protein that binds to phosphatidylserine released from the inner leaflet of apoptosing cells, whereas propidium iodide stains necrosed cells whose cell membranes have broken down(Wlodkowic et al., 2011). Co-staining with propidium iodide and fluorescein isothiocyanate (FITC)-conjugated annexin V allows determination of the proportion of cells that are alive, in early and late apoptosis or have undergone necrosis (Figure 2.5B). As the emission spectra of FITC and PI overlap (see Figure 2.5C) the data must be compensated in order to identify true staining; this was achieved using controls for each treatment (unstained, annexin V only, PI only).

Adherent cells were washed, trypsinised, centrifuged and washed in cold PBS before being resuspended in annexin V binding buffer. For each treatment condition, cells were stained with annexin V and propidium iodide alongside appropriate compensation controls: unstained, annexin V alone and propidium iodide alone. Cells were stained for 15 minutes in the dark at room temperature, resuspended in more annexin binding buffer and analysed immediately on the flow cytometer. The FCSFortessa gates a total of 10,000 cells per sample for analysis. Data was analysed in FACS Diva software: data was compensated for appropriate staining controls for each treatment and the proportion of live/dead cells was determined as a percentage of the total gated cells.

2.12.2. Cell cycle analysis

Cell cycle analysis using flow cytometry aims to quantify the amount of DNA in each stage of the cell cycle. This utilises fluorescent dyes such as propidium iodide, which intercalates with DNA of fixed and permeabilised cells and fluoresces when it is bound to nucleic acids. These dyes are stoichiometric, with the amount of binding

75

being proportionate to the amount of DNA in each cell cycle phase(Ormerod, 2008). This generates a DNA histogram that illustrates the number of cells in each cell cycle phase, plotting intensity of fluorescence against the cell count (Figure 2.5D).

At the time of cell harvesting, well media and PBS washes were saved in order to store any detached cells. Trypsinised cells were added to this and the suspension was spun and washed twice in ice cold PBS. The cells were fixed by continual vortexing and dropwise addition of ice cold 70% ethanol, and samples stored in the freezer at -20°C overnight. At the time of analysis, cells were washed twice and resuspended in PBS. RNase was added along with the propidium iodide to remove any contaminating RNA that would otherwise invalidate the results. The stained samples were protected from light and immediately transferred to the flow cytometer for analysis.

2.13. Imaging

Light microscope images were taken on the Zeiss AX10 microscope within the Zen Software at 10x and 20x objectives. Cell culture images were also taken using the Incucyte and the Incucyte Zoom 2011 machine, with software capturing at x10 objective.

2.14. Data Analysis

A minimum of 3 biological repeats were carried out for each complete experiment before statistical analysis was carried out. Statistical analysis was carried out on three or more treatment conditions using a one-way ANOVA with Bonferroni-Holm correction. Two conditions were compared using paired t-test. Statistical significance was reached when p-value was at or below 0.05.
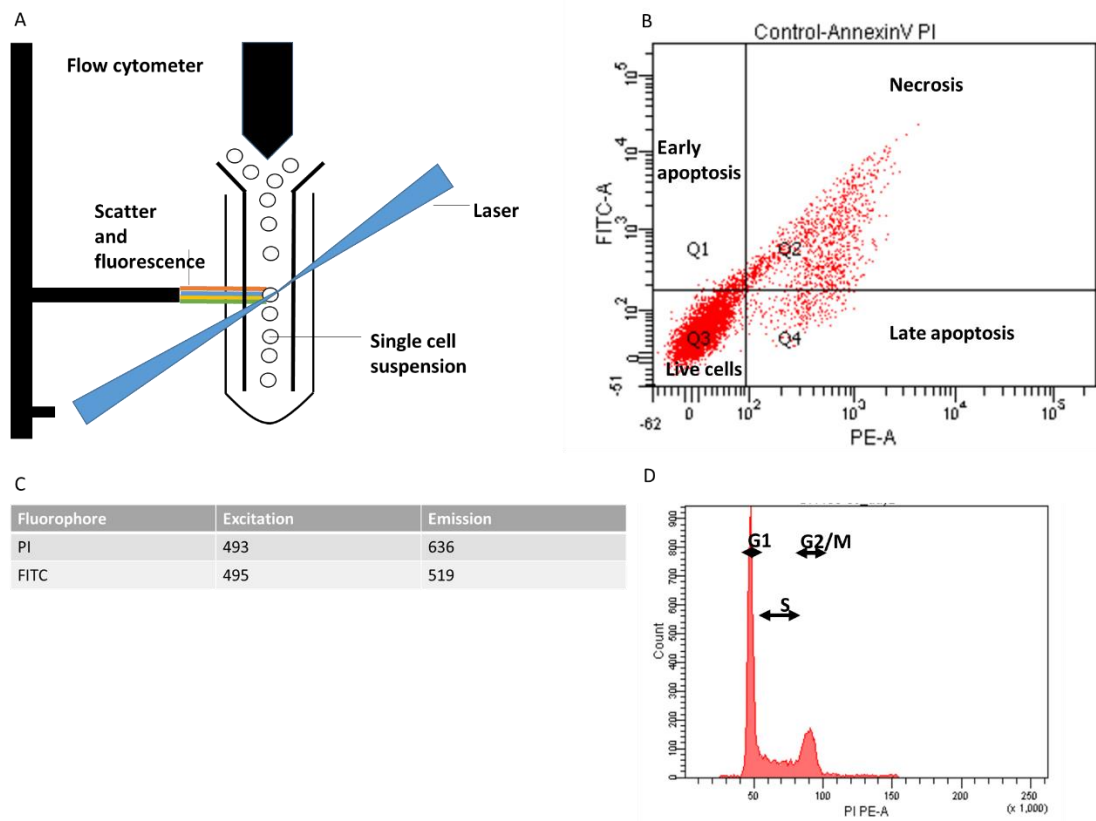
Figure 2.5. Flow cytometry. A. Illustration of the main mechanics of the flow cytometry machine. A single cell suspension is sucked up through the sheath and a pre-set laser excites the appropriate fluorophore. Fluorescence and cell scatter are detected by the flow cytometer and this information is translated onto the computer. B. Representative staining demonstrating the 4 populations of cells: live, early apoptosis, late apoptosis and necrotic cells. C. Table of the excitation and emission spectra of annexin V-FITC and PI. D. A DNA histogram of fixed cells stained with PI as part of cell cycle analysis.

2.15. The Cancer Genome Atlas (TCGA)

The aim of the TCGA project was to characterise the molecular and genomic landscape of a range of human tumours. Hundreds of tissue samples were collected for each of the 33 different cancer types that were ultimately included in the TCGA project, alongside a limited number of tissue samples from adjacent normal tissue. This project was run in collaboration with the National Cancer Institute (NCI) and National Human Genome Research Institute (NHGRI) primarily in the USA, starting in 2006 and running until 2017(The National Institute of Health, 2019).

Tissue underwent comprehensive analysis including single nucleotide polymorphism (SNP) arrays, chromosome and sub-chromosomal copy number changes and translocations using low pass (3-5X coverage) whole genome sequencing, mRNA expression profiling using Agilent microarrays and RNA-Seq, DNA promoter methylation analysis using Illumina Infinium HumanMethylation27 arrays, miRNA quantification via Illumina sequencing and profiling of coding mutations using whole exome sequencing. DNA from blood samples was extracted and sequenced for germline mutations.

Both tissue and blood samples were collected along with key clinical data for each patient, which underwent histopathological diagnostic checks and laboratory quality control at the designated Biospecimen Core Resource centre prior to DNA and RNA extraction and sample storage(Tomczak et al., 2015). The samples were then processed at genomic characterization and sequencing centres to generate copy number alteration and single nucleotide polymorphism (SNP) data, epigenomics, mRNA expression profiles, microRNA analysis, targeted sequencing and functional proteomic profiles. The data was stored at data coordinating centres internally and eventually released for open access. The Genome Data Analysis Centres generated informatics tools to facilitate the research community as a whole to be able to interface and explore these data(Tomczak et al., 2015), such as cBioportal.

The Cancer Genome Atlas Network published results on genome-scale analysis on 276 samples of colorectal cancer in 2012(The Cancer Genome Atlas Network et al., 2012). The study continued to collect 461 samples. There have been many publications using these data characterising the molecular landscape of cancers such as breast(Network, 2012b), colorectal cancer(The Cancer Genome Atlas Network et al., 2012) and ovarian cancer(Cancer Genome Atlas Research Network, 2011).

Now that TCGA has effectively finished, the data is archived at the NCI genomic Data Commons. Genomic profiling on normal colon and colon cancer tissue is available to download, but not data from the blood samples.

Colorectal cancer samples were taken from newly diagnosed consenting adults who did not receive neoadjuvant therapy prior to surgical resection(The Cancer Genome Atlas Network et al., 2012). Samples were a minimum of 60mg in weight. Frozen tissue was embedded in optimal cutting temperature (OCT) medium for transport to the Biospecimen Core Resource. Frozen samples were taken from both the top and bottom of the tissue block for histological assessment using haematoxylin and eosin (H&E) staining. These were reviewed by a certified pathologist to verify that the tissue and determine whether it met the tissue criteria. An example H&E slide is presented in Figure 2.6. Tumour tissue with a minimum of 60% tumour nuclei and less than 20% necrosis was included. Normal tissue was taken from at least 2cm away from the primary tumour site(The Cancer Genome Atlas Network et al., 2012). Sequencing data was made available for open access download and analysis: initially this was through the TCGA Data Portal, however following the completion of the TCGA project in 2017 the data is now archived on the Broad Institute GDAC portal.

2.14.1. Data file assimilation

There were 3 different forms of cancer mRNA data used in this study:

1. Raw counts.
2. Fragments per kilobase of transcript per million mapped reads (FPKMs) from the TCGA portal.
3. Reads per kilobase of transcript per million (RPKMs) from the 2012 TCGA paper.

Raw counts were downloaded from the original TCGA National Institute of Health (NIH) data portal in 2015. This provided accessible data on 453 colon cancer samples and 41 normal colon samples.

For differential expression analysis, data for 41 matched tumour and normal tissue samples was extracted from the large database. Individual sample data files provided raw counts that were calculated per gene by the TCGA data analysis teams using the Seqware framework via the RNASeqAlignmentBWA workflow. These

count files were compiled into one using the "multmerge" function in the r statistical software suite and were used for differential expression analysis via the edgeR package. Raw counts were filtered for low reads (defined as counts per million (cpm)<1) and normalised within edgeR using the trimmed mean of M values (TMM) method(Robinson and Oshlack, 2010). The cpm values were log 2-transformed and then used for plotting principal component analysis (PCA) charts and for differential gene correlation analysis (DCGA).

FPKMs were subsequently accessed through the GDAC portal and assimilated into a .txt file by Dr Lucy Stead in 2017. This data was transformed prior to analysis: addition of a pseudocount of 1 to all readings before log 2 transformation of fold-change. The purpose of downloading this data was to allow closer inspection and further analysis to follow up on results from the differential expression analysis.

RPKM data used for further analysis of the data presented in the 2012 TCGA colorectal cancer paper was downloaded from the supplementary data of the paper in 2018. This provided a larger cohort for exploratory analyses. Data was filtered to generate a dataset of the 195 patients who had complete sequencing of mutation status and genetic pathway alterations. Data was 1+log2 transformed prior to analysis. The size of this file was within the remit of the computer resources available.
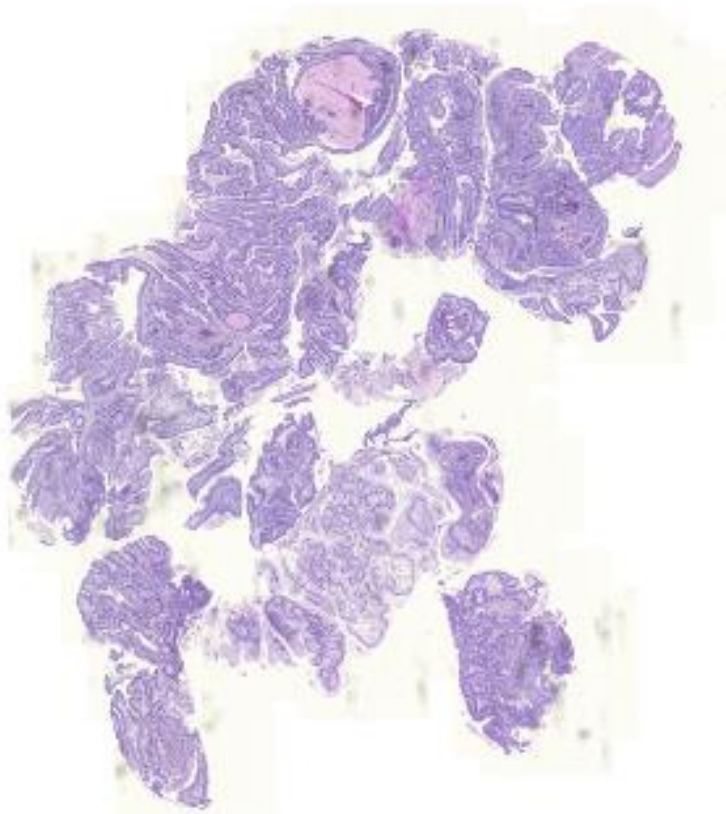
Figure 2.6. Representative haemoxylin and eosin (H&E) slide taken from a TCGA colorectal cancer specimen. Downloaded from the National Cancer Institute GDC Data Portal on 02.01.2019 from case TCGA-AA-A00L.Size marker was not available with the digital download.

2.14.2. Clinical characteristics and outcome data

Clinical data was originally downloaded from the NIH data portal. This provided patient demographics such as age, weight and racial classification, as well as initial tumour staging (in both Dukes and the AJCC TNM staging classification systems) and histopathological data such as resection margins and microscopic invasion. This dataset was incomplete in those fields that reported on future treatment following resection, particularly adjuvant treatment details and data on survival outcomes. Initial attempts were made to contact the TCGA team to enquire about an update of the outcome data but there was no reply. In 2018 Liu and colleagues comment on the paucity of clinical data, explaining that collating a comprehensive clinical dataset over the course of the project was not within the scope or capability of the original project(Liu et al., 2018). Liu *et al* found that the follow-up times varied between cancers but were essentially short: the colorectal cancer dataset had a median follow-up time of 22 months, but they varied from 12 months for glioblastoma to 48.3 months in kidney chromophobe tumours(Liu et al., 2018). They performed a systematic analysis that generated a curated and filtered clinical and survival outcome dataset for 33 cancers studied in TCGA. Therefore, survival outcomes for colorectal cancers were extracted from this dataset and used with the sequencing data to generate survival analyses. As part of the calculations in this systematic analysis, Liu and colleagues found that there were 221 missing data fields (190/459, 41%) from the fields of first-course treatment, residual tumour and margin status. Furthermore, the disease specific survival (DSS) outcome was estimated with assumptions drawn on included data in the majority of cancers due to the paucity of longer-term data. Therefore, only outcome data for progression-free interval and overall survival were felt to be the most robust survival data (Liu et al., 2018)and were used in the data analysis in this study.

2.14.3. Genomic profiling

Copy number variation (CNV) data was downloaded from the UCSC Xena browser(Goldman et al., 2019). Information on mutational profiles of each individual sample included in the analysis in the 2012 TCGA paper was obtained from the supplementary data files from the publication and aligned with expression data for further analysis.

2.14.4. Data analysis

2.14.4.1. r

r is a unique combination of programming language and a software that allows statistical computing and analysis along with generation of appropriate graphics from this analysis(R Core Team, 2013). It is part of the GNU project (http://www.gnu.org). It is open access and free for desktop use. The user can download different packages for different types of analysis.

2.14.4.1.1. edgeR

edgeR is a package that is designed specifically for differential expression analysis of RNA-seq expression profiles, and allows implementation of a range of negative binomial-based statistical analysis methods for this purpose such as generalised linear modelling (Robinson et al., 2010), which was used for this purpose. This methodology has previously been used with TCGA data to identify differentially expressed genes(Peng et al., 2015). This package is designed to carry out differential expression analyses on raw counts, at gene, exon, transcript or tag level. Raw counts undergo scaling normalisation using the TMM normalisation method, normalising it against estimated library size and sequencing depth(Robinson and Oshlack, 2010). It implements statistical methods that take into account biological variation across the gene pool of the samples. Low reads were filtered out of the 41 pairs of matched tumour-normal tissue by keeping those counts with counts per million (cpm) over 1 in at least 41 of the 82 samples.

edgeR also allows the user to annotate differentially expressed genes with gene ontology (GO) terms in order to aid functional interpretation. This was achieved using the *goana* function within the edgeR package.

2.14.4.1.2. Weighted gene correlation network analysis (WGCNA)

The R package WGCNA is a validated method of exploring gene expression within different conditions, as it uses a weighted correlation method to identify correlated genes within a dataset(Langfelder and Horvath, 2008). This was used to identify and explore networks of correlated genes within samples with different histopathological qualities, e.g. lymphatic and venous invasion.

The data was inputted and filtered for low reads. The data was scrutinised for outliers using clustering into a dendrogram but no outliers were identified (Figure 2.7A). Selected clinical data was inputted for further analysis and clustered beneath the sample dendrogram (Figure 2.7A). A weighted gene network was constructed using a soft thresholding power β, which was derived from the scale-free fit index of the data against the soft-thresholding power. This β value was chosen as the lowest power for which the scale-free topology fit index curve plateaus at a high soft-thresholding power of 0.9 (Figure 2.7B). Module detection settings included a minimum module size of 30, a medium sensitivity (deepSplit=2) to cluster splitting and a threshold of 0.25 for merging modules, which are default to the package as detailed in the programme manual.

The resulting identified modules were correlated with the uploaded clinical factors to generate a module-trait relationship chart (Figure 2.7C), that is generated from the correlation of the module eigengene to the gene expression profile. These correlative values are provided within the module-relationship chart (Figure 2.7C).

2.14.4.1.3. Differential gene correlation analysis (DGCA)
The DGCA r package can identify differential correlations between gene pairs in multiple conditions(McKenzie et al., 2016), e.g. between normal and tumour tissue. This package was specifically used to explore differential correlation between ORAI1 and PIEZO1 in normal and colon cancer tissue.

2.14.4.1.4. Survival analyses
The r packages survival(Therneau, 2015) and survminer(Kassambara, 2019) were used to generate estimated survival data and the log rank statistics for some of the Kaplan Meier charts, as well as carrying out univariate and multivariate cox regression analyses to identify hazard ratios for parameters associated with overall survival (OS) and progression free interval (PFI). SPSS version 25 was used to create Kaplan Meier charts.
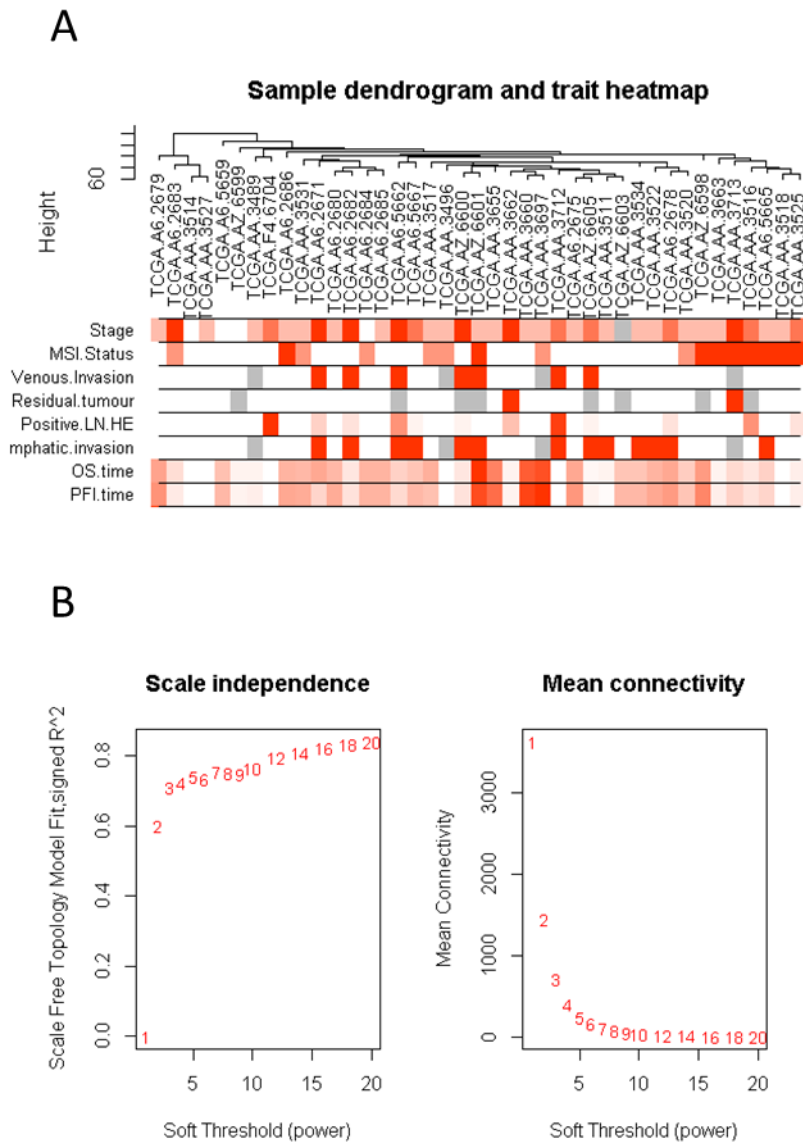
Figure 2.7. Data figures generated from the WGCNA analysis. A. Sample dendogram identified no outliers. Trait heatmap identifies clustering between samples for different traits. B. Chart of scale free topology identified a soft threshold of 20 where data would start to plateau.

2.14.4.2. GraphPad Prism

Dot plot and box whisker plots were made in GraphPad Prism version 7.04.

2.14.4.3. SPSS

Kaplan Meier charts were created in IBM SPSS Statistics version 25.

2.14.5. Gene set enrichment analysis

Gene set enrichment analysis (GSEA) differs to the gene ontology analysis as it aims to identify gene sets that are positively or negatively enriched within the entire list of genes. It is a more robust analysis as it calculates the degree of enrichment within the entire gene list and calculates significance. Enrichment is represented by the enrichment score, which interprets the degree to which a given set of genes (in an ontological class or preset pathway) is highly or lowly enriched to the phenotype relative to the entire set of genes included within the analysis: the greater the number the more enriched it is(Subramanian et al., 2005). Enrichment can be positive or negative. Significance is calculated using an empirical phenotype-based permutation test that makes multiple comparisons (or permutations) between genes. The normalized enrichment score (NES) normalises the gene set by the size of the gene set and calculates the false discovery rate in order to control for false positive findings(Subramanian et al., 2005). It can be carried out with the actual data or with a pre-ranked gene list.

Pre-ranked GSEA analysis was carried out within the Broad Institute GSEA Java-based platform. The results of the GSEA analysis was imported into Cytoscape 3.7.1 for pathway visualisation.

2.14.6. Cytoscape 3.7.1

The Enrichment Map application within Cytoscape was used to visualise and explore the pathway enrichment results from GSEA. This app clusters major biological themes that arise from the results to facilitate clearer interpretation of the data(Reimand et al., 2019).

2.14.7. Hierarchical clustering and heatmap generation

The Broad Institute Morpheus web-based interface was used to convert log2-transformed cpm to z scores prior to hierarchical clustering to identify clustering of samples. Samples were clustered by one minus pearson correlation.

Chapter 3: CRAC Channel Pharmacology in Colorectal Cancer

3.1. Introduction

Calcium release activated calcium (CRAC) channels were first described by James Putney in 1986(Putney, 1986a) and were subsequently discovered to consist of ORAI subunits, dependent on STIM1 clustering for their function. Their function has been established in T cells (Hoth and Penner, 1992), and more recently T cell-mediated pathology such as inflammatory bowel disease (Di Sabatino et al., 2009), asthma(Spinelli et al., 2012) and dermatitis(The et al., 2013). CRAC channel function has also been demonstrated in human umbilical vein endothelial cells (Oike et al., 1994) and vascular smooth muscle cells(Li et al., 2011b). Our laboratory had previously reported functional effects of treating HUVECs with small molecule CRAC channel inhibitor S66 alongside siRNA knockdown, reducing cell migration and endothelial tube formation(Bae C, 2011), making this a potential target for anti-angiogenic therapy for diseases including cancer.

Furthermore, ORAI1 has been reported to be functionally upregulated in a number of cancers including clear cell renal carcinoma(Kim, 2014), oesophageal(Zhu et al., 2014) and melanoma(Umemura et al., 2014). Sobradillo and colleagues reported differential upregulation of ORAI1, 2, 3 and STIM1 and differential downregulation of STIM1 in colorectal cancer cell line HT-29 relative to normal colonic mucosal cells MCM460 (Sobradillo et al., 2014). Differential overexpression of ORAI1 has also been reported in immunohistochemical studies of paired cancer-normal samples of patients with hepatocellular carcinoma(Tang et al., 2017) and colorectal cancer (Deng, 2016).

CRAC channel function may be clinically relevant in cancer therapy. Tang and colleagues reported that 5FU treatment of HepG2 cells reduced CRAC channel activity in HepG2 cells, and CRAC channel inhibition enhanced autophagy-induced cell death in this cell line (Tang et al., 2017).

In essence, evidence suggests that this holds potential as a target for clinical treatments. At the time of starting this project, there were no studies that had defined ORAI1 function in CRC and the functional effects of small molecule inhibition.

3.2. Chapter Aims and Objectives

The aim of this work was to assess the role of CRAC channel signalling in colorectal cancer.

Objectives include:

- Characterising whether CRAC channels are functional in colorectal cancer
- Determining the effects of CRAC channel function on cancer cell function, namely cell viability, cell migration and invasion.
- Determining the effects of CRAC channel function on endothelial cell function, namely endothelial proliferation, cell migration and invasion.

3.3. CRAC channels are activated by thapsigargin-induced store depletion in cancer cell lines

Endoplasmic reticulum stores can be depleted by a number of experimental methods: inhibiting the sarcoplasmic reticulum calcium transport ATPase (SERCA) pump on the endoplasmic reticulum membrane, application of a calcium ionophore or by intracellular application of inositol 1, 4, 5-triphosphate (IP3). Thapsigargin is a sesquiterpene lactone and weak tumour stage promoter that is derived from the plant *Thapsia garganica*. It has been shown to irreversibly inhibit the SERCA pump, preventing replenishment of calcium that has been released from the intraorganelle store, and activating CRAC channel function through redistribution of STIM1(Lytton, 1991).

Unlike IP3, extracellular application of thapsigargin can reliably deplete the stores, making this a useful experimental tool for studying CRAC channel activation downstream of store depletion and is widely used in CRAC channel studies. Therefore, experiments studying CRAC channel inhibition were carried out using thapsigargin to induce store depletion.

3.3.1. Thapsigargin-induced CRAC channel activity

Thapsigargin-induced CRAC channel activity was determined in the colorectal cell lines HT-29, SW480 and HCT116. CRAC channel activity was demonstrated in all cell lines (Figure 3.1). All cell lines had lower cytoplasmic calcium levels following thapsigargin pre-treatment at baseline compared to the cells that were pre-treated with the DMSO vehicle control (Figures 3.1A-C), which suggests that the intracellular calcium pool is depleted following SERCA inhibition. There was a small

rise in intracellular calcium in vehicle-treated cells upon calcium addback that can be seen in Figures 3.1A-C, but this was not significant: this is likely to have been precipitated by a small degree of store depletion from prolonged incubation in calcium-free buffer.

All cell lines demonstrated calcium entry over the first 60 seconds following calcium add-back (Figure 3.1D). The kinetics of the CRAC channel calcium entry varied between the cell lines. HT-29 demonstrated a rapid transient peak with a fall in calcium signalling before calcium levels plateaued to give a sustained calcium entry (termed the sustained response). HCT116 and SW480 both demonstrated a steady rise in calcium signalling to generate a steady plateau with sustained calcium entry. The rate of rise in both HT-29 and HCT116 did not differ (HT-29 0.13/s and HCT116 0.19/s, $p>0.05$). However, the rate of rise is significantly lower in SW480 cells (0.04/s). Peak amplitude was the same for HT-29 (1.24) and HCT116 (1.1) ($p>0.05$) but the peak amplitude of SW480 was significantly lower than both HT-29 ($p=0.004$) and HCT116 ($p=0.009$) (Figure 3.1E). Area under the curve analysis showed no difference between calcium entry between the two cell lines (HT-29 524.7 vs HCT116 539.9) (Figure 3.1F). Area under the curve analysis also showed that calcium entry was lower in SW480 (349.2) compared to HT-29 ($p=7.3E-4$) and HCT116 ($p=4.6E-4$). In conclusion, all cell lines demonstrated CRAC channel activity, with lower CRAC channel calcium responses in SW480 compared to the other cell lines.

3.3.2. Thapsigargin-induced store depletion

The rate, amplitude and total amount of calcium entry differed between HT-29 and SW480. Thapsigargin add-back was used to determine whether this could be related to a difference in store depletion. Cells were washed in calcium-free salt buffered solution and 1 µM of thapsigargin was added to the cells in calcium-free solution while calcium traces were recorded to capture the amplitude of intracellular calcium rise from endoplasmic reticulum store depletion for HT-29 (Figure 3.2A) and SW480 (Figure 3.2B).

The peak amplitude of store depletion Ca^{2+} release was 0.44 (SEM 0.09) for HT-29 and 0.53 (SEM 0.03) for SW480 and did not differ from one another ($p=0.66$) (Figure 3.2C). In conclusion, Ca^{2+}-release and therefore store depletion does not differ between HT-29 and SW480 cell lines.
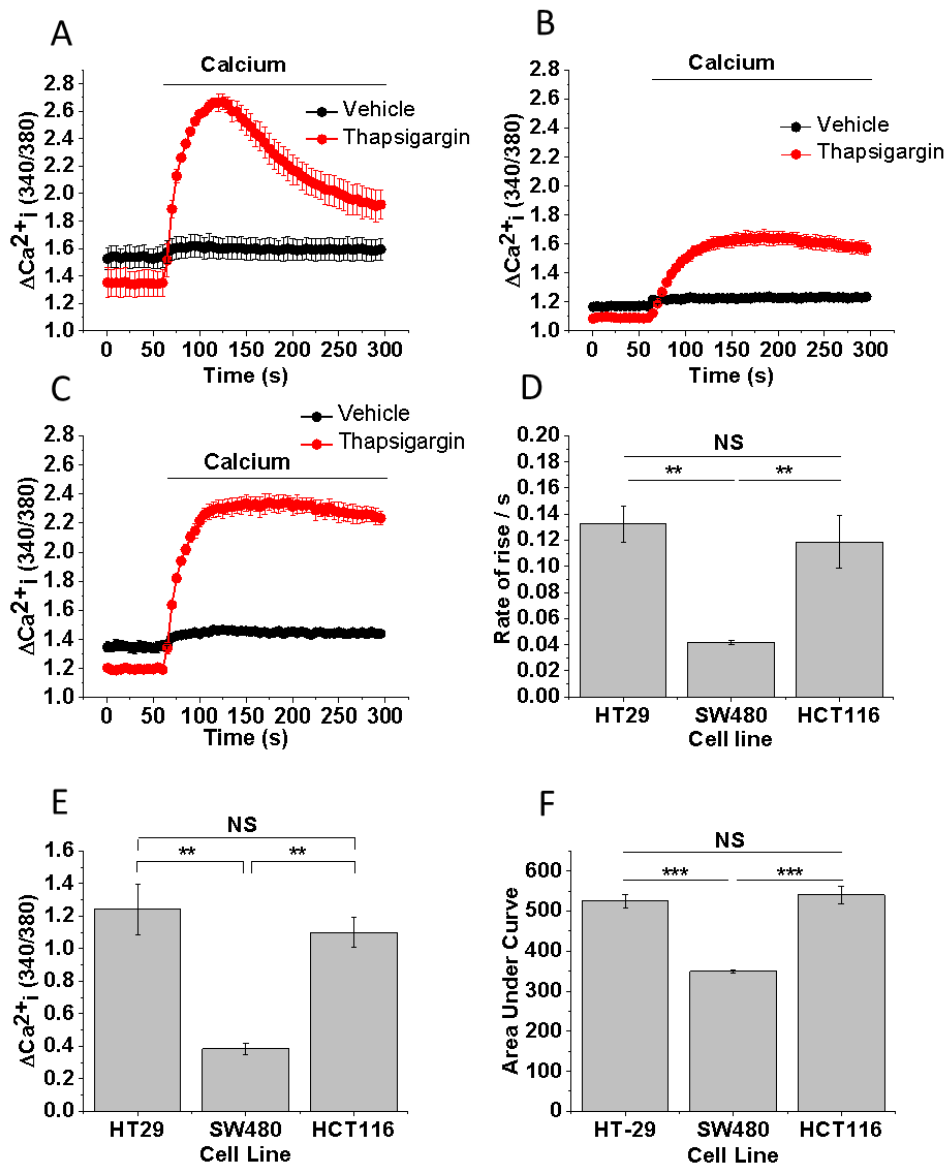
Figure 3.1. A-C: CRAC channel calcium traces in CRC cell lines. Cytoplasmic calcium traces obtained after calcium addback following pre-treatment with thapsigargin (red line) and vehicle (black line) in calcium-free buffer of 3 CRC cell lines recorded on the Flexstation. A. HT-29; B. SW480; C. HCT116; D. Bar chart presenting mean±SEM of the initial rate of calcium rise in the 3 cell lines; E. Bar chart presenting mean±SEM of the peak calcium amplitude obtained in the 3 cell lines; F. Bar chart presenting mean±SEM of the area under the curve of calcium entry derived from traces of the 3 cell lines. Key: s = seconds. ΔCa^{2+}_i = change in intracellular calcium flux. ANOVA testing: * = p≤0.05; ** p=≤0.01; *** p=≤0.001; NS = not significant. All experiments n/N=3/4.
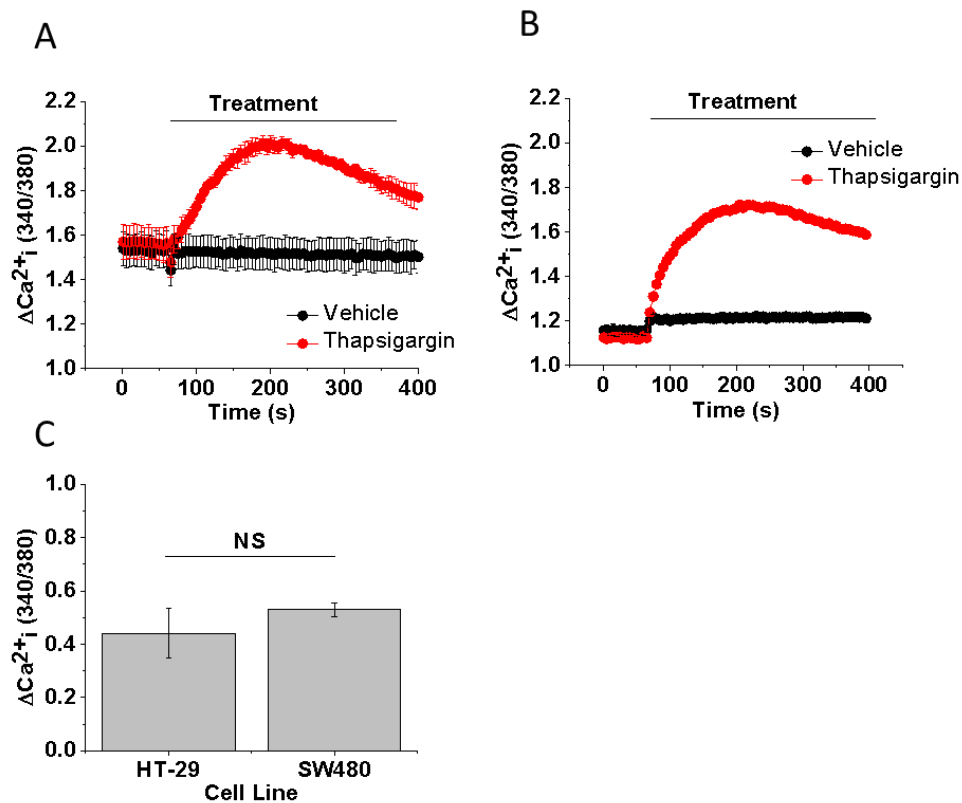
Figure 3.2. A-B: Store depletion calcium traces in CRC cell lines. Cytoplasmic calcium traces of cells in calcium-free buffer with the addition of either vehicle (black line) or thapsigargin (red line) in CRC cell lines recorded on the Flexstation. A. HT-29; B. SW480. C. Bar chart presenting mean±SEM of the peak amplitude of calcium entry obtained in colorectal cancer cell lines derived from both A and B. T test: * = p≤0.05; ** p=≤0.01; *** p=≤0.001; NS = not significant Key: s = seconds. ΔCa^{2+}_i = change in intracellular calcium flux. All experiments n/N=3/4.

3.3.3. qRT-PCR

The expression profiles of *ORAI1* for the 3 cell lines was determined using semi-quantitative real time PCR (qRT-PCR). There was no normal colonic epithelial cell line to use in order to determine differential expression. The laboratory has previously shown *ORAI1* expression in HUVECs by real time RT-PCR as well as demonstrating functional effect in migration, invasion and endothelial tube formation (Bae C, 2011). Therefore, *ORAI1* expression in HUVEC cells was determined and used as a positive control, but it was not an appropriate cell line to use for comparative purposes, therefore the $2^{-\Delta CT}$ was reported. Expression of *ORAI1* RNA was detected in all cell lines. The $2^{-\Delta CT}$ values of the 3 colorectal cancer cell lines do not differ from one another (HT-29 vs SW480, p=1; SW480 vs HCT116, p=1; HT-29 vs HCT116, p=1) (Figure 3.3). The $2^{-\Delta CT}$ for each cell line was compared to HUVEC samples. There was lower *ORAI1* expression in HT-29 (p=0.047) and HCT116 (p=0.047) relative to the HUVEC control (Figure 3.3). There was no difference between SW480 and HUVEC samples (p=0.39).

3.3.4. siRNA

ORAI1 siRNA transfection was used to determine whether CRAC channel activity was specific to ORAI1. Cells were transfected with a scrambled sequence pool transfection control and ORAI1 SMARTpool alongside mock-transfected cells then cultured in fresh medium overnight. Cells were seeded the following day into microplates to give confluent monolayers for testing the day after, 48 hours post transfection. Fura2AM-loaded cells were treated with thapsigargin or vehicle control in calcium-free SBS before calcium-containing SBS was added back to the wells.

In HT-29 cells, there was no discernible difference in calcium traces between the mock-transfected and scrambled-transfected cells (relative amplitude 92.5% in scrambled vs mock control, p=0.28) (Figure 3.4A). This demonstrated that the scrambled sequence pool did not interfere with CRAC channel function and validated it as a suitable control for the siRNA experiments. Transfection resulted
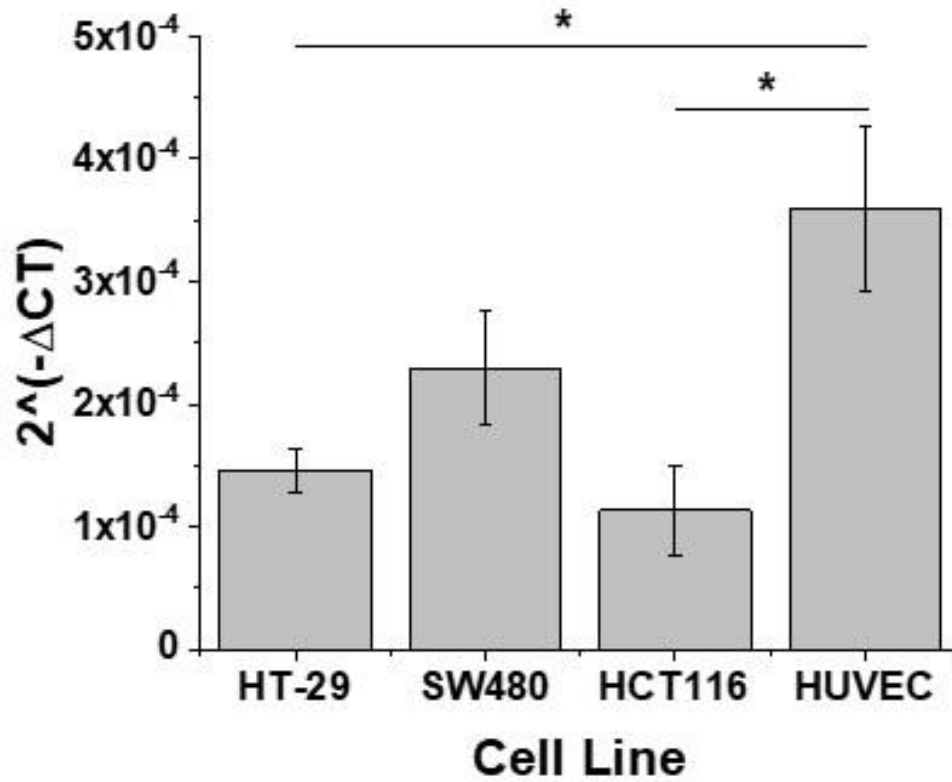
Figure 3.3. qRT-PCR expression profiling of ORAI1 in colorectal cancer cell lines. Bar chart presenting the $2^{(-\Delta CT)}$ values of *ORAI1* expression in the 3 colorectal cancer cell lines SW480, HT-29 and HCT116 alongside a HUVEC positive control. ANOVA testing: * = p≤0.05; ** p=≤0.01; *** p=≤0.001; NS = not significant Experiments n/N=3/3.

in a global reduction in calcium entry without altering the kinetics of CRAC channel calcium entry (Figure 3.4B). Transfection reduced the peak amplitude from 1.45 to 0.84 (Figure 3.4C), equating to 58.8% calcium entry relative to the scrambled control (p=0.018) (Figure 3.4D).

In SW-480 cells, there was no discernible difference in calcium traces between the mock-transfected and scrambled-transfected cells in SW480 (Figure 3.5A). This demonstrated that the scrambled sequence pool did not interfere with CRAC channel function and validated it as a suitable control for the siRNA experiments.

The trace of the transfected cells follows the same kinetics as the scrambled trace with similar transient rise then initial fall of calcium signalling before it started to plateau (Figure 3.5B). There was a globally lower rate of calcium entry in the ORAI1 siRNA-transfected cells (Figure 3.5B). siRNA transfection resulted in a reduction of the peak amplitude from 0.58 to 0.31 (Figure 3.5C), equating to 52.6% calcium entry relative to the scrambled control (p=0.017) (Figure 3.5D). In conclusion, transfection demonstrates that ORAI1 is necessary for CRAC channel function.

3.3.5. Conclusion
In conclusion, this work has determined that CRAC channels are present and functional in the selected colorectal cancer cell lines.
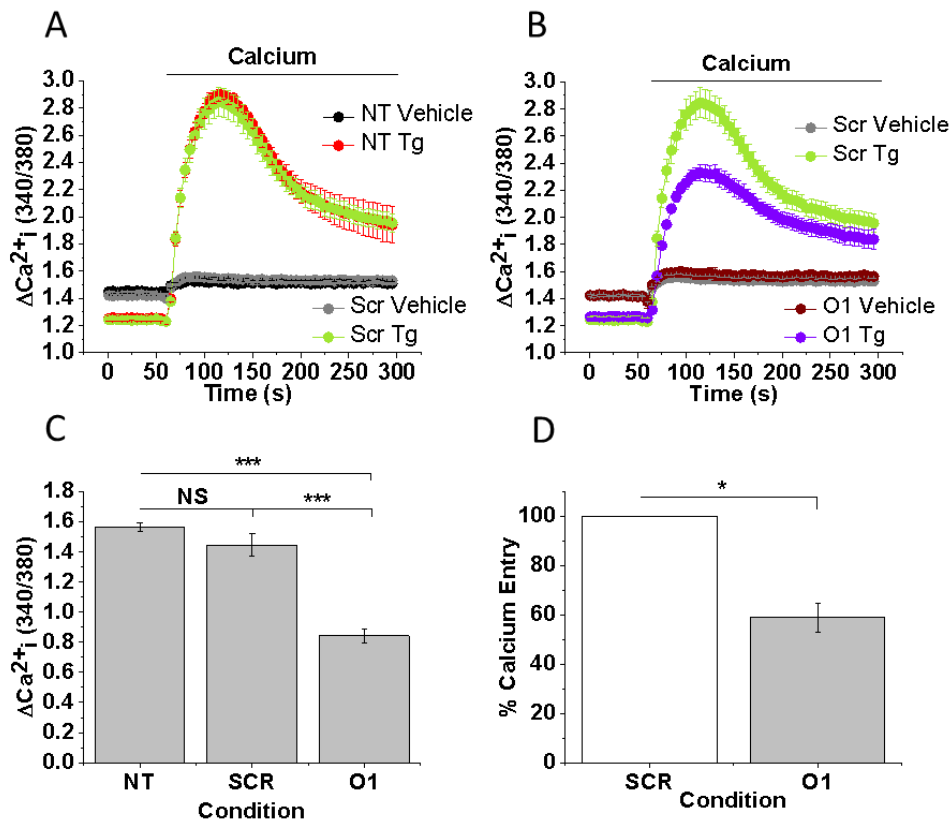
Figure 3.4. CRAC channel signalling in HT-29 following ORAI1 siRNA transfection. A-B: Cytoplasmic calcium traces of transfected HT-29 cells following calcium addback after thapsigargin-induced store depletion in calcium-free buffer recorded on the Flexstation. A. Calcium traces of mock-transfected (red line) and scrambled sequence-transfected (green line) cells; B. Cytoplasmic calcium traces of scrambled sequence-transfected (green line) and ORAI1 siRNA-transfected (purple) cells. C. Bar chart presenting the mean±SEM of the peak amplitude of calcium entry in mock-transfected, scrambled sequence-transfected and ORAI1 siRNA-transfected cells derived from B. D. Bar chart presenting the mean±SEM of the percentage calcium entry in ORAI1 siRNA-transfected cells relative to the scrambled sequence-control cells derived from C. Key: NT = non-transfected (mock); SCR = scrambled; O1 = ORAI1; s = seconds; $\Delta Ca^{2+}{}_i$ = change in intracellular calcium flux. ANOVA or t testing: * = $p \leq 0.05$; ** $p = \leq 0.01$; *** $p = \leq 0.001$; NS = not significant All experiments n/N=3/4.
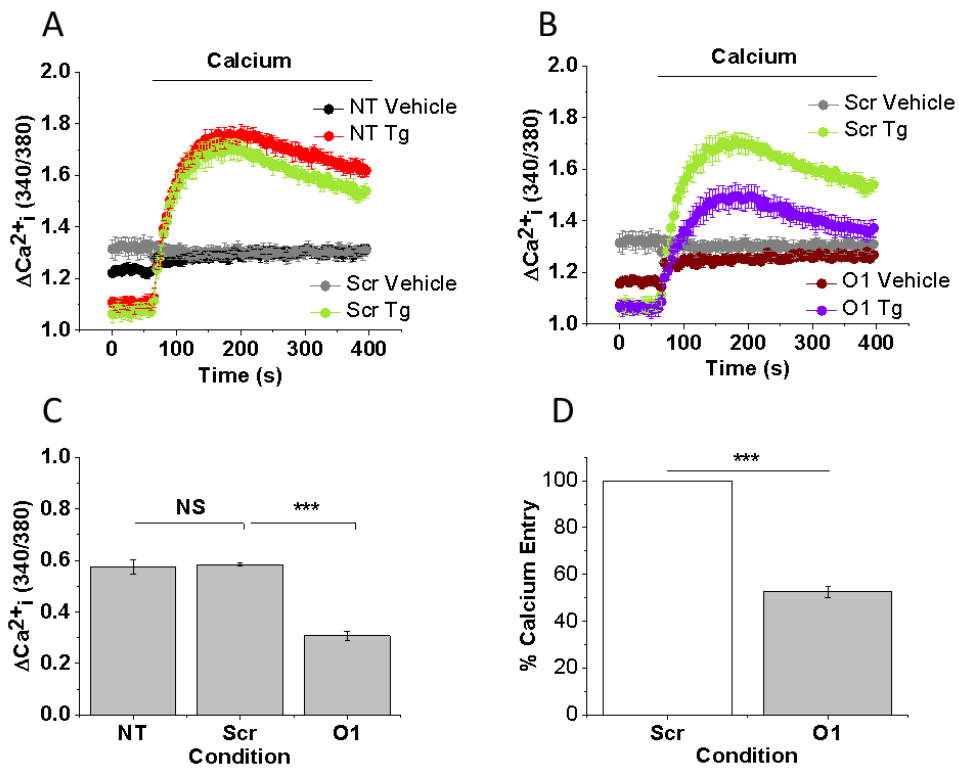
Figure 3.5. CRAC channel signalling in SW480 following ORAI1 siRNA transfection. A-B: Cytoplasmic calcium traces of transfected cells obtained after calcium addback following thapsigargin-induced store depletion in calcium-free buffer A. Calcium traces of mock-transfected (red line) and scrambled sequence-transfected (green line) cells; B. Cytoplasmic calcium traces of scrambled sequence-transfected and ORAI1 siRNA-transfected cells. C. Bar chart presenting mean±SEM of the peak amplitude of calcium entry in mock-transfected, scrambled sequence-transfected and ORAI1 siRNA-transfected cells (n/N=3/4). D. Bar chart presenting mean±SEM of the percentage calcium entry in ORAI1 siRNA-transfected cells relative to the scrambled sequence-control cells. Key: NT = non-transfected (mock); Scr = scrambled; O1 = ORAI1; ΔCa^{2+}_I = change in intracellular calcium flux. ANOVA or t test: * = p≤0.05; ** p=≤0.01; *** p=≤0.001; NS = not significant All experiments n/N=3/4.

3.4. CRAC channel activity is inhibited by established and novel CRAC channel inhibitors in colorectal cancer cell lines

3.4.1. CRAC channel inhibition

A number of studies have reported CRAC channel signalling inhibition in colorectal cancer cells. The commercially available inhibitor SFK96365 inhibited CRAC channel calcium traces in a concentration-dependent manner in both Hct116 and HT-29 cell lines(Jing et al., 2016). Intracellular calcium measurements were performed on the FlexStation in order to determine whether CRAC channels could be pharmacologically inhibited in the cell lines.

3.4.1.1. Synta66 (S66)

Our laboratory has reported on the potent ability of S66 to inhibit CRAC channel activity in human umbilical vein endothelial cells (HUVECs) (Li et al., 2011a) and vascular smooth muscle cells(Li et al., 2011b). It inhibits CRAC channel calcium re-entry in breast cancer cells MDA-MB-468(Azimi et al., 2018) but its use has not been reported in colorectal cancer. Therefore, CRAC channel inhibition using S66 was tested in the colorectal cancer cell lines HT-29 and SW-480.

Cells were treated with Tg in the presence of different concentrations of S66 alongside the DMSO vehicle control of the drug. S66 inhibited CRAC channel activity in both HT-29 (Figure 3.6A) and SW480 (Figure 3.6C). Dose-response curves generated from peak calcium amplitudes derived IC50s within the nanomolar range in both cell lines. Residual calcium entry was 15.2% at 5 µM concentration in HT-29 cells with an IC50 of 671 nM of the dose-response curve (Figure 3.6B). S66 appeared to be more potent in SW480 cells with residual calcium entry of 4.85% at the maximum 5 µM concentration and an IC50 concentration of 144 µM of the dose-response curve (Figure 3.6D).

3.4.1.2. The history of the novel CRAC inhibitor JPIII

S66 solubility limited the maximum concentration that could be used on the cells. 10 µM was seen to macroscopically precipitate out of solution therefore 5 µM was the maximum concentration used. The solubility of S66 has previously been a problem for *in vitro* testing in other laboratory projects. The solubility index of S66

was confirmed to be very narrow using the turbidimetric solubility assay performed by Cyprotex Limited. This demonstrated a compound mid-range solubility of 6.5 µM (upper to lower range 3-10 µM).

Solubility was an issue for testing in multiple projects *in vitro* within the laboratory. This small solubility range also prevented progression onto *in vivo* testing. Therefore, work was undertaken with members of our lab and postdoctoral scientists in the Department of Chemistry to generate S66 analogue compounds with better solubility and similar if not better pharmacokinetic properties. Of the compounds screened, JPIII was the most promising compound. This analogue was derived by removing the fluorine group from the pyridine ring of the S66 structure (Synta66 Figures 3.7A and JPIII Figure 3.7B). This compound demonstrated comparable CRAC channel inhibition in FlexStation testing in HUVECs and HEK cells. The solubility range was broader, with a mid-range solubility of 37.5µM (range 10-65µM) (Figure 3.8). Furthermore, the compound has been used *in vivo* successfully in other projects within the lab. Therefore, this compound was tested further *in vitro* as a wider concentration range could be tested *in vitro* and this compound would be more likely to be used successfully *in vivo*.
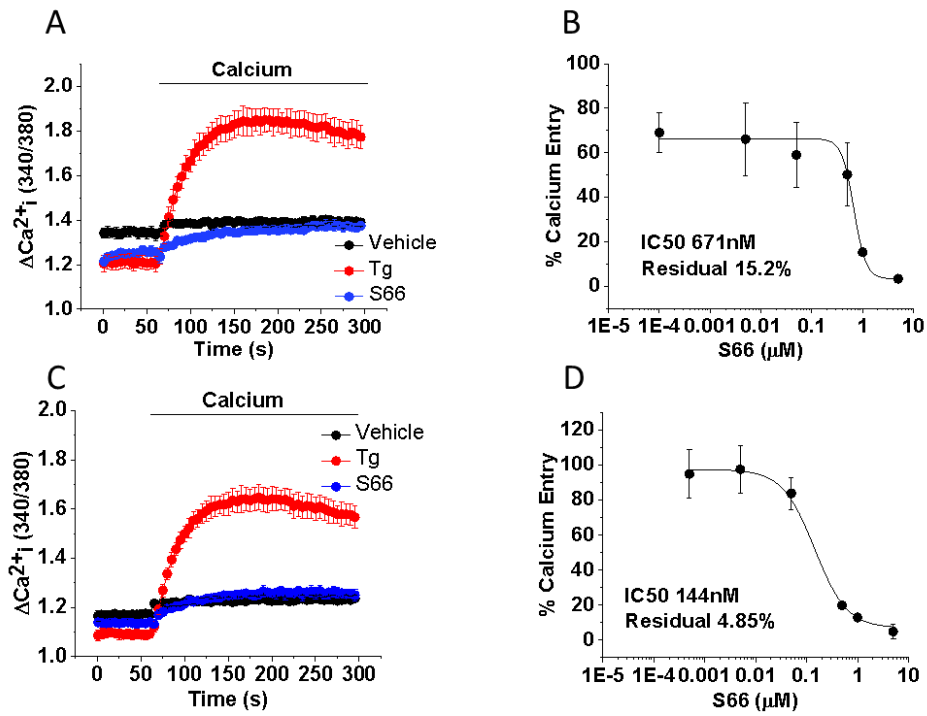
Figure 3.6. CRAC channel inhibition by S66 in CRC cell lines. A and C. Cytoplasmic calcium traces of CRAC channel signalling in HT-29 cells following the addition of calcium to cells that have been treated in calcium free buffer with vehicle (black line), thapsigargin (red line) and thapsigargin/1μM S66 (blue line): A. HT-29; C. SW480. B. Dose-response curve of calcium inhibition by S66 in HT-29 cells. D. Dose-response curve of calcium inhibition by S66 in SW480 cells. Key: s = seconds. ΔCa^{2+}_I = change in intracellular calcium flux. All experiments n/N 3/4.
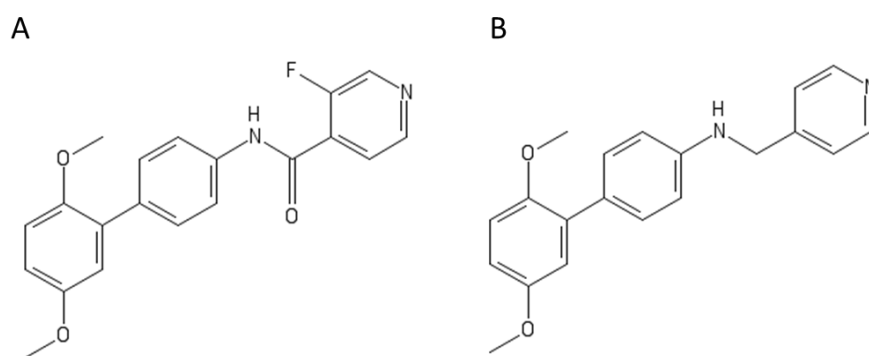
Figure 3.7. Chemical structures of CRAC channel inhibitors used in this study. A. S66; B. JPIII.
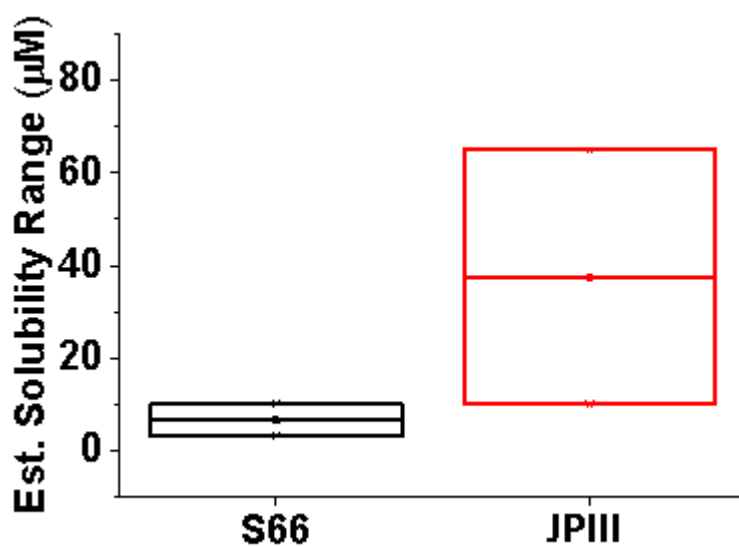
Figure 3.8. The solubility range of the compounds S66 and JPIII. Box plot presenting results of turbidimetric solubility testing for estimated solubility range (µM) of compound for both S66 (black box) and JPIII (red box), with the middle line representing the calculated mid-range precipitation dose, with the upper and lower bound edges representing the higher bound and lower bound estimated precipitation range. Turbidimetric solubility experiments were carried out by Cyprotex Ltd. Data was provided by Dr Marc Bailey and Dr Richard Foster. Key: Est. = estimated.

3.4.2. JPIII inhibits CRAC Channel Function in Colorectal Cancer Cell Lines

Intracellular calcium measurements were carried out on pre-treated cells using the FlexStation in order to determine the efficacy of JPIII at inhibiting CRAC channel calcium entry in the selected colorectal cancer cell lines. The peak calcium amplitude obtained with each dose was determined from calcium traces on the Flexstation and used to generate dose-response curves. In order to determine whether there was any difference in the total calcium entry at each concentration, the area under the curve was also derived for each concentration from the calcium traces from each repeat.

Calcium traces of HT-29 cells are presented in Figure 3.9A. Peak calcium amplitudes were used to create a dose-response curve (Figure 3.9B). An IC50 concentration of 740 nM was extrapolated from this curve. There was 17.84% residual calcium entry at 10 µM concentration. JPIII inhibited calcium entry at 1 µM and 10 µM only, discernible from peak calcium amplitude (Figure 3.9C) and area under the curve (Figure 3.9D). The kinetics of calcium entry differed for higher concentrations than it did for the lower concentrations, with a slower, sustained calcium re-entry at 1 µM and 10 µM compared to the rapid and transient rise in calcium entry with the lower concentrations (Figure 3.9A). This demonstrated that there was only a difference in total calcium entry at 1 µM and 10 µM (Figure 3.9D).

Calcium traces of SW480 cells are presented in Figure 3.10A. Peak calcium amplitudes were used to create a dose-response curve (Figure 3.10B). An IC50 concentration of 553 nM was extrapolated from this curve. There was 27.8% residual calcium entry at 10 µM concentration. JPIII inhibited calcium entry at 0.5 µM, 1 µM and 10 µM only (Figure 3.10C). Data from area under the curve showed similarly that there was only a reduction in total calcium entry at 0.5 µM, 1 µM and 10 µM (Figure 3.10D).

Calcium traces of HCT116 are presented in Figure 3.11A. Peak calcium amplitudes were used to create a dose-response curve (Figure 3.11B). An IC50 dose of 160 nM was extrapolated from this curve. There was 26.5% residual calcium entry at 10 µM. JPIII significantly inhibited calcium entry at 0.5 µM, 1 µM and 10 µM only (Figure 3.11C). Data from the area under the curve showed similarly that there was only a reduction in total calcium entry at 0.5 µM, 1 µM and 10 µM (Figure 3.11D).

In conclusion, CRAC channel inhibition was achieved in all cell lines. CRAC channel inhibition was only achieved at higher concentrations in all cell lines. JPIII was

unable to obtain total inhibition of CRAC channel activity at the highest concentration in this assay. CRAC channel inhibition was relatively more potent in HCT116 and SW480 cells than HT-29.

3.5. Data mining existing datasets to look at the effect of CRAC channel inhibition

A literature search was carried out to identify studies that studied gene expression profiles in cells treated with CRAC channel inhibitors. PubMed, GEO and ArrayExpress were used to identify studies that had carried out RNASeq or microarray analysis of gene expression following treatment with known CRAC channel inhibitors. The aim of this search was to identify multiple datasets that could allow exploratory analysis of the effect of drug treatment on the transcriptome. The objective was to determine whether genes were differentially regulated following CRAC channel inhibition and to perform pathway analysis of these genes in order to identify potential functional effects of CRAC channel inhibition *in vitro*. The objective of this work was to determine whether CRAC channel inhibition had been shown to impact on cellular signalling pathways such as survival, cell death and cell cycle, which could further justify *in vitro* studies.

Pubmed searches were carried out for the following CRAC channel inhibitors S66, RO2959, SFK-96365, GSK5505A and GSK7975A. Only one study was identified by Chen and colleagues. No such study was found in cancer research.

Chen studied the compound RO2959, a CRAC channel inhibitor that has been characterised relatively recently. They studied the effect of 24 hours of treatment of CRAC channel inhibitor RO2959 and the calcineurin inhibitor cyclosporin A on activated T cells by using human peripheral blood mononuclear cells (PBMC) stimulated with anti-CD3/CD28 (Chen et al., 2013). Treatment was carried out on cells from 4 patients. RNA was extracted from cells and hybridised to Affymetrix Human U133 plus 2 Genechips. Gene transcription profiles were generated and differentially expressed genes were identified.
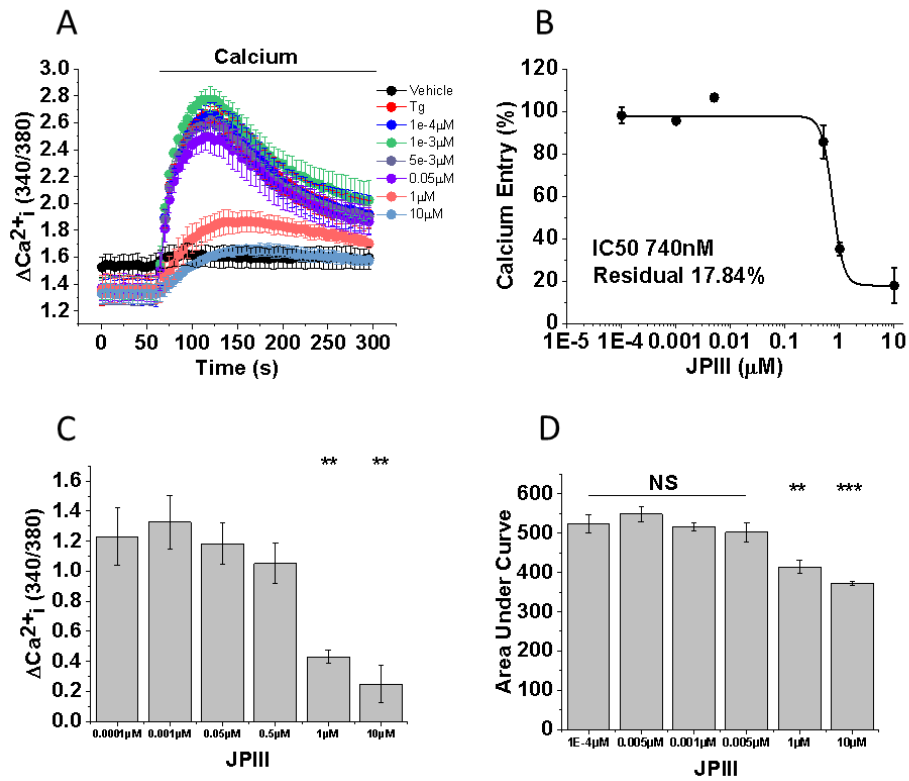
Figure 3.9. CRAC channel inhibition by JPIII in HT-29 cells. A. Cytoplasmic calcium traces following addition of calcium to cells pre-treated with thapsigargin and a range of JPIII concentrations in calcium-free buffer alongside vehicle-treated (black line) and thapsigargin-treated (red line) cells; B. Dose-response curve of calcium inhibition by JPIII in HT-29 cells derived from A; C. Bar chart presenting mean±SEM of the peak calcium amplitude for each JPIII concentration derived from A; D. Bar chart presenting mean±SEM of the area under the curve for each JPIII concentration derived from A. Key: s = seconds. ΔCa^{2+}_I = change in intracellular calcium flux. ANOVA testing: * = p≤0.05; ** p=≤0.01; *** p=≤0.001; NS = not significant All experiments are n/N=3/4.

Figure 3.10. CRAC channel inhibition by JPIII in SW480 cells. A. Cytoplasmic calcium traces following the addition of calcium to cells that were pre-treated with thapsigargin in calcium-free buffer with a range of JPIII concentrations alongside vehicle only (black line) and thapsigargin only (red line); B. Dose-response curve of calcium inhibition by JPIII derived from the peak calcium amplitudes from A; C. Bar chart presenting mean±SEM of the peak calcium amplitude by concentration derived from A. D. Bar chart presenting mean±SEM of the area under the curve for each concentration derived from A. Key: s = seconds; ΔCa2+I = change in intracellular calcium flux. ANOVA testing: * = p≤0.05; ** p=≤0.01; *** p=≤0.001; NS = not significant. All experiments n/N=3/4.

Figure 3.11. CRAC channel inhibition by JPIII in HCT116 cells. A. Cytoplasmic calcium traces following the addition of calcium to cells pre-treated with thapsigargin in calcium-free buffer with a range of concentrations of JPIII, alongside vehicle only (black line) and thapsigargin only (red line); B. Dose-response curve of calcium inhibition by JPIII derived from the peak calcium amplitudes from A; C. Bar chart presenting mean±SEM of the peak calcium amplitude by concentration derived from A. D. Bar chart presenting mean±SEM of the area under the curve for each concentration derived from A. Key: s = seconds; $\Delta Ca2+I$ = change in intracellular calcium flux. ANOVA testing: * = $p \leq 0.05$; ** $p = \leq 0.01$; *** $p = \leq 0.001$; NS = not significant. All experiments n/N=3/4.

3.5.1. Gene set enrichment analysis of differentially modulated genes treated by pharmacological CRAC channel inhibition.

Limma analysis identified 2098 genes that were differentially expressed: 18 had a mean log FC under 1 and 126 under 0.5; 131 had a mean log FC of over 1 and 9 had a log FC over 1. String network analysis was carried out within Cytoscape for differentially upregulated and downregulated genes in treated cells and are visually presented in Figures 3.12 and 3.13 respectively. Upregulated and downregulated gene ontology processes are presented in Tables 3.1 and 3.2 respectively.

3.5.2. Conclusion and further direction

In conclusion, RO2959 treatment resulted in differential expression in activated T cells, with downregulation of genes involved in cell proliferation as well as DNA damage pathways and cell cycle checkpoints. Conversely though, there was a significant upregulation of genes involved in cell migration and immunity. The results indicate that CRAC channel inhibition does impact on molecular signalling processes. It should be borne in mind that the results are not directly applicable to cancer cells, as the work was carried out on T cells. This data was used to explore whether CRAC channel inhibition may have an impact on cellular function, and was carried out prior to *in vitro* testing to drive hypotheses.

An effective anti-cancer drug needs to be able to target the hallmarks of cancer as outlined by Hanahan and Weinberg (Hanahan and Weinberg, 2011):

1. Sustained proliferative signalling.
2. Evasion of growth suppressors.
3. Activating invasion and metastases.
4. Enabling replicative immortality.
5. Induction of angiogenesis.
6. Resisting cell death.
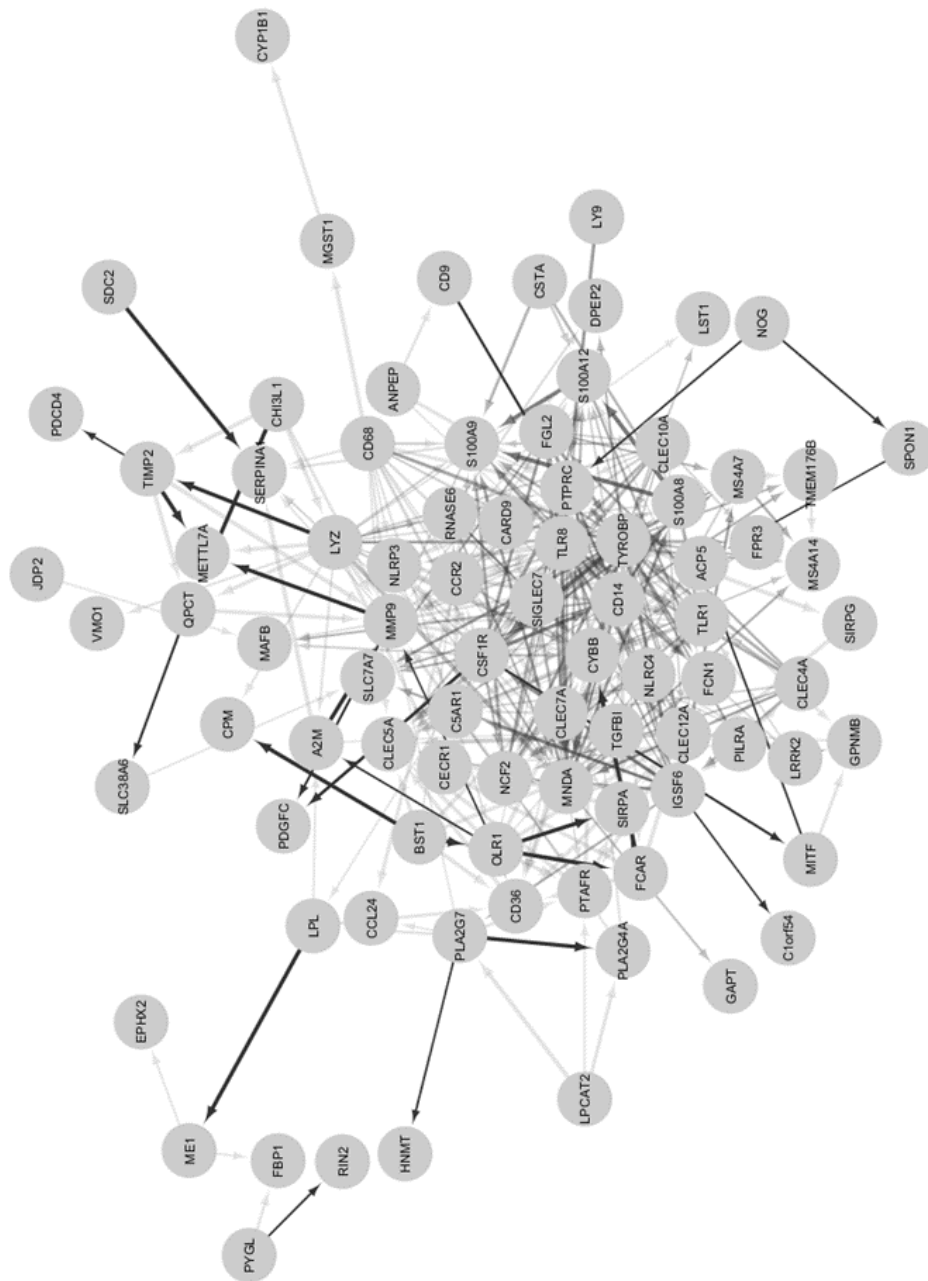
Figure 3.12. Network analysis of differentially upregulated genes of activated T cells treated with RO2959. Generated from data from (Chen et al., 2013). Fold changes of 0.5 and above. n/N=4/1. The genes show as round notes, the edges denote co-expression scores based on the quality of the published data. Co-expression scores are calculated within the String app of Cytoscape. The stronger the edge, the higher the score; the more transparent the edge, the lower the score.

Figure 3.13. Network analysis of differentially downregulated genes of activated T cells treated with RO2959. Generated from data from (Chen et al., 2013). Fold changes of 0.5 and above. n/N=4/1. The genes show as round notes, the edges denote co-expression scores based on the quality of the published data. Co-expression scores are calculated within the String app of Cytoscape. The stronger the edge, the higher the score; the more transparent the edge, the lower the score.

	No. of Enriched Genes	% enriched genes in GO category	FDR q-value
Inflammatory response	17	26.2	6.83E-06
innate immune response	21	2.5	3.81E-04
immune response	25	1.5	3.81E-04
leukocyte migration	11	3.2	4.26E-04
defence response to other organism	13	11	4.26E-04
response to molecule of bacterial origin	12	3.1	4.26E-04
defence response	25	1.5	5.22E-04
positive regulation of defence response	13	10	5.22E-04
response to biotic stimulus	17	1.1	9.60E-04
regulation of tumour necrosis factor (TNF) production	7	4.2	0.00172
response to other organism	16	1	0.00172
cellular defence response	6	37.5	0.00172
response to bacterium	13	1.4	0.00217
cell adhesion	19	1.5	0.00217
Defence response to bacterium	9	2.1	0.00217
positive regulation of protein metabolic process	23	1.4	0.00242
regulation of defence response	16	4.4	0.0036
response to lipopolysaccharide	10	2.7	0.00369
cytokine production	7	0.9	0.00375
cell migration	16	1.1	0.00412
positive regulation of cytokine production	11	2.4	0.00468
positive regulation of TNF production	5	5.1	0.0065
regulation of cytokine secretion	7	3.2	0.00694
immune system process	27	1	0.00697
response to stress	38	1	0.00738
cell activation	14	1.3	0.00767
localization of cell	16	1	0.00875
positive regulation of programmed cell death	13	2	0.00959

Table 3.1. Summative table of the gene ontology processes upregulated in activated T cells treated with CRAC channel inhibitor RO2959 relative to the untreated control. Number of genes upregulated in each process is also presented as a proportion of genes annotated to that process.

GO Process	No. of Enriched Genes	% enriched genes in GO category	FDR q-value
cell cycle	59	3.6	6.54E-34
mitotic cell cycle	49	6.1	1.01E-32
mitotic cell cycle process	47	7.2	1.21E-32
cell cycle process	51	4.6	8.64E-31
organelle fission	35	7.7	9.39E-26
nuclear division	34	8.4	1.83E-25
mitotic nuclear division	31	3.8	1.18E-24
cell division	34	5.9	3.66E-24
mitotic cell cycle phase transition	24	6.6	1.07E-16
chromosome segregation	20	6.3	2.18E-16
G1/S transition of mitotic cell cycle	19	95	1.02E-15
regulation of cell cycle	34	3.5	4.22E-15
DNA metabolic process	28	3.4	3.76E-13
single-organism organelle organization	44	1.2	4.08E-13
DNA conformation change	18	8.5	5.25E-13
cell cycle checkpoint	18	10	1.26E-12
DNA replication	17	7.2	4.60E-12
organelle organization	50	1.4	2.46E-11
regulation of cell proliferation	35	2.1	1.45E-10
positive regulation of JAK-STAT cascade	11	10.7	1.57E-10
regulation of cell cycle process	22	3.8	2.91E-10
regulation of JAK-STAT cascade	12	7.2	2.91E-10
regulation of transcription involved in G1/S transition of mitotic cell cycle	8	57.1	1.48E-09
chromosome organization	26	2.3	2.73E-09
regulation of chromosome segregation	10	10	3.74E-09

DNA packaging	13	7.7	4.86E-09
cellular response to stimulus	68	0.9	1.59E-08
positive regulation of cytokine production	17	3.7	1.67E-08
regulation of cell division	15	9.6	1.93E-08
regulation of cytokine production	19	2.8	8.45E-08
regulation of protein modification process	32	1.8	8.95E-08
regulation of mitotic cell cycle	18	3.6	1.00E-07
DNA replication initiation	7	24.1	1.00E-07
regulation of mitotic nuclear division	11	6.8	1.02E-07
positive regulation of cell cycle process	14	5.6	1.08E-07
regulation of chromosome organization	13	3.6	1.28E-07
single-organism cellular process	90	0.6	1.32E-07
response to stress	48	1.3	1.36E-07
negative regulation of cell division	9	64.3	1.75E-07
positive regulation of cell cycle	15	4.2	1.79E-07
DNA repair	17	3.6	1.94E-07
regulation of protein metabolic process	39	1.4	2.80E-07
positive regulation of cell proliferation	22	2.3	3.67E-07
positive regulation of tyrosine phosphorylation of STAT protein	8	14.3	3.95E-07
negative regulation of cell cycle	17	3.8	3.98E-07
sister chromatid segregation	9	5.2	4.52E-07
regulation of nuclear division	11	5.7	5.22E-07
DNA integrity checkpoint	11	9.6	6.36E-07
regulation of protein phosphorylation	26	1.8	7.31E-07
nuclear chromosome segregation	10	3.9	8.50E-07

Table 3.2. Summative table of the top 50 most significant gene ontology processes that are downregulated in T cells treated with CRAC channel inhibitor RO2959 relative to the untreated control. Number of genes upregulated in each process is also presented as a proportion of genes annotated to that process.

The results of the gene set enrichment analysis from the Chen study of RO2959 inhibition of activated T cell function highlighted that CRAC channel inhibitor treatment affects genes related with cell proliferation and the cell cycle(Chen et al., 2013). A number of studies have reported that CRAC channel inhibitors impact on cancer cell growth(Azimi et al., 2018) as well as migration and invasion(Motiani et al., 2013a). Our laboratory have previously described the anti-angiogenic effects of JPIII's parent compound S66 *in vitro* on human umbilical vein endothelial cells (HUVECs) with inhibition of CRAC channel function, migration and invasion as well as tube formation alongside ORAI1 siRNA knockdown(Bae C, 2011). There is therefore the potential for JPIII to target tumour endothelium as well as the cancer cell. Targeting angiogenesis with the human VEGF monoclonal antibody bevacizumab proved to have potent effects in xenograft studies *in vivo(Kim et al., 1993)*. Bevacizumab did not have such impact on patient survival as sole therapy in metastatic CRC *in vitro* (Giantonio et al., 2007). However, combining it with standard chemotherapeutic regimes results in greater response and improved survival outcomes (Hurwitz et al., 2004). Therefore, the concept of a drug therapy that can target both tumour tissue and vasculature is an ideal.

Therefore, further studies were carried out using JPIII to determine whether JPIII treatment displayed anti-cancer effects in the selected colorectal cancer cell lines. *In vitro* study looked to determine whether JPIII had any impact on some of the hallmarks of cancer: proliferation, replicative immortality, cell death, invasion and migration. In addition, the effect of treatment was studied in endothelial cells to determine whether the compound affected endothelial cell function.

3.6. The effect of JPIII on colorectal cancer cell viability

The WST1 viability assay was used to determine whether JPIII affected cellular viability. The validity of the cellular response was concomitantly determined by using a positive control. Both SW480 and HT-29 cells are known to respond to 5-fluouracil (5-FU), however microplate viability is only reduced with prolonged exposure to high concentrations(Mhaidat et al., 2014).

Firstly, the viability of HT-29 cells treated with the DMSO vehicle compound was compared to untreated cells to determine whether DMSO affected cell viability. DMSO treatment over 6 days did not affect viability, with raw absorbance of 1.45 in untreated cells vs 1.34 in vehicle-treated cells (p=0.09) (Figure 3.14A). A range of concentrations of JPIII were tested on HT-29 cells between 0.03-30 µM. There was no effect with any concentrations following 4 days of continual treatment (Figure 3.14C). The validity of the cellular response was concomitantly tested with the 5-FU positive control. The relative viability of HT-29 cells treated with 100 µM of 5-FU was reduced to 22.03% (p=0.003) (Figure 3.14C).

The treatment period was prolonged to 6 days. Again, there was no difference in viability between untreated and vehicle-treated cells (Figure 3.15A). There was a dose-dependent reduction in relative viability following 6 days of treatment for concentrations between 1 µM and 30 µM (Figure 3.15B): 40.8% with 30 µM (p=3.8E-5), 53.5% with 20 µM (p=0.002) and 59.1% with 10 µM (p=0.007), 68.8% with 3 µM (p=0.002) and 67.2% with 1 µM (p=0.05) (Figure 3.15B). The viability of HT-29 cells was reduced to 22.09% with 6 days of continuous treatment with 5-FU (p=0.003) (Figure 3.15C).

Viability of SW480 cells was tested with DMSO vehicle control alongside untreated cells to determine whether the vehicle compound affected cell viability. Viability was unaffected by the vehicle control over 4 days, with raw absorbance of 0.934 in untreated cells and 1.203 in DMSO treated cells (p=0.06) (Figure 3.16A). Following 4 days of continuous treatment with JPIII, the viability of SW480 cells was reduced to 47.7% with 30 µM and 42.6% with 20 µM relative to the vehicle control (Figure 3.16B). The validity of the cellular response was concomitantly tested with the 5-FU positive control. Viability of SW480 cells was reduced to 27.6% after 4 days of continuous treatment with 100 µM 5-FU (p=0.008) (Figure 3.16C).

Viability of HCT116 cells was tested with the DMSO vehicle control alongside untreated cells to determine whether the vehicle compound affected cell viability.

Viability was unaffected by the vehicle control over 4 days, with raw absorbance of 0.754 in untreated cells and 0.573 in DMSO treated cells (p=0.13) (Figure 3.17A). Following 4 days of continuous treatment with JPIII, HCT116 cell viability was reduced to 25% with 30 µM (p<0.001) (Figure 3.17B). The validity of the cellular response was concomitantly tested with the 5-FU positive control. Viability was reduced to 14.1% after 4 days of continuous treatment with 100 µM 5FU (p=0.034) (Figure 3.17C).

In conclusion, the WST1 viability assays suggest that JPIII affects the cellular viability of colorectal cancer cells at the highest micromolar concentrations of the concentration range used.
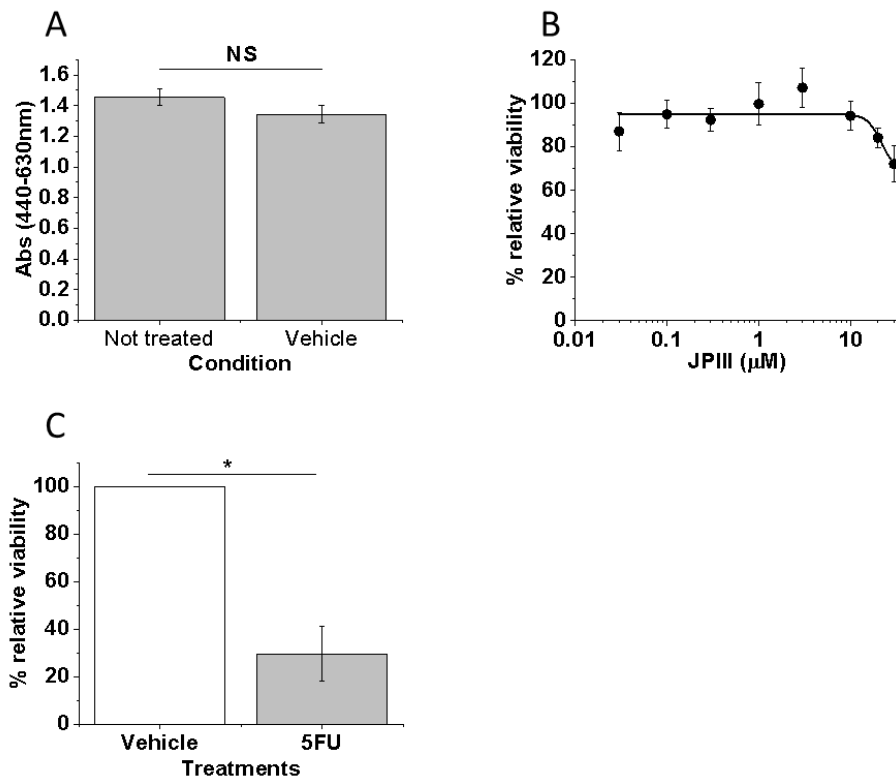
Figure 3.14. Viability of HT-29 cancer cells treated with JPIII for 4 days. A. Bar chart presenting the mean±SEM of the raw absorbance readings obtained from the WST1 cell viability assay for non-treated and DMSO vehicle-treated HT-29 cells; B. Dose-response curve presenting viability of HT-29 treated with JPIII relative to the vehicle control as % viability relative to the vehicle control; C. Bar chart presenting the mean±SEM of the percentage relative viability of HT-29 cells treated with 5-FU (grey bar) relative to the vehicle control (white bar). Key: 5FU = 5 flurouracil. Abs = absorbance. ANOVA testing: * = p≤0.05; ** p=≤0.01; *** p=≤0.001; NS = not significant. All experiments are n/N = 3/3.
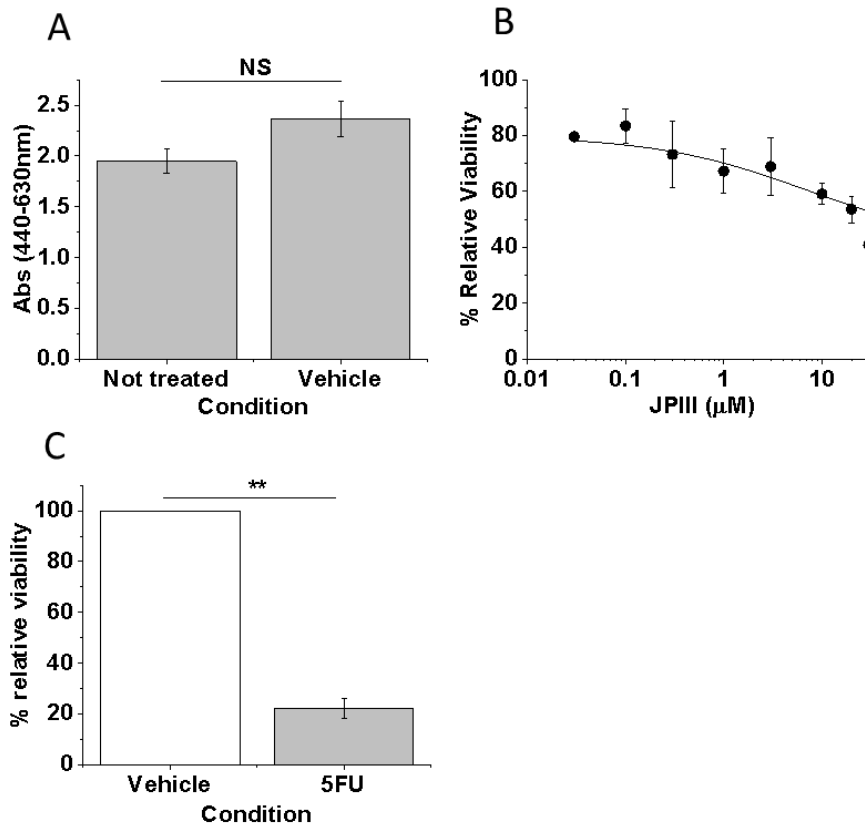
Figure 3.15. Viability of HT-29 cancer cells treated with JPIII for 6 days. A. Bar chart presenting the mean±SEM of the raw absorbance readings from the WST1 cell viability assay for non-treated and DMSO vehicle-treated cells; B. Dose-response curve presenting viability of treated with JPIII relative to the vehicle control; C. Bar chart presenting the mean±SEM of the viability of cells treated with 5-FU (grey bar) relative to the vehicle control (white bar). Key: NS = not significant; Abs = absorbance. ANOVA testing: * = p≤0.05; ** p=≤0.01; *** p=≤0.001; NS = not significant. All experiments n/N = 3/3.

117
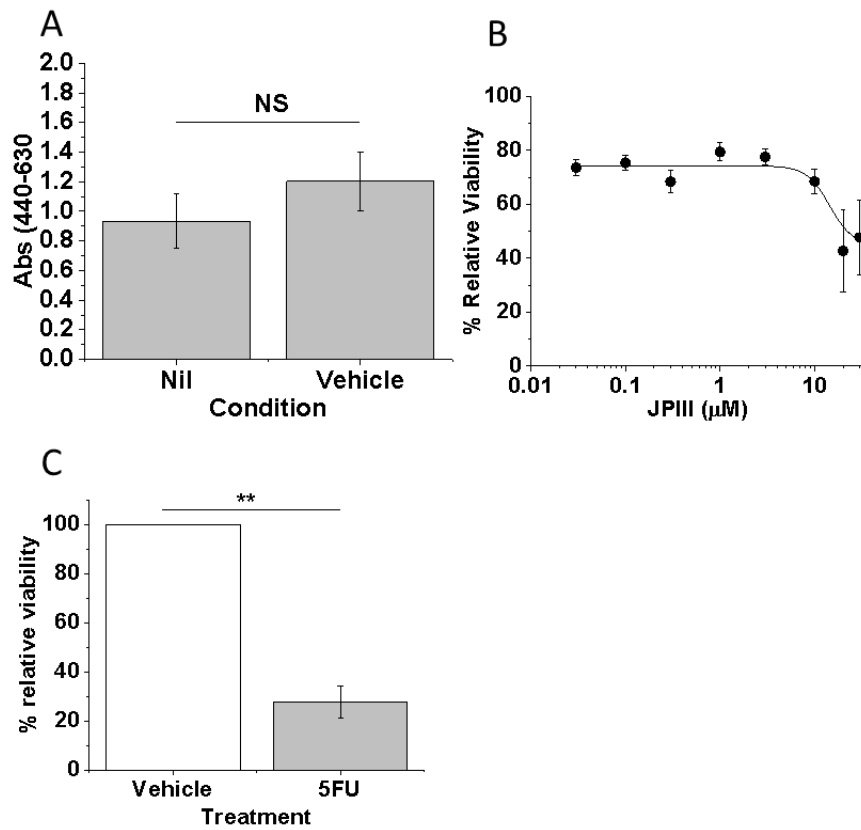
Figure 3.16. Viability of SW480 cancer cells treated with JPIII for 4 days. A. Bar chart presenting the mean±SEM of the raw absorbance readings for the WST1 assay for non-treated and DMSO vehicle-treated SW480 cells (control); B. Dose-response curve presenting viability of SW480 treated with JPIII relative to the vehicle control; C. Bar chart presenting the mean±SEM of the viability of SW480 cells treated with 5-FU (grey box) relative to the vehicle control (white box).Key: Abs = absorbance; $\Delta Ca2+I$ = change in intracellular calcium flux. T testing: * = $p \leq 0.05$; ** $p = \leq 0.01$; *** $p = \leq 0.001$; NS = not significant. All experiments are n/N = 3/3.
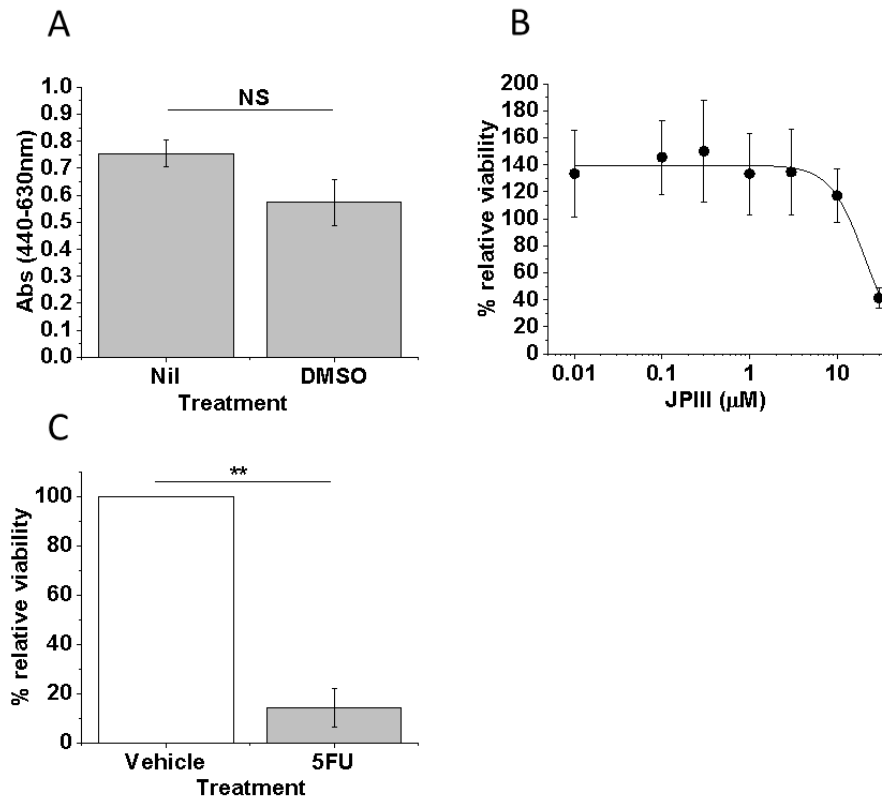
Figure 3.17. Viability of HCT116 cancer cells treated with JPIII for 4 days. A. Mean±SEM of the raw absorbance readings for non-treated and DMSO vehicle-treated HCT116 cells (control); B. Dose-response curve presenting viability of HCT116 treated with JPIII relative to the vehicle control; C. Mean±SEM of the viability of HCT116 cells treated with 5-FU relative to the vehicle control. Key: Abs = absorbance.; $\Delta Ca2+I$ = change in intracellular calcium flux. T testing: * = $p \leq 0.05$; ** $p = \leq 0.01$; *** $p = \leq 0.001$; NS = not significant. All experiments are n/N = 3/3.

3.7. The effect of JPIII on colorectal cancer cell viability and growth characteristics and cell death: growth curves with trypan blue exclusion assay

Growth curves were used to determine the effect of JPIII treatment on growth characteristics. The trypan blue live dead cell viability assay was used to determine whether the reduction in WST1 viability seen with JPIII treatment was cytostatic or cytotoxic. Cell counts were taken over 6 days for both cell lines for cells treated with 30 µM, 10 µM and 3 µM.

HT-29 cells cultured in the DMSO vehicle control displayed the same growth characteristics as untreated cells (Figure 3.18A) and counts did not differ between the two conditions. Viability was reduced by 30 µM and 10 µM JPIII at day 5 and day 6 (Figure 3.18B). Relative viability was 53.5% with 30 µM (p=1.8E-4) and 76.8% at 10 µM (p=0.02) on day 5, and 47.9% at 30 µM (p=4.17E-6) and 83.6% at 10 µM (p=0.013) on day 6 (Figure 3.18B, 3.18C). The other concentrations did not affect cellular viability. Trypan blue count of dead cells showed no difference in the number of dead cells in the presence of all conditions over the duration of the assay (Figure 3.18D).

SW480 cells cultured in the DMSO vehicle control displayed the same growth characteristics as untreated cells (Figure 3.19A) and counts did not differ between the two conditions. Viability was reduced by 30 µM JPIII at day 3, day 4 and day 6 (Figure 3.19B, 3.19C), with a relative viability of 50.9% at day 3 (p=0.036), 45.9% at day 4 (p=0.042) and 48% at day 6 (p=0.03) (Figure 3.19C). There was no effect seen with the other concentrations. Trypan blue count of dead cells showed no difference in cell death with all concentrations over the course of the assay (Figures 3.19D).

In conclusion, the assay validated the results from the WST1 viability assays. JPIII did not cause cell death at any of the higher effective concentration over the course of the assay in either cell line.
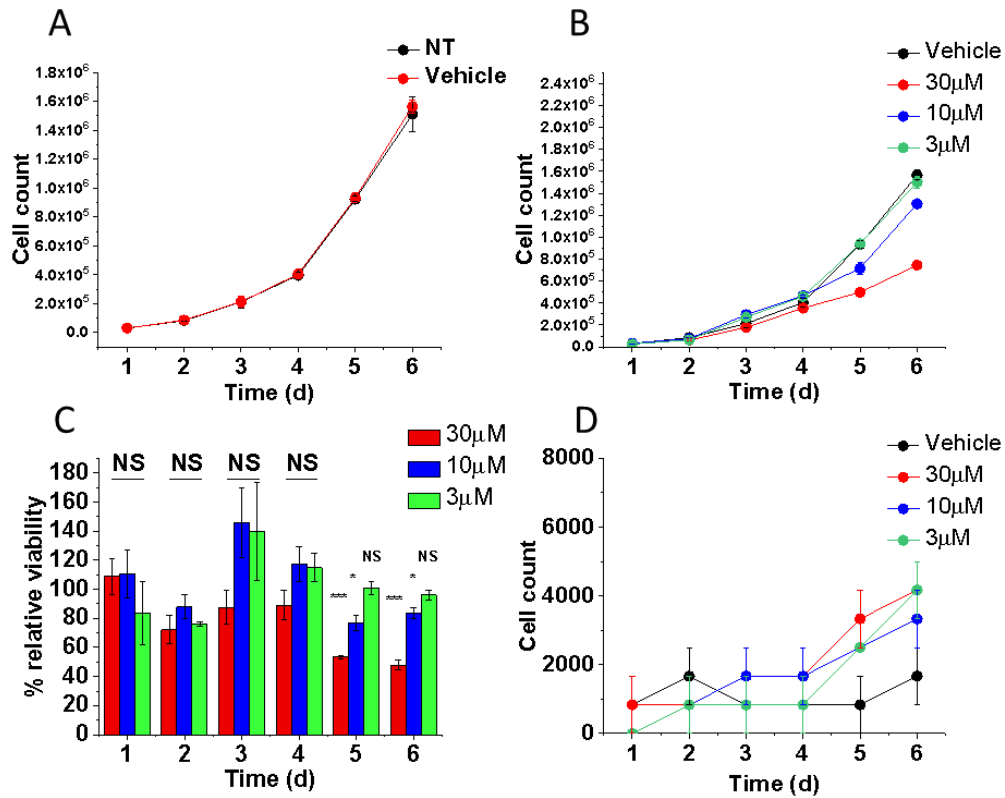
Figure 3.18. The effect of JPIII on HT-29 viability and growth characteristics.

A. Line graph presenting cell growth and viability over 6 days of continuous treatment with no treatment (NT, black line) and DMSO vehicle control (vehicle, red line). B. Line graph presenting viable cell counts over 6 days of continuous treatment with different concentrations of JPIII alongside the vehicle control (black line). C. Bar chart presenting the mean±SEM percentage of viable cells treated with specified concentrations of JPIII relative to the vehicle control. D. Line graph presenting the dead cell count of cells treated with specified concentrations of JPIII alongside vehicle control (black line). Key: d = days. ANOVA testing: * = $p \leq 0.05$; ** $p = \leq 0.01$; *** $p = \leq 0.001$; NS = not significant. All experiments are n/N=3/3.
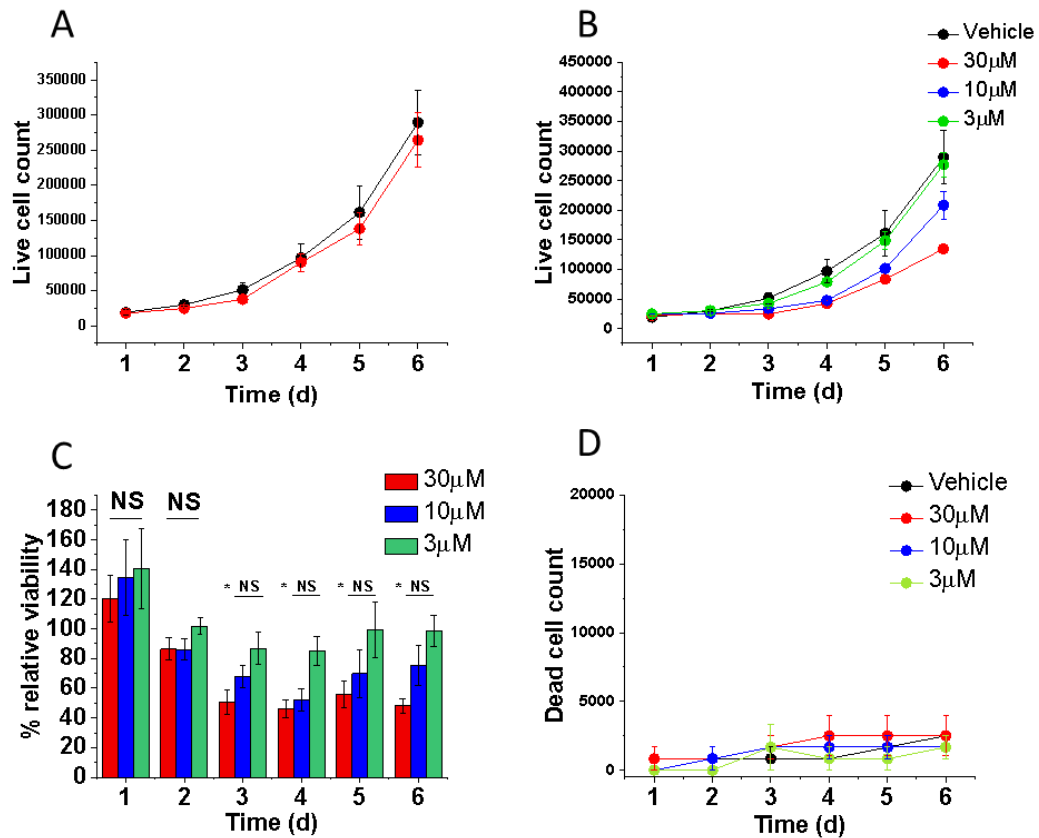
Figure 3.19. The effect of JPIII on SW480 viability and growth characteristics.

The effect of JPIII on HT-29 cell growth and viability. A. Line graph presenting viability and growth over 6 days of continuous treatment with no treatment (NT, black line) and DMSO vehicle control (red line). B. Line graph presenting live/viable cell counts over 6 days of continuous treatment with different concentrations of JPIII alongside the vehicle control (black line). C. Bar chart presenting mean±SEM percentage of viable cells treated with specified concentrations of JPIII relative to the vehicle control. D. Line graph presenting the dead cell count of cells treated with specified concentrations of JPIII alongside vehicle control (black line). Key: d = days. ANOVA testing: * = p≤0.05; ** p=≤0.01; *** p=≤0.001; NS = not significant. All experiments are n/N=3/3.

3.8. The effect of JPIII on colorectal cancer cell clonogenicity

The effect of JPIII on replicative immortality was studied using the colony formation assay. Cells were seeded in a 6-well plate and DMSO vehicle and different concentrations of JPIII were added 4 hours later.

HT-29 cells formed clean colonies. A mean of 101 colonies formed in the presence of DMSO vehicle. Cellular clonogenicity was reduced in response to treatment with concentrations at and above 1 µM (Figure 3.20A). Clonogenicity was reduced to 64.7% with 1 µM (p=0.018), 44.3% with 3 µM (p= 6.04E-4), 33.7% with 10 µM (p= 1.13E-4) and 20.7% with 30 µM (p= 1.8E-5) (Figure 3.20A). Plotting a Hill curve through the colony data allowed extrapolation of an IC50 concentration of 1.79 µM (Figure 3.20B). There were no colonies formed in the presence of 100µM 5FU positive control.

In conclusion, JPIII reduces clonogenicity and replicative immortality. This assay shows that functional effect is only seen using micromolar concentrations. However, the effects are more potent than those seen with the WST1 assay over a longer period of time.
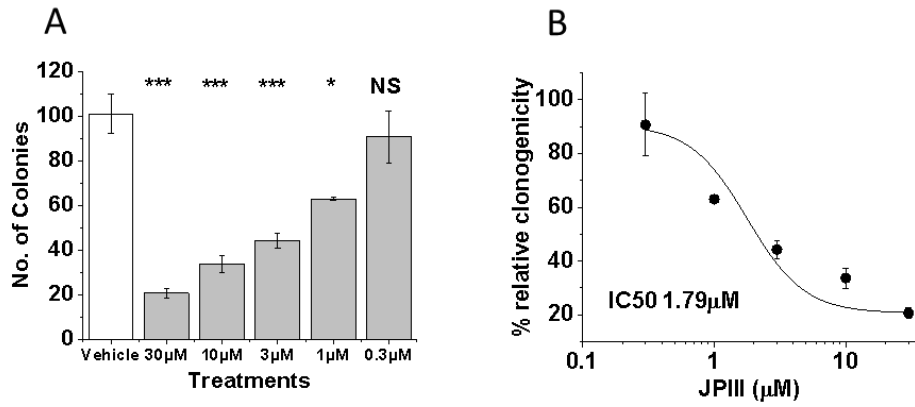
Figure 3.20. The effect of JPIII on HT-29 clonogenicity. A. Bar chart presenting the mean±SEM number of colonies formed in the presence of a range of JPIII concentrations (grey bars) alongside the vehicle control (white bar). B. Dose-response curve fitted to number of colonies treated with each dose relative to the vehicle control. Key: No. = number. ANOVA testing: * = p≤0.05; ** p=≤0.01; *** p=≤0.001; NS = not significant. Experiments are n/N=3/1.

3.9. JPIII reduces colorectal cancer cell migration

The scratch wound assay was used to test anti-migratory effects of JPIII against the colorectal cancer cell lines. A number of important optimisation steps were undertaken with each cell line prior to carrying out the assay, namely serum culture conditions and the choice of mitogen.

3.9.1. Optimisation

The effect of different levels of serum deprivation on cellular proliferation were tested using trypan blue growth counts. HT-29 cells that were serum starved for 24 hours continued to proliferate, with an increase of cell number from 12,139 to 24,992 (p=2.02E-4). However, following subsequent culture in 0.5% serum media the cells did not proliferate (cell count 29,188, p=0.16) (Figure 3.21A). There was no increase in cell death over this 24-hour culture period (p=1) (Figure 3.21B), therefore 0.5% serum culture following a 24-hour serum starvation period was deemed optimal for arresting proliferation without causing cell death. Proliferation of cells cultured in 48 hours did not alter significantly (from 24,992 to 20,028, p=0.07) (Figure 3.21A). However, the number of dead cells increased from 1,667 to 26,333 (p=0.01) (Figure 3.21B). Therefore, prolonged serum starvation was not used.

SW480 cells that were serum starved for 24 hours continued to proliferate, with an increase of cell number from 20,833 to 34,444 (p=0.02) (Figure 3.21C). However, following subsequent culture in 0.5% serum media the cells did not proliferate (cell count 35,972, p=1). There was no increase in cell death over this 24-hour culture period (p=1) (Figure 3.21D), therefore 0.5% serum culture following a 24-hour serum starvation period was deemed optimal for arresting proliferation without causing cell death. There was a fall in the number of proliferating cells following 48 hours of continuous serum starvation (24 hour mean cell count 34444, 48-hour mean cell count 22361, p=0.045) (Figure 3.21C). In addition, the number of dead cells increased from 1,667 to 25,000 (p=0.033) (Figure 3.21D). Therefore, prolonged serum starvation was not used.

Following serum starvation, the migratory response of the colorectal cells to different mitogens was tested in 0.5% serum. In HT-29 cells, the relative wound density (RWD) of untreated (vehicle control) cells at 24 hours was 25.1%, whereas 50 ng/ml of EGF stimulated migration (RWD of 42.3%, p=2.19E-5) (Figure3.21E). However, 30 ng/ml of VEGF and PDGF did not have any effect on migration (VEGF

27.1%, p=1; PDGF 28.9%, p=0.64) (Figure 3.21E). In SW480, the RWD of untreated (vehicle control) cells at 24 hours was 31%, whereas 50 ng/ml of EGF stimulated migration (RWD of 43.6%, p=1.63E-4) (Figure 3.21F). However, 30 ng/ml of VEGF and PDGF did not have any effect on migration (24 hours VEGF 33% p=1, PDGF 33.7% p=0.61) (Figure 3.21F).

In order to determine whether this concentration of EGF was affecting cellular proliferation, the trypan live dead cell assay was used to quantify cellular proliferation using the same conditions of serum starvation and culture in reduced-serum media with and without EGF for 24 hours, the length of the kinetic migration assay. Following 24 hours of serum starvation, 24 hours of culture of HT-29 cells in 0.5% serum media with 50 ng/ml EGF did not increase cellular proliferation (cell count 28778 in serum-only, 30,493 in EGF-supplemented media, p=0.96) (Figure 3.21G). SW480 cells cultured in the same conditions did not proliferate (cell count 39,028 in serum-only, 40489 in EGF-supplemented media, p=1) (Figure 3.21H). In conclusion, this verified that 50 ng/ml of EGF did not affect cellular proliferation in the migration assay conditions.

VEGF has been shown to induce endothelial cell migration in previous angiogenic studies. Intracellular calcium measurements carried out using the FlexStation have also shown that adding VEGF to the cells induces calcium store release and induces an influx of calcium(Li et al., 2015b), which will also be seen later in this chapter. EGF-induced store depletion has previously been reported in the breast cancer cell line MDA-MB-468, and EGF-induced store depletion could be inhibited by S66 and YM58483(Azimi et al., 2018). Intracellular calcium measurements were therefore carried out on the FlexStation in order to determine whether EGF would induce store depletion.

EGF was added to Fura2-loaded cells in calcium-free recording buffer. There was no change in the intracellular calcium levels in HT-29 (Figure 3.22A) or SW480 (Figure 3.22B) over a 10-minute recording period. This suggests that EGF did not induce depletion of intracellular stores.

EGF was added to Fura2-loaded cells in calcium-containing recording buffer. There was no change in the intracellular calcium levels in HT-29 (Figure 3.22C) and SW480 (Figure 3.22D). This suggests that EGF did not induce calcium entry from the extracellular environment.

3.9.2. Effect of JPIII on Cell Migration

Cellular migration was tested with different concentrations of JPIII in EGF-supplemented media alongside an EGF-free vehicle control to validate cellular response. EGF stimulated migration in both cell lines. HT-29 cells responded appropriately with an RWD of 14.9% in vehicle-treated cells and 41.8% in EGF-treated cells (Figure 3.23A). In HT-29, 30 µM JPIII reduced EGF-induced migration, with 28.8% migration at 24 hours (p=0.05) (Figure 3.23B, 3.23C), but 10 µM did not affect cellular migration (38.4%, p=1) (Figure 3.23B, Figure 3.23C).

In SW480, cells responded to EGF stimulation appropriately with an RWD of 29.44% in vehicle-treated cells and 42.98% in EGF-treated cells (p=0.007) (Figure 3.24A, Figure 3.26C). JPIII reduced EGF-induced migration to 21.3% with 30 µM (p=1.9E-4) and to 24.9% with 10 µM (p=8.53E-4). However, 3 µM did not reduce migration (RWD 39.6%, p=1) (Figure 3.24B, Figure 3.24C). In conclusion, JPIII reduced EGF-induced migration at high concentrations only.
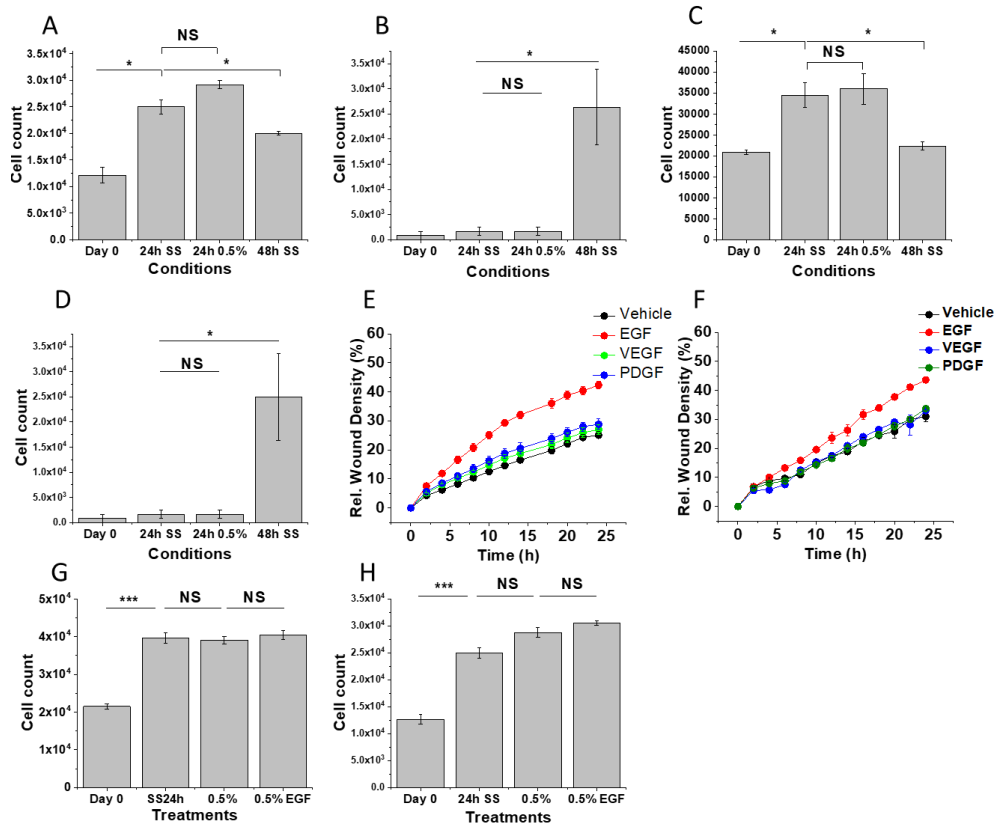
Figure 3.21. Optimisation of conditions for the scratch wound assay. A and C. Bar charts presenting mean±SEM cell counts of cells cultured in different serum conditions: A. HT-29; C. SW480. B and D. Nar chart presenting the mean±SEM cell counts of dead cells cultured in different serum conditions: B. HT-29; D. SW480. E-F. Line graph presenting kinetic migration of cells treated with different mitogens EGF (red), VEGF (green) and PDGF (blue) alongside vehicle (black): F. HT-29; G. SW480. G-H. Bar charts presenting mean±SEM cell counts in different serum culture conditions with and without EGF: G. HT-29; H. SW480. Key: standard culture serum (baseline); 0% serum media for 24 hours (24h SS); cells serum starved for 24 hours then cultured in 0.5% serum for a further 24 hours (0.5%); cells cultured in 0% serum media for 48 hours (48h SS); cells serum starved for 24 hours then treated with 50 ng/ml EGF in 0.5% serum for 48 hours (0.5%EGF). h=hours. ANOVA testing: * = p≤0.05; ** p=≤0.01; *** p=≤0.001; NS = not significant.All experiments n/N=3/3
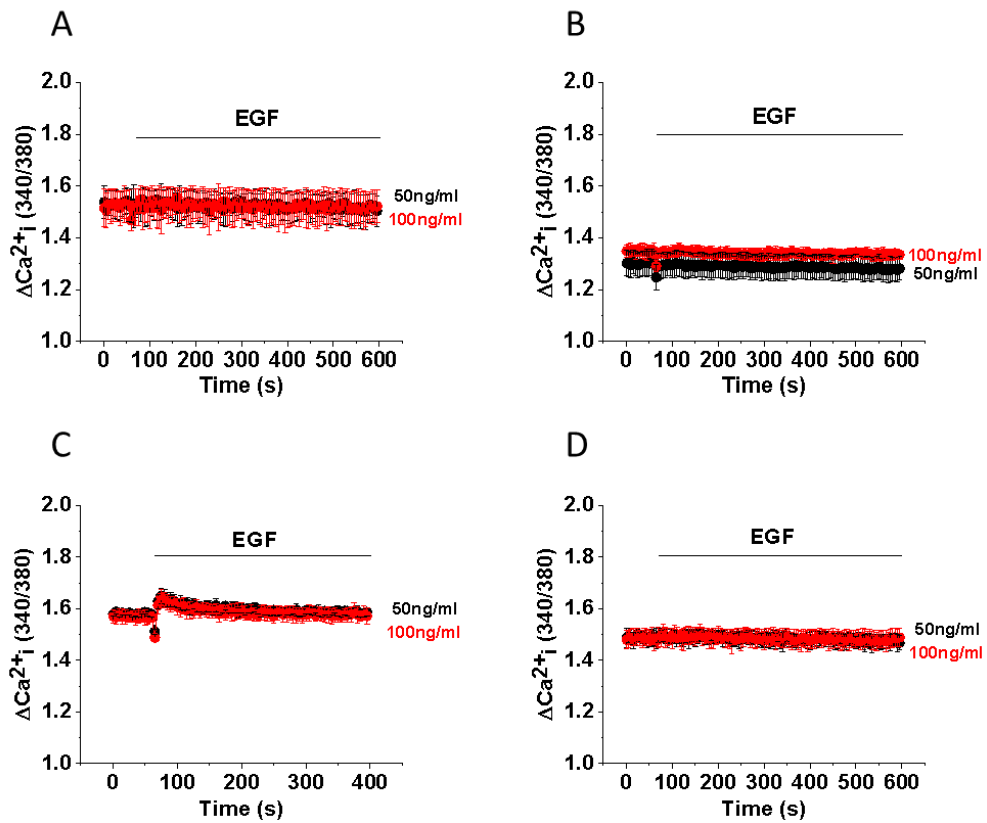
Figure 3.22. The effect of EGF on store depletion and CRAC channel activity. A-B. Cytoplasmic calcium traces of cells in calcium-free recording buffer treated with 50ng/ml (black line) and 100ng/ml (red line) of EGF added to the cells 60 seconds into the trace: A. HT-29; B. SW480. C-D. Cytoplasmic calcium traces of cells in calcium-containing recording buffer treated with the 2 concentrations of EGF at 60 seconds: C. HT-29; D. SW480. Key: s = seconds; EGF = epidermal growth factor. All experiments n/N=3/4.
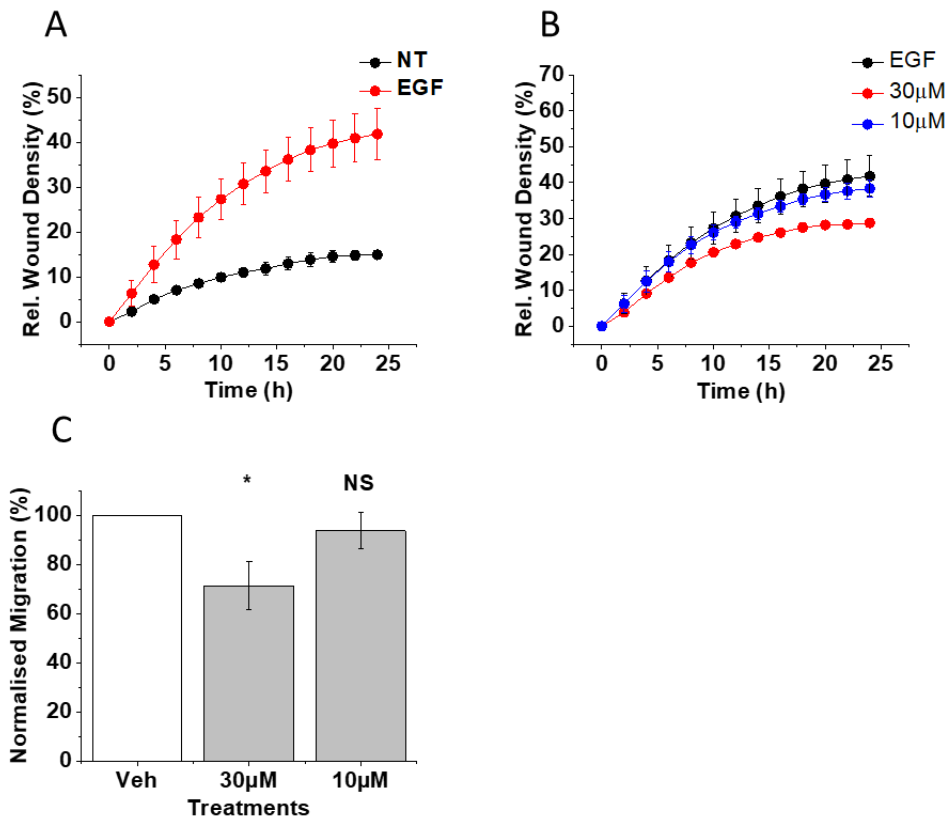
Figure 3.23. The effect of JPIII on HT-29 migration. A. Line graph presenting kinetic migration of untreated (NT, black line) cells and cells treated with 50ng/ml EGF (EGF, red line). B. Line graph presenting kinetic migration of cells treated with JPIII alongside the EGF control (black line). C. Bar chart presenting mean±SEM migration at 24 hours of cells treated with JPIII relative to the vehicle control, derived from data in Figure B. Key: h = hours; Rel. = relative. ANOVA testing: * = p≤0.05; ** p=≤0.01; *** p=≤0.001; NS = not significant. All experiments are n/N = 3/3.
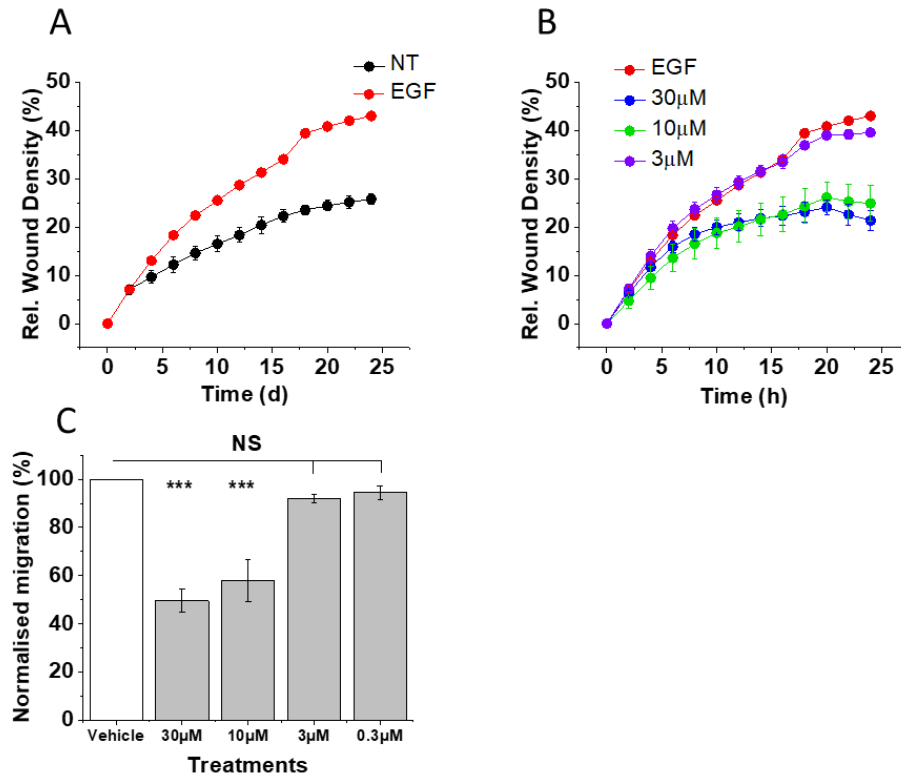
Figure 3.24. The effect of JPIII on SW480 migration. A. Line graph presenting kinetic migration of untreated cells (NT, black line) and cells treated with 50 ng/ml EGF (EGF, red line). B. Line graph presenting kinetic migration of cells treated with JPIII alongside the EGF control (red line). C. Bar chart presenting mean±SEM migration at 24 hours of cells treated with JPIII relative to the vehicle/EGF control (white bar), derived from data from Figure B. Key: h = hours; Rel. = relative. ANOVA testing: * = $p \leq 0.05$; ** $p = \leq 0.01$; *** $p = \leq 0.001$; NS = not significant. All experiments are n/N = 3/3.

3.10. JPIII reduces colorectal cancer invasion

The Transwell chamber assay was used to test whether JPIII would inhibit cellular invasion. The Transwell inserts were coated with Matrigel within the laboratory. The seeding density was also optimised prior to initiating the assay. Only the 30 µM concentration was tested, chosen as the only concentration that inhibited migration in the scratch wound assay.

In HT-29, JPIII inhibited invasion. There was a mean of 58 invaded cells following treatment with 30 µM JPIII compared to 170 cells treated with the vehicle control (p=0.012) (Figure 3.25A). There was no invasion with the serum-free negative control (serum-free media 3 cells, vehicle control 170 cells, p=0.004) (Figure 3.25A).

In SW480, JPIII inhibited invasion. There was a mean of 60 invaded cells following treatment with 30 µM JPIII compared to 95 cells (p=0.04) (Figure 3.25B). There was no invasion with the serum-free negative control (serum-free media 3 cells, vehicle control 95 cells, p=0.012) (Figure 3.25B).

In conclusion, JPIII inhibits cancer cell invasion.
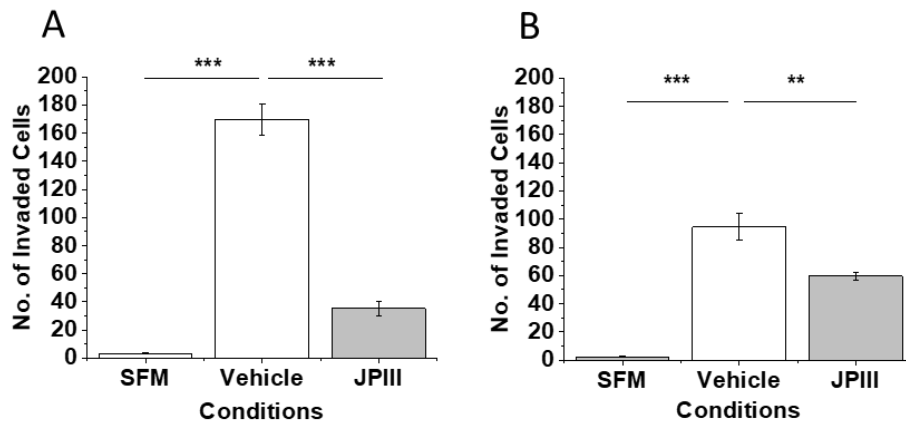
Figure 3.25. The effect of JPIII on cell invasion. A-B: Bar charts presenting the mean±SEM number of invaded cells, with data for the vehicle (white bar) and 30µM JPIII (JPIII, grey bar) alongside a serum free chemoattractant control (SFM, grey bar). A. HT-29; B. SW480. ANOVA testing: * = p≤0.05; ** p=≤0.01; *** p=≤0.001; NS = not significant. All experiments are n/N=3/2. SFM = serum free media.

3.11. JPIII results in acidification of the culture medium

Treatment with JPIII resulted in a visible change in colour of the culture medium at higher concentrations of 30 µM and 10 µM that was visible within the first 24 hours of treatment (HT-29 Figure 3.26). This phenomenon was present in both HT-29 and SW480 cell lines. The pH of the culture media was therefore determined over a 72-hour period.

In HT-29 cells, changes in culture medium pH over the 3 time points were compared for each treatment condition (Table 3.3). The pH of the vehicle-control media did not change between 24 and 48 hours of culture but it did fall at 72 hours. This would be expected as the nutrients would start to be depleted by the cells and metabolic waste products would be accumulating in a closed culture system. The pH of the medium containing 30 µM fell steadily over each time point. The pH of the medium containing 10 µM fell from 24 to 48 hours of treatment but did not fall further between 48 and 72 hours. In HT-29 cells, the media pH was compared to the vehicle control for each time point (Table 3.3). Treatment with 30 µM JPIII resulted in acidification of the culture medium compared to the vehicle control at 24 hours (p=0.018), 48 hours (p=9E-6) and 72 hours (p=1.2E-6), with steadily falling pH at each time point. The pH of 10 µM-containing medium was not altered compared to the vehicle control at 24 hours (p=1), but was acidified at 48 hours (p= 9.6E-5). However, there was no difference between drug and vehicle-containing medium at 72 hours (p=0.06).

For SW480 cells, changes in culture medium pH over the 3 time points were compared for each treatment condition (Table 3.4). The pH of the vehicle-control media fell between 24 to 48 hours and fell further from 48 hours to 72 hours. The pH also fell steadily over the 3 time points for 30 µM-containing media. The pH of 10 µM containing media also steadily fell over the 3 time points. In SW480 cells, the media pH was compared to the vehicle control for each time point (Table 3.4). The pH of 30 µM containing media was lower than that of the vehicle (p= 1.2E-4) but there was no difference between vehicle and 10 µM. However, at 48 hours the pH of both 30 µM- and 10 µM-containing media was lower than the vehicle media at 48 hours (30µM, p= 8.14E-5; 10µM p= 0.004). Similarly, at 72 hours the pH of both 30 µM- and 10 µM-containing media was lower (30µM p= 3.12E-6; 10µM p= 7.1E-5).

In order to determine whether variations in pH were independent of cellular processes (e.g. drug stability in serum-containing media in a HCO_3/CO_2 buffering

system), the pH of drug-containing media was tested following culture in the 5% CO_2 37°C incubator in a cell free environment. pH was not altered in cell-free DMEM media cultured over the three time points. Similarly, pH was not altered in cell-free RPMI media cultured over the three time points. The pH of media containing 30μM and 10μM JPIII was not altered over any of the time points. These results demonstrate that neither the vehicle compound nor the drug at the tested concentrations had any independent effect on the pH of the culture media.

In conclusion, cancer cell treatment with JPIII at concentrations with proven functional effect on the cancer cell lines was seen to generate acidity in the culture environment.
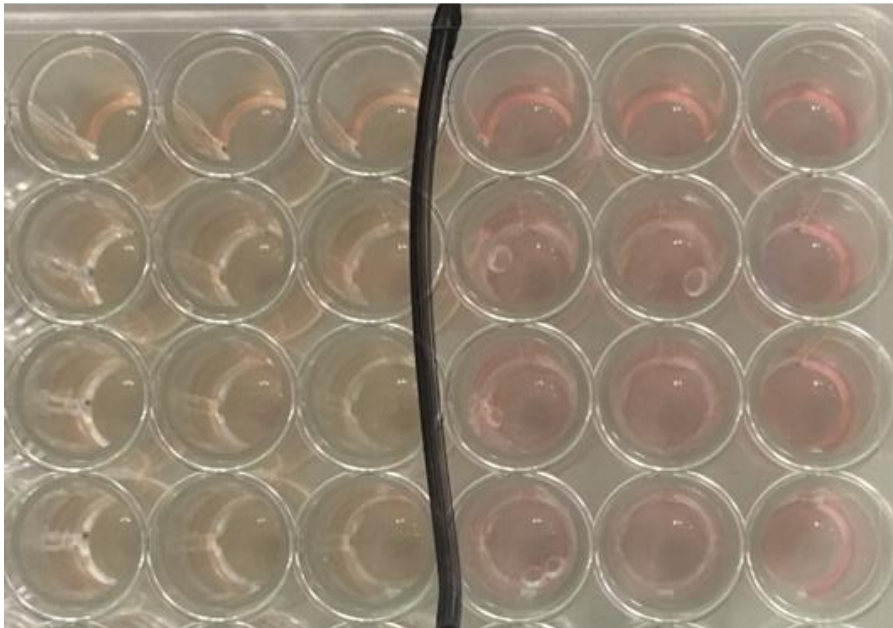
Figure 3.26. Representative photomicrograph of HT-29 cells in DMEM media culture that demonstrates the visible colour difference between vehicle-treated cells to the right of the plate and JPIII-treated cells to the left of the plate following 24 hours of culture.

	24 hours	48 hours	72 hours
Media only	7.9	7.88 (NS)	7.64 (NS)
Vehicle	7.83	7.67 (NS)	7.38 (p=0.016)
30µM JPIII	7.62	7.08 (p=2.5E-5)	6.62 (p=5.8E-5)
10µM JPIII	7.85	7.28 (p= 1E-6)	7.28 (p=1)
Media only cell free	7.78	7.86 (NS)	7.63 (NS)
Vehicle media cell free	7.82	7.82 (NS)	7.68 (NS)
30µM JPIII cell free	7.82	7.79 (NS)	7.77 (NS)
10µM JPIII cell free	7.8	7.82 (NS)	7.75 (NS)

Table 3.3. pH measurements of drug-containing DMEM media. NS = not significant.

	24 hours	48 hours	72 hours
Media only	7.45	7.42 (NS)	7.42 (NS)
Vehicle	7.42	7.2 (p= 0.004)	7.06 (p= 0.02)
30µM JPIII	7.12	6.66 (p= 7.2E-7)	6.6 (p=0.03)
10µM JPIII	7.49	6.94 (p= 4E-5)	6.79 (p= 0.04)
Media only cell free	7.47	7.45 (NS)	7.47 (NS)
Vehicle media cell free	7.46	7.45 (NS)	7.49 (NS)
30µM JPIII cell free	7.44	7.46 (NS)	7.45 (NS)
10µM JPIII cell free	7.46	7.45 (NS)	7.47 (NS)

Table 3.4. pH measurements of drug-containing RPMI 1640 media. NS = not significant.

3.12. pH modulates CRAC Channel Activity

Tumours grow into three- dimensional structures that experience fluxes of nutrients such as oxygen, glucose and amino acids, with metabolic by-product accumulation due to poor neovasculature. These deficient conditions have been shown to have clinicopathological consequences with disease progression and responses to treatment (Vaupel et al., 2001, Schlappack et al., 1991). These conditions have also been found to create an acidotic extracellular environment within the tumour. Acidic or nutrient deficient conditions have been reported to alter signalling pathways, including iCRAC signalling. Acidification of the extracellular media to pH 6.4 has been found to inhibit ORAI1-mediated CRAC channel signalling in vascular smooth muscle cells. Beck and colleagues found that acidification to pH 6 completely blocked CRAC channel signalling whereas alkalinisation to pH 8.3 potentiated CRAC signalling(Beck et al., 2014).

In order to determine the effect of pH on CRAC channel function in colorectal cancer cells, intracellular calcium measurements were carried out on cells using the FlexStation with salt-buffered pH solutions of 6, 6.8, 7.4 and 8.3. This range encompassed the pH ranges found in the cancer culture conditions found in JPIII culture detailed in the last section, whilst also including the extreme ranges studied in the study by Beck and colleagues. Calcium was added back to cells in salt-buffered solutions of the same pH ranges.

In HT-29 cells, CRAC channel function was completely abrogated at pH 6 (corrected calcium amplitude -0.00535) (Figure 3.27A) compared to standard pH 7.4 conditions (p=4.1E-7). Calcium traces of CRAC channel activity are presented for cells treated in pH 6.8 (Figure 3.27B) and pH 7.4 (Figure 3.27C) conditions. The peak amplitude for cells in pH 6.8 was 0.66 (Figure 3.27E) and the area under the curve was 605.2 (Figure 3.27F). However, the peak amplitude for cells in pH 7.4 was 0.61 (Figure 3.27E) and the area under the curve was 602.1 (Figure 3.27F). There was no difference between the amplitude (p=1) or the area under the curve (p=1) between these 2 conditions. Time to reach the peak calcium amplitude did not differ between cells at pH 6.8 than at pH 7.4 (pH 6.8 168.5 seconds, pH 7.4 155.1 seconds, p= 0.34) (Figure 3.27G). Calcium traces for cells treated in pH 8.3 are presented in Figure 3.27D. The peak calcium amplitude did not differ from pH 7.4 (amplitude 0.69, p=0.3) (Figure 3.27E). However, there was a faster calcium rise to peak amplitude (100.1 seconds, p=7.9E-4) (Figure 3.27G). Intracellular calcium levels fell quicker, which is demonstrated by a relative fall in the area under the curve (area

under the curve 486.5, p=0.002) (Figure 3.27F). This data suggests that alkalinisation of the media potentiates a more rapid calcium entry that may then contribute to a more rapid inactivation of CRAC channel signalling.

In SW480 cells, CRAC channel function was completely abrogated at pH 6 (corrected calcium amplitude 0.00137) (Figure 3.28A) compared to standard pH 7.4 conditions (corrected calcium amplitude 0.5, p=1.4E-6). Calcium traces of CRAC channel activity are presented for cells treated in pH 6.8 (Figure 3.28B) and pH 7.4 (Figure 3.28C) conditions. The peak amplitude for cells in pH 6.8 was 0.59 (Figure 3.28E) and the area under the curve was 548.5 (Figure 3.28G). However, the peak amplitude for cells in pH 7.4 was 0.53 (Figure 3.28E) and the area under the curve was 540.9) (Figure 3.28G). There was no difference between the amplitude (p=0.78) or the area under the curve (p=0.96) between these 2 conditions. However, time to reach the peak calcium amplitude was slower in pH 6.8 than in pH 7.4 (pH 6.8 220 seconds, pH 7.4 208 seconds, p= 0.007) (Figure 3.28F). Calcium traces for cells treated in pH 8.3 are presented in Figure 3.28D. The peak calcium amplitude did not differ from pH 7.4 (amplitude 0.54, p=1) (Figure 3.28E). However, there was a faster calcium rise to peak amplitude (141.8, p=0.017) (Figure 3.28F). Intracellular calcium levels fell quicker, which is demonstrated by a fall in the area under the curve (under the curve 490.8, p=0.001) (Figure 3.28G). This data suggests that alkalinisation of the media potentiates a more rapid calcium entry that may then contribute to a more rapid inactivation of CRAC channel signalling.

In conclusion, this work successfully reproduced the effects of acidity (pH 6) and alkalinity (pH 8.3), whilst determining that the range of acidity found following JPIII treatments do not impact on CRAC channel function.
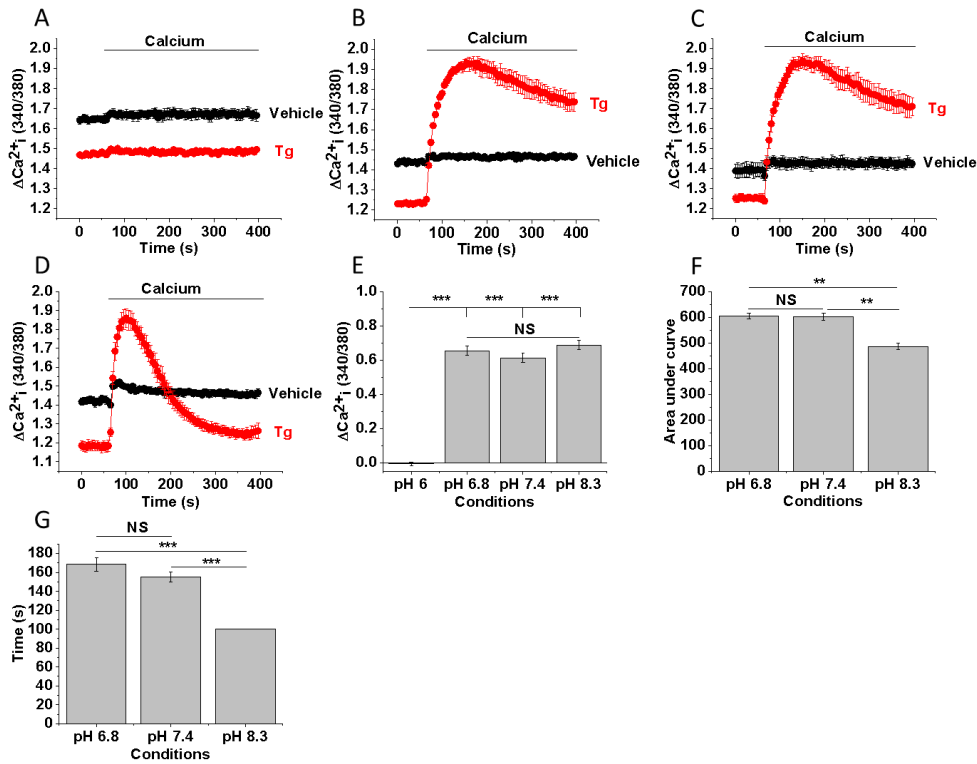
Figure 3.27. The effect of pH on CRAC channel function in HT-29 cells. A-D. Cytoplasmic calcium traces of cells pre-incubated in calcium-free buffer with either 1 μM thapsigargin (Tg, red line) or vehicle (black line) prior to calcium addback. All buffers were calibrated to 4 different pH ranges: A. pH 6; B. pH 6.8; C. pH 7.4; D. pH 8.3. E-G. Bar charts presenting mean±SEM calcium data obtained across the 4 pH ranges: E. Peak amplitude; F. Area under the curve. G. Time to peak amplitude. Key: s = seconds. ANOVA testing: * = p≤0.05; ** p=≤0.01; *** p=≤0.001; NS = not significant. All experiments are n/N=3/3.
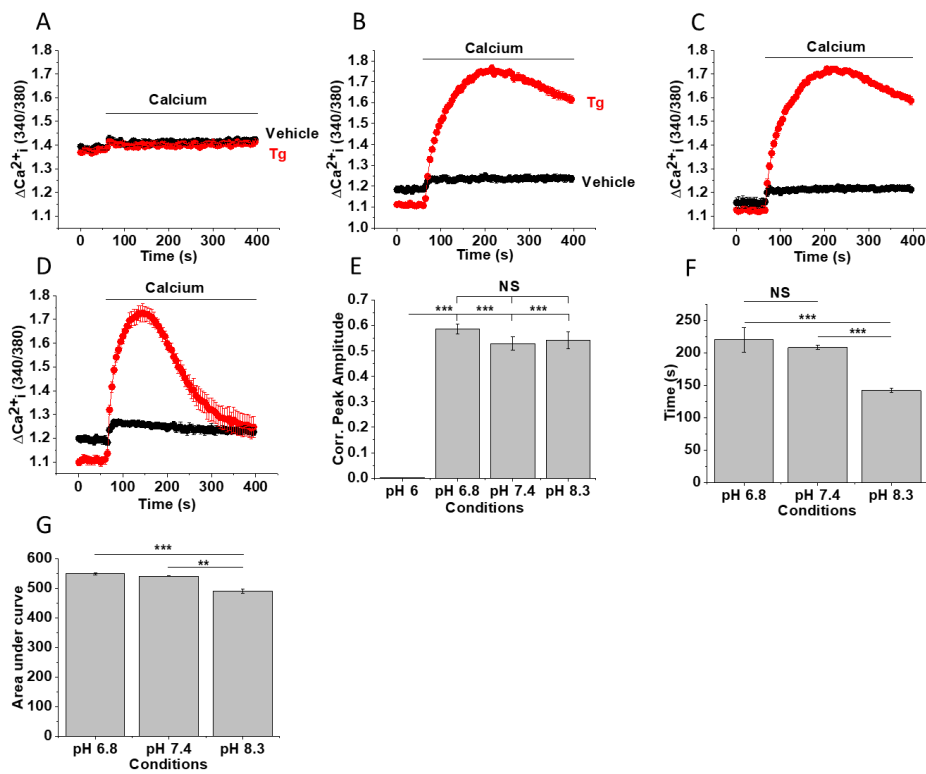
Figure 3.28. The effect of pH on CRAC channel function in SW480. Cytoplasmic calcium traces of cells pre-incubated in calcium-free buffer with either 1 µM thapsigargin (Tg, red line) or vehicle (black line) prior to calcium addback. All buffers were calibrated to 4 different pH ranges: A. pH 6; B. pH 6.8; C. pH 7.4; D. pH 8.3. E-F. Bar chart presenting the mean±SEM calcium data across the 4 pH ranges: E. Peak amplitude; F. Rate of rise; G. Area under the curve. Key: s = seconds. ANOVA testing: * = p≤0.05; ** p=≤0.01; *** p=≤0.001; NS = not significant. All experiments are n/N=3/3.

Intracellular calcium measurements were taken on the FlexStation to further explore the effect of acidity on CRAC channel signalling, to determine whether alterations of pH affect store depletion.

Fura2-loaded cells were incubated in calcium-free recording buffer calibrated to the 4 different pH ranges for 20 minutes prior to addition of 1 μM thapsigargin. The kinetics of store depletion in the 4 conditions were studied.

In HT-29 cells, store depletion was seen in all 4 pH conditions. The kinetics of the calcium responses were similar across all 4 pH ranges (Figures 3.29A-D). The peak amplitude of the calcium response did not differ between the 4 conditions (pH 6 0.55, pH 6.8 0.43, pH 7.4 0.44, pH 8.3 0.3, $p > 0.05$) (Figure 3.29E). The area under the curve did not differ between pH 6, 6.8 and 7.4 (pH 6 AUC 970.9, pH 6.8 AUC 940.6, pH 7.4 962.8, $p > 0.05$). However, the AUC of cells in pH 8.3 was lower than that at pH 6 ($p = 0.015$) and pH 7.4 (0.026) (Figure 3.29F). This data suggested that there was minimal effect of pH on store depletion in HT-29 cells.

In SW480 cells, store depletion was seen in all 4 pH conditions. The kinetics of the calcium responses were similar across all 4 pH ranges (Figures 3.30A-D). The peak amplitude of the calcium response did not differ between the 4 conditions (pH 6 = 0.17, pH 6.8 = 0.21, pH 7.4 = 0.1, pH 8.3 = 0.21, $p > 0.05$) (Figure 3.30E). The area under the curve did not differ between the 4 conditions (pH 6 = 729, pH 6.8 = 725, pH 7.4 = 697, pH 8 = 3 668) (Figure 3.30F). This data suggested that there was no effect of pH on store depletion in SW480 cells.
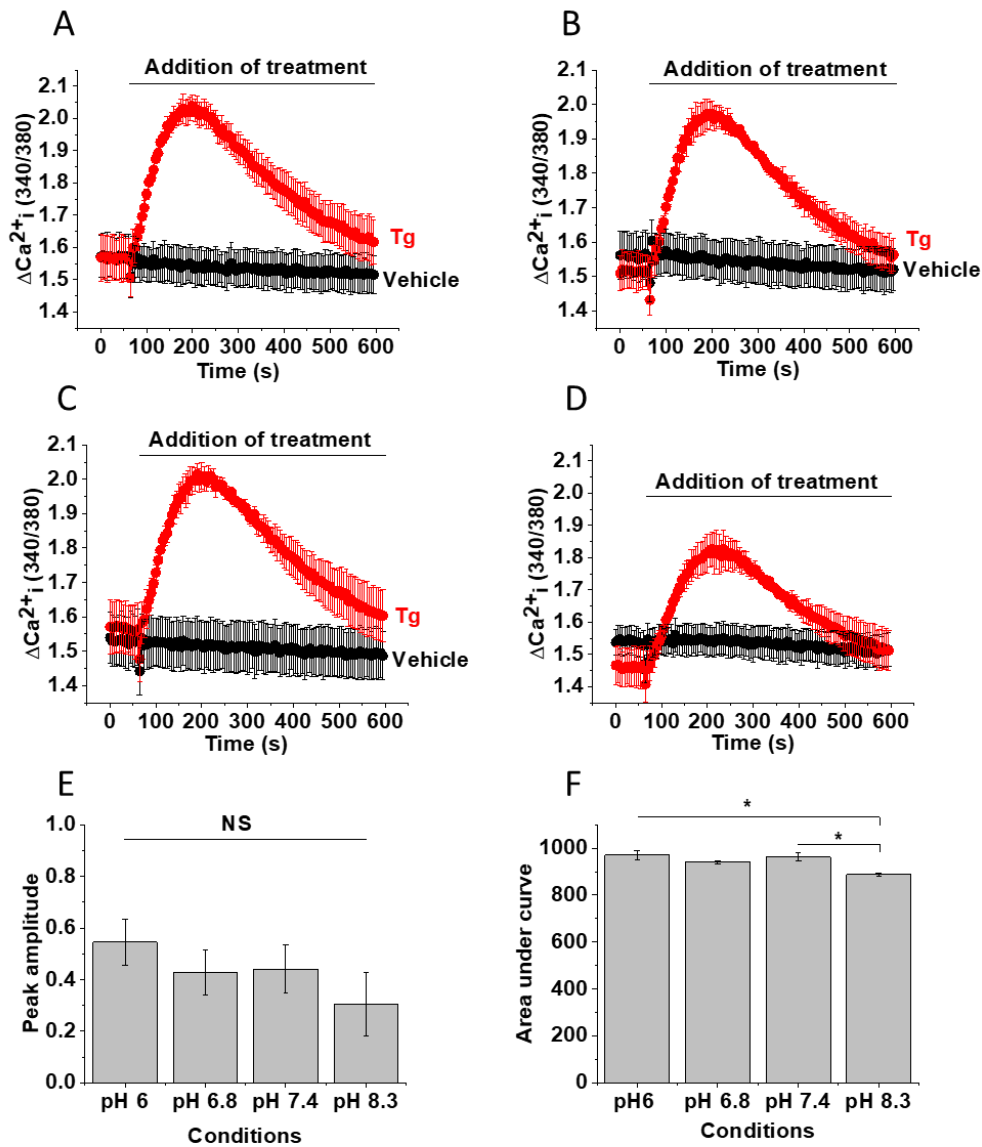
Figure 3.29. The effect of pH on store depletion in HT-29 cells.

A-D. Cytoplasmic calcium traces of HT-29 cells treated with thapsigargin (Tg, red line) or vehicle control (black line) in calcium free recording buffer. All buffer conditions were calibrated to 4 different pH conditions: A. pH 6; B. pH 6.8; C. pH 7.4; D. pH 8.3. E. Bar chart presenting mean±SEM peak calcium amplitude derived from A-D. F. Bar chart presenting area under the curve derived from figures A-D. Key: s = seconds. ANOVA testing: * = p≤0.05; ** p=≤0.01; *** p=≤0.001; NS = not significant. All experiments n/N are 3/4.
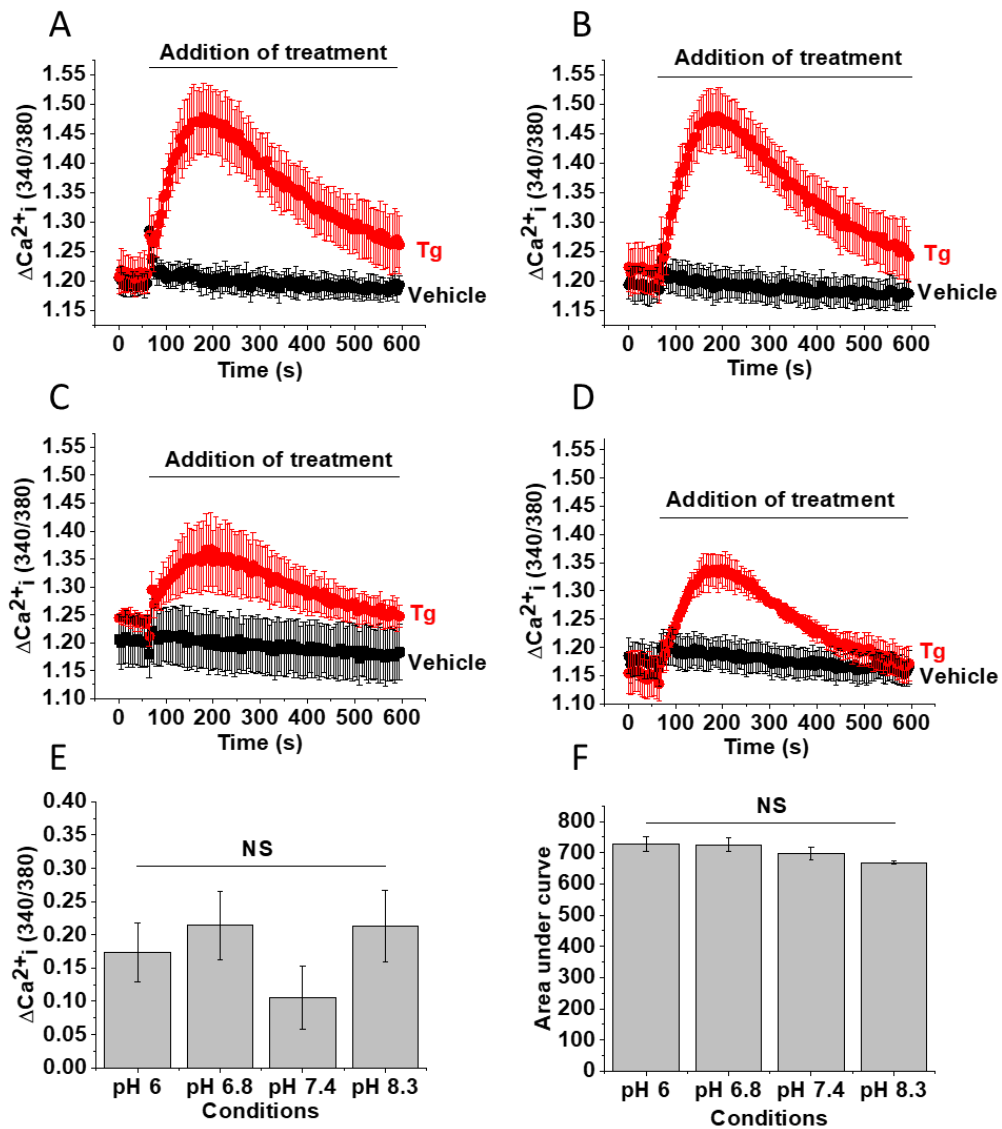
Figure 3.30. The effect of pH on store depletion in SW480 cells.

A-D. Cytoplasmic calcium traces of HT-29 cells treated with thapsigargin (Tg, red line) or vehicle control (black line) in calcium free recording buffer. All buffer conditions were calibrated to 4 different pH conditions: A. pH 6; B. pH 6.8; C. pH 7.4; D. pH 8.3. E. Mean±SEM of the peak calcium amplitude derived from A-D. F. Bar chart presenting area under the curve derived from figures A-D. All experiments n/N are 3/4.

3.13. The effect of *in vitro* JPIII treatment on CRAC channel activity

So far, work has described the anti-cancer effects of JPIII on cancer cell functions relevant to tumourigenesis following prolonged *in vitro* treatment over a number of days. However, the effect of CRAC channel inhibitors in serum culture on CRAC channel function has not previously been reported in the literature. HT-29 cells were plated at a seeding density to generate confluent monolayers for FlexStation testing, and media changed to drug- or vehicle-containing media once the cells had attached to the microplate 6 hours later. Following 24 hours of drug culture, cells were loaded with Fura2 and store depleted with thapsigargin in calcium-free buffer. Calcium addback traces were recorded.

Cells that had been cultured in DMSO vehicle control (vehicle-culture cells) displayed thapsigargin-induced CRAC channel activity (Figure 3.31A) with a peak calcium rise of 0.66. JPIII at 10 µM resulted in 75.3% inhibition of calcium entry (Figure 3.31B). There was no difference in peak calcium amplitude of the vehicle control for either the vehicle-precultured or JPIII-precultured cells (Figure 3.31C). However, in JPIII-precultured cells, there was a drastic decrease in CRAC channel activity (Figure 3.31D). Peak amplitude for CRAC channel calcium entry fell from 0.75 in vehicle-pretreated cells to 0.20 in JPIII-pretreated cells (p=0.007) (Figure 3.31E). The peak amplitude of CRAC channel calcium entry did not differ between vehicle-pretreated cells that were treated with 10 µM JPIII and the JPIII-pretreated cells treated with both vehicle (0.17, p=1) and 10 µM JPIII (0.15, p=0.78) (Figure 3.31E). Similarly, JPIII treatment reduced calcium entry in the vehicle-precultured cells (vehicle 434.1, JPIII 324, p=3.2E-4) as expected. The AUC of the JPIII-precultured cells was lower than that of the vehicle-precultured cells (vehicle 434.1, JPIII 314.4, p=1.71E-4) (Figure 3.31F). The AUC of CRAC calcium entry did not differ between that of JPIII-precultured cells incubated with vehicle and vehicle-precultured cells incubated with JPIII (AUC 314.3 vs 324.2, p=1) (Figure 3.31F).

The effect of prolonged JPIII treatment on ORAI1 expression was explored using qRT-PCR to determine whether JPIII culture affected the level of *ORAI1* expression in the cells. *ORAI1* expression was reduced in HT-29 cells treated with JPIII (Figure 3.32). ORAI1 culture resulted in a reduction in ORAI1 expression. This data indicates that pharmacological ORAI1 inhibition results in suppression of *ORAI1* gene expression. However, an RNA concentration curve is required in treated and vehicle-treated cells to validate the effect of CRAC channel inhibition at the RNA level.
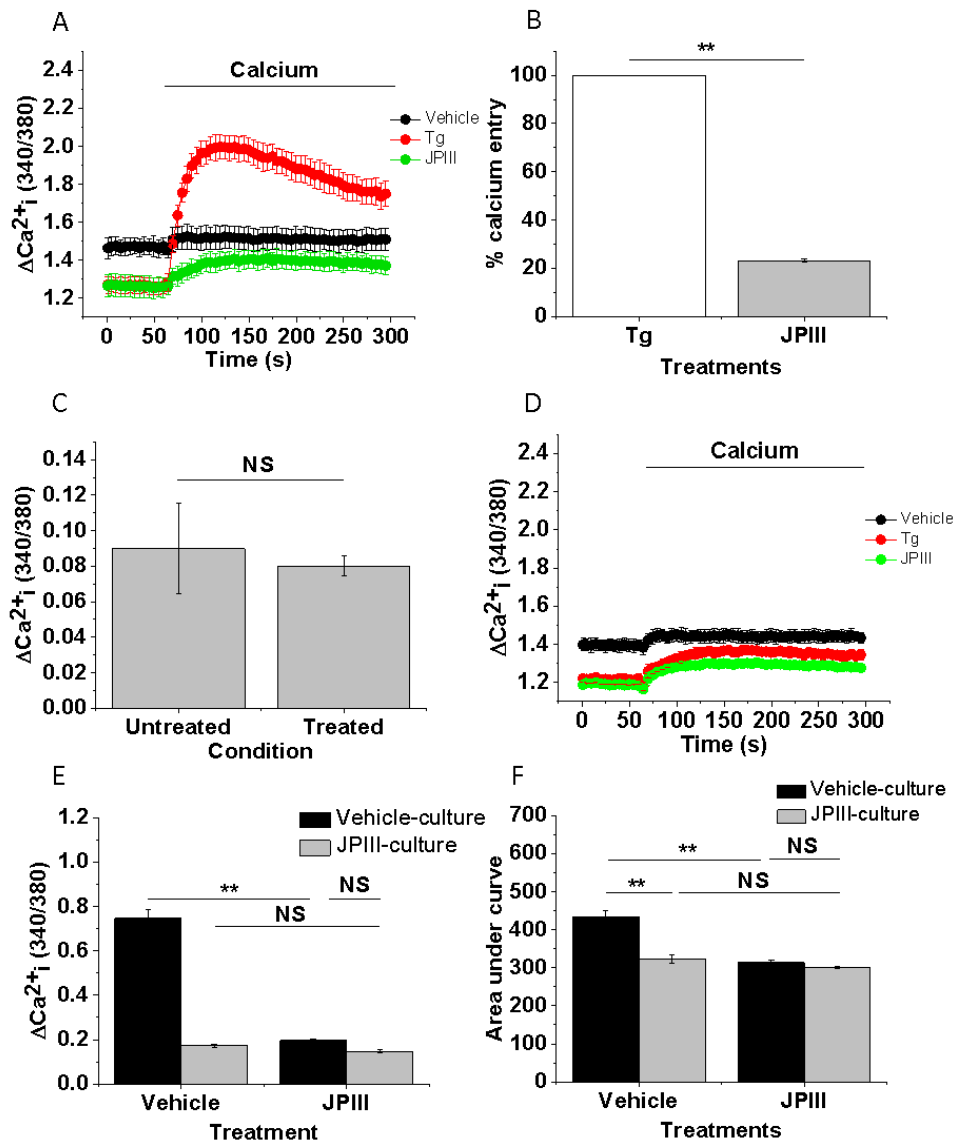
Figure 3.31. The effect of prolonged culture with JPIII on calcium signalling in HT-29 cells. A. Cytoplasmic calcium traces of cells following calcium addition after pre-treatment in calcium-free buffer with either thapsigargin only (Tg, red line) or thapsigargin and 10μM JPIII (JPIII, green) alongside the vehicle control (vehicle, black). B. Mbar chart presenting mean±SEM percentage calcium entry in JPIII-treated cells (grey bar) relative to the vehicle control (white bar) derived from A. C. Bar chart presenting mean±SEM peak calcium amplitudes following calcium addback after thapsigargin-induced store depletion in non-treated (untreated) or vehicle-cultured (treated) cells. D. Calcium traces of cells that were cultured in JPIII for 12 hours prior to thapsigargin-induced store depletion in calcium-free buffer with thapsigargin alone (Tg, red), thapsigargin and 10 μM JPIII (JPIII) and vehicle only (black). E-F. Bar chart presenting mean±SEM calcium data derived from A and D: E. Peak calcium amplitude; F. Area under the curveAll experiments n/N are 3/4. ANOVA testing: * = p≤0.05; ** p=≤0.01; *** p=≤0.001; NS = not significant.

146
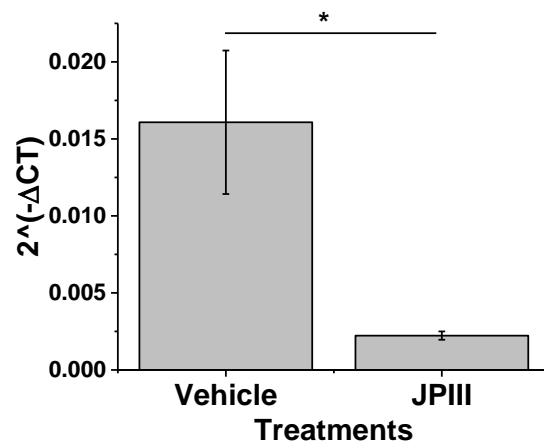
Figure 3.32. The effect of prolonged JPIII culture on ORAI1 expression. Bar chart presenting mean±SEM of the 2^(-ΔCT) values of HT-29 cells treated for 24 hours with DMSO vehicle (vehicle) and 30μM JPIII (JPIII). T testing: * = p≤0.05; ** p=≤0.01; *** p=≤0.001; NS = not significant. Experiments are n/N=3/3.

3.14. The effect of JPIII on AKT phosphorylation

Jing and colleagues have recently reported that 24 hours of treatment of HCT116 and HT-29 cells with the CRAC channel inhibitor SKF-96365 initiates autophagy that protects cells from apoptosis(Jing et al., 2016). Autophagy inhibition and AKT overexpression were shown to decrease cellular viability and increase apoptosis, suggesting that AKT and autophagy are cytoprotective during CRAC channel treatment. This group also found that AKT phosphorylation was reduced with both SFK-96365 treatment and ORAI1 siRNA(Jing et al., 2016). Phospho-blotting for phospho-AKT was carried out on cells treated for 36 hours in order to determine whether JPIII treatment would have a similar effect.

In HT-29 cells, there was a reduction in band intensity in JPIII-treated cells compared to the vehicle control (Figure 3.33A). Image J was used to carry out quantitative analysis of pixel intensity. The mean pixel intensity of vehicle control cells was 8391 whereas the pixel intensity of JPIII-treated cells was lower at 2392 (p=0.05) (Figure 3.33B).

In SW480 cells, there was a reduction in band intensity in JPIII-treated cells compared to the vehicle control (Figure 3.33C). Using Image J, the mean pixel intensity of vehicle control cells was determined to be 30,547 whereas the pixel intensity of JPIII-treated cells was lower at 15,069 (p=0.018) (Figure 3.33D).

In conclusion, JPIII treatment results in reduced AKT phosphorylation.
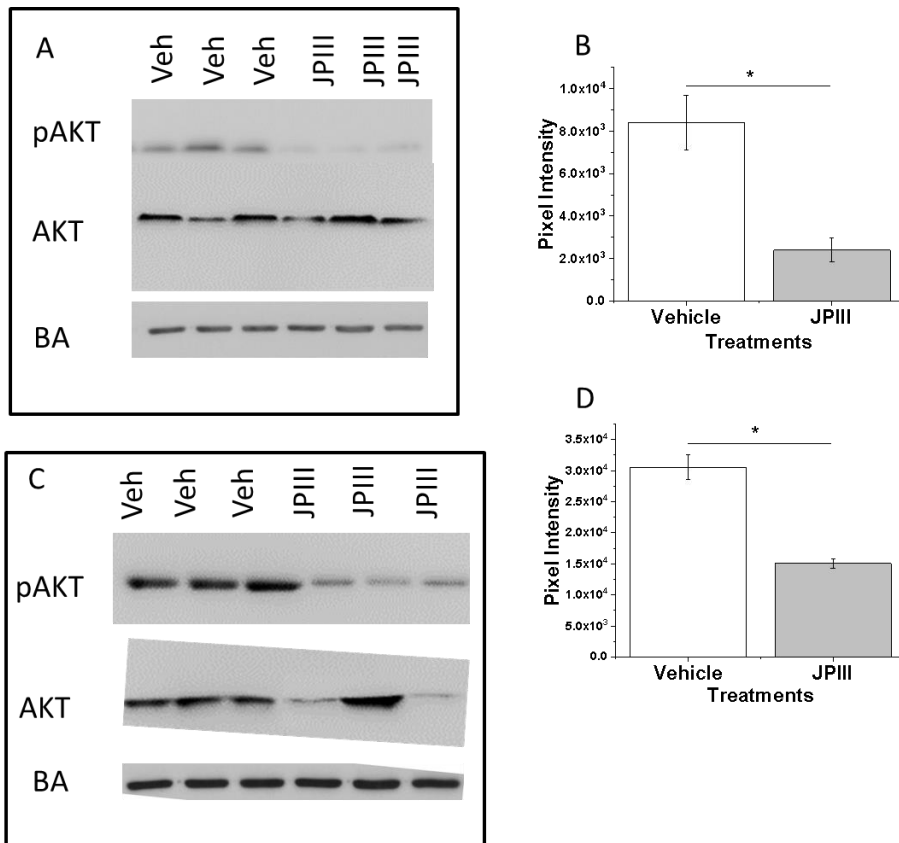
Figure 3.33. phosphoAKT blotting of JPIII treated cells. A-C. Image presentation of phosphoAKT and AKT blots of cells treated with DMSO vehicle control (veh) and 30μM JPIII (JPIII) for 36 hours: A. HT-29. C. SW480. B-D. Bar chart presenting mean±SEM pixel intensity measurements of phospho-AKT derived from data from the western blots: C. HT-29. D. SW480. Key: pAKT = phosphorylated AKT; AKT = total AKT; BA = β-actin. T testing: * = p≤0.05; ** p=≤0.01; *** p=≤0.001; NS = not significant. All experiments are n/N of 3/1.

3.15. The effect of JPIII on autophagy

As previously discussed, CRAC channel inhibition with SKF-96365 in HT-29 and HCT116 cells had been shown to result in autophagy activation with an increased number of autophagosomes and an increased expression of autophagy markers including p62, LC3 and PARP (Jing et al., 2016). Further western blotting was used to determine whether there was an increase in L3CB expression. HT-29 cells were treated with 30 µM JPIII or vehicle control for 36 hours before they were lysed and probed for LC3B. There was an increase in band intensity following JPIII treatment (Figure 3.34A). Using Image J, the mean pixel intensity was determined to be 53.9 whereas the pixel intensity of JPIII-treated cells was 149.6 (p=0.012) (Figure 3.34B). This result suggests that JPIII may initiate cellular autophagy, and this finding validates further study into this looking at other markers of autophagy.

3.16. JPIII blocks CRAC Channel Function in Human Endothelial Cells

Our laboratory have previously shown that CRAC channels are activated by thapsigargin-induced store depletion in human umbilical endothelial cells and can be inhibited by synta 66(Li et al., 2011a). Furthermore, this study demonstrated that CRAC channel inhibition inhibited endothelial function including tube formation, migration and invasion(Li et al., 2011b). Therefore, JPIII was also tested on human umbilical vein endothelial cells (HUVECs) to determine whether the compound could have similar anti-angiogenic effects.

ORAI1 expression has been demonstrated in HUVECs using qRT-PCR and is presented in Figure 3.3. Intracellular calcium measurements were carried out on the FlexStation to determine whether JPIII would similarly inhibit CRAC channel signalling in HUVEC cells. Thapsigargin induced CRAC channel signalling successfully (Figure 3.35A). Vehicle-treated control cells showed no evidence of store depletion as there was no calcium influx upon calcium add-back in these cells (mean peak calcium amplitude of 1.38 vs 1.41, p>0.05).

JPIII inhibited CRAC channel calcium entry in a concentration-dependent manner (Figure 3.35B). The mean peak calcium amplitudes were inhibited by 0.1 µM (0.59, p= 0.001), 0.5 µM (0.4, p=8.4E-7) and 1 µM (0.32, p=3.5E-8) (Figure 5.35C). The area under the curve was inhibited by the same concentrations (0.5µM 401.5, p=0.013; 1µM 360.9, p=1.2E-5; 1µM 345.8, p=9.8E-7) (Figure 3.35D). The peak calcium amplitudes were used to plot a dose-response curve. From the fitted Hill curve, an
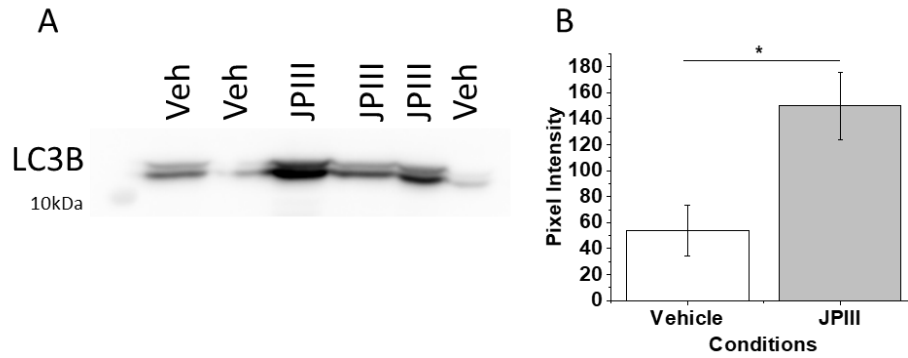
Figure 3.34. LC3B western blotting of JPIII-treated HT-29 cells. A. Image presentation of L3CB western blotting of cells treated with DMSO vehicle control (veh) and 30 μM JPIII (JPIII) for 36 hours. The protein marker on the left of the bands determines the appropriate molecular weight (LC3B protein delineated by LC3B; molecular marker delineated by 10kDa). B. Bar chart presenting the mean±SEM pixel intensity measurements of LC3B derived from data from the western blot images in A. T testing: * = p≤0.05; ** p=≤0.01; *** p=≤0.001; NS = not significant. Experiment is n/N = 3/1.

IC50 concentration was extrapolated of 126nM. The residual calcium entry at the highest concentration range was 29.88% (Figure 3.35E).

In conclusion, JPIII inhibited thapsigargin-induced CRAC channel signalling in HUVECs.
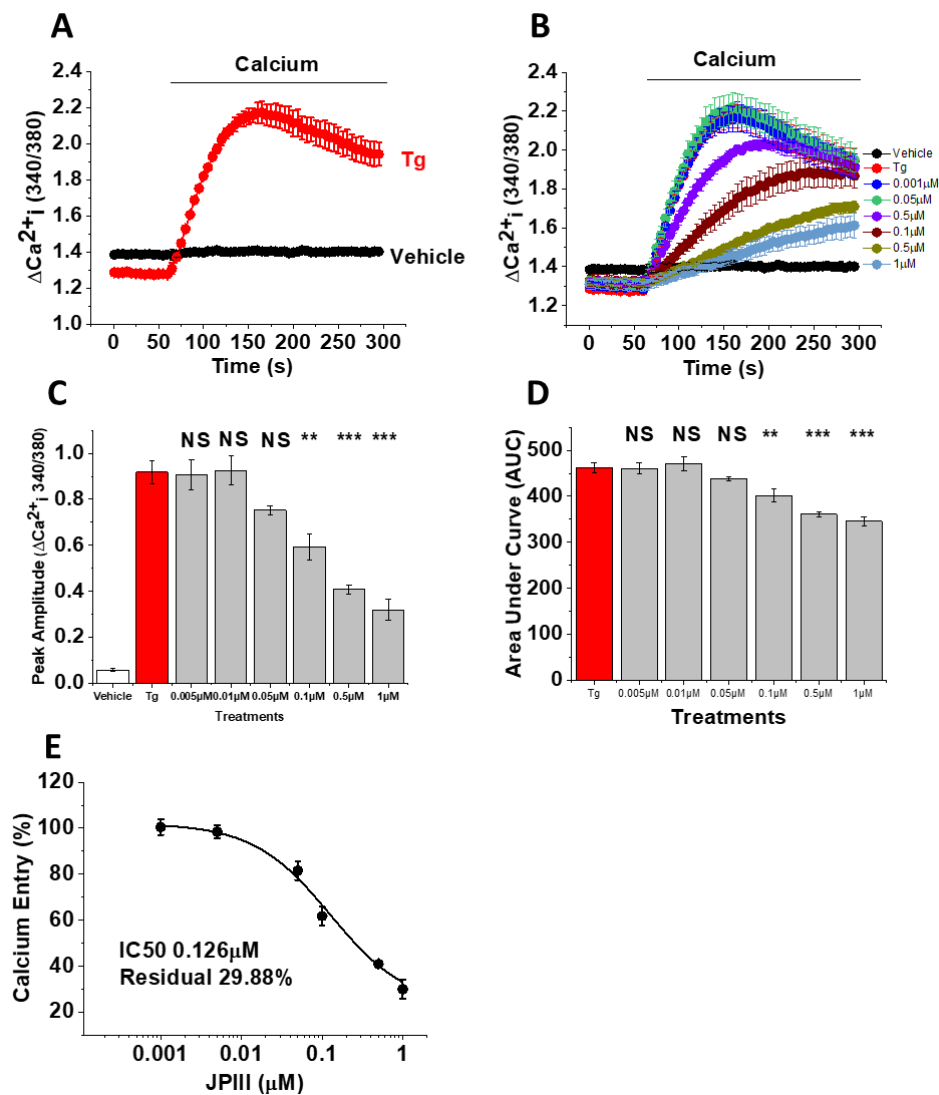
Figure 3.35. The effect of JPIII on thapsigargin-induced CRAC channel signalling in HUVEC cells. A-B. Cytoplasmic calcium traces measured on the Flexstation: A. Calcium traces of HUVEC cells following calcium addback after treatment with thapsigargin (Tg, red line) or vehicle (black line) in calcium-free buffer prior to calcium addback. B. HUVEC calcium traces following calcium addback after thapsigargin pre-treatment in calcium-free buffer with varying concentrations of JPIII. C. Bar chart presenting mean±SEM peak amplitude of calcium traces from Figure B for each concentration (grey) alongside thapsigargin alone (red bar) and vehicle (white). D. Bar chart presenting mean±SEM cumulative area under the curve (AUC) derived from the calcium traces in Figure B. E. Dose-response curve derived from the peak amplitudes of the traces from Figure B. E. ANOVA testing: * = p≤0.05; ** p=≤0.01; *** p=≤0.001; NS = not significant.All experiments are n/N=5/4.

153

3.17. JPIII inhibits endothelial cell viability

Li *et al* presented data that demonstrated no adverse effect to endothelial cell proliferation following 24 hours of treatment with 2, 5 and 10 μM of synta 66(Bae C, 2011). Otherwise there is no other published data detailing the effect of JPIII on endothelial cell viability. The WST1 viability assay was used to determine the effect of prolonged treatment with varying concentrations of JPIII in standard culture media. Following 3 days of treatment, concentrations at and below 10 μM did not affect cell viability (Figure 3.36A). However, 30 μM JPIII reduced viability to 66% (p=0.009). Sorafenib 0.5 μM posed as a positive control, reducing viability to 71.5% (Figure 3.36B).

In conclusion, JPIII did reduce viability but only at the highest possible concentration.

3.18. The effect of JPIII on cell survival and cell death

Annexin V propidium iodide staining was used to determine whether the reduction in viability seen at 30 μM was cytotoxic or cytostatic. Cells were treated with JPIII for 3 days, following which cells were lifted into suspension and stained with annexin V propidium iodide and analysed by flow cytometry. This demonstrated that cells treated for 3 days with 30 μM JPIII were alive and were not undergoing apoptosis or necrosis (Figure 3.37). Therefore, the effect of prolonged CRAC channel inhibition appears to be cytostatic rather than cytotoxic.
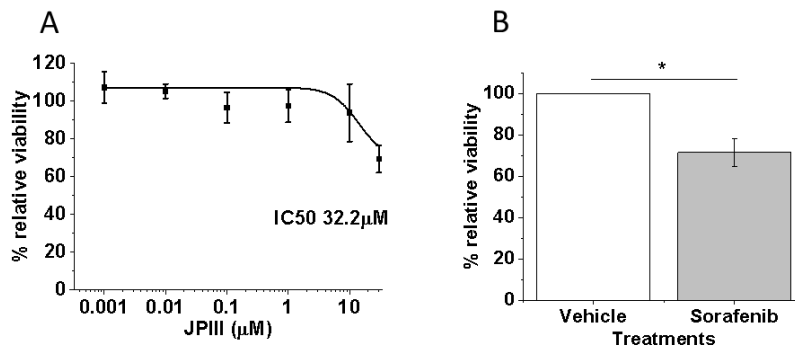
Figure 3.36. Endothelial cell viability. A. Dose-response curve of HUVEC cell viability from the WST1 cell viability assay treated with a range of JPIII concentrations over 3 days relative to the viability of the vehicle-treated cells. The IC50 was extrapolated; it may be inaccurate because 30μM JPIII had less than 50% effect. B. Bar chart presenting mean±SEM viability of 0.5μM sorafenib relative to the vehicle control. ANOVA or T testing: * = p≤0.05; ** p=≤0.01; *** p=≤0.001; NS = not significant. Experiments n/N = 3/4.
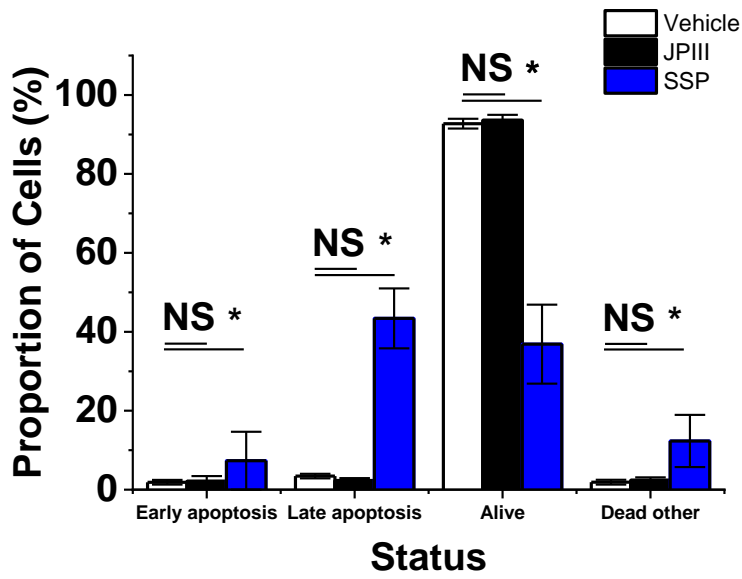
Figure 3.37. Annexin V PI staining of JPIII-treated HUVEC cells and the effect of JPIII on HUVEC cell survival and cell death. Bar chart presenting mean±SEM annexin V PI staining of cells treated with 30 µM JPIII (black bar) alongside the vehicle control (white bar) 100µM staurosporine (SSP, blue bar) control for 72 hours. n/N=4/1. ANOVA testing: * = p≤0.05; ** p=≤0.01; *** p=≤0.001; NS = not significant.

3.19. JPIII blocks VEGF-induced Endothelial Cell Migration

Our laboratory has shown that HUVEC migration through the Boyden chamber inserts was inhibited by 2 μM and 5 μM synta 66 as well as ORAI1 siRNA transfection(Bae C, 2011) demonstrating the functional relevance of ORAI1 to HUVEC function. The scratch wound assay was used with the Incucyte Zoom live kinetic cell imaging platform to determine whether JPIII would inhibit endothelial cell migration. Over a 24-hour period, migration is inhibited at the highest concentration (Figure 3.38A). Plotting the relative wound densities at the 24-hour endpoint demonstrates that migration is only inhibited at 30 μM to 62.4% relative to the control, with no effect seen at lower concentrations (Figure 3.38B). The 1 μM sorafenib positive control inhibited migration to 29.7% relative to the control (p=6.8E-4).

In conclusion, the data indicates that JPIII can inhibit endothelial cell migration but only at the highest possible concentration.

3.20. JPIII blocks VEGF-induced Endothelial Cell Invasion

The microplate scratch wound assay with the application of Matrigel extracellular matrix is a validated method of studying cell invasion and has been established for testing endothelial invasion within our laboratory(Webster et al., 2017). This method was used to test whether CRAC channel inhibition would alter endothelial cell invasion. Only the 30μM concentration was tested, as this was the only concentration that inhibited both cellular migration and proliferation. JPIII inhibited invasion of endothelial cells (Figure 3.39A), with 21.4% relative wound density versus 69.2% of the vehicle control at 24 hours (p= p=6.6E-4), equivalent to 32.6% invasion relative to the vehicle control (Figure 3.39B). The 1 μM sorafenib positive control also inhibited invasion to 12.1%, equivalent to 18% invasion relative to the vehicle control (Figure 3.39B).

In conclusion, the data indicates that JPIII can inhibit endothelial cell invasion.
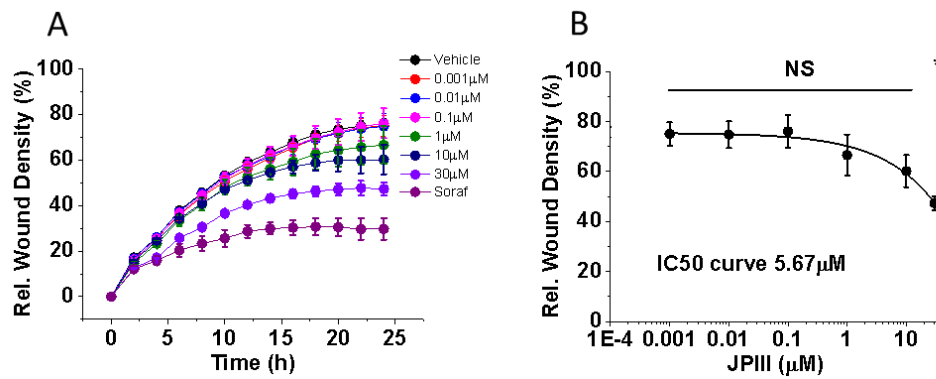
Figure 3.38. The effect of JPIII on HUVEC scratch wound migration. A. Line graph presenting the kinetic migration of HUVEC cells treated with a range of concentrations of JPIII and positive control 1 μM sorafenib (mauve) and the vehicle control (black). B. Dose-response curve generated from the relative wound densities normalised to the vehicle control (as %) derived from the 24 hour time point from the data in Figure A. ANOVA testing: * = p≤0.05; ** p=≤0.01; *** p=≤0.001; NS = not significant. Experiments are n/N=3/3.
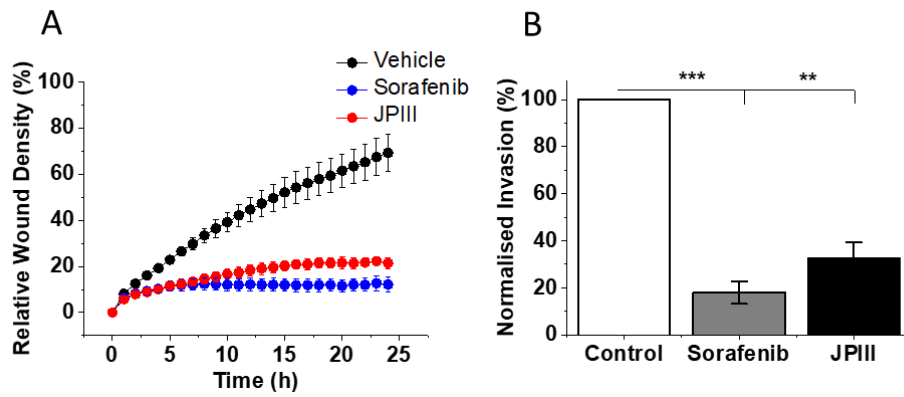
Figure 3.39. The effect of JPIII on HUVEC scratch wound Matrigel invasion. A. Line graph presenting the kinetic invasion of HUVEC cells treated with 30 μM JPIII (JPIII, red line) and the 1 μM sorafenib positive control (sorafenib, blue line). B. Bar chart presenting mean±SEM relative wound density of invading cells treated with JPIII (black bar) and sorafenib (grey bar) at the 24-hour timepoint derived from Figure A. Key: h = hours. ANOVA testing: * = p≤0.05; ** p=≤0.01; *** p=≤0.001; NS = not significant. Experiment is n/N=3/3.

3.21. Sorafenib inhibits CRAC channel activity

Sorafenib (Figure 3.40A) has been used as a positive control as it has been widely reported to have potent effects against endothelial cell viability and micro-vessel density of xenograft experiments (Wilhelm et al., 2004), as well as tube formation (an assay that has not been carried out as part of this study). Sorafenib has also been reported to have anti-angiogenic effects in a number of human tumours including hepatocellular carcinoma(Coriat et al., 2012) as well as breath, colon and non-small lung cancers(Wilhelm et al., 2004). CRAC channel inhibitory properties have not been described previously in the literature. However, given the similar effects seen in these *in vitro* endothelial assays, intracellular calcium measurements were carried out on the FlexStation to determine whether sorafenib could inhibit thapsigargin-induced CRAC channel function.

Sorafenib was found to inhibit thapsigargin-induced CRAC channel activity (Figure 3.40B). There was inhibition of peak calcium amplitudes at 1 µM (59%, p=0.001), 5 µM (34.3%, p=1.2E-5) and 10 µM, 8.9%, p=3.3E-7) (Figure 3.40B, 3.40C). Similarly, there was a reduction in the AUC at 1 µM (422.6, p=0.001), 5 µM (422.6, p=3E-6) and 10 µM (6.7E-8) (Figure 3.40D). Plotting the peak amplitudes generated a dose-response curve (Figure 3.40B). However, the Hill curve could not be fitted in order to extrapolate an IC50. The curve can be seen to be bowed and skewed to the right, therefore inhibition is likely to be less potent.

In conclusion, sorafenib is a CRAC channel inhibitor that is comparable in potency to other CRAC channel inhibitors used in this study.
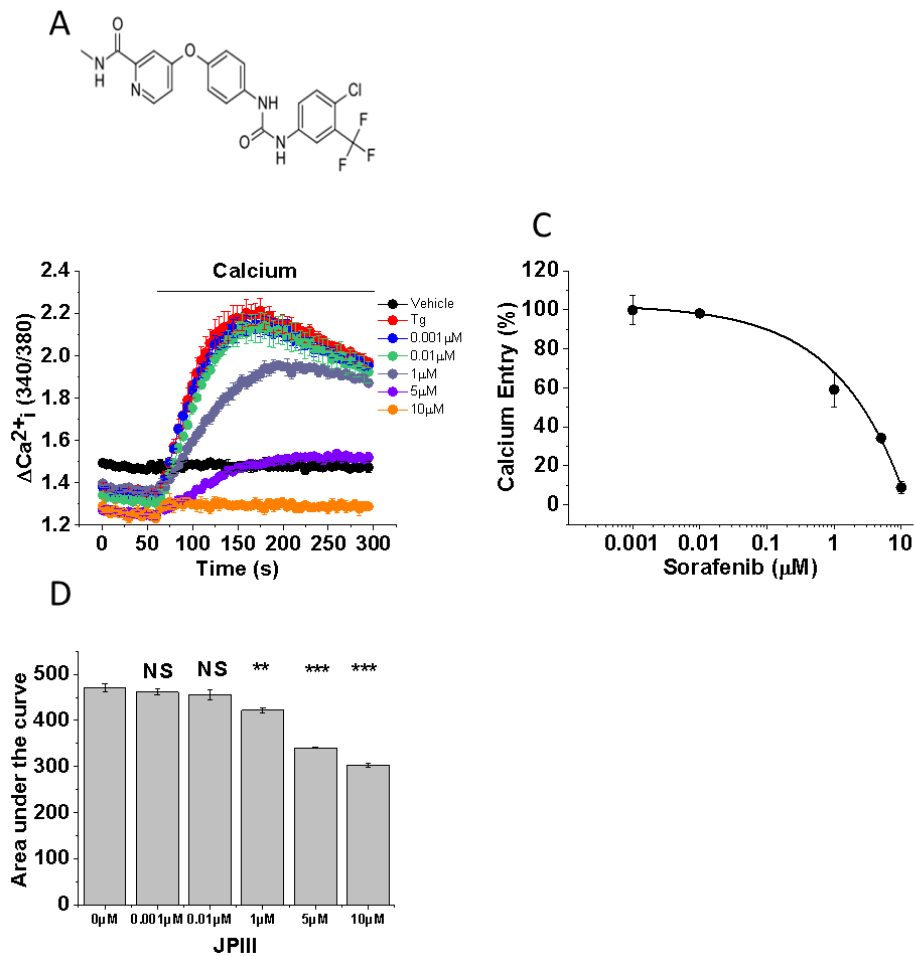
Figure 3.40. The effect of sorafenib on CRAC channel signalling in HUVEC cells. A. Chemical structure of sorafenib. B. Cytoplasmic calcium traces of HUVECs following calcium addback after incubation in calcium-free buffer with thapsigargin and a range of sorafenib concentrations alongside the vehicle only (black line) and thapsigargin only (red line). C. Dose response curve derived from the peak calcium amplitudes derived from the data traces in Figure B. D. Bar chart presenting mean±SEM cumulative area under the curve (AUC) derived from the calcium traces in Figure B. ANOVA testing: * = p≤0.05; ** p=≤0.01; *** p=≤0.001; NS = not significant.Key: s= seconds. Experiments n/N=3/4.

3.22. Summary of findings

• The CRAC channel is expressed in CRC cell lines. It is expressed and functionally responsive to thapsigargin-induced store depletion.

• ORAI1 knockdown reduced CRAC channel calcium re-entry, demonstrating the role of ORAI1 in CRAC channel function.

• CRAC channel calcium re-entry is inhibited by the commercially available CRAC channel inhibitor synta 66 (S66), as well as the novel CRAC channel inhibitor JPIII, in colorectal cancer cell lines.

• Microarray analysis of immune cells treated with CRAC channel inhibitor demonstrated transcriptional upregulation of genes involved in immune responses, cell migration, TNF production and cell death. It also demonstrated downregulation of genes involved in mitosis, cell cycling, cell cycle checkpoints, JAK-STAT signalling and cell proliferation

• JPIII treatment resulted in a reduction of cell viability in all cell lines but at high concentrations only. JPIII also reduced tumour clonogenicity.

• JPIII inhibits EGF-induced migration and invasion. However, EGF does not induce store depletion.

• JPIII treatment results in acidification of the culture media after 24 and 48 hours. Although CRAC channel function was affected by the extremes of pH reported in the literature, the change in pH seen in response to drug treatment was not found to alter store depletion or CRAC channel function in either cell line.

• Serum culture with JPIII was found to depress CRAC channel function and suppress ORAI1 mRNA expression, suggesting that pharmacological inhibition induces CRAC channel remodelling.

• JPIII treatment was found to reduce AKT phosphorylation and initiate autophagy, which is consistent with findings following SFK-96365 treatment *in vitro* in HCT116 and HT-29 cell lines.

• JPIII potently inhibits CRAC channel activity in HUVECs.

• JPIII inhibits endothelial cell viability at high concentration only. The anti-proliferative effect is cytostatic rather than cytotoxic.

• JPIII blocks VEGF-induced migration and invasion.

- Sorafenib, a multi-tyrosine kinase inhibitor with some structural similarity to S66 and JPIII, was also found to inhibit CRAC channel activity.

3.23. Discussion

In conclusion, this work has demonstrated that CRAC channel inhibition with JPIII has a functional effect against both colorectal cancer cell lines and endothelial cells.

Current data suggests that JPIII does have a significant effect on cancer cell function as the drug reduces cell viability and growth in the WST1 viability assay and growth studies, and the clonogenic assay results demonstrate a greater impact on clonogenicity over the 11-day window. A more prolonged time course of treatment may capture the effects of JPIII treatment better and define the switch between cell survival and cell death. Furthermore, JPIII treatment reduced migration and invasion of CRC cells. This has been seen previously in other cancers. Both siRNA knockdown of ORAI1 and STIM1 and SFK-96365 treatment inhibited migration of MDA-MB-231 breast cancer cells(Yang, 2009) by impairing focal adhesion turnover.

CRAC channel assays carried out on the FlexStation demonstrated potent CRAC channel inhibition with IC50 doses within the nanomolar range, 126nM in HUVECs, 740nM in HT-29, 553nM in SW480 and 160nM in HCT116. These IC50 doses were similar to those seen with S66 in the CRC cell lines (671nM in HT-29 and 144nM in SW480). The IC50 concentration in HUVECs is less potent than the concentration published by our group for S66 in HUVEC cells of 25.5 nM (Li, 2011), but this should be interpreted with caution and ideally retested with HUVECs.

There was a difference in compound sensitivities seen with CRAC channel inhibition experiments carried out on the FlexStation and the functional assays, more so for SW480 and HCT116 than HT-29. FlexStation testing demonstrated immediate inhibition above 0.5µM, inhibiting between 72-82% of CRAC channel re-entry at 10µM. However, functional effects were subtler. Viability effects took days to manifest, and required high concentrations: 20µM and 30µM over 4 days in SW480 and HCT116 cells respectively, whereas HT-29 cells demonstrated sensitivity above 1µM after 6 days. It should be noted that some of the most important chemotherapeutic agents in clinical use for metastatic CRC today, such as 5-

FU(Mhaidat et al., 2014) and oxaliplatin(Flis, 2009), have demonstrated a similar requirement for high micromolar concentrations in *in vitro* assays that take days for functional effects to manifest. The requirement for high concentrations required for functional effects is likely due to a number of factors. The media of cultured cells requires serum, and serum binding of JPIII may reduce the free fraction in culture. Protein binding of CRAC channel inhibitors has been reported as a common issue by others, particularly with *in vivo* studies(Stauderman, 2018). However, the work in this thesis suggests that this difference is equally likely to be due to the drug's effects on the cell. This work has demonstrated that JPIII treatment initiates the cytoprotective process of autophagy as well as having an inhibitory effect on the PI3/AKT/mTOR pathway by reducing AKT phosphorylation, which impacts on cell survival, growth and migration processes downstream. The drug therefore simultaneously activates 2 opposing processes. This has previously been reported with the ORAI1 channel inhibitor SFK-96365 treatment in colorectal cancer cell lines HCT116 and HT-29(Jing et al., 2016). The interaction between ORAI1 and Akt has previously been shown in CRC. ORAI1 silencing in LOVO cells reduces AKT and GSK3β phosphorylation whereas overexpression in Hct116 cells enhances it(Deng, 2016), implicating ORAI1 in the WNT signalling pathway. The data in this thesis suggests that JPIII works in a similar way to SFK-96365, and may be due to interplay between these processes of cell survival and cell death. The interplay between these 2 processes has been partially revealed by Jing and colleagues, who found the calcium-dependent serine/threonine protein kinase CAMKII phosphorylates AKT and that CRAC channel blockade negatively impacted on that. They also found that prolonged SFK-96365 treatment eventually resulted in apoptosis with a rise in cytochrome c and caspase 3 activation, perhaps by overwhelming its capacity to maintain viability in the face of mounting cell stress(Jing et al., 2016). The trypan blue exclusion assay showed that there was no increase in cell death over the 6-day period. This is in stark contrast to the apoptotic effects of SFK-96365, which resulted in apoptosis of 15% of cells after 48 hours of treatment with 10μM in HCT116 and HT-29(Jing et al., 2016). Cell death may have been initiated later than the timepoint of the assay, and a prolonged time course may demonstrate this.

An intriguing finding of this study was the acidification of the media following CRC treatment with JPIII. This is a novel finding that has not been described in the literature. This will likely be due to high glycolytic flux from within the cell resulting

from increased intracellular metabolic activity. However, it also led to the question as to whether the alteration in extracellular pH could impact on CRAC channel function. Acidity has also been previously shown to inhibit CRAC channel function(Beck et al., 2014). This is also pertinent in cancer as the tumour environment *in vivo* has been found to be acidic relative to the extracellular environment of normal tissue, whilst maintaining a neutral intracellular pH(Gerweck and Seetharaman, 1996). This is thought to impact on chemosensitivity, in particular increasing the efficacy of weak acids(Kozin et al., 2001) and decreasing the efficacy of weak bases(Parkins et al., 1996) by a process called ion trapping. It is reported to result in increased drug resistance, potentially as lower pH upregulates multi-resistance machinery such as p-glycoprotein expression and function(Thews et al., 2006). This work has shown that the pH levels attained following JPIII treatment did not impact on store depletion or CRAC channel entry, and could mean that acidity of the tumour environment would not impact on treatment response *in vivo*. However, this interpretation is limited by the short-term incubation of the cells in acidic solution for this experiment. Cells *in vivo* are subjected to acidic conditions for a longer time scale, which may have more profound effects on cellular function. It would be interesting to study CRAC channel signalling in cells that have been cultured in acidic culture medium, in particular the impact that CRAC channel inhibition would have on channel activity and expression, cellular proliferation and cellular migration and invasion.

An equally novel and intriguing finding from this study is that JPIII treatment actually resulted in a downregulation of ORAI1 expression and CRAC channel function. This suggests that pharmacological inhibition results in calcium channel remodelling. ORAI channel remodelling has been described in cancer in response to upstream receptors that can influence the cell. Motiani and colleagues found that CRAC channel signalling in oestrogen-positive cell lines was mediated by ORAI3 and STIM1/2, whereas CRAC signalling in oestrogen-negative cell lines was mediated by ORAI1 and STIM1(Motiani et al., 2010). Furthermore, Azimi and colleagues found hypoxia induced ORAI3 expression in basal breast cancer(Azimi et al., 2019). It has also been reported in different molecular subtypes of breast cancer, with higher ORAI1 expression in basal-like breast cancers but higher ORAI3 expression in triple-negative breast cancers(Azimi et al., 2019). However, channel remodelling in response to CRAC channel inhibitors has not previously been

described. This should be explored with further transcriptional characterisation of CRAC channels such as ORAI2 and ORAI3. As we do not have a reliable antibody for determining protein expression, treatment of cancer cell lines with stably-transfected fluorescently-tagged or HA-tagged proteins may allow protein determination using microscopy or pull-down western blots.

This work has demonstrated the functional efficacy of the novel CRAC channel inhibitor JPIII, developed as part of a drug discovery project within the Beech laboratory. However, the use of the drug is limited by the fact that it only dissolves in 100% DMSO at stock concentration. This makes *in vivo* use for testing in mouse cancer models problematic. Normally animals are dosed with liquid oral gavage, intravenous (IV) tail vein injections, transdermal applications or intraperitoneal (IP) injections. DMSO has been shown to result in dermatitis following dermal application, perivascular inflammation and thrombosis following IV injection, cataracts, lower body weights and abdominal discomfort following oral administration (Noel et al., 1975) as well as cardiotoxicity, intraperitoneal scarring and organ abnormalities following IP injections(Kramer et al., 1995), and is not favoured by the local veterinarian. One other member of the laboratory has been successful in dosing mice with the drug in 100% DMSO delivered in mini-osmotic pumps that are implanted subcutaneously in C57B/6 mice, and demonstrated drug absorbance into the serum and drug uptake and metabolism in the liver, without systemic toxicity. Work is ongoing within the Beech laboratory in association with the Department of Chemistry to develop derivative compounds with improved absorbance in more hydrophobic solvents without affecting the pharmacokinetic profile that could be used *in vivo*. However, the next logical step for this work is to proceed onto *in vivo* studies using either ectopic or orthotopic xenografts or PDX models in nude mice under an appropriate Home Office license with the mini-osmotic pumps.

3.24. Conclusion

In conclusion, this work provides *in vitro* evidence of the functional effects of CRAC channel inhibition on both cancer and endothelial cell viability, migration and invasion that is supported by other more recent work in the field. The findings in

this work warrant further molecular characterisation of the signalling processes involved, but also supports progression on to *in vivo* study.

Chapter 4. A role for PIEZO1 in colorectal cancer

4.1. Introduction

PIEZO1 forms a mechanically activated ion channel(Lewis, 2015) that is highly conserved in mammalian species (Coste et al., 2010a). Physiological roles have been described for this channel, such as embryonic development of the vasculature(Li et al., 2014). In addition, functional PIEZO1 mutations have pathological consequences, for instance M2225R and R2456K mutations of PIEZO1 have been identified in pedigree sequencing studies of familial hereditary xerocytosis (Zarychanski et al., 2012), two gain-of-function mutations that result in delayed channel inactivation(Bae, 2013).

Research on oncogenic PIEZO1 is in its infancy, however it has been reported in a number of cancers. PIEZO1 has been shown to drive tumour cell proliferation in osteosarcoma cells(Jiang, 2017), migration in breast cancer(Li et al., 2015a), and invasion in osteosarcoma (Jiang, 2017). PIEZO1 expression levels have been reported to have prognostic significance, with greater levels of PIEZO1 expression reported to correlate with poorer prognosis in breast cancer(Li et al., 2015a). Conversely a reduction in PIEZO1 expression has been postulated to drive tumour cell metastasis in a number of cancers. It has been suggested that it has tumour suppressor function in gastric cancer cell lines(Jiang, 2017) by binding to trefoil factor family 1 (TFF1) at the C-terminal domain, with PIEZO1 knockdown in these cell lines resulting in increased tumour metastasis both *in vitro* and *in vivo*. Knock-down of PIEZO1 in normal lung epithelial cultures has been reported to reduce cell adhesion but drive anchorage-independent colony survival, migration and invasion *in vitro* (McHugh et al., 2012). More recently, differential upregulation of PIEZO1 has been reported in breast cancer cell line MCF-7 relative to the normal mammary epithelial cell line MCF-10A (Li et al., 2015a). In contrast, a reduction in PIEZO1 expression has been reported in a panel of small cell lung cancer cell lines relative to normal lung epithelial cell lines (McHugh et al., 2012). A role for PIEZO1 has not been reported in colorectal cancer.

There are a number of recent papers that have identified PIEZO1 mutations in colorectal cancer syndromes. Spier and colleagues screened the adenoma tissue of 12 patients with unexplained polyposis (i.e. those who did not carry any somatic APC, MUTYH, POLE or POLD1 mutations) using exome sequencing of DNA from both leucocytes and the polyps. This work identified homozygous loss-of-function

germline mutations in PIEZO1(Spier et al., 2016), which suggests that PIEZO1 germline mutation could predispose to adenoma formation and subsequent tumourigenesis. Interestingly, Donnard and colleagues performed exome-capture sequencing on 3,594 cell surface genes in 23 colorectal cancer cell lines, and identified PIEZO1 (which was previously known as FAM38A) as one of 48 surface protein genes that was mutated and expressed in over 10% of these cell lines(Donnard et al., 2014), which included HT-29 but not SW480. ORAI1 was screened but no such mutation was identified. In addition, loss of heterozygosity of the chromosomal locus of PIEZO1 has been reported in gastric(Mori et al., 1999) and breast(Tsuda et al., 1994) cancers.

Open access data was downloaded from The Cancer Genome Atlas (TCGA). The RSEM expression values for 460 colorectal cancer samples and 41 normal colon samples were pooled and gave a 1.1-log fold increase in expression in the colorectal cancer samples relative to the normal colon tissue. This led to the hypothesis that PIEZO1 may be important in colorectal cancer function.

4.2. Aims and Objectives

The aim of this *in vitro* study was to determine whether PIEZO1 has a role in carcinogenesis.

The objectives of this work were:

1. To determine whether PIEZO1 was functionally active in colorectal cancer cell lines.
2. Whether altering PIEZO1 expression or function had any impact on cancer cell morphology, growth characteristics, survival, migration and invasion.

Study of PIEZO1 function utilised a range of published tools, including compounds that are known to activate and inhibit PIEZO1 as well as commercially available siRNA sequences to knock down PIEZO1 expression.

4.3. PIEZO1 is functional in CRC lines

4.3.1. Yoda1 treatment activates calcium influx

Yoda1 is the first chemical activator of PIEZO1. Syeda and colleagues discovered this compound from a chemical screen as an activator of both human and mouse PIEZO1 channels transfected into HEK293T cells, which do not endogenously express PIEZO1 and are therefore not have an inducible calcium flux in response to Yoda1 treatment(Syeda et al., 2015). Yoda1 has not been tested against other channels to clarify specificity. Yoda1 has been validated in experiments looking at PIEZO1 function. Both Yoda1-induced and patch clamp pressure-induced calcium influx were similarly reduced in the erythrocytes of paediatric patients suffering from congenital lymphatic dysplasia(Lukacs et al., 2015). A different study found similar effects on calcium entry and downstream signalling with both Yoda1 treatment and shear stress on endothelial cells(Wang, 2016). Yoda1 has been shown to exert its effects directly on the PIEZO1 channel rather than through indirect mechanisms, as Yoda1 induced current through purified reconstituted mouse PIEZO1 protein isolated in symmetric lipid bilayers in an acellular environment (Syeda et al., 2015).

In this work, Yoda1 was used to determine whether PIEZO1 channels are functionally active in the colorectal cancer cell lines HT-29, SW480 and HCT116. Cells were loaded with the ratiometric dye Fura2-AM prior to the addition of a range of concentrations of Yoda1 between 0.5µM and 10µM, and resultant changes in intracellular calcium concentration were measured on the FlexStation 3 platform.

Yoda1 induced a rise in intracellular calcium in both HT-29 (Figure 4.1A-B) and SW480 (Figures 4.1C-D), demonstrating a concentration-dependent rise in intracellular calcium entry (HT-29 Figure 4.1B; SW480 Figure 4.1D). However, Yoda1 did not induce calcium entry in HCT116 (Figure 4.1E). Probing the Genome Browser of the COSMIC Cell Line Project(Tate et al., 2018) reveals that there is a deep deletion of the portion of chromosome 16 that encodes the PIEZO1 gene. Deletion of the gene could be the reason as to why there is no Yoda1 response. This needs to be clarified in the HCT116 cells with DNA polymerase chain reaction (PCR) to verify whether loss of expression is due to gene deletion. Subsequent cell work was carried out with the HT-29 and SW480 cell lines.

The calcium responses to Yoda1 treatment differed between the 2 cell lines. Immediately following application of Yoda1 to HT-29, initial calcium entry was

rapid, achieving the fastest rate of calcium entry within the first 10 seconds of Yoda1 addition to the cells (Figure 4.1A). This rapid calcium entry was seen in all concentrations (1-10µM). Following this rapid rise, steady and constant calcium entry continued over the 300 seconds for all concentrations except 10µM, where a plateau was reached at 140 seconds. Calcium levels did not fall during the traces, indicating that the PIEZO1 channel remained open in the presence of Yoda1 throughout the experiment. The peak calcium amplitude was significant for 10µM (p=0.006) and 5µM (p=0.03). In SW480 cells, the initial rate of calcium entry was not as rapid as was seen in HT-29 cells. There was a steady rate of calcium entry seen for all concentrations tested (0.5-10µM) following the addition of Yoda1 (Figure 4.1C). The calcium signal plateaued at 65 seconds for concentrations of 0.5-2µM after Yoda1 treatment, suggesting that an equilibrium of channel activity, calcium influx and calcium efflux from the cell had been reached. Calcium entry for concentrations of 4-10µM did not plateau but there was a slow and gradual increase in calcium signalling. Again, calcium fluorescence did not decay during the trace recordings, indicating that the PIEZO1 channel remained open in the presence of Yoda1 throughout the experiment. The Yoda1 responses were significant for 10µM (p=1.6E-9), 7.5µM (p=4.8E-8) and 4µM (p=3.8E-4).
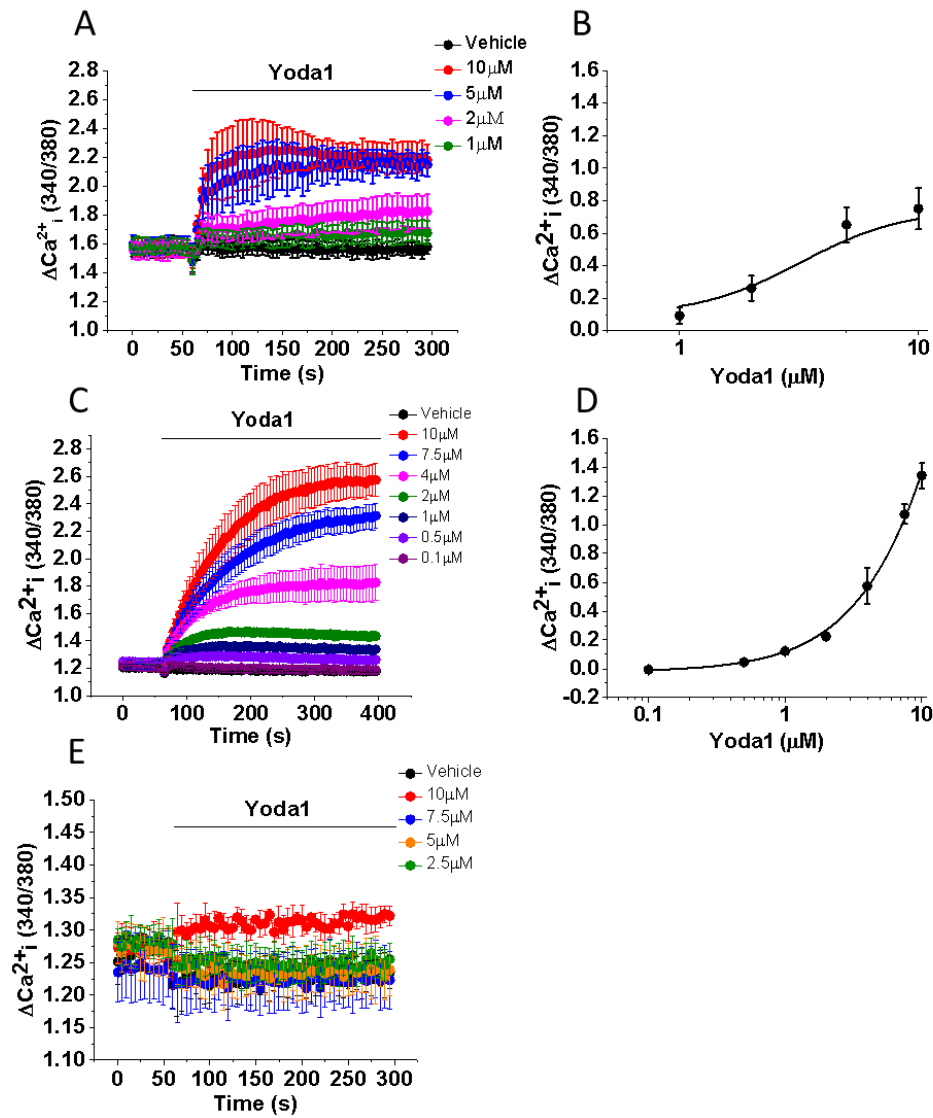
Figure 4.1. The effect of Yoda1 on intracellular calcium levels in CRC lines. A. Cytoplasmic calcium traces in HT-29 following the addition of a range of concentrations of Yoda1 in calcium-containing buffer. B. Dose-response curve demonstrating dose-dependent calcium entry derived from the peak calcium amplitude from Figure A.

C. Cytoplasmic calcium traces in SW480 following the addition of a range of concentrations of Yoda1 in calcium-containing buffer. D. Dose-response curve demonstrating dose-dependent calcium entry derived from the peak calcium amplitude from Figure C. E. Cytoplasmic calcium traces in HCT116 following Yoda1 treatment. All experiments are n/N=3/4.

4.3.1.1. Yoda1 does not cause calcium entry in calcium-free conditions.

As previously discussed, Yoda1 has been reported to activate PIEZO1 in order to induce extracellular calcium entry into the cell through the channel (Syeda et al., 2015). However, it is not clear whether Yoda1 may also deplete intracellular calcium stores downstream of its application. In a study looking at the molecular pathway of PIEZO1-induced calcium response in endothelial cells, Gαq/11 knockdown reduced Yoda1-induced calcium influx(Wang, 2016). Gαq/11 activates phospholipase C, which cleaves cytoplasmic phosphatidylinositol 4,5-bisphosphate into inositol 1,4,5-trisphosphate (IP3)(Lee et al., 1992) and diacylglyercol. IP3 binds to IP3 receptors on the ER surface and depletes the intracellular calcium store(Parekh, 1997). Furthermore, Fluorescence Resonance Energy Transfer (FRET) imaging of the spatiotemporal distribution of calcium in HUVECs has shown that vibrationally-induced calcium entry in HUVECs was followed by store depletion downstream of phospholipase C (Nishitani et al., 2011). No such result has been reported in epithelial or cancer cells. If IP3-stimulated ER store release occurs in a calcium-free extracellular recording buffer, a rise in intracellular calcium would be seen as an increase in Fura2 fluorescence (Parekh, 1997, Wu, 1994). Therefore, it is possible that store depletion may occur downstream of PIEZO1 activation and may therefore contribute to the intracellular calcium entry seen in Yoda1-induced calcium traces in Figure 4.1. To explore this further, Fura2-loaded cells were treated with 5μM and 10μM Yoda1 that had been washed in calcium-free salt buffered recording solution for 5 minutes. There was no change in fluorescence following Yoda1 treatment in SW480 (Figure 4.2A) or HT-29 (Figure 4.2B) cells. In conclusion, this data suggests that Yoda1 does not induce store depletion in these malignant epithelial cells, and that Yoda1-induced calcium elevation is due to calcium entry from the extracellular environment.

4.3.2. PIEZO1 knockdown indicates Yoda1 specificity in colorectal cancer cells

PIEZO1 small interfering RNA treatment is a useful investigative tool in PIEZO1 studies. It allows specificity as it prevents production of the protein of interest by targeted mRNA degradation. siRNA treatment of PIEZO1 has been used extensively in the literature, for instance siRNA knockdown resulted in a reduction in amplitude of inward mechanically-activated currents in murine N2A cells(Coste et al., 2010a).

Two commercially available PIEZO1 siRNA sequences were used that targeted 2 independent sequences of the PIEZO1 mRNA transcript: s18891 and s138387 (ThermoFisher Scientific), and transfection protocols were optimised in the HT-29 and SW480 cell lines. SW480 and HT-29 cells were both seeded 48 hours after transfection and seeded in microplates for Flexstation testing the following day (72 hours post transfection).

In SW480 cells, there was no difference in response to 10μM Yoda1 in both the scrambled-transfected and non-transfected cells (Figure 4.3A). Calcium entry was reduced in transfected cells, with a 60.4% (p<0.01) and 52% (p<0.01) reduction using siRNA sequences 18891 and 138387 respectively (Figure 4.3B). qRT-PCR was used to validate knockdown. There was a reduction of PIEZO1 expression in transfected cells relative to the scrambled-transfected control (Figure 4.3C).

In HT-29 cells, there was no difference in response to 10μM Yoda1 in both the scrambled-transfected and non-transfected cells (Figure 4.3D). Calcium entry was reduced in transfected cells, with a 46.5% (p<0.01) and 40.3% (p<0.01) reduction in calcium entry with sequences 18891 and 138387 respectively (Figure 4.3E). qRT-PCR was used to validate knockdown. There was a reduction of PIEZO1 expression in transfected cells relative to scrambled-transfected control (Figure 4.3F). The knockdown was very effective, but this did not correlate with the degree of Yoda1-induced calcium entry seen in transfected cells. The mRNA level may not correlate well with protein expression, and this should be clarified further by looking at protein expression in mock-transfected and PIEZO1 siRNA-transfected cells.

In conclusion, PIEZO1 siRNA transfection demonstrated Yoda1 specificity to PIEZO1 activation with a significant reduction in calcium entry in both cell lines with 2 targeted sequences.
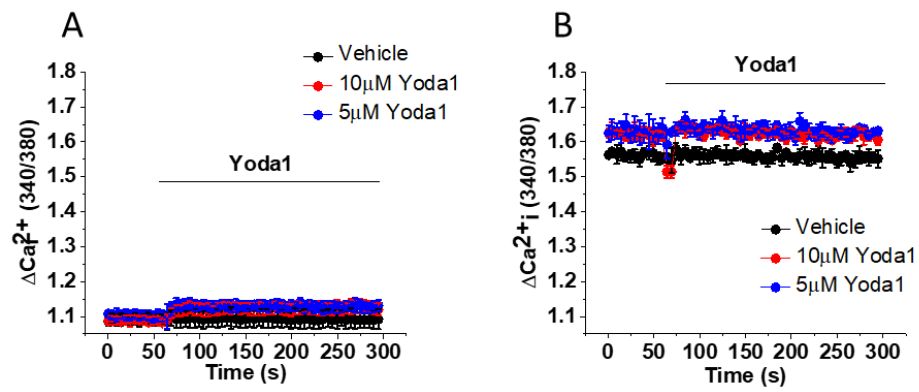
Figure 4.2. The effect of Yoda1 on CRC cells in calcium-free recording solution. A-B. Cytoplasmic calcium traces following the addition of Yoda1 to cells in calcium-free recording solution. A. SW480; B. HT-29 cells. Key: s = seconds. All experiments are n/N=3/4.
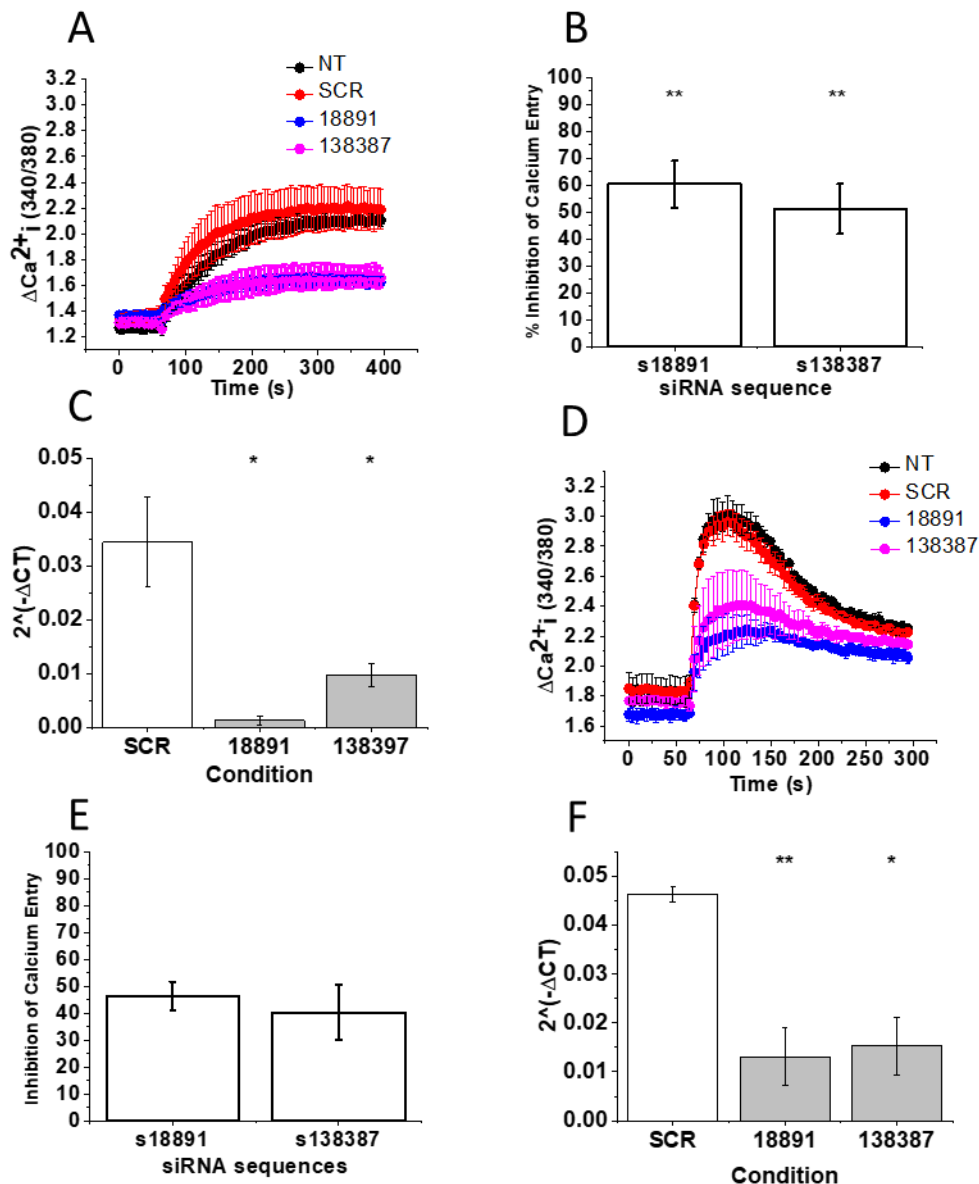
Figure 4.3. The effect of PIEZO1 knockdown on Yoda1-induced calcium response in CRC cells. A. Cytoplasmic calcium traces following 10μM Yoda1 treatment of PIEZO1 siRNA-transfected SW480 cells (pink 138387; blue 18891) relative to the non-transfected (black) and scrambled-treated control (red). B. Bar chart presenting mean±SEM calcium inhibition in SW480 transfected cells as a percentage of the scrambled-treated cells derived from the data in A. C. Bar chart presenting mean±SEM PIEZO1 mRNA expression in SW480 PIEZO1 siRNA-transfected cells as $2^{(-\Delta CT)}$ (n/Ns=3/2). D. Cytoplasmic calcium traces for HT-29 PIEZO1 siRNA-transfected cells (conditions as in A). E. Bar chart presenting mean±SEM calcium inhibition in HT-29 as a percentage of the scrambled-treated cells derived from C. F. Mean±SEM PIEZO1 mRNA expression in HT-29 PIEZO1 siRNA-transfected cells as $2^{(-\Delta CT)}$ (n/n=3/2). ANOVA or T testing: * = p≤0.05; ** p=≤0.01; *** p=≤0.001; NS = not significant. Key: s = seconds.

4.3.3. Cation channel Inhibitors known to inhibit PIEZO1 inhibit Yoda1-induced intracellular calcium influx

Cation channel inhibitors ruthenium red, GsMTx4 and gadolinium have been reported to inhibit PIEZO1 current and calcium entry in a number of cell lines. Ruthenium red is a non-selective cationic channel blocker that has been shown to inhibit PIEZO1 currents in channels cloned into GFP-positive vectors expressed into a number of murine and rat cell lines at 30μM (Coste et al., 2010a). It inhibits PIEZO1-induced currents in HEK cells transfected with the PIEZO1 channel with an IC50 of 5.4μM (Coste et al., 2012). Ruthenium red has also been reported to inhibit Yoda1-induced calcium current(Coste et al., 2012) as well as a number of TRPV channels. Gadolinium is a trivalent lanthanide ion. It was first described as a potent inhibitor of voltage-gated calcium uptake and noradrenaline release in bovine chromaffin cells(Bourne, 1982). It is known to inhibit a number of channels including PIEZO1 (Syeda et al., 2015) and ORAI1(Hou et al., 2012). GsMTX4 is a 35 amino acid peptide toxin isolated from the venom of the Grammostola spatulata spider, that was identified as an inhibitor of stretch-activated current in astrocytes and cardiac myocytes (Suchyna, 2000). GsMTx4 was first reported to block PIEZO1 pressure-induced currents in PIEZO1-transfected HEK cells from both open and closed channels using concentrations between 2.5-3μM (Bae C, 2011). In addition, the compound does not display stereochemical specificity as both the D- and L-enantiomers inhibit PIEZO1 currents effectively(Bae C, 2011). However, it has also reported effects against other mechanosensitive channels such as TRPV6(Spassova, 2006). It has also been shown to inhibit shear stress-induced calcium entry in HUVECs(Li et al., 2014).

These compounds were used to determine whether they would have a similar inhibitory effect against Yoda1-induced calcium elevation in SW480 and HT-29 cells.

4.3.3.1. Ruthenium Red

In order to determine whether ruthenium red would inhibit Yoda1-induced calcium elevation, cells were pre-incubated with a range of concentrations of ruthenium red between 0.01μM and 40μM prior to treatment with 5μM of Yoda1.

In SW480 cells ruthenium red inhibited Yoda1-induced calcium entry at high concentrations only (Figure 4.4A). Measuring peak calcium amplitudes, there was inhibition at 10μM (80.1%) (p= 1.3E-4), 20μM (91.9%) (p=4E-5) and 40μM (97%) (p=2.4E-5). A Hill curve fitted to the inhibition data from Figure 4.4B derived an IC50

concentration of 3.7µM (Figure 4.4B). The inhibitor had a very similar effect on the area under the curve with inhibition at 10µM (74.8%) (p=5.7E-6), 20µM (86.9%) (p=1.2E-6) and 40µM (89.3%) (p=9.3E-7), generating an IC50 of 4.37µM (Figure 4.4C).

In HT-29 cells, ruthenium red inhibited Yoda1-induced calcium entry at high concentrations only (Figure 4.5A). Measuring peak calcium amplitudes, ruthenium red was relatively more potent with inhibition at 5µM (52.7%), 10µM (79.8%), 20µM (89.7%) and 40µM (97.3%) (Figure 4.5B). However, a Hill curve fitted to the inhibition data from Figure 4.4B derived an IC50 concentration of 4.1µM, very similar to that in SW480 cells. Again, the inhibitor had a very similar effect on the area under the curve with inhibition at 5µM (43.4%), 10µM (75.2%), 20µM (73.1%) and 40µM (75.5%), generating an IC50 of 4.37µM (Figure 4.5C).
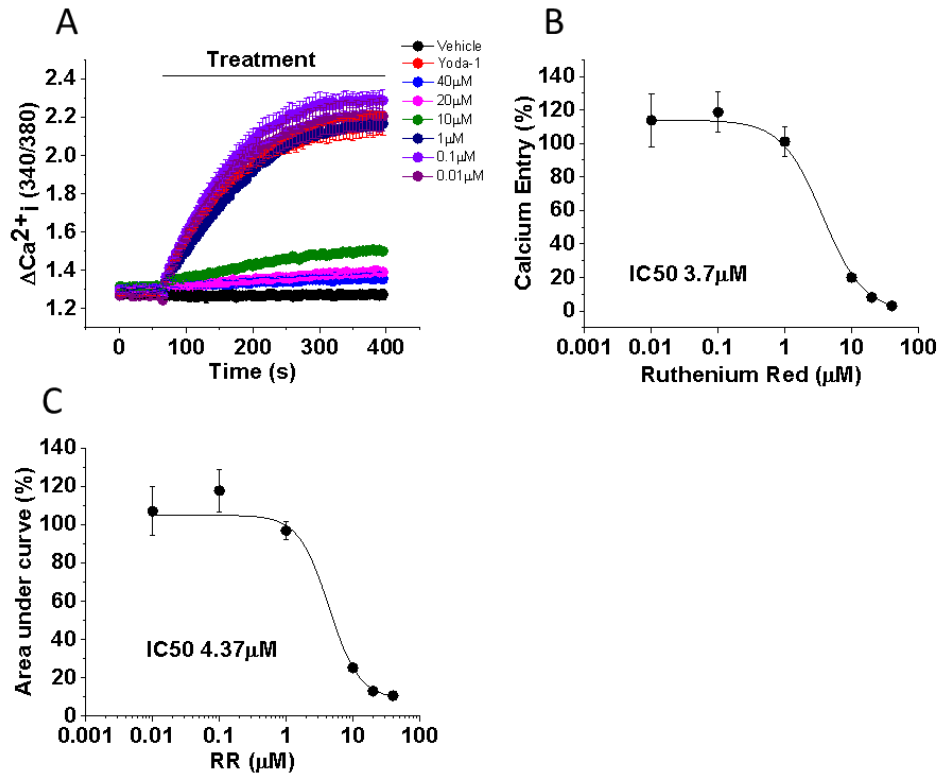
Figure 4.4. The effect of ruthenium red (RR) on Yoda1 calcium response in SW480. A. Cytoplasmic calcium traces of SW480 cells following addition of Yoda1 following pre-incubation with a range of concentrations of ruthenium red. B. Dose-response curve derived from the peak calcium amplitude data presented in A. C. Dose-response curve derived from area under the curve data for each dose, derived from the data in A. Key: s = seconds. All experiments n/N = 3/3.
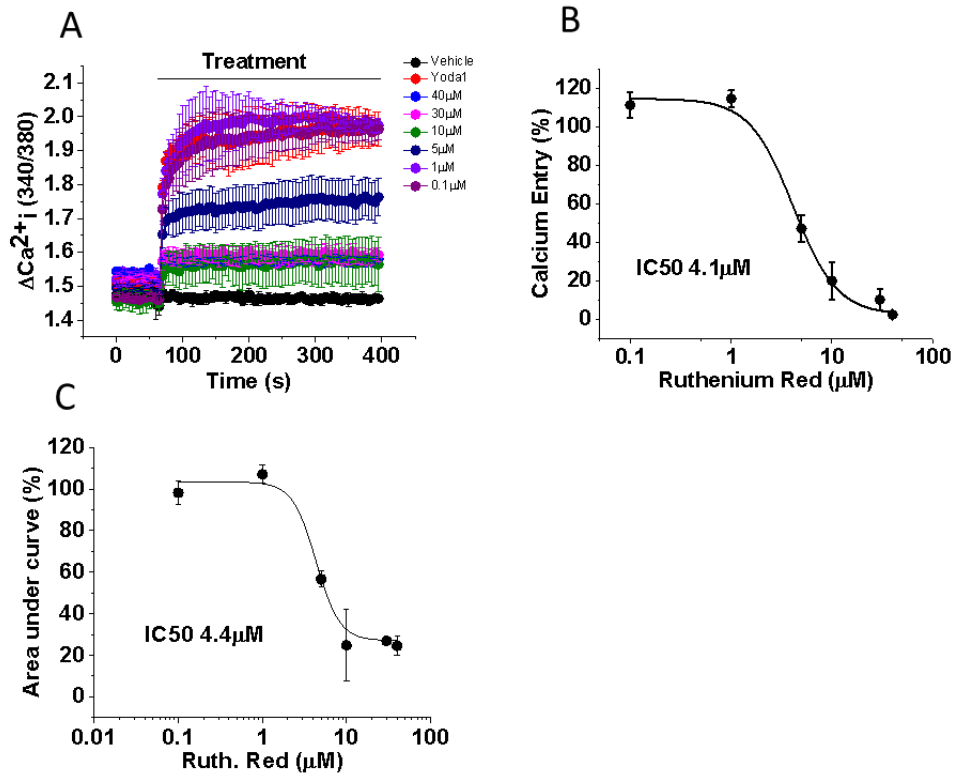
Figure 4.5. The effect of ruthenium red (RR) on Yoda1 calcium response in HT-29.

A. Cytoplasmic calcium traces in HT-29 following the addition of Yoda1 to cells following pre-incubation with a range of concentrations of ruthenium red. B. Dose-response curve derived from the peak calcium amplitude data presented in A. C. Dose-response curve derived from the area under the curve for each dose, derived from the data in A. Key: s = seconds. All experiments are n/N=3/3.

4.3.3.2. Gadolinium

In order to determine whether gadolinium inhibited Yoda1-induced calcium elevation, cells were pre-incubated with various concentrations of gadolinium prior to addition of Yoda1.

Gadolinium inhibited Yoda1-induced calcium entry in both SW480 and HT-29 cell lines.

In SW480 cells, gadolinium inhibited Yoda1-induced calcium entry (Figure 4.6A). Measuring peak calcium amplitudes, there was inhibition at 5μM (52.7%) (p=3.5E-4), 15μM (79.6%) (p=2.9E-6), 30μM (89.7%) (p=6.8E-7) and 100μM (97.3%) (p=2.4E-7) (Figure 4.6B). Plotting a Hill curve to the peak calcium amplitudes allowed extrapolation of an IC50 concentration of 2.17μM (Figure 4.6B). There was greater inhibition seen when measuring the area under the curve, with inhibition at 1μM (49.7%, p=3E-4), 5μM (83%, p=7.1E-7), 15μM (95%, p=1.3E-7), 30μM (88.6%, p=3.1E-7) and 100μM (96%, p=1.1E-7) (Figure 4.6C). However, plotting the percentage area under the curve relative to Yoda1 generated an IC50 of 1.9μM, similar to that from the peak calcium amplitudes.

In HT-29 cells, gadolinium inhibited Yoda1-induced calcium entry (Figure 4.7A). Measuring peak calcium amplitudes, there was inhibition at 30μM (68.8%, p=6.4E-7), 90μM (100%, p=9.2E-6) and 100μM (98%, p=1.2E-5) (Figure 4.7B). Plotting a Hill curve to the peak calcium amplitudes allowed extrapolation of an IC50 concentration of 23.3μM (Figure 4.7B). There was similar inhibitory effect seen on analysing the area under the curve, with inhibition at 30μM (71.8%, p=0.005), 90μM (95.4%, p=2.9E-4) and 100μM (3.1%, p=2.5E-4) (Figure 4.7C). Plotting the percentage area under the curve relative to Yoda1 generated an IC50 of 23.7μM, similar to that from the peak calcium amplitudes.

4.3.3.3. GsMTx4

In order to determine whether GsMTx4 inhibited Yoda1-induced calcium entry, cells were pre-incubated with 2.5μM of GsMTX4 prior to addition of 10μM Yoda1.

GsMTx4 inhibited Yoda1-induced calcium influx in HT-29 cells (Figure 4.8A). Similarly, GsMTx4 inhibits Yoda1-induced calcium influx in SW480 cells (Figure 4.8B). The inhibition was small in both cell lines, with 20.7% calcium blockade in SW480 (p=0.02) and 24.8% blockade in HT-29 (p=0.03) (Figure 4.8C). It did not alter the initial rate of calcium entry but reduced the total amount of calcium entry in

both cell lines. However, there is no effect on the area under the curve relative to the Yoda1 alone (SW480 19.2% inhibition, p=0.09; HT-29 24.7% inhibition p=0.09) (Figure 4.8D).

4.3.4. Conclusion

In summary, all cation channel inhibitors with proven inhibitory effect against the PIEZO1 channel inhibited Yoda1-induced calcium entry in SW480 and HT-29 cells. The potency of Yoda1-induced calcium entry for both cell lines was similar to the IC50 inhibitory concentration for PIEZO1 current reported by Coste *et al* against patch pressure-induced current (Coste et al., 2012). However, the degree of GsMTx4 inhibition of Yoda1-induced calcium entry was weak in both the SW480 and HT-29 cells, which contrasts to reported potency against the PIEZO1 channel. However, literature reporting on GsMTx4 in PIEZO1 studies have tested it against methods of mechanical activation using pressure clamp measuring current (Bae C, 2011) rather than chemical activation. The potency of the effect of GsMTx4 is thought to be mechano-pharmacological: GsMTx4 is thought to be a gating modifier, modifying the conformation of the channel to that of a closed state by altering the properties of the adjacent lipid bilayer without modifying the channel itself (Suchyna, 2004). Yoda1 has been shown to activate the channel by binding directly to the channel (Syeda et al., 2015), so it may be hypothesized that GsMTx4 would not have the same degree of effect against Yoda1.

There is a clear difference in inhibitory potency of gadolinium between the two cell lines.

In whole, this pharmacological data does support the hypothesis that PIEZO1 channels mediate the Yoda1-induced calcium entry in both cell lines. However, it should be borne in mind that these three compounds are known to be non-selective with reported effects against a number of cation channels. Targeted siRNA knockdown of the PIEZO1 channel was successfully used to demonstrate specificity of Yoda1 against the PIEZO1 channel in both cell lines. Complete knockdown of the channel is not feasibly attained with siRNA transfection. Creation of modified HT-29 or SW480 cell lines would generate more robust models for better determination of this, for example shRNA or deletion of the PIEZO1 gene, or PIEZO1 gene overexpression.
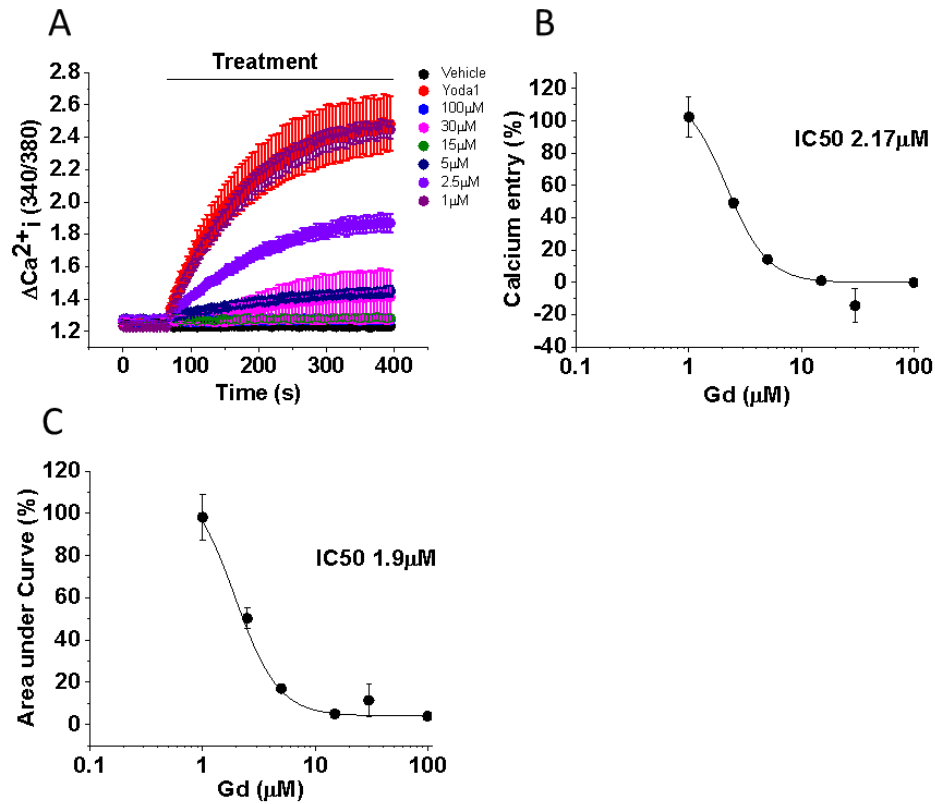
Figure 4.6. The effect of gadolinium on Yoda1-induced calcium entry in SW480. A. Cytoplasmic calcium traces of SW480 cells following the addition of Yoda1 to cells that have been pre-incubated with a range of concentrations of gadolinium. B. Dose-response curve generated from the data presented in A. C. Dose-response curve generated from the area under the curve data for each dose. Key: Gd = gadolinium; s = seconds. All experiments n/N=3/4.
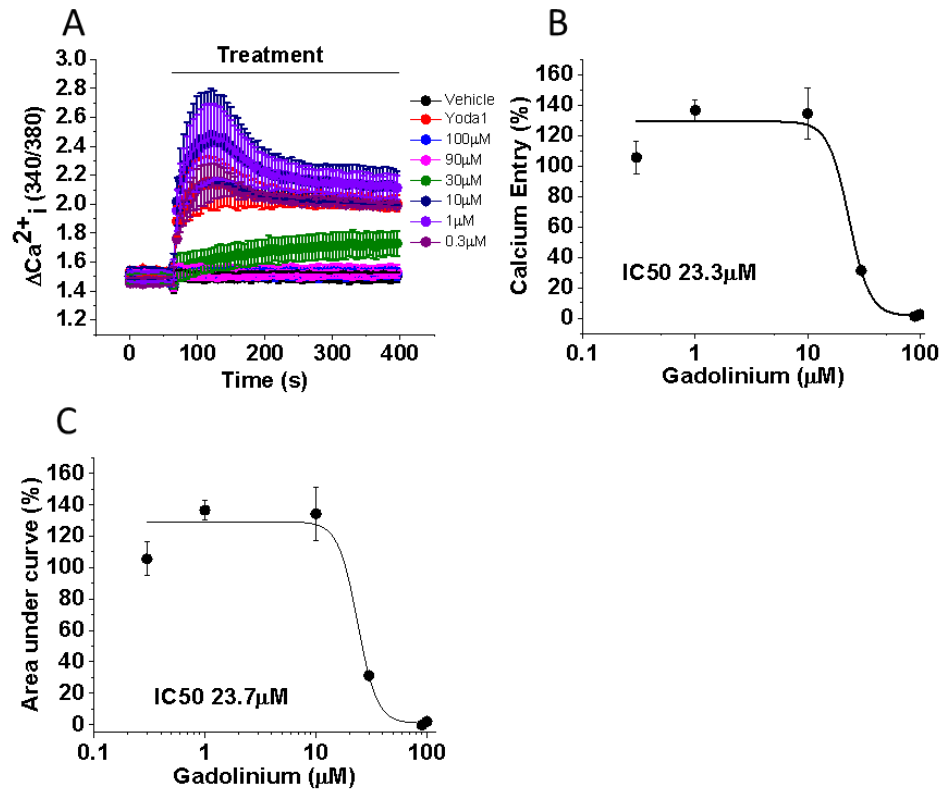
Figure 4.7. The effect of gadolinium on Yoda1-induced calcium entry in HT-29.

A. Cytoplasmic calcium traces of HT-29 cells following the addition of Yoda1 to cells that have been pre-incubated with a range of concentrations of gadolinium. B. Dose-response curve generated from the data presented in A. C. Dose-response curve generated from the area under the curve data for each dose. Key: Gd = gadolinium; s = seconds. All experiments n/N=3/4.
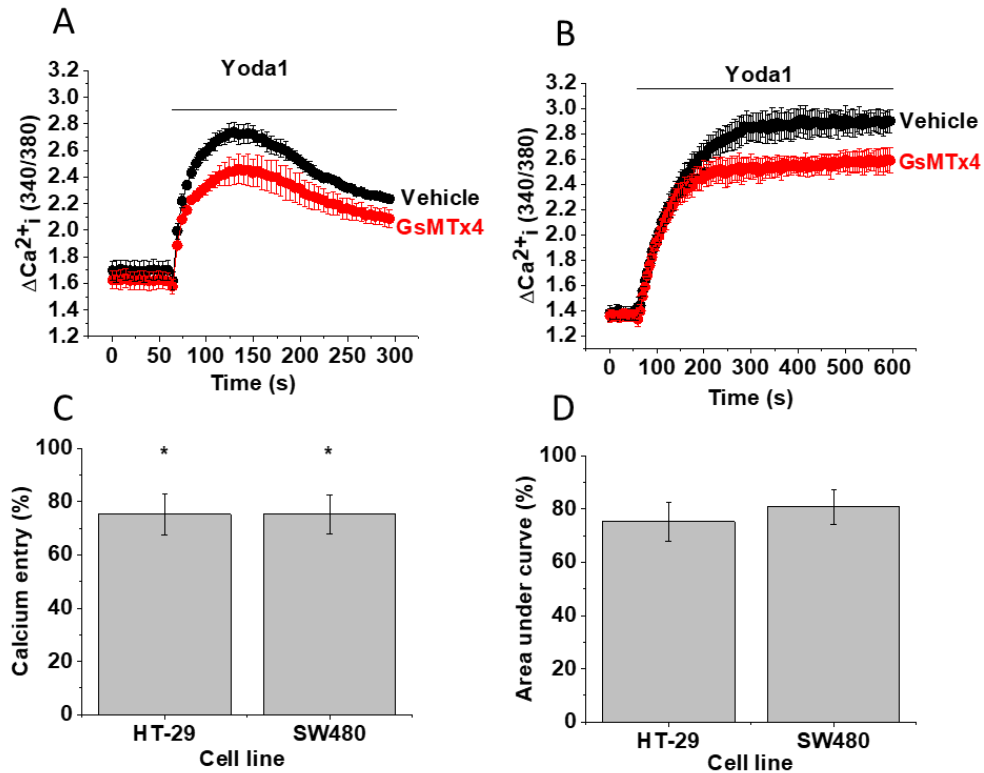
Figure 4.8. The effect of GsMTx4 on Yoda1-induced calcium entry in CRC cell lines.

A-B. A. Cytoplasmic calcium traces of cells following the addition of Yoda1 to cells that have been pre-incubated with 2.5µM GsMTx4 for 20 minutes: A. HT-29; B. SW480. C. Bar chart presenting mean±SEM percentage blockade of Yoda1-induced calcium entry in both cell lines calculated from the peak calcium amplitude, derived from the data in A and B. D. Bar chart presenting mean±SEM percentage blockade of Yoda1-induced calcium entry in both cell lines calculated from the area under the curve, derived from the data in A and B. Key: s = seconds. T testing: * = p≤0.05; ** p=≤0.01; *** p=≤0.001; NS = not significant. All experiments n/N=3/4.

4.4. The role of PIEZO1 in colorectal cancer cell function

It has been established in the previous section that the PIEZO1 gene is expressed in the chosen colorectal cancer cell lines. Furthermore, the protein is functional and can be both activated by Yoda1 and expression can be reduced using siRNA transfection. Therefore, work in this section will determine whether PIEZO1 has a functional role in the hallmark functions of tumourigenesis: proliferation, replicative immortality, migration and invasion.

Transfection of 2 siRNA sequences targeting PIEZO1 was the tool predominantly used for this.

Transfection of the siRNA sequences did not alter tumour cell morphology as can be seen in Figure 4.9 for SW480 and Figure 4.10 for HT-29.

4.4.1. The role of PIEZO1 in colorectal cancer cell viability and growth

4.4.1.1. WST-1 cellular viability assay

The WST-1 cellular viability assay was used to determine the viability of cells transfected with siRNA relative to the scrambled-transfected control, over a 5-day period in SW480 cells and over a 4-day period in HT-29 cells.

In SW480 cells, the viability of scrambled-transfected cells was determined alongside non-transfected cells to determine whether the scrambled sequence had an effect on cellular viability. There was no difference in viability between the 2 conditions (Figure 4.11A). Therefore, the scrambled sequence was deemed an appropriate control in this cell line for this study. There was no difference in viability across the first 2 days of the assay. At day 3 viability was lower in s18891-transfected cells relative to scrambled but not s138387-transfected cells. However, there was lower viability in both PIEZO1 siRNA-transfected sequences on day 4 and day 5 (Figure 4.11B). The validity of the cellular response was concomitantly tested with a 50µM 5-FU positive control, which demonstrated a 47.7% reduction in viability at day 4 (Figure 4.11C).

In HT-29 cells, the viability of scrambled-transfected cells was determined alongside non-transfected cells. There was no difference in viability between the 2 conditions
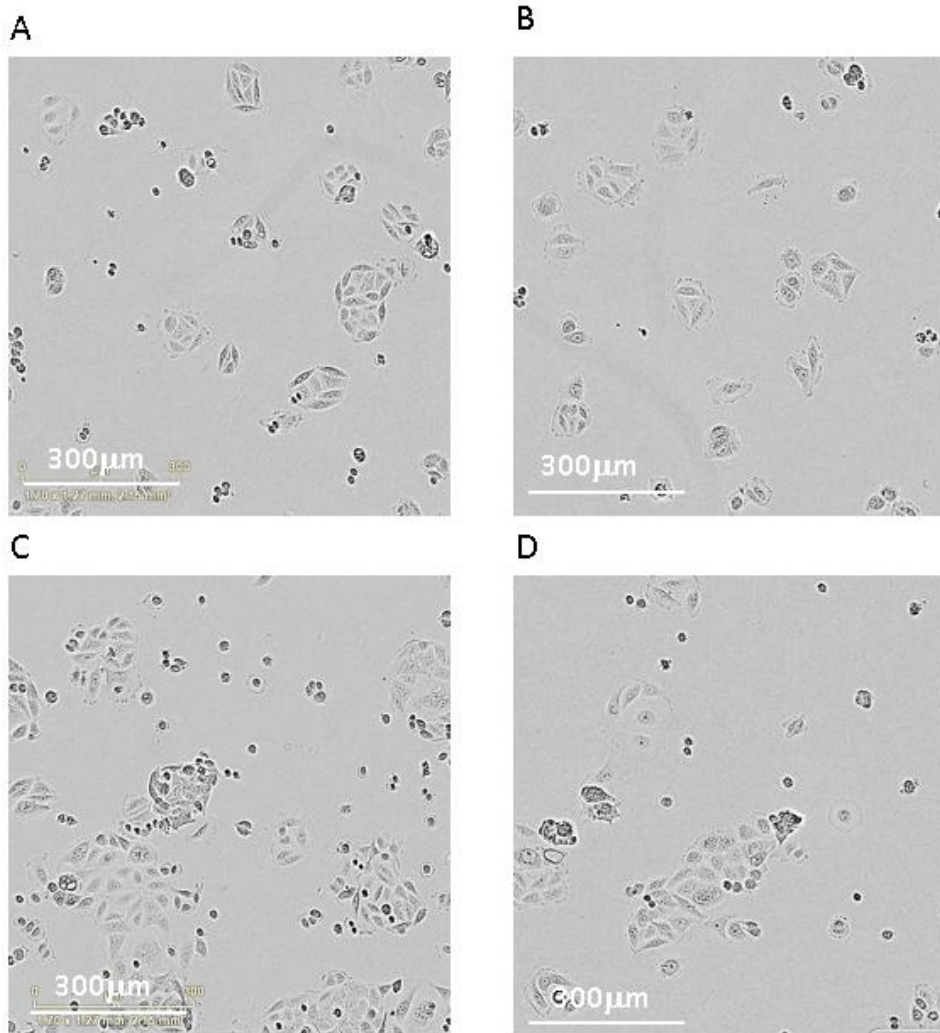
Figure 4.9. Representative bright field microscope images of SW480 cells transfected with control and PIEZO1 siRNA.

Representative light microscope bright field images of scrambled-transfected control cells at 72 hours (A) and 120 hours post-transfection (C) and PIEZO1 siRNA-transfected at 72 hours (B) and 120 hours (D) post-transfection cells. x10 magnification.
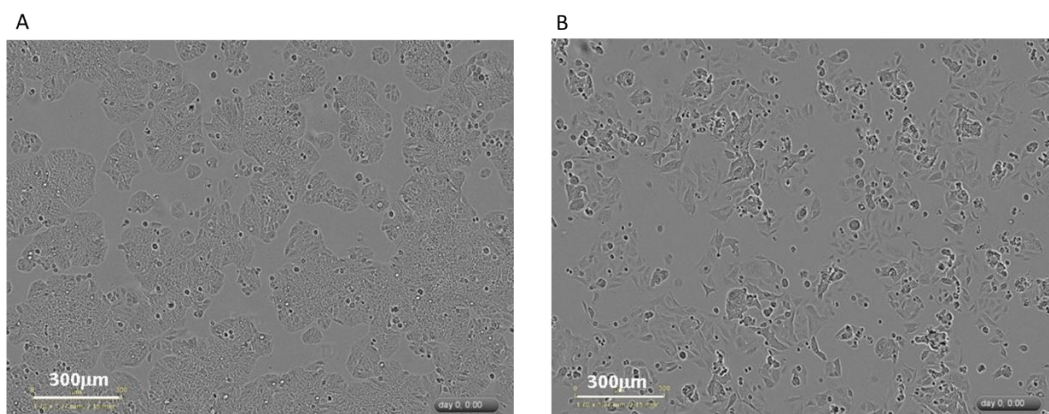
Figure 4.10. Representative bright field microscope images of HT-29 PIEZO1 siRNA-transfected cells.

Representative light microscope bright field images of scrambled-transfected (control) cells (A) and PIEZO1 siRNA-transfected at 72 hours (B). x10 magnification.
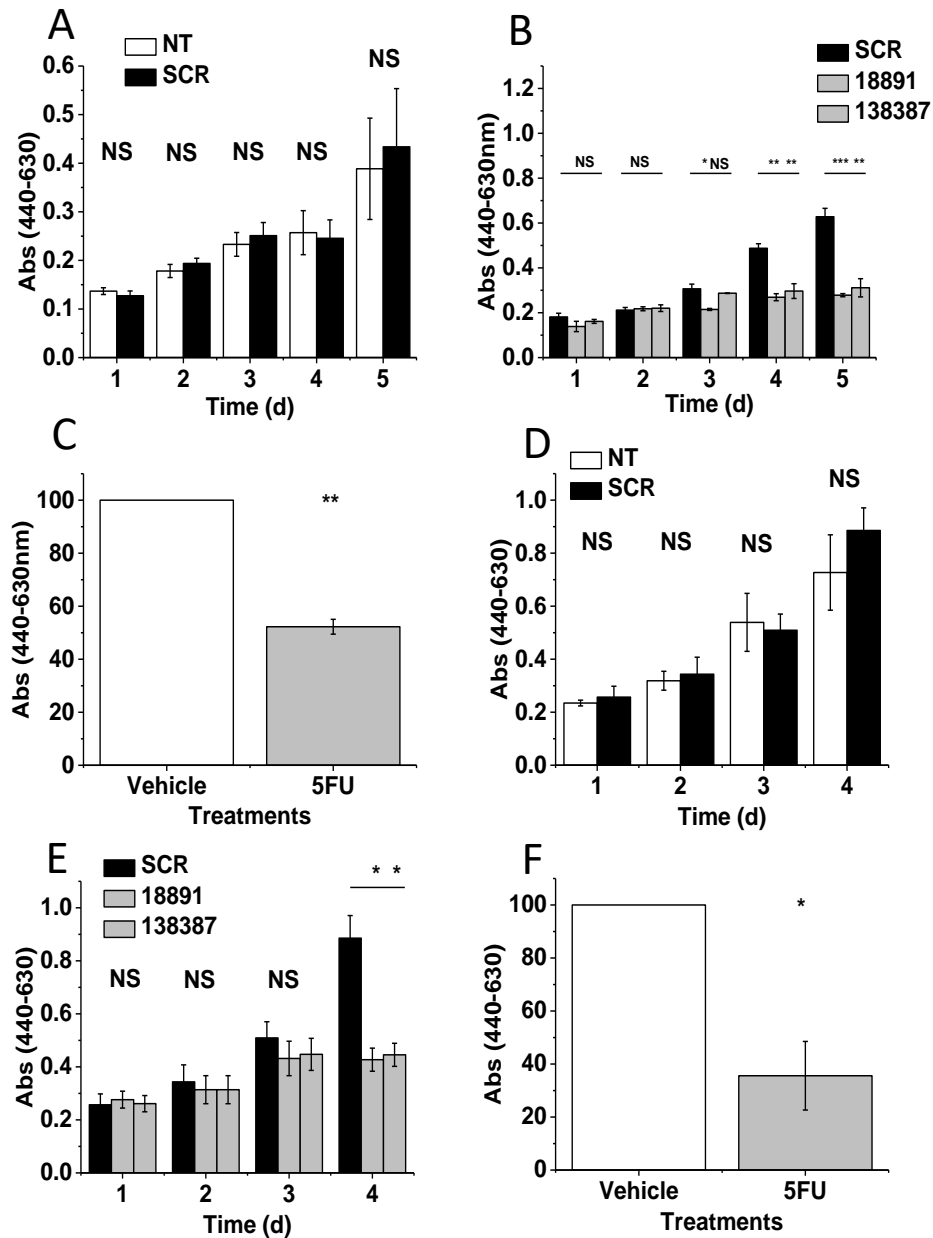
Figure 4.11. The effect of PIEZO1 on cellular viability.

A and D. Bar charts presenting mean±SEM absorbance data from the WST1 cell viability assay, for non-transfected (NT, white bar) and scrambled-transfected (scrambled, black bar) cells over a time course: A. SW480 over 5 days; D. HT-29 over 4 days. B and E. Bar chart presenting mean±SEM viability of scrambled-transfected (black bar) and PIEZO1-transfected (grey bars) cells over a time course: B. SW480 over 5 days; E. HT-29 over 4 days. C and F. Bar charts presenting mean±SEM viability of cells treated with 40µM 5-FU (grey bars) against vehicle control (white bars) against over 4 days: C. SW480; D. HT-29. Key: 5FU = 5flurouracil; Abs = absorbance; d = days. ANOVA and T testing: * = p≤0.05; ** p=≤0.01; *** p=≤0.001; NS = not significant. All experiments n/N=3/3.

(Figure 4.11D). Therefore, the scrambled sequence was deemed an appropriate control in this cell line for this study. There was no difference in viability for the first 3 days of the assay (Figure 4.11E). At day 4 viability is significantly lower than the scrambled in both transfected conditions (Figure 4.11E). The validity of the cellular response was concomitantly tested with a 50µM 5-FU positive control, which showed a 73.6% reduction in viability at day 4 (Figure 4.11F).

This assay has identified an effect of PIEZO1 knockdown on cellular viability, however it is unable to characterise whether the effect is cytostatic or cytotoxic. Therefore, proliferation studies were carried out using growth studies with trypan blue to quantify live and dead cell fractions at each time point.

4.4.1.2. Growth curves using trypan blue exclusion assay

PIEZO1 siRNA was used to study whether PIEZO1 knockdown affects cancer cell viability and growth in both cell lines.

In SW480 cells, the viability of scrambled-transfected cells was determined alongside mock-transfected cells. Both cells displayed identical growth characteristics with a lag phase carrying into exponential growth at day 5 (Figure 4.12A). There were slightly more cells in the non-transfected versus the scrambled-transfected at day 1 (NT 10,867 vs scrambled 9,583, p=0.045), however there was no difference in viable cells between the 2 conditions at each subsequent time point. By day 7, wells for both conditions were approaching confluence. This data validated the scrambled sequence as an appropriate control for this experiment.

There was no difference in viable cells between the scrambled-transfected control and PIEZO1 siRNA-transfected cells at day 1, suggesting that the plating efficiency of cells was not affected by transfection with scrambled and siRNA sequences (Figure 4.12B, 4.12C). The lag phase for cells transfected with both PIEZO1 siRNA sequences was the same as that seen in the non-transfected and scrambled-transfected cells. However, growth characteristics were slower than the scrambled-transfected, and was lower than the scrambled from day 3 (Figure 4.12B, 4.12C).

There was no difference in the number of dead cells between scrambled-transfected and PIEZO1-transfected cells (Figure 4.12D). As expected, there was a significantly higher number of dead cells in the 5-FU treated cells from day 3 onwards (Figure 4.12D).

190

In HT-29 cells, the viability of scrambled-transfected cells was compared to non-transfected cells. Both cells displayed identical growth characteristics with a lag phase carrying into exponential growth at day 4 (Figure 4.13A). By day 7, wells for both conditions were approaching confluence. This data validated the scrambled sequence as an appropriate control for this experiment.

There was no difference in viable cells between scrambled-transfected and PIEZO1-transfected cells for the first 3 days (Figure 4.13B). However, there were fewer s18891-transfected cells at day 4 but no difference between scrambled- and s138387-transfected cells (Figure 4.13B, Figure 4.13C). There were significantly less viable cells in both PIEZO1-transfected sequences relative to the scrambled control on days 5 and 6 (Figure 4.13B, 4.13C). On day 7 there was no difference between the scrambled-transfected and s18891- and s138387-transfected cells (Figure 4.13C).

There was no difference in the number of dead cells seen between the scrambled-transfected and PIEZO1-transfected cells across the 7-day period (Figure 4.13D). There was greater cell death seen in the 5-FU treated cells from day 4 onwards (Figure 4.13D).

This data indicates that PIEZO1 is important in cellular viability. Knockdown reduces viability and impacts on growth characteristics without causing cell death.
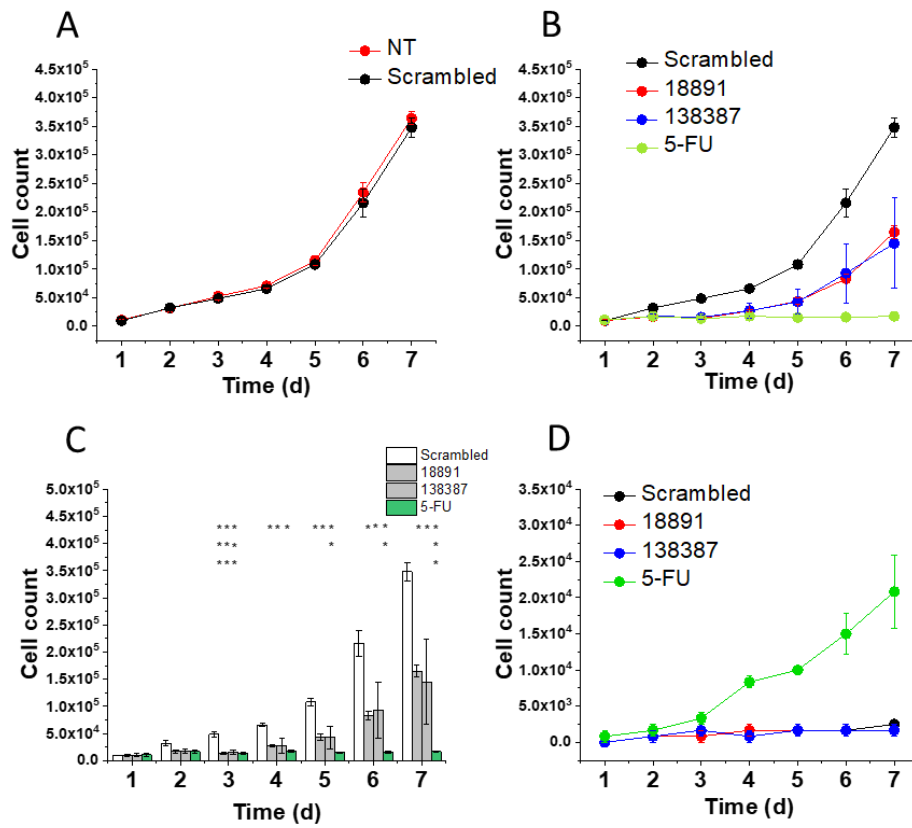
Figure 4.12. The effect of PIEZO1 on cell viability in SW480: trypan blue exclusion assay and growth curve.

A. Growth curve presenting the growth characteristics of non-transfected (NT) and scrambled-transfected (scrambled, black) cells. B. Growth curve presenting the live cell fraction of scrambled-transfected (black), PIEZO1-transfected (red and blue) and 5-FU-treated (40µM, green) cells over 7 days following plating. C. Bar chart presenting mean±SEM live cell fractions (vehicle, white bars; PIEZO1 siRNA grey bars; 5-FU green bars). D. Growth curve presenting the dead cell fraction of scrambled-transfected (black), PIEZO1-transfected (red and blue) and 5-FU-treated (green) cells. Key: d = days; 5FU = 5-flurouracil. ANOVA testing: * = $p \leq 0.05$; ** $p = \leq 0.01$; *** $p = \leq 0.001$; NS = not significant. All experiments n/N=3/3.

Figure 4.13. The effect of PIEZO1 on cell viability in HT-29: trypan blue exclusion assay and growth curve.

A. Growth curve presenting the growth characteristics of non-transfected (NT) and scrambled-transfected (scrambled, black) cells. B. Growth curve presenting the live cell fraction of scrambled-transfected (black), PIEZO1-transfected (red and blue) and 5-FU-treated (40µM, green) cells over 7 days following plating. C. Bar chart presenting mean±SEM live cell fractions (vehicle, white bars; PIEZO1 siRNA grey bars; 5-FU green bars). D. Growth curve presenting the dead cell fraction of scrambled-transfected (black), PIEZO1-transfected (red and blue) and 5-FU-treated (green) cells. Key: d = days; 5FU = 5-flurouracil. ANOVA testing: * = p≤0.05; ** p=≤0.01; *** p=≤0.001; NS = not significant. All experiments n/N=3/3.

4.4.1.3. Colony formation assay

The clonogenic assay is a validated and effective method of looking at the survival capacity of a cell. It determines the cellular ability to proliferate indefinitely, which is quantified by the number of large-number colonies formed(Munshi, 2005). The assay runs over a number of weeks, which is beyond the scope of most other *in vitro* survival assays. In order to determine the clonogenicity of cells with PIEZO1 knockdown, transfected cells were prepared in single-cell suspensions and plated in 6 well plates. Plates were fixed and stained in methylene blue in 100% ethanol, washed and dried, and visible adherent colonies were counted under a dissecting microscope.

The clonogenic assay was only carried out in SW480 cells with the s18891 siRNA sequence. The clonogenic potential of PIEZO1-transfected cells was reduced relative to the scrambled-transfected control, with 9 colonies formed from transfected cells compared to 232 from the scrambled-transfected cells (4% of control), p<0.001. This result however indicates that PIEZO1 is important for cell division and survival.

4.4.2. Transwell migration assay

Cancer cell motility is an important factor in tumour progression and metastasis. The Boyden chamber assay is a validated and reproducible assay to study single cell migration through a porous membrane(Moutasim et al., 2011). This assay was used to study the effect of PIEZO1 on cancer cell migration. This assay studies cell migration towards a chemoattractant substance(Falasca, 2011). A number of important optimisation steps were undertaken with each cell line prior to carrying out the assay, namely serum culture conditions and the choice of mitogen.

The effect of different levels of serum deprivation on the cells was previously determined (and presented in Chapter 3) using trypan blue growth counts in sub-confluent conditions to establish the optimal culture conditions to arrest proliferation without cytotoxic effect, to allow focused study of the migratory and invasive capacity of the cancer cells. These were used again in this assay prior to initiating the migration assay.

Previous studies have used the Boyden chamber migration assays in both HT-29 and SW480 cells with migration incubation periods of 24 hours(Roh et al., 2010).

During initial testing, there was no difference in migration of non-transfected and scrambled–transfected cells in HT-29 (non-transfected 34.6, scrambled 35, p=0.963) (Figure 4.14A) or SW480 cells (non-transfected 95.8, scrambled 92.6, p=1) (Figure 4.14B).

In HT-29, migration was reduced in cells transfected with both PIEZO1 siRNA sequences (scrambled 35.5, s18891 8.98, p=6.3E-4; s138387 7.75, p=4.9E-4) (Figure 4.14C). A serum-free media (SFM) negative control was included and demonstrated minimal migration versus the scrambled-control.

In SW480, migration was reduced in cells transfected with both PIEZO1 siRNA sequences (scrambled 92.6, s18891 32.7, p=1.1E-4; s138387, p=1.1E-4) (Figure 4.14D). An SFM negative control was included and demonstrated minimal migration versus the scrambled-control.

In conclusion, this data indicates that PIEZO1 is an important protein in the process of cellular migration.

4.4.3. Transwell invasion assay.

Matrigel-coated Transwell chambers are a validated assay for studying cell invasion(Moutasim et al., 2011).

In HT-29, invasion was reduced in PIEZO1-transfected cells relative to the scrambled-transfected cells (scrambled 158.8, s18891 40.3, p=5.3E-5; s138387 44.7, p=7E-5) (Figure 4.15A). A serum-free media (SFM) negative control demonstrated no invasion relative to the scrambled control.

In SW480, invasion was reduced in PIEZO1-transfected cells relative to the scrambled-transfected cells (scrambled 83.3, s18891 17.4, p=9.7E-6; s138387 30, p=4.8E-5) (Figure 4.15B). A serum-free media negative control demonstrated no migration relative to the scrambled control.

In conclusion, the data indicates that PIEZO1 is involved in cancer cell invasion.
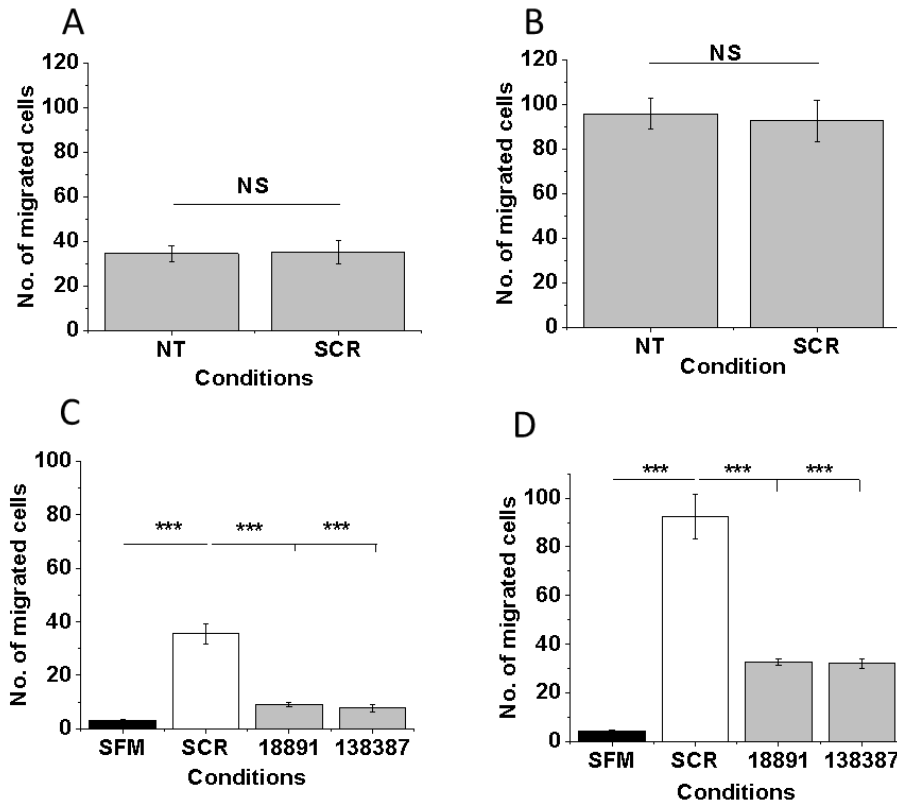
Figure 4.14. The effect of PIEZO1 on cancer cell migration.

A-B. Bar chart presenting mean±SEM migration of non-transfected (NT) and scrambled-transfected cells: A. HT-29; B. SW480. C-D. Bar chart presenting mean±SEM migration of scrambled-transfected (white bar), PIEZO1-transfected cells (grey bars) and the serum-free media (black bar) negative control: C. HT-29; D. SW480. All experiments are n/N=3/2. Key: SFM = serum free media; SCR = scrambled. ANOVA testing: * = p≤0.05; ** p=≤0.01; *** p=≤0.001; NS = not significant.
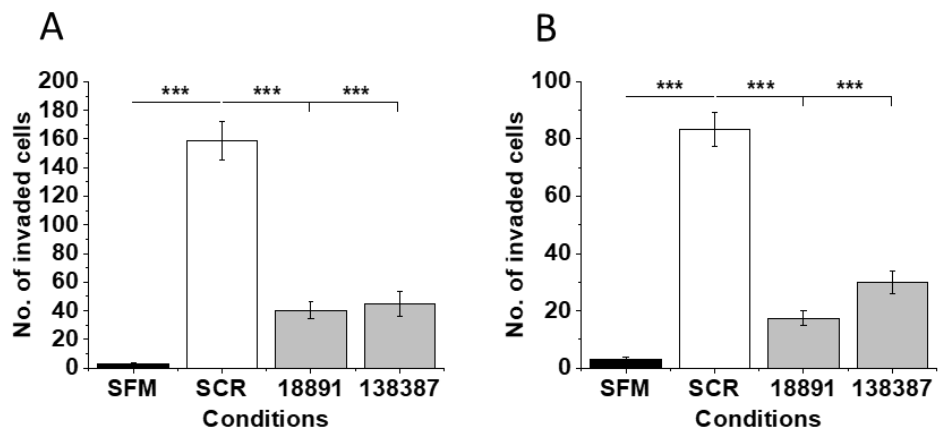
Figure 4.15. The effect of PIEZO1 on cancer cell invasion.

A-B. Bar chart presenting mean±SEM number of Boyden chamber invaded cells, with data from scrambled-transfected (SCR, white bar), PIEZO1 siRNA (grey bars) and the SFM negative control (black bar): A. HT-29; B. SW480. All experiments are n/N=3/1. ANOVA testing: * = p≤0.05; ** p=≤0.01; *** p=≤0.001; NS = not significant.

4.4.4. Cell cycle profiling

PIEZO1 has previously been found to be important in stretch-activated mitosis of cells at the G2/M checkpoint of the cell cycle(Gudipaty et al., 2017). It was therefore postulated that the effects against cell viability and growth seen with PIEZO1 knockdown could affect cell cycling.

Propidium iodide flow cytometry was used to analyse the cell cycling profile of transfected SW480 cells. Cell cycle profiling of scrambled-transfected cells was compared to non-transfected cells. There was no difference in cell cycle profiles at day 2 (Figure 4.16A) and day 3 post-seeding (Figure 4.16B). This validated that the scrambled sequence did not have effect on the cell cycle profile.

Cell cycle profiles were collected over 2-4 days to determine any effects of PIEZO1 siRNA (Figure 4.16C-E). There was no difference in the cell cycle profiles at day 2 (Figure 4.16C). At day 3, there was a reduction of the number of cells in the G1 phase in PIEZO1 siRNA-transfected cells and an increased number of cells in the G2M phase (Figure 4.16D). However, there was no difference in the proportion of cells in S phase. At day 4, there was a reduction in the number of cells in G1 phase in PIEZO1 siRNA-transfected cells with an increase in the proportion of cells in S phase and G2M phase (Figure 4.16E).

This data indicates that PIEZO1 knockdown generates G2M arrest.
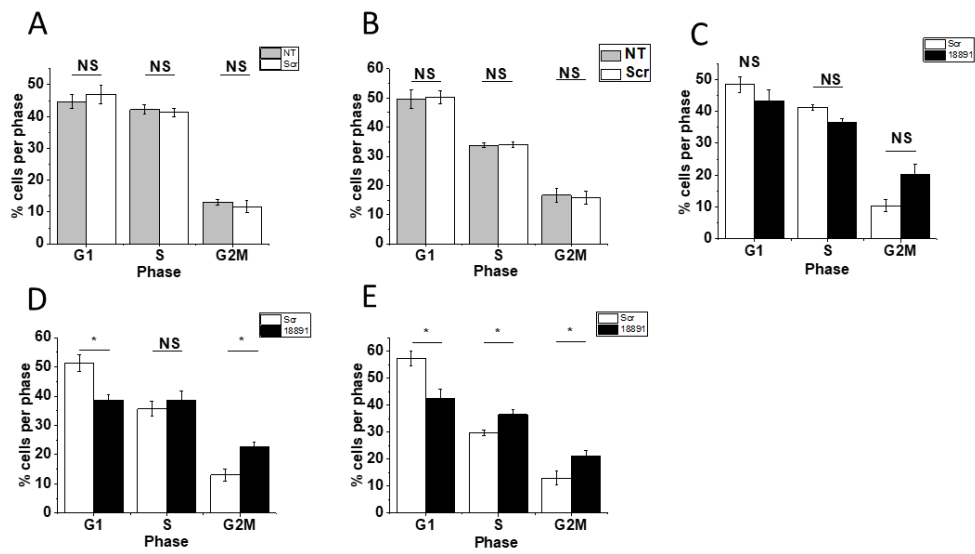
Figure 4.16. The effect of PIEZO1 on cell cycle profiling in asynchronised SW480 cells.

A-E. Bar charts presenting the mean±SEM percentage of cells in each cell cycle phase. A-B. Cell cycle phase profiles of non-transfected (NT, grey bar) and scrambled-transfected (SCR, white bar): A. Day 2; B. Day 3. C-E. Cell cycle phase profiles of scrambled-transfected (SCR, white bar) and PIEZO1-transfected (s18891, black bar) cells: C. Day 2; D. Day 3; E. Day 4. All experiments are n/N 3/1. ANOVA testing: * = p≤0.05; ** p=≤0.01; *** p=≤0.001; NS = not significant.

4.5. The effect of Yoda1 on cancer cell viability

The data indicates that PIEZO1 is important in cellular proliferation. Intracellular influx of calcium has previously been shown to activate the Ras/MEK/ERK proliferation pathway. Calcium influx from store release and membrane depolarisation through L type voltage gated calcium channels have both previously been reported to activate MEK1 downstream of Ras to activate MAPK in the PC12 rat phaeochromocytoma cell line(Rosen et al., 1994). Furthermore, PIEZO1 has been shown to induce a calcium-dependent activation of ERK1/2 that is abrogated with PIEZO1 knockdown in MDCK cells(Gudipaty et al., 2017). Therefore, the effect of Yoda1 on the Ras/MEK/ERK pathway was explored using phospho-blotting for phosphorylation of pERK.

4.5.1. Phospho-pERK western blotting

Cells were transfected with scrambled-sequence or PIEZO1 siRNA sequences. At 48 hours post transfection, cells were serum starved for 24 hours. Cells were treated with 10µM Yoda1 or DMSO vehicle control for 30 minutes then cells were harvested on ice for western blotting. MEK1/2 are activated by growth factors such as EGF(Mizuno et al., 2006). EGF-induced pERK phosphorylation is inhibited by the MEK inhibitor PD98059. Therefore, cells were concomitantly treated with 50ng/ml of EGF following a 20-minute incubation with either the MEK inhibitor PD98059 or the DMSO vehicle control as a positive control.

Visible inspection of the blots indicated that there was minimal phospho-pERK band intensity in the vehicle control cells for scrambled-transfected and PIEZO1-transfected cells (Figure 4.17A). Yoda1 treatment increased band intensity of all 3 transfected conditions (Figure 4.17A). The total ERK (pERK) loading control demonstrated equal protein loading in all conditions (Figure 4.17A). Image J was used to quantify band intensities. This confirmed an increase in phospho-pERK signalling in scrambled-transfected (vehicle 37.9, Yoda1 123.5, p=0.007), s18891-transfected (vehicle 41.3, Yoda1 109, p=0.05) and s138387-transfected cells (vehicle mean 39.8, Yoda1 116.4, p=0.017) (Figure 4.17B). This data indicates that Yoda1 activates Ras/MEK/ERK signalling. However, there was no difference in the band intensities between the scrambled-transfected and PIEZO1-transfected cells (p=1). Therefore, PIEZO1 is not essential in Yoda1-induced Ras/MEK/ERK signalling.

EGF phosphorylated pERK (Figure 4.17C, 4.17D) (mean intensity 129). The MEK inhibitor PD98059 inhibited EGF-induced pERK phosphorylation (mean intensity 23.1, p=3.5E-4) (Figure 4.17C, 4.17D). These findings were consistent with findings from the literature and validated that the cells were responding appropriately.

4.5.2. Trypan blue exclusion cellular viability assay

The data thus far suggests that PIEZO1 is important in cellular proliferation. Therefore, Yoda1 was used in cell culture to determine whether it can induce cellular proliferation. A concentration range was chosen by considering those concentrations that had previously shown significant effect on calcium response: in HT-29 these were 10µM (p=0.006) and 5µM (p=0.026); in SW480 these were 10µM (p=1.6E-9), 7.5µM (p=4.8E-8) and 4µM (p=3.75878E-4). Therefore, 10µM and 5µM concentrations were chosen for use in both cell lines. Cells were plated in a 24 well plate and counted over 4 days.

HT-29 cells treated with vehicle displayed normal growth characteristics, with a lag phase and entering exponential growth after day 2 (Figure 4.18A). Both concentrations of Yoda1 did not affect cellular proliferation for the first 2 days (Figure 4.18A and 4.18B). Cellular proliferation was reduced with both concentrations at day 3 (Figure 4.18A, 4.18B). At day 4, cellular proliferation was arrested at 5µM but there was a fall in cellular counts with 10µM (Figure 4.18A and 4.18B). Trypan blue allowed quantification of the dead cell fraction (Figure 4.18C). There was an increased dead cell fraction in cells treated with 10µM at day 3 but not with 5µM. There was no increase in cell death at day 4 (Figure 4.18C).

SW480 cells treated with vehicle compound entered exponential phase immediately (Figure 4.18D), which may have been due to the different cell seeding density and different culture conditions to the previous growth studies. Yoda1 had an immediate effect on cellular proliferation (Figure 4.18D). There was a reduction in proliferating cells from day 2 to day 4 with 10µM relative to the vehicle control (Figure 4.18E). There was a reduction in proliferation from day 2 to 4 in 5µM and a fall in proliferating cells at day 4 (Figure 4.18E). However, there was no difference in cellular count between day 3 and day 4. Trypan blue allowed quantification of the dead cell fraction (Figure 4.18F). There was no difference in dead cell counts across all treatment conditions at all time points.
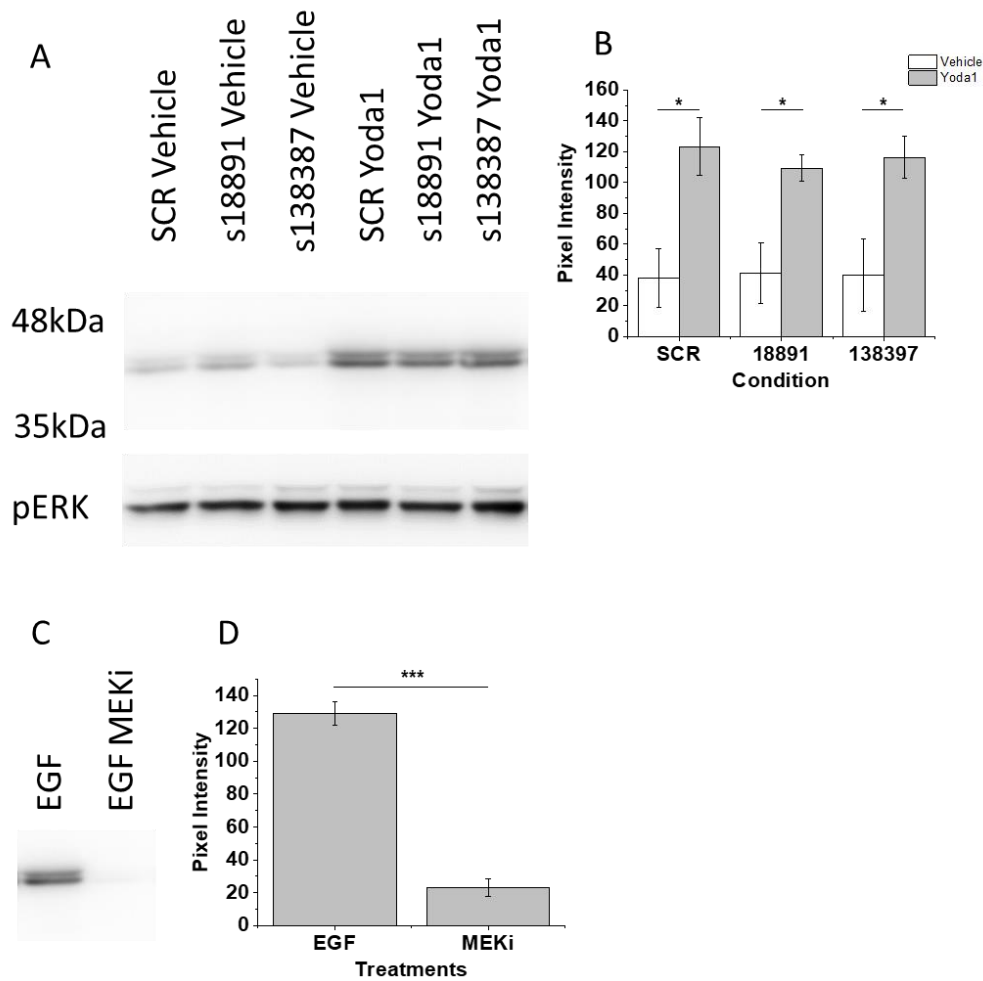
Figure 4.17. The effect of Yoda1 on pERK phosphorylation.

A. Phospho-blot of ERK phosphorylation in transfected SW480 cells treated with Yoda1 for 30 minutes, alongside the pERK (total ERK) loading control. The position of the protein markers is denoted on the left-hand side of the blot with their respective molecular weights. B. Bae chart presenting the mean±SEM pixel intensity of the Western blot expression bands for scrambled-transfected (SCR, white bar) and PIEZO1-transfected (18891, grey bar) from Figure A. C. Representative phospho-blot of SW480 cells treated with 50ng/ml of EGF for 30 minutes in the presence and absence of PD98058 MEK inhibitor (MEKi). D. Bar chart presenting mean±SEM pixel intensity of ERK phosphorylation (phosphoERK) from the bands in Figure C. All experiments n/N=3/1. ANOVA testing: * = p≤0.05; ** p=≤0.01; *** p=≤0.001; NS = not significant.
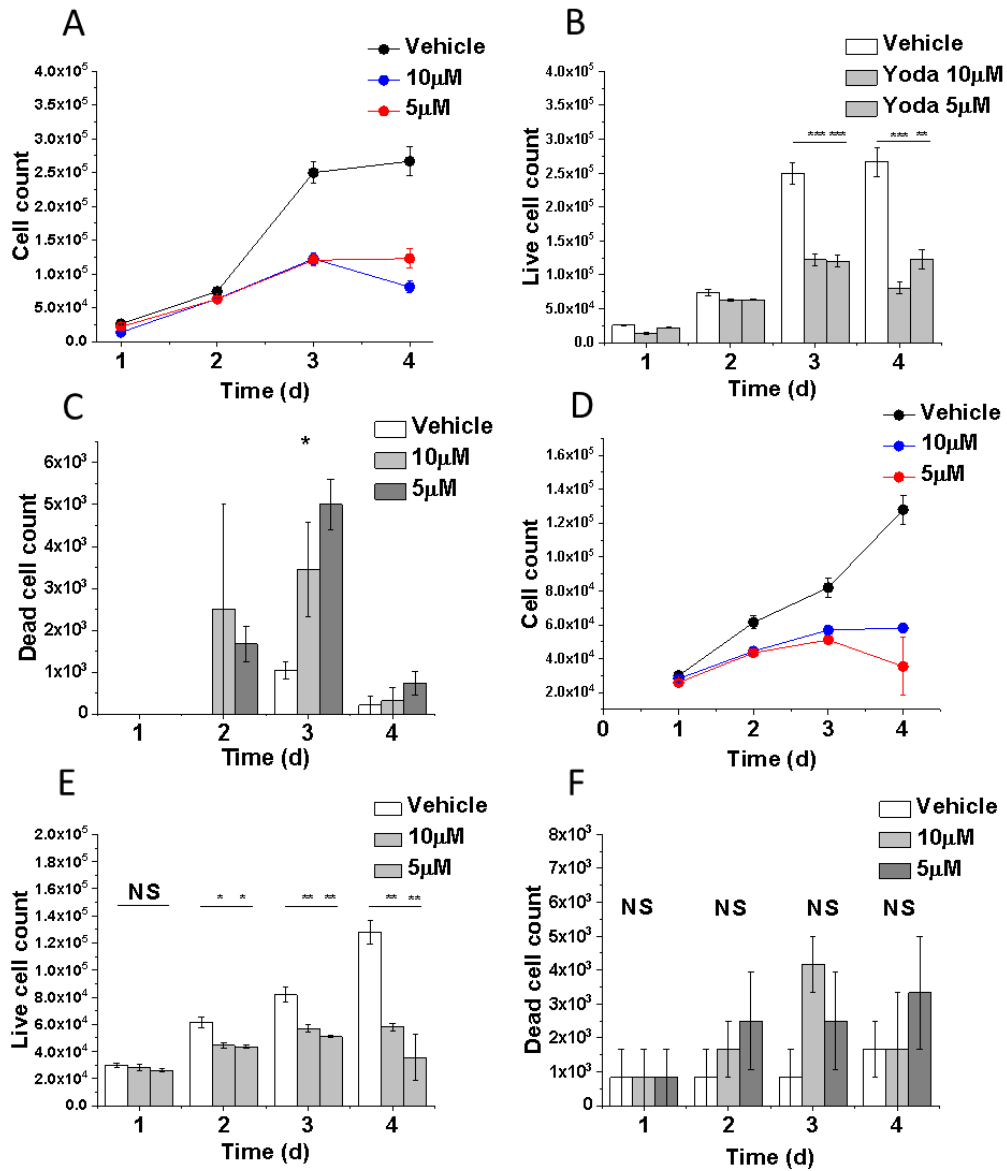
Figure 4.18. The effect of Yoda1 on cancer cell viability.

A and D. Line graph presenting live cell counts of cells treated with DMSO (vehicle, black line) and 2 concentrations of Yoda1: A. HT-29; D. SW480. B and E. Bar chart of mean±SEM live cell counts: B. HT-29; E. SW480. C and F. Bar chart of mean±SEM dead cell counts over the 4 days of treatment: C. HT-29; F. SW480. Key: d = days. ANOVA testing: * = p≤0.05; ** p=≤0.01; *** p=≤0.001; NS = not significant. All experiments n/N=3/2.

In conclusion, this data indicates that Yoda1 impacts on cell viability and growth but is not cytotoxic.

4.6. Summary of Findings

• Yoda1 induces calcium influx in HT-29 and SW480 cells but not HCT116 cells.

• Yoda1 does not result in changes in intracellular calcium levels in the absence of extracellular calcium, suggesting that Yoda1 does not induce store operated calcium release.

• The specificity of Yoda1 in inducing PIEZO1-dependent calcium entry is demonstrated using PIEZO1 siRNA as well as a number of cation channel inhibitors that have been shown to block PIEZO1 current.

• PIEZO1 siRNA knockdown results in a reduction in cell viability and proliferation. There is no increase in cell death in PIEZO1-transfected cells, suggesting that PIEZO1 knockdown is cytostatic. PIEZO1 knockdown also reduces clonogenicity.

• PIEZO1 siRNA knockdown reduces migration and ECM invasion.

• PIEZO1 siRNA results in a reduction in cells in G1 and an increase in cells arrested in G2/M.

• Yoda1 phosphorylates pERK but PIEZO1 siRNA knockdown does not affect the level of pERK phosphorylation.

4.7. Discussion

In conclusion, this chapter has shown an important role of PIEZO1 in colorectal cancer cell function. The *in vitro* work presented here has revealed a role for PIEZO1 in CRC viability. This finding is novel and has not been reported previously in colorectal cancer. It has been reported in other tumours, including synovial sarcoma cells (Suzuki et al., 2018) and glioma cells(Chen et al., 2018b). PIEZO1 has previously been found to be important in cellular proliferation in normal epithelial cells. PIEZO1 knockdown resulted in a reduction of proliferation, both *in vitro* in MDCK epithelial cells and *in vivo* in zebrafish (Gudipaty et al., 2017). The channel's mechanosensitive properties appear to play an important role in this. Epithelial cell stretch has been shown to induce PIEZO1-dependent stretch-induced mitosis and ERK1/2-dependent proliferation in a calcium-dependent manner(Gudipaty et al., 2017). Yoda1-induced ERK phosphorylation has been demonstrated in this thesis, which is consistent with previous work, but it is the first time it has been described

in CRC. Recent PIEZO1 cancer studies suggest that PIEZO1-mediated proliferation is activated by the tension of the tumour mass. Chen and colleagues have reported that PIEZO1 cell division and cell cycling is increased in GBM cell culture in polyacrylamide gels of increasing stiffness, and that siRNA knockdown resulted in reduced tumour volume *in vivo* (Chen et al., 2018b). However, pressure is unlikely to be the sole activator of the channel, particularly given the proliferative arrest seen on siRNA knockdown in HT-29 and SW480 that were cultured in pressure-free sub-confluent monolayers in routine cell culture. There is evidence that the association of PIEZO1 with integrin β1 and other cell adhesion molecules are important in cell division, so the channel may also influence proliferation this way. Chen and colleagues characterised PIEZO1 association with the cell adhesion molecules integrin β1, vinculin and focal adhesion kinase (FAK) and demonstrated a positive role for this interaction in mediating cell mitosis(Chen et al., 2018b), which may play an important role in cytoskeletal rearrangements required during mitosis. PIEZO1 involvement in cytoskeletal arrangement has previously been described by McHugh and colleagues, who found that PIEZO1 knockdown in lung epithelial cells resulted in reduced integrin β1 activation and an altered actin cytoskeleton to a more rounded phenotype(McHugh et al., 2012). However, PIEZO1 knockdown in SW480 and HT-29 cells did not result in any such altered phenotype. However, PIEZO1's interaction with integrins in CRC should be explored further.

PIEZO1 siRNA reduced cancer cell proliferation without inducing cell death, suggesting that the effect of knockdown was cytostatic. However, clonogenicity was markedly reduced, suggesting that the proliferative arrest was not reversible. PIEZO1 knockdown also resulted in an increase in cells arresting in G2/M of the cell cycle. It is possible that cell cycle checkpoints at G2/M could trigger cell death, and further work should clarify this. This finding has also not been reported in cancer to date. PIEZO1 function has been associated with G2/M cell cycle in epithelial cells previously. Epithelial cell stretch induces cyclin B1 production and mitosis with a resultant transient burst of cell division of cells paused at G2/M but not of those cells at other cell cycle checkpoints (Gudipaty et al., 2017). It is therefore reasonable to consider that PIEZO1 knockdown could impair the molecular signalling process required for mitosis at G2/M, causing cells dependent on PIEZO1 function to arrest there. Western blotting for cyclin B1 would be a logical next step in beginning to characterise this further.

PIEZO1 siRNA knockdown resulted in proliferative arrest, and Gudipaty and colleagues have previously reported that cell stretch generated a transient PIEZO1-dependent burst of cell division over a 1-hour window with an increase of 1.4% above baseline, returning to basal levels of proliferation thereafter(Gudipaty et al., 2017). It was therefore hypothesized that Yoda1 treatment would enhance proliferation. However, in this work 4 days of Yoda1 treatment resulted in a reduction in viable cells. Other researchers have also found that Yoda1 does not induce cell proliferation either. Chen and colleagues who did not see a difference in cell proliferation of GBM cells treated with Yoda1(Chen et al., 2018b), who concluded that increasing endogenous channel activity wasn't sufficient to promote cell growth. It could be postulated that the reduction in proliferation and increasing cell death of the Yoda1-treated CRC cells could be due to intracellular calcium overload by over-stimulation of the PIEZO1 channel that could overwhelm the cell's ability to handle the excess calcium, which could cause mitochondrial calcium overload, cytochrome c release and caspase-induced apoptosis, and is an area for further work in the laboratory. The molecular machinery for calcium homeostasis in cell lines such as GBM may be better primed to deal with the calcium influx to generate better calcium homeostasis.

In this thesis, PIEZO1 knockdown resulted in reduced CRC cell migration and invasion. This is in contrast to the findings of McHugh *et al*, who reported that PIEZO1 knockdown in normal lung epithelial cell line 16HBE cells increased 2D single cell migration and substrate invasion as well as cell detachment and anchorage-independent growth (McHugh et al., 2012). In further contrast to this, there was no increase in cell detachment in transfected cells in this thesis work, purely an arrest in proliferation. As they found that small cell lung carcinoma cell lines H510, H345 and H69 had very low levels of PIEZO1 expression relative to the normal epithelial lines, they used the knockdown study in normal lung epithelia as a proxy for the cancer lines. This suggests that loss of PIEZO1 expression in lung cancers results in anchorage-independent growth and a more invasive phenotype, such as that which has been shown to occur with epithelial-mesenchymal transition (EMT), a key driver in the development of the anchorage-independent phenotype and a key feature of NSCLC cell lines(Takeyama et al., 2010). This isn't to say that PIEZO1 is protective against invasion. PIEZO1 plays an important role in cell adhesion, as it is

necessary for integrinβ1 activation(McHugh et al., 2010). Integrins are involved in cancer metastasis and invasion, particularly important in establishing metastatic cell uptake into distant tissues such as the liver(Enns et al., 2004). Integrin α1β1 complexes have been demonstrated in two thirds of colorectal cancers(Boudjadi et al., 2016) and their expression has been found to be controlled by c-MYC(Boudjadi et al., 2016), an oncogene that is upregulated in 70% of colorectal cancers(Erisman et al., 1985) and that has been shown to drive tumour cell migration and invasion. Further work should look into whether PIEZO1 signalling is influenced by c-MYC, particularly in terms of migration and invasion. As well as its association with integrins, PIEZO1 may drive metastasis *in vivo* through cell extrusion. The cellular layers of the colon are constantly proliferating, and where this proliferation leads to overcrowding, both live, viable cells and apoptosing epithelial cells are extruded in order to maintain the gut's functional barrier(Eisenhoffer et al., 2012). PIEZO1 likely senses crowding through an increase of pressure within the cell monolayer, as the channel is activated by pressure(Wu et al., 2016). PIEZO1 has been shown to be inherent in the process of cell extrusion via Rho kinase-mediated actomyosin contraction, which is disrupted by both knockdown of the channel and inhibition by gadolinium in MDCK cells (Eisenhoffer et al., 2012). Basal rather than the normal apical cell extrusion has been reported in the presence of oncogenic mutations such as those occurring in APC(Marshall et al., 2011) and K-RAS(Slattum et al., 2014), and it is feasible to hypothesize that PIEZO1 may be important in the mechanical aspect of such basal cell extrusion that could propagate local tumour invasion.

Work in this chapter has also found that Yoda1 phosphorylates ERK, which has been shown previously in other cancers, suggesting that PIEZO1 signalling activates the Raf/MEK/ERK proliferation pathway. However, there was no discernible reduction in pERK phosphorylation in PIEZO1 knockdown cells relative to the control. This could be due to the fact that siRNA is not going to result in 100% transfection efficiency, so some channels will still be expressed, and their Yoda1-induced calcium entry may be sufficient to phosphorylate pERK - it is not clear whether the effect of calcium entry has a 'concentration-dependent' effect on the level of pERK phosphorylation. To this end, dela Paz and Frangos did not see a concentration-dependent Yoda1-induced increase in pERK phosphorylation(Dela Paz and Frangos, 2018). The use of some of the inhibitors used earlier in the chapter such as gadolinium and ruthenium red could also be used alongside siRNA-transfected cells

as they have demonstrated potent (albeit non-specific) inhibition. However, a recent study by dela Paz and Frangos has found that even with such potent inhibitors as gadolinium and ruthenium red did not inhibit Yoda1-induced pERK phosphorylation(Dela Paz and Frangos, 2018). However, they do inhibit Akt phosphorylation. This suggests that Yoda1 could be inducing pERK phosphorylation independently of PIEZO1 by other targets, and that PIEZO1 may preferentially activate Akt signalling and proliferation. Similar studies on Akt phosphorylation in the CRC cell lines needs to be carried out.

In conclusion, this work provides evidentiary support for a role of PIEZO1 signalling in colorectal cancer cell proliferation, migration and invasion.

4.9. Rationale to chapter 5

Study of PIEZO1 was driven by initial interrogation of the TCGA colorectal cancer dataset, following a publication by Li and colleagues who reported higher PIEZO1 expression in the MCF7 cell line relative to the normal mammary epithelial cell line MCF10A(Li et al., 2015a). This initial analysis, albeit crude, demonstrated a 1.1-fold increase in PIEZO1 expression in colon cancer relative to normal colon that led into *in vitro* work.

The work in these two chapters presents evidence of an important role for PIEZO1 in CRC growth *in vitro*. Furthermore, the work from the preceding chapter presents evidence that CRAC channel function is also important. It was therefore a logical next step to explore the role of these receptors in human tumourigenesis. We did not have access to human tissue and clinical data for the purposes of this analysis. TCGA provides open access to their comprehensive genomic dataset. Therefore, TCGA data was interrogated with the aim of characterising the role of calcium channel signalling in colorectal cancer, with particular focus on PIEZO1 and ORAI1.

Chapter 5: Transcriptome Analysis of Calcium Channel Signalling in Colorectal Cancer

5.1. Introduction

Work so far has shown that pharmacological inhibition and siRNA knockdown of ORAI1 and PIEZO1 has anti-proliferative and anti-migratory effects in CRC cell lines *in vitro*. The next logical step was to explore the significance of these receptors in cancer development. In particular, we have very little information about the ligand-based receptors that activate PIEZO1 and CRAC channel signalling in CRC, or how signalling through these receptors interplays with cell cycling, viability an proliferation, migration and apoptosis. This can be approached using *in vitro* techniques such as RNAi screens, which can identify the dependency of genes on survival or migration but are a time-consuming and labour-intensive process that was beyond the time limits of this PhD. Recently, next generation sequencing techniques such as microarray, RNASeq and proteomic analysis have become a lot more affordable and accessible to individual laboratories and are generating publications from *in vitro* cell line work, as well as human tumour and PDX tissues. This type of data is useful for generating targeted hypotheses that can then be taken back into the laboratory.

TCGA is an international multi-centre project that has sought to better understand the genomic landscape of different types of cancers. Tissue underwent comprehensive analysis including single nucleotide polymorphism (SNP) arrays, chromosome and sub-chromosomal copy number changes and translocation analysis, mRNA and miRNA expression profiling and DNA promoter methylation, generating the most comprehensive cancer dataset to date. Furthermore, the project collected baseline demographic data and clinicopathological characteristics including cancer staging, micro- and macroscopic measures of disease invasion and metastases and survival data that can be used to generate clinically relevant molecular analyses. A number of landmark papers have resulted from this project that have defined the molecular landscape of a number of cancers including colorectal cancer in 2012(The Cancer Genome Atlas et al., 2012). All of the research data is available through open access via the International Cancer Genome Consortium Data Portal since 2010 for download and individual analysis, facilitating its use in cancer research across the globe. In the body of papers generated from cancer research, there are relatively fewer papers carrying out differential analysis

between tumour and normal tissue. This may be due to the limited technical feasibility of acquiring a normal colon sample at an appropriate distance away from the tumour site at the time of resection, particularly with the increasing use of laparoscopic or robotic surgical techniques. It may also be due to concerns of 'field cancerization' of normal tissue, something that Slaughter and colleagues described from a histological analysis of normal oral mucosa adjacent to squamous cell carcinoma (SCC) showing histological preconditioning to developing neoplasia (Slaughter et al., 1953). The concern is that the normal samples may not be 'normal' as they will carry genomic aberrations in particular with cancers that have an established multistep carcinogenetic process such as colon cancer that may not have yet developed histological neoplastic changes. However, there is evidence that matched tumour-normal analysis generates clinically meaningful biological insight. A recent systematic analysis of TCGA transcriptional data from matched samples from breast, head and neck, kidney clear cell and liver carcinoma as well as adenocarcinoma and SCC of the lung report that differential analysis provides reliable and powerful results, particularly in terms of predicted survival(Huang et al., 2016).

The TCGA project has unarguably performed one of the most comprehensive genomic analyses to date. However, proteomic data is lacking relative to the genomic data. The project used reverse phase protein analysis (RPPA), a dot-blot antibody-based microarray that allows quantitative analysis of protein expression of hundreds to thousands of samples simultaneously(Spurrier et al., 2008). However, the antibody panel for colorectal cancer is limited to 208 antibodies (which do not include ORAI1 and PIEZO1) compared to the RNASeq data yielding expression data on 60,000 genes. Still, there is a significant amount of information that can be yielded from probing the cancer transcriptome that is available from TCGA without the accompanying proteomic data, in order to understand the functional elements of the cancer genome. Gene ontology and gene set enrichment analysis can allow computational functional interpretation of both differentially expressed genes as well as the cancer transcriptome in its entirety(Subramanian et al., 2005).

5.2. Aims and Objectives

The aim of this analysis was to determine whether calcium channels and calcium signalling pathways are involved in human CRC growth and metastases.

The objectives of this study include:

1. Determining whether calcium channels are differentially expressed between colorectal tumours and normal tissue.

2. Determining whether ORAI1 and PIEZO1 expression is associated with any particular clinicopathological features such as tumour stage and histopathological markers of invasion, as well as prognostic outcomes such as overall survival and progression free interval.

3. Determining whether, in colorectal tumours, ORAI1 and PIEZO1 expression correlates with other genes, and using gene ontology and pathway analysis to identify whether these genes have any functional effect.

4. Explore whether ORAI1 and PIEZO1 are associated with any of the molecular characteristics that have been described in the landmark 2012 colorectal cancer paper from The Cancer Genome Network.

The results shown here are in whole based upon data generated by the TCGA Research Network: https://www.cancer.gov/tcga.

5.3. Data characterisation

There was RNASeq data available for download for 453 colon cancer and 41 normal colon samples at the time of download. Rather than pooling datasets for normal and cancer tissue, differential expression analysis was carried out on matched normal colon and cancer tissue samples, as this generates more robust and meaningful analysis. From hereon out, the 41 patients for which matched normal tissue was available is referred to as the subgroup. The entire dataset of 453 patients is referred to as the cohort.

Prior to undertaking analysis, a number of steps were taken to determine the acceptability of the data from both tumour and normal tissue by looking at quality of the data as well as the clinical, pathological and expression characteristics of the subgroup and the cohort.

211

5.3.1. Characterisation of the paired tumour-normal dataset

5.3.1.1. The quality of the data

Before undertaking any analysis, a number of steps were taken in order to verify that the available data was of sufficient quality for analysis.

Analysis of the GC content from the raw data files prior to alignment, processing and generation of read counts is a standard quality control step. This process is referred to in the supplementary methods page 10 of the 2012 TCGA COAD paper. However, TCGA only provides processed read counts for open access, therefore we did not have access to the GC data or the raw files on which to carry out the GC analysis. The colon cancer dataset has been extensively utilised by the research community and has generated a broad range of high-quality publications. Therefore, in the current circumstances It is assumed that this quality control process was satisfactorily completed prior to generation of read counts.

5.3.1.2. Histological data

There are strict sampling criteria for including cancer and normal samples within the TCGA project, as detailed in the Methods. Biospecimen data for both cancer and normal tissue was downloaded from the TCGA website. Biospecimen data for the 41 colorectal cancer samples is presented in Figure 5.1. The median percentage of tumour nuclei was 80% (range 60-95%), all meeting the minimum criteria of 60% tumour nuclei. However, there was a varying amount of both normal and stromal tissue included in the tissue samples: the median percentage of normal cells was 1.5% with a range encompassing from 0-50%; the median stromal cell percentage was 10% with a range of 0-50%. There was minimal inflammatory cell infiltration, with no eosinophils, minimal monocyte (median 1%, range 0-1%), neutrophil (median 2%, range 0-3%) and lymphocyte (median 5%, 1-20%) infiltration. Data was not filtered for samples with no infiltration as this would reduce the number of paired samples available for analysis and impact on the statistical power. However, there was no biospecimen data recorded for the normal colon tissue. Therefore, the 41 H&E digital slides were downloaded from the GDAC portal and the tissue phenotype was validated by myself and independently by a consultant pathologist (Dr Ali Khurram), and this ascertained that these 41 normal tissue samples were normal colon.

5.3.1.3. Principal component analysis

PCA plotting of the 41 matched tumour and normal samples demonstrated distinct clustering of the colon cancer and normal colon tissue (Figure 5.2). This distinct clustering between cancer and normal colon has been reported in the literature previously in a paper carrying out PCA on 77 normal colon and 78 colorectal cancer samples(Xu et al., 2017).

5.3.1.4. Hierarchical clustering

Hierarchical clustering of the z-scores of the log2-transformed raw read counts of the 41 tumour and normal samples also demonstrated clear clustering of tumour versus normal samples (Figure 5.3). This distinct clustering has previously been shown in other paired normal analyses of TCGA data for breast cancer(Huang et al., 2016).

5.3.2. The subgroup versus the cohort

5.3.2.1. Clinicopathological characteristics

Clinicopathological characteristics and outcome data of the cancer samples in both groups were compared to determine whether the 2 groups differed in any way, as any such differences could generate bias that could skew analysis. The clinicopathological characteristics were compiled for the subgroup and compared to the cohort. The clinicopathological and demographic data are summarised for both the cohort in Table 5.1 and the subgroup of 41 patients in Table 5.2.

There was no difference in overall survival (OS) or progression free survival (PFS) between patients in the subgroup and the entire cohort (Figure 5.4). Estimated 1-, 3-, and 5- year survival of the subgroup was 94% (86.3-100%), 86.9% (75.7-99.8%) and 69.5% (43.9-100%) respectively compared to 93% (91-95%), 86% (82-90%) and 80.4% (74-87%). Equally there was no difference in survival in terms of age and sex.

There was no difference in lymphatic invasion in the subgroup but there was lower survival in patients with lymphatic invasion (p<0.0001). Univariate and multivariate analyses showed that there was no difference in sex, age, disease stage in overall survival (Table 5.3) or progression-free survival (Table 5.4). Both univariate and multivariate analyses of progression free survival showed that there was significantly higher chance of progression with venous invasion (p=0.033) (Table 5.4).
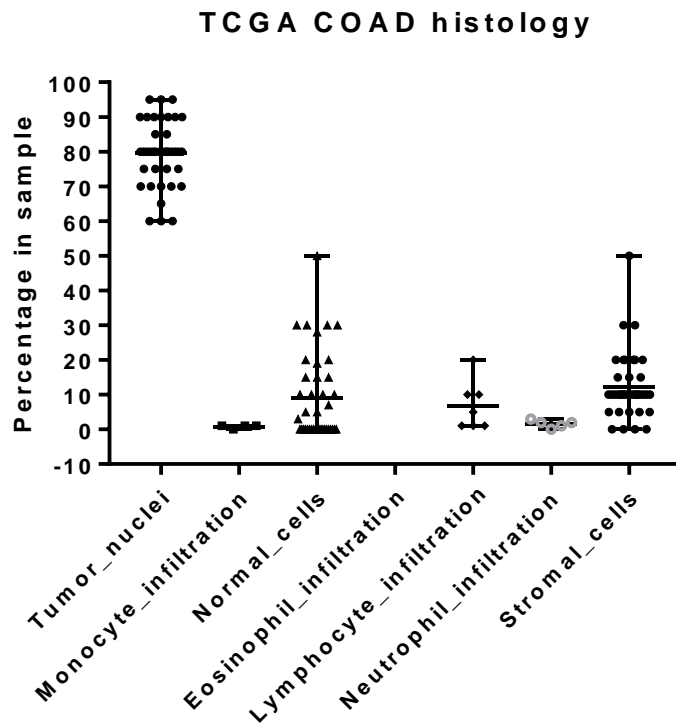
Figure 5.1. Dot whisker plot summarising the histological biospecimen data from the 41 colon cancer samples.
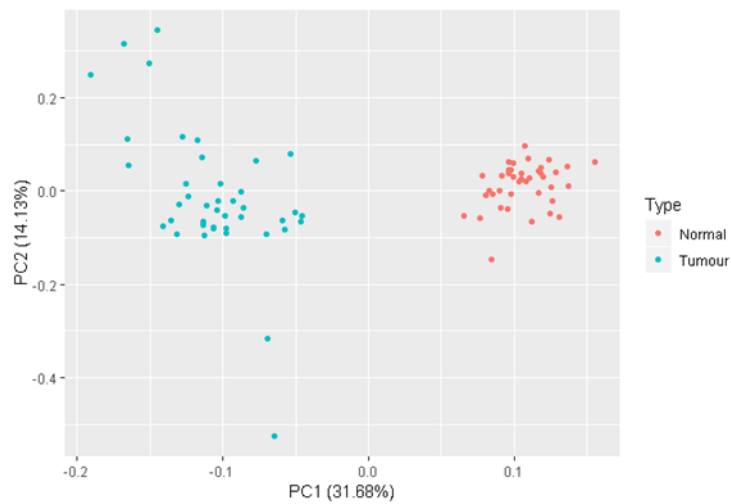
Figure 5.2. PCA plot of 41 colon tumour and normal colon samples. Tumour samples are coloured blue (key = tumour); normal samples are coloured red (key = normal).

In conclusion, there was no discernible difference in the clinicopathological characteristics or outcomes of the patients with matched tumour and normal colon tissue to the entire cancer cohort.
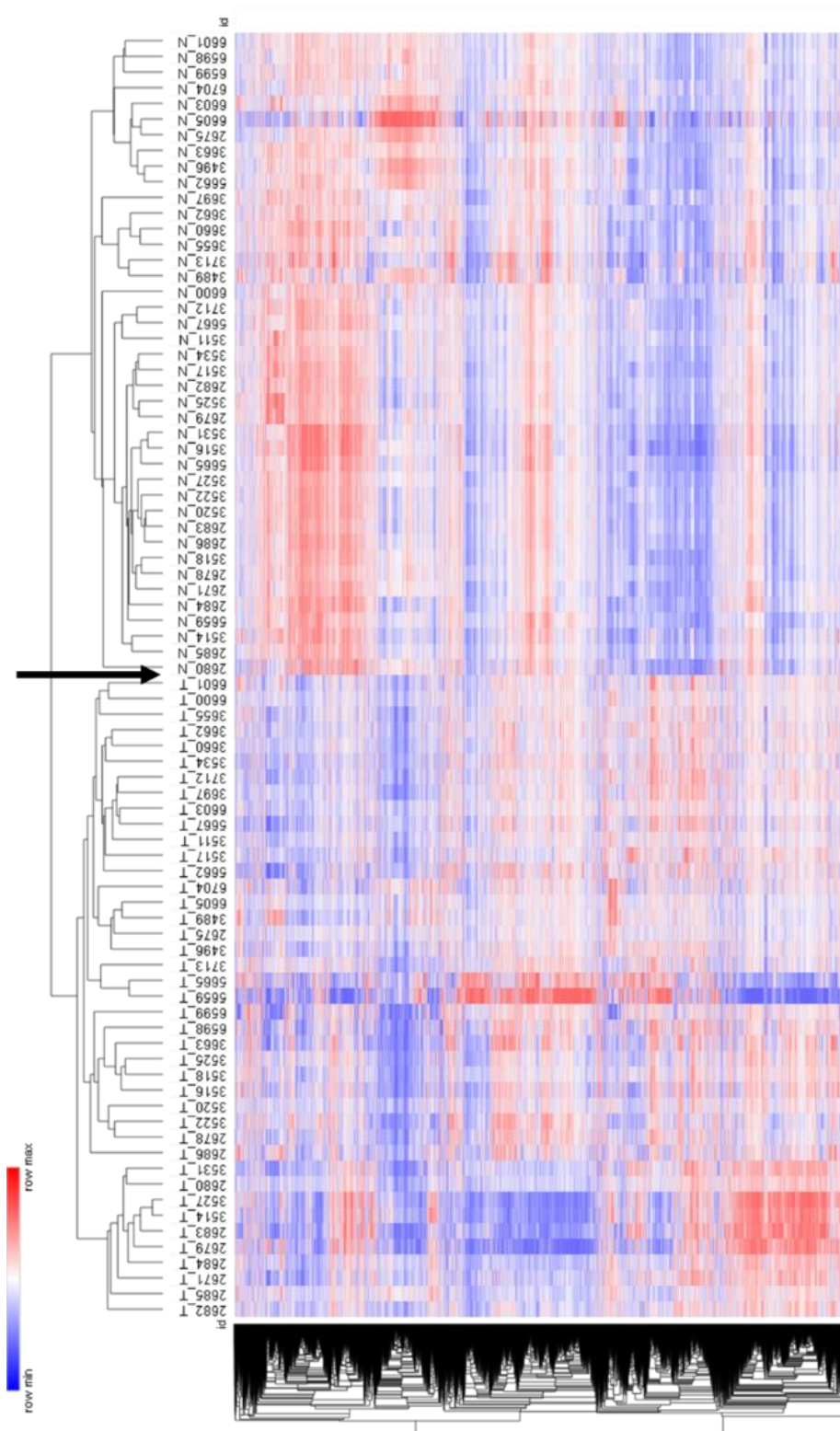
Figure 5.3. Heat map presenting hierarchical clustering of gene expression of the 41 tumour and normal samples. Tumour is denoted by T; normal colon is denoted by N. Expression was transformed into z scores and clustered using one minus pearson method. There is clear clustering of the two groups (demarcated with the black arrow). Heat map created in the Broad Institute matrix visualization and analysis software Morpheus (https://software.broadinstitute.org/morpheus/).
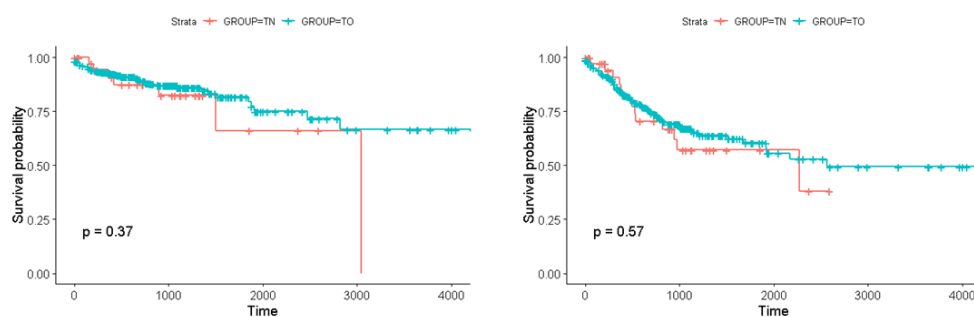
Figure 5.4. Kaplan Meier curves comparing disease outcome data in the subgroup and the entire cancer cohort. Group TN denotes the subgroup; Group TO denotes the cohort. A. Overall survival; B. Progression-free survival.

Clinical Data	Number of patients with available data	Overall	Male	Female
Age	470: 218 female 246 male	Median (range): 69 (30-90) Mean (SD): 66.7 ± 13.7	69 (31-90)	68 (34-90)
Sex	464	-	246	218
Stage	438		233	199
1		78 (17.8%)	43 (18.5%)	33
2		184 (42%)	95 (40.8%)	87
3		108 (24.7%)	57 (24.5%)	49
4		68 (15.5%)	38 (16.3%)	30

Table 5.1. Tabulated summary of the demographics and clinical characteristics of the entire TCGA COAD dataset (n=470).

Clinical Data	Number of patients with available data	Overall	Male	Female
Age	41	Median 74 years (range 40-90) Mean (SD): 70±13.3	Median (range): 73.5 (42-90) Mean (SD): 70.2±13.4	Median (range): 73 (40-90) Mean (SD): 69±13.3
Sex	41	-	20 (49%)	21 (51%)
Stage	40			
1		4 (10%)	2	2
2		22 (54%)	9	13
3		7 (17%)	4	3
4		7 (17%)	5	2

Table 5.2. Tabulated summary of the clinical demographics and characteristics of the 41 patients with available matched tumour-normal tissue.

Clinical characteristic	Regression coefficient	Hazard ratio (95% CI)	Univariate P value (log rank)	Multivariate P value (log rank)
Age	0.03	1.031 (0.95-1.11)	0.39	0.44
Sex (female vs male)	0.75	2.12 (0.39-11.74)	0.39	0.39
Stage (Stage 2-4 versus Stage 1)	-1.7	0.18 (0.02-1.99)	0.1	0.16
Venous Invasion (absent versus present)	1.5	4.66 (0.93-23.42)	0.04	0.062
Lymphatic invasion (absent versus present)	0.72	2.05 (0.4-10.34)	0.4	0.38

Table 5.3. Univariate and multivariate analysis of the clinicopathological characteristics in overall survival in the 41 patients.

Clinical characteristic	Regression coefficient	Hazard ratio (95% CI)	Univariate P value (log rank)	Multivariate P value (log rank)
Age	0.03	1 (0.96-1.1)	0.44	0.44
Sex (female vs male)	0.94	2.6 (0.49-14)	0.27	0.27
Stage (Stage 2-4 versus Stage 1)	-1.7	0.18 (0.017-2)	0.1	0.17
Venous Invasion (absent versus present)	1.7	5.6 (1.2-27)	0.033	0.033
Lymphatic invasion (absent versus present)	0.96	2.6 (0.57-12)	0.22	0.22

Table 5.4. Univariate and multivariate analysis of the clinicopathological characteristics in progression free survival in the 41 patients.

5.3.2.2. Principal Component Analysis

In order to determine how comparable both the 41-sample cohort are to the large dataset of 453 colorectal cancer samples, principal component analysis (PCA) was used to generate PCA plots that allow a visual summary of the variance of the datasets. The 41 tumour samples demonstrated similar dimensionality and variance to the 453 colorectal cancer samples (Figure 5.5).

5.3.3. Conclusion

In conclusion, data available from TCGA for normal colon tissue was limited but internal control measures determined that this tissue was appropriate for further analysis. The analysis has verified that the cohort of 41 patients is comparable and therefore sufficiently representative of the entire cohort. In addition, calculations determined that the paired dataset is sufficiently powered to generate robust differential expression analysis.

5.4. Differential expression analysis

5.4.1. Summary of differentially expressed genes

Differential expression analysis of the colorectal cancer samples relative to their paired normal colon tissue found that there were 15,057 differentially expressed genes, which was 25% of the total gene list. Of these, differential expression was significant in 7930 (52.7%) with an FDR of ≤ 0.01: 3,658 were upregulated and 4225 genes downregulated (Figure 5.6A and 5.6B). A similar number of differentially expressed genes has been reported in the literature, with 10,255 differentially expressed genes of 78 matched tumour-normal colon samples filtered by a less stringent FDR of 0.05(Xu et al., 2017). Furthermore, principal component analysis of the 41 paired tumour and normal samples demonstrated distinct clustering between the two tissues, so it is not surprising that there are so many differentially expressed genes.

5.4.2. Differential expression of calcium channel genes

One of the aims of this chapter was to determine whether calcium channels were differentially expressed in cancer relative to normal colon tissue. The differentially expressed gene list was interrogated for TRP, ORAI and PIEZO channels. 4 calcium
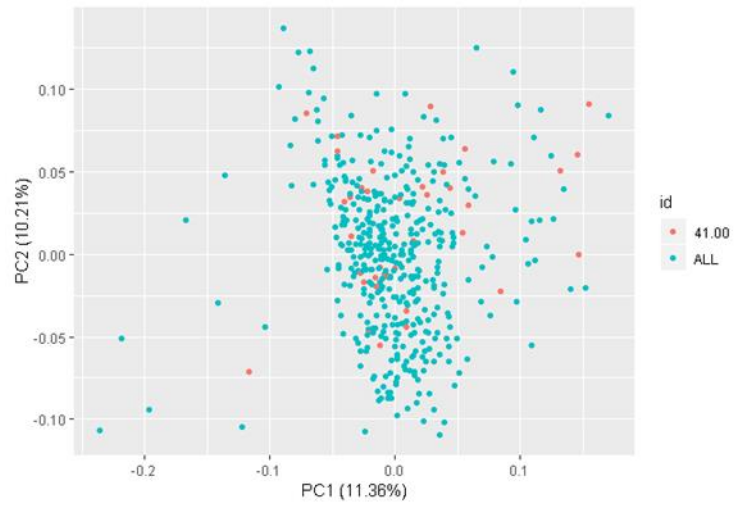
Figure 5.5. PCA plot presenting the variance of the 41 tumour samples and the 453 cancer samples. The 41 CRC samples are coloured red (key=red); the larger cohort of CRC samples are coloured blue (key = all).

channels were upregulated: TRPV4, TRPM2, PIEZO1 and ORAI1 and 10 channels were downregulated: TRPM7, PIEZO2, TRPS1, TRPM4, TRPC1, TRPM5, TRPA1, TRPC6, TRPV3 and TRPM6 (Table 5.5).

Differentially upregulated genes could represent pathophysiologically relevant gene signalling and potentially druggable targets. From hereon, further analysis focused on ORAI1 and PIEZO1. Some of the known upstream and downstream components of the store operated calcium signalling process were interrogated from the list of differentially expressed genes in order to determine whether more components of the signalling process were also differentially expressed in tumour tissue. There was downregulation of some of the important signalling components used by ORAI1 in store operated calcium entry. STIM1, which has been shown to be pivotal in ORAI1 clustering and activation, was downregulated (Log FC -0.98, p=1.36-8).

Furthermore, IP3 receptors that are pivotal in endoplasmic reticulum store depletion, the molecular process that activates CRAC channel signalling, were not differentially expressed (ITPR3 (log FC 0.27, p=0.15)). Proteins involved in downstream signalling cascades were also downregulated, such as calmodulin (CALM2, log FC -0.61, q=3.45E-4; CALM3 -0.44, q=0.01; CALM1 log FC -0.79, q=2.5E-6).

5.4.3. Conclusion

In conclusion, this analysis has demonstrated that ORAI1 and PIEZO1 are differentially overexpressed in colorectal cancer. However, there is differential downregulation of known calcium machinery both upstream and downstream of the ORAI1 channel.

5.5. Correlation of Clinicopathological Characteristics

Further analysis was carried out to determine whether ORAI1 and PIEZO1 expression correlates with disease progression and clinical outcome.

5.5.1. Log fold changes

In order to determine whether the level of differential expression was associated with clinical outcome, the fold changes were compared across disease stage as well
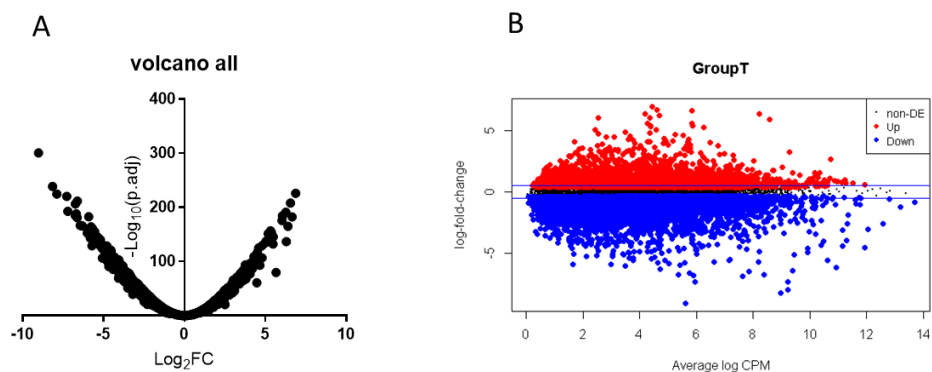
Figure 5.6. Pictorial representation of differentially expressed genes between cancer and normal colon. A. Volcano plot plotting the log fold change (x axis) by the -log10 of the adjusted q value. B. MA plot demonstrating the differential expression of the dataset, demonstrating the small window of non-differentially expressed genes (black), upregulated (red) and downregulated (blue) genes.
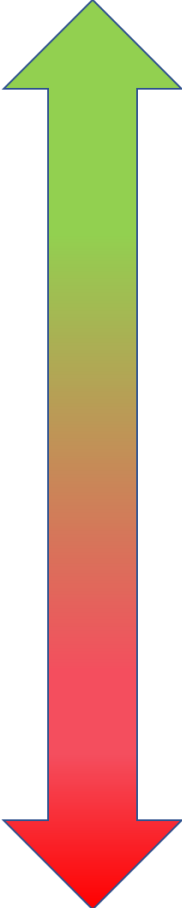
Gene	Log Fold Change	Likelihood Ratio	p.Adj
TRPV4	1.8168	103.4	3.21E-23
TRPM2	1.6001	85.1	2.75E-19
PIEZO1	1.0871	45.1	4.42E-10
ORAI1	0.50956	9.6	4.01E-3
TRPM7	-0.38504	5.63	3.02E-2
PIEZO2	-0.7923	21.6	1.02E-05
TRPS1	-0.8008	21.1	1.33E-05
TRPM4	-0.9011	29.5	2.16E-07
TRPC1	-1.0509	37.5	4.10E-9
TRPM5	-1.1939	40.5	9.42E-10
TRPA1	-1.5171	73.9	6.97E-17
TRPC6	-1.8525	48.6	1.83E-11
TRPV3	-2.9067	238.6	3.19E-52
TRPM6	-4.6897	511	7.67E-111

Table 5.5. Table of differentially expressed calcium genes.

223

as lymphatic and venous invasion for both ORAI1 and PIEZO1. Perineural invasion was not analysed as there was insufficient data available on perineural invasion to do this for the 41 patients.

There was no difference in the fold change expression of ORAI1 expression across disease stage (p=0.9) or venous invasion (0.45) (Figure 5.7A and Figure 5.7B). However, there was a reduction in fold change where there was lymphatic invasion (p=0.047) (Figure 5.7C).

There was no difference in fold change expression of PIEZO1 expression in disease stage (p=0.35) or venous invasion (p=0.3) (Figure 5.7D and 5.7E). There was a reduction in fold change in lymphatic invasion (p=0.02) (Figure 5.7F).

5.5.2. Survival analysis

Kaplan-Meier analysis was carried out to determine whether there was a difference in overall survival and progression-free survival across both PIEZO1 and ORAI1 expression. This tested for differences in survival in high or low median expression. There was no difference in overall survival (p=0.412, Figure 5.8A) or progression-free survival (p=0.847, Figure 5.8B) for PIEZO1. In addition, there was no difference in overall survival (p=0.62, Figure 5.8C) or progression-free survival (p=0.85, Figure 5.8D).

Analysis was then carried out to determine whether clinicopathological characteristics were prognostic across PIEZO1 and ORAI1 expression. With ORAI1, there was no difference in overall survival for lymphatic invasion (p=0.38) or disease stage (p=0.11) but there was a poorer prognosis for venous invasion in the lower ORAI1 group (p=0.004) but no difference in the higher ORAI1 group (p=0.583).

With ORAI1, there was no difference in progression-free survival for lymphatic invasion (p=0.2) or disease stage (p=0.11). There was a poorer prognosis for venous invasion in the lower ORAI1 group (p=0.005) but no difference in the higher ORAI1 group (p=0.314).

For PIEZO1, there was no difference in overall survival for lymphatic invasion (p=0.38) and disease stage (p=0.11). There was a poorer prognosis for venous invasion in the lower PIEZO1 group in both overall survival (p=0.017), but no difference for the higher PIEZO1 group (p=0.307).

For PIEZO1, there was no difference in progression-free survival for lymphatic invasion (p=0.2) and disease stage (p=0.11). There was a poorer prognosis for venous invasion in the lower PIEZO1 group (p=0.018), but no difference in the higher PIEZO1 group (p=0.229).

5.5.3. Conclusion

In conclusion, this data suggests an inverse relationship between both ORAI1 and PIEZO1 tumour expression and lymphatic invasion, however this did not impact on survival outcomes. However, there was poor prognosis for patients with lower ORAI1 and PIEZO1 expression in venous invasion.
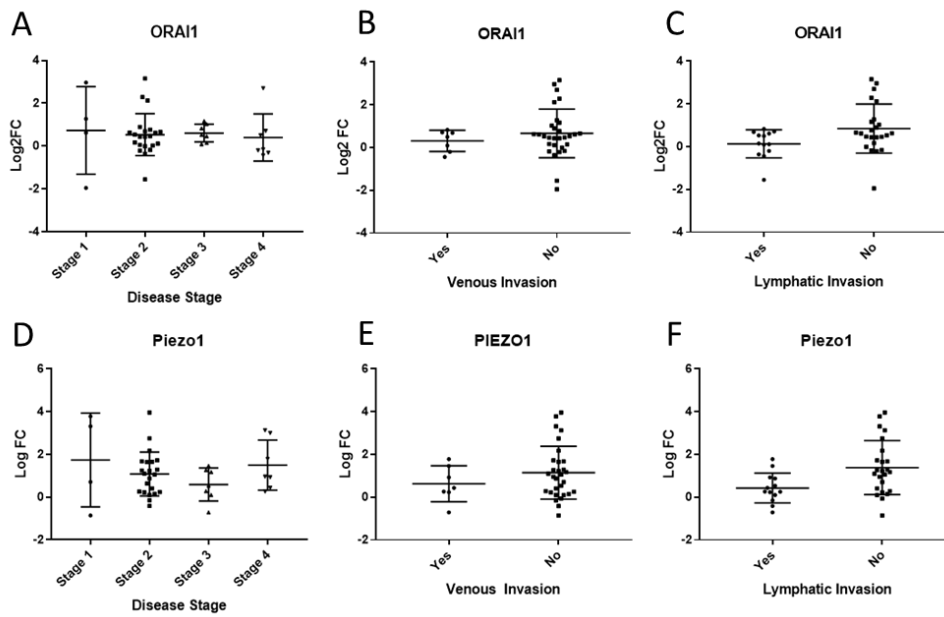
Figure 5.7. Dot plot graphs representing the variation of log fold changes across clinicopathological parameters: A-C. ORAI1; D-F. PIEZO1. A and D. Disease stage; B and E. Venous invasion; C and F. Lymphatic invasion.
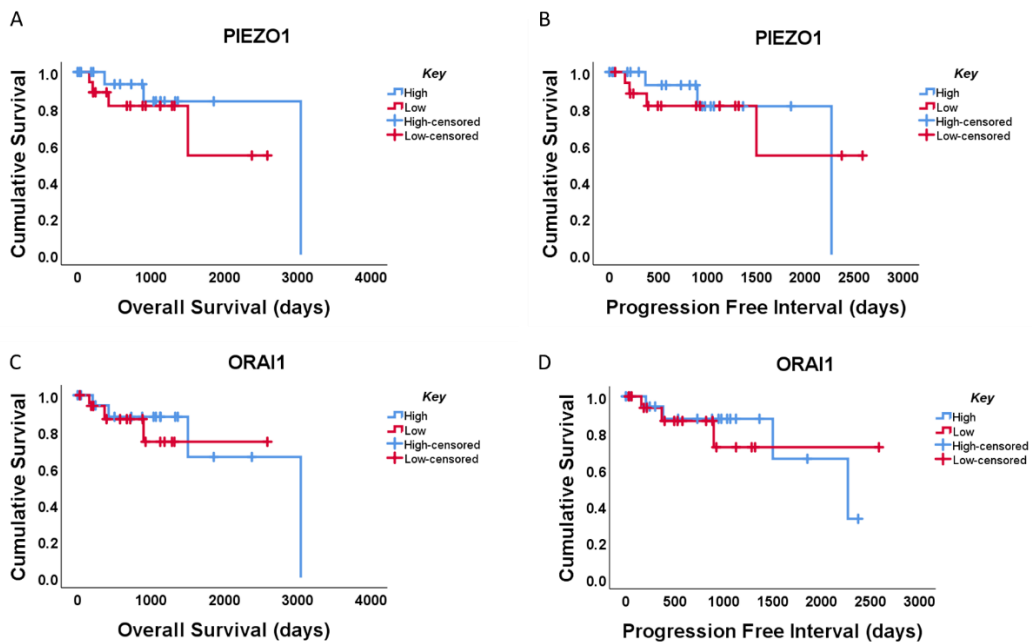
Figure 5.8. Kaplan Meier survival analysis by PIEZO1 and ORAI1 expression. A-D: Kaplan Meier survival curves for high (blue line) and low (red line) expression: A. PIEZO1 overall survival; B. PIEZO1 progression free interval; C. ORAI1 overall survival; D. ORAI1 progression free interval.

5.6. Functional analysis of differentially expressed genes

Further analysis was carried out to interpret what these genes meant on a biological, cellular and molecular basis. Gene ontology is a resource overseen by the Gene Ontology consortium that provides a computational representation of the current scientific knowledge about the functions of genes, creating annotations that describe the molecular, cellular or biological process for each gene. Two methods were used: gene ontology enrichment analysis within the goana programme in r and pre-ranked gene set enrichment analysis (GSEA).

5.6.1. Gene ontology enrichment analysis

The differentially expressed genes were tagged with their assigned gene ontology (GO) terms using the Goana function within edgeR. This assigned the genes to 14,132 GO terms for biological processes (BP), 1,802 terms for cellular components (CC) and 3,693 terms for molecular functions (MF).

All differentially expressed GO terms were clustered under headings relevant to their biological function. There were 28 positively enriched processes (summarised in Table 6.1 in the Appendix), with the highest number of positively enriched GO terms occurring in metabolic cell signalling pathways, immunity, cellular structure and formation, embryogenesis and stem cells and synaptic function. Other relevant processes include cell proliferation, Wnt signalling, endocytosis and exocytosis. Xu and colleagues have previously found the biological processes cell proliferation, inflammation and immunity to be differentially overexpressed in human colorectal cancer(Xu et al., 2017).

There were 37 negatively enriched processes (summarised in Table 6.2 in the Appendix), with the highest number of negatively enriched gene ontology terms in metabolic processes, nucleoside and nucleotide processing, metabolic energy processes, catabolic processes, cellular response to external stimuli and immunity. Other processes include endocytosis and exocytosis, ion and cation transport, acidic pH response and DNA repair. Xu and colleagues have previously found the biological processes metabolic processes have previously been found to be differentially under-expressed in human colorectal cancer(Xu et al., 2017).

227

5.6.1.1. Calcium related gene ontology enrichment analysis

Calcium-related GO terms were identified by searching for the word 'calcium' in the GO titles. This resulted in 122 biological process terms. However, only 10 were downregulated and 0 were upregulated.

There were 10 negatively enriched calcium-related BP gene sets (Table 5.6). Five of the 10 enriched BP terms are specific to tissue: 4 relating to calcium-induced exocytosis in the neurone and 1 related to cardiac muscle signalling. Of the remaining 5, 3 GO terms are related to calcium import into the cell, 1 is related to calcium-mediated signalling and 1 relating to endoplasmic reticulum calcium homeostasis (Table 5.6).

There were 4 negatively enriched calcium-related MF gene sets (Table 5.7). There were no enriched CC datasets.

In addition, the KEGG calcium pathway is downregulated (Figure 5.9). Of this pathway, 90 genes are differentially expressed: 62 were underexpressed (Figure 5.12A) and 16 were overexpressed (Figure 5.12B). PIEZO1 was not included in this pathway.

From hereon, biological process GO terms were further scrutinised.

5.6.2. Gene set enrichment analysis

Gene set enrichment analysis was carried out in the Broad Institute GSEA Java platform, preranked by the log fold change values. All 15,025 genes were recognised by GSEA in this analysis.

The analysis classified by biological process gene ontology terms, recognising 3,976 separate gene sets within this category. There were 1,453 (37%) positively enriched gene sets, of which 57 (3.9%) were significant (FDR < 25%). There were 2,523 (63%) negatively enriched gene sets, of which 70 (2.8) were negatively enriched (adjusted p value ≤0.01). The top 50 positively and negatively enriched are graphically presented in the appendix (Positively enriched data in Figure 6.1, negatively enriched data in Figure 6.2).

Of the positively enriched gene sets, the top 50 GO terms represented positive enrichment of genes related to DNA replication, division, cell cycle and cellular machinery for protein transcription and translation (Appendix Figure 6.13A, Figure 6.3A).

Of the negatively enriched gene sets, the top 50 negatively enriched GO terms include G protein-coupled receptors (GPCR), non-calcium ion channel function, cation transport, immunity, calcium ion-related transport and membrane potential (Appendix Figure 6.3B).

5.6.2.1. Calcium related gene set enrichment

None of the positively enriched gene sets were related to calcium signalling or transport.

Of the negatively enriched gene sets, 9 were related to calcium: 4 were related to transmembrane calcium ion entry and transporter activity, 1 related to sarcoplasmic reticulum calcium release, 1 for calcium-mediated cardiac muscle contraction, 2 for calcium-mediated signalling and 1 for cytosolic calcium ion control (Table 5.8).

GSEA enrichment mapping revealed clustering of the downregulated calcium ion transmembrane transport GO terms (Figure 5.10). ORAI1 and PIEZO1 both mapped to the gene sets 'ion transmembrane transport', 'cation transport', 'transmembrane transport' and 'ion transport', which collectively contained 922 genes (Figure 5.10). These pathways were all negatively enriched (Table 5.8).

5.6.3. Conclusion

In conclusion, gene set enrichment analysis has found that calcium signalling processes and ion transport are negatively enriched in colon cancer relative to normal colon tissue.

Term	No. of genes	No. Up-regulated	No. down-regulated	P.Up	P.Down
Calcium-mediated signaling	128	35	51	0.756	0.031
Calcium ion import into cytosol	7	2	5	0.666	0.037
Calcium ion import across plasma membrane	7	2	5	0.666	0.037
Regulation of cardiac muscle contraction by calcium ion signaling	23	7	12	0.55	0.033
Induction of synaptic vesicle exocytosis by positive regulation of presynaptic cytosolic calcium ion concentration	4	0	4	1	0.01
Positive regulation of presynaptic cytosolic calcium concentration	4	0	4	1	0.01
Calcium ion import	46	9	22	0.958	0.016
Endoplasmic reticulum calcium ion homeostasis	14	2	8	0.951	0.043
Regulation of calcium ion-dependent exocytosis	64	20	28	0.443	0.028
Calcium ion regulated exocytosis	82	25	37	0.484	0.007

Table 5.6. Tabulated summary of the differential expression of calcium-related GO terms for biological processes (p<0.05).

Term	No. of genes	No. up-regulated	No. down-regulated	P. Up	P. Down
Voltage-gated calcium channel activity involved in positive regulation of presynaptic cytosolic calcium levels	4	0	4	1	0.01
Calcium-dependent ATPase activity	3	0	3	1	0.032
Voltage-gated calcium channel activity involved in cardiac muscle cell action potential	5	0	5	1	0.003
Voltage-gated calcium channel activity involved in AV node cell action potential	3	0	3	1	0.032

Table 5.7. Tabulated summary of the differential expression of calcium-related GO terms for molecular function (p<0.05).
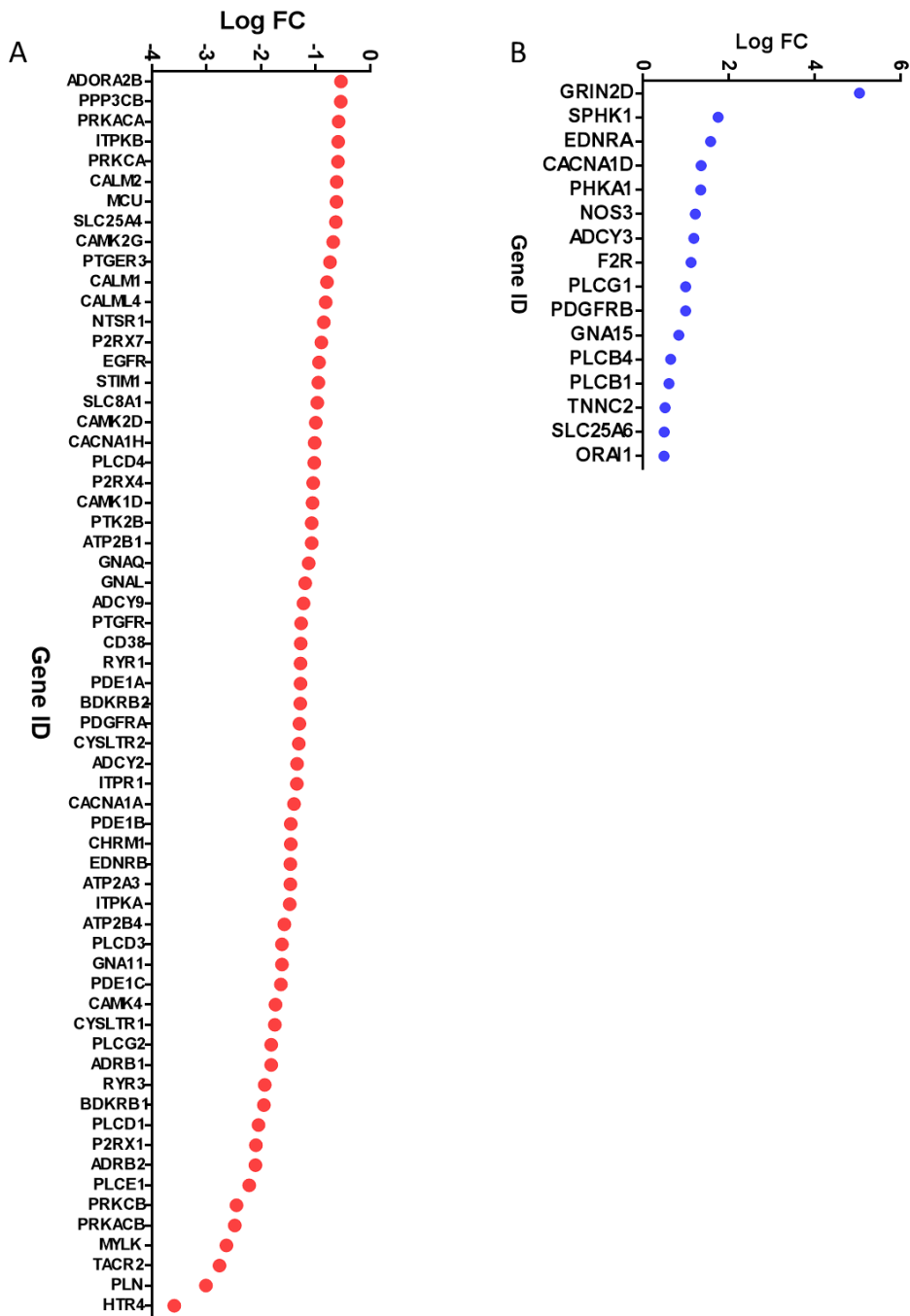
Figure 5.9. A-B. Dot plots presenting the differentially expressed genes from the KEGG calcium pathway: A. Negatively enriched terms; B. Positively enriched terms.

Term	Size	ES	NES	P.adj (FDR)
Regulation of calcium ion transmembrane transporter activity	50	-0.62	-1.91	0.01
Regulation of release of sequestered calcium ion into cytosol by sarcoplasmic reticulum	21	-0.73	-1.89	0.01
Negative regulation of calcium ion transmembrane transport	22	-0.70	-1.84	0.01
Regulation of calcium-mediated signalling	61	-0.59	-1.84	0.01
Calcium ion transport	134	-0.52	-1.82	0.02
Regulation of cardiac muscle contraction by calcium ion signalling	22	-0.69	-1.81	0.02
Calcium ion transmembrane transport	91	-0.53	-1.76	0.03
Calcium mediated signalling	72	-0.54	-1.72	0.05
Regulation of cytosolic calcium ion concentration	128	-0.58	-2.00	0.00

Table 5.8. Tabulated summary of the GSEA analysis identifying the negatively enriched genes for calcium-related function within the GO terms for biological process. q<0.05.

A

234

B

GO_TRANSMEMBRANE_TRANSPORT

GO_CATION_TRANSPORT

GO_ION_TRANSPORT

GO_ION_TRANSMEMBRANE_TRANSPORT
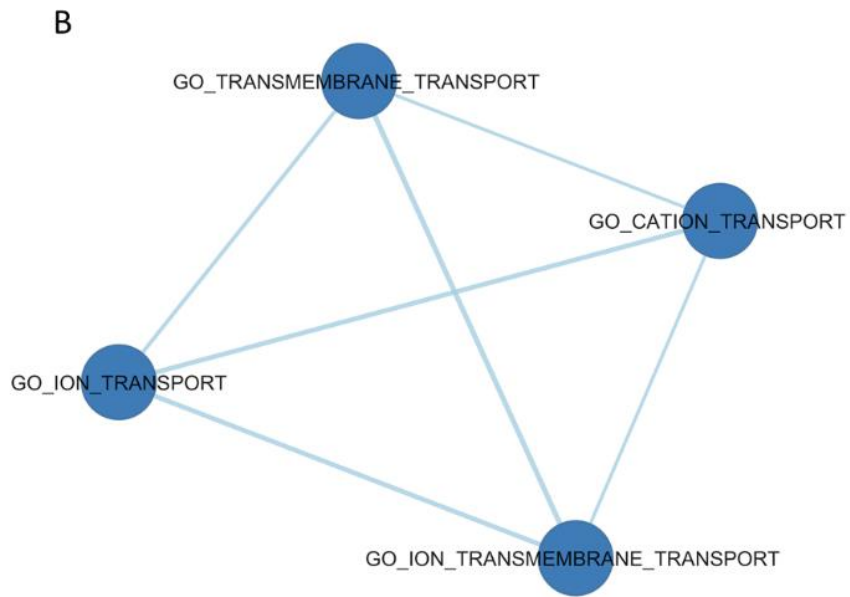
Figure 5.9. A. Diagram presenting the cluster of gene ontology terms pertaining to calcium signalling. The nodes are sized to represent the number of genes mapping to the gene ontology term. B. Node diagram highlighting the nodes from A to which ORAI1 and PIEZO1 were mapped.

5.7. Gene co-expression

So far, analysis has determined that ORAI1 and PIEZO1 are differentially overexpressed in colorectal cancer relative to normal cancer, but analysis of structured GO datasets of calcium transport and signalling processes are negatively enriched in tumour relative to normal colon. Further analysis was undertaken to identify gene co-expression outside of the structured GO terms, which may allow identification of novel gene relationships. Correlation is a common measure of co-expression and was used in the methods employed in these analyses.

Analysis was carried out to identify genes that co-expressed with both ORAI1 and PIEZO1. Furthermore, analysis was carried out to identify gene co-expression with clinicopathological traits.

5.7.1. Differential gene correlation

The differential gene correlation analysis package was used to explore gene co-expression in the tumour tissue. The top 100 positively and top 100 negatively co-expressed genes are presented in the Appendix in Figure 6.4 and 6.5 respectively.

5.7.1.1. Gene co-expression with ORAI1 and PIEZO1 in tumour tissue

The differential gene correlation analysis package was used to identify gene correlations with ORAI1 and PIEZO1 in tumour tissue that did not exist in normal colon tissue.

There were 3,602 genes that correlated with PIEZO1 in tumour tissue where they did not correlate in normal colon tissue. Filtering these above correlation coefficients above 0.3 and below -0.3, this resulted in 1,924 positive correlations, and 1,678 negative correlations. Gene set enrichment of the genes co-expressing with PIEZO1 in tumour tissue found that there was positive enrichment of genes pertaining to lipid catabolism and small molecule catabolism, and negative enrichment of RNA localization, nucleobase-containing compound transport, protein-containing complex localization, RNA polymerase I transcription and ribonucleoprotein complex localization (Table 5.9). The top 50 positive and negative gene co-expression with PIEZO1 are presented in Figure 5.11.

There were 6,952 genes that correlated with ORAI1 in tumour tissue where they did not correlate in normal colon tissue. Filtering these above 0.3 and below -0.3,

this resulted in 3,491 positive correlations and 3,461 negative correlations. Gene set enrichment analysis of the genes correlating with ORAI1 in tumour tissue found that there was negative enrichment of genes pertaining to protein-containing complex localization, RNA polymerase 1 transcription, ribonucleoprotein complex localization and meiotic cell division (Table 5.10). No gene sets were positively enriched in tumour relative to normal tissue. The top 50 positive and negative gene co-expression with PIEZO1 are presented in Figure 5.10.

ORAI1 and PIEZO1 correlated strongly with one another in tumour tissue (correlation coefficient of 0.94, p=0), whereas there was no correlation in the normal colon tissue (correlation coefficient 0.01, p=0.9).

5.7.1.2. Conclusion
In conclusion, PIEZO1 and ORAI1 both negatively co-express with genes involved in transcriptional processes. ORAI1 and PIEZO1 are strongly co-expressed in tumour tissue where there is no correlation in expression in normal tissue.

5.7.2. Weighted gene correlation analysis
It has already been demonstrated earlier in Section 5.5 that ORAI1 and PIEZO1 expression is inversely associated with lymphatic invasion. In order to explore gene co-expression by clinicopathological factors, the log transformed FPKM from the 41 tumour samples was subjected to weighted gene correlation network analysis (WGCNA). This uses a weighted correlation analysis to identify clusters, or modules, of highly interconnected genes, which are labelled by colour within the r programme. These modules can be explored using gene ontology terms to identify functional clusters, as well as correlated with clinicopathological factors.

5.7.2.1. Exploration of the clustered modules
WGCNA analysis identified 7 modules (black, blue, brown, green, turquoise, red, yellow). Genes that did not cluster by correlation were labelled as the grey cluster, therefore these were not analysed further.

There were 40 genes mapped to the genes in the black module, 805 in the blue module, 318 in the brown module, 318 genes in the brown module, 59 genes in the

Description	Size	Number of leading edges	NES	P value	FDR (q value)
Lipid catabolic process	51	42	2.34	0	0.03
Small molecule catabolic process	91	58	2.22	0	0.05
RNA localization	74	30	-2.16	0	0.03
Nucleobase-containing compound transport	73	30	-2.17	0	0.04
Protein-containing complex localization	77	39	-2.23	0	0.03
RNA polymerase I transcription	21	12	-2.38	0	0.01
Ribonucleoprotein complex localization	50	33	-2.7	0	0.002

Table 5.9. Table of differentially enriched gene sets that correlate with PIEZO1 in tumour tissue.

Description	Size	Number of leading edges	NES	P value	FDR (q value)
Protein-containing complex localization	148	57	-2.16	0	0.04
RNA polymerase I transcription	38	15	-2.19	0	0.05
Ribonucleoprotein complex localization	78	35	-2.27	0	0.04
Meiotic cell cycle	81	46	-2.4	0	0.03

Table 5.10. Table of differentially enriched gene sets correlated with ORAI1 in tumour tissue.
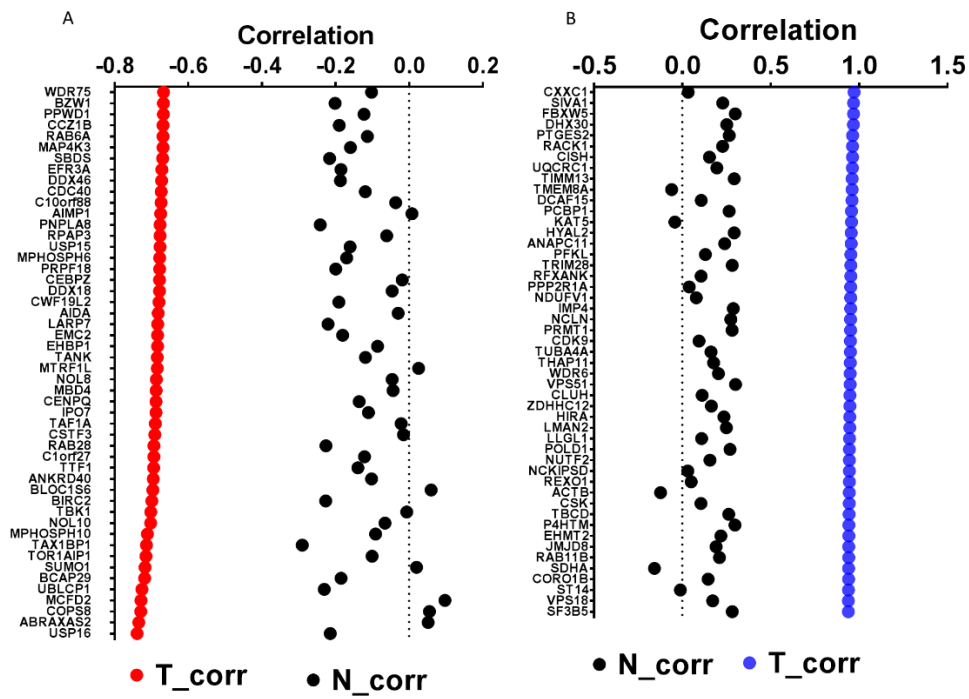
Figure 5.10. Dot plots of the correlation values of genes with ORAI1 in tumour (T_corr) and normal tissue (N_corr). A. Genes that are negatively co-expressed. B. Genes that are positively co-expressed.
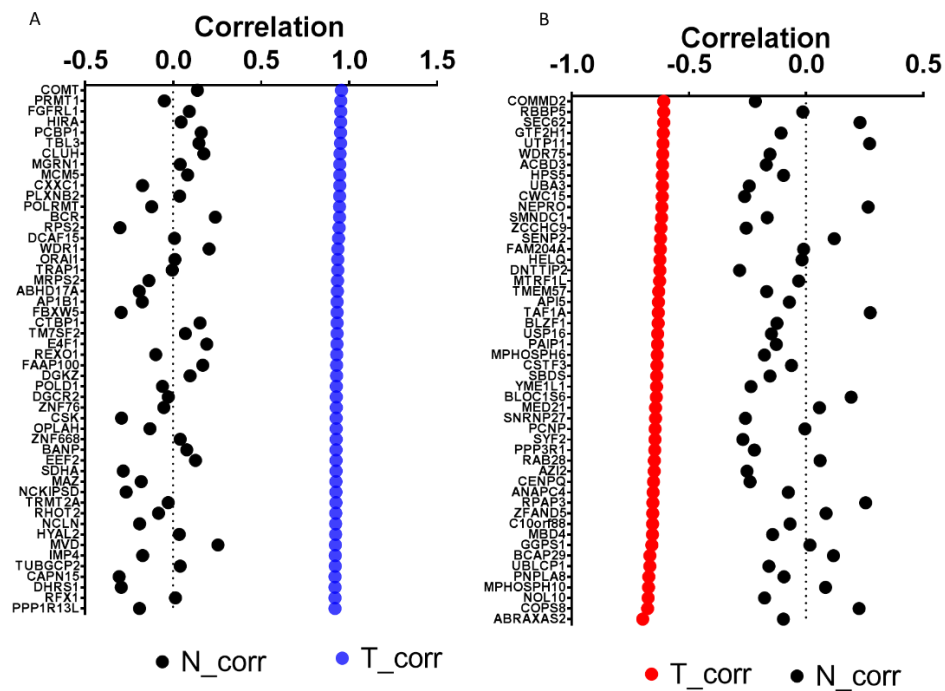
Figure 5.11. Dot plots of the correlation values of genes with PIEZO1 in tumour and normal tissue. T_corr denotes correlation in tumour tissue; N_corr denotes correlation in normal tissue. A. Genes that are negatively co-expressed. B. Genes that are positively co-expressed.

green module, 4,148 genes in the turquoise module, 44 genes in the red module and 94 in the yellow module.

The networks are visually summarised in a network heatmap plot in Figure 5.12. This demonstrates high interconnected co-expression predominantly occurring within the turquoise module (Figure 5.12), implicating the functional relevance of this module. ORAI1 and PIEZO1 were included within the turquoise module.

The Cytoscape app was used to cluster and visualise the genes by their biological functions (Figure 5.13). No GO terms mapped to the blue, green, brown, red and brown modules. There were 342 GO terms enriched within the turquoise module, including ion transport (p=5.1E-6). Other GO terms also clustered to cell cycle process and regulation, cellular metabolism of cellular nitrogen, RNA processing and cellular macromolecule localisation and breakdown (Figure 5.13). ORAI1 was only enriched with ion transport, which did not interrelate to any of the other nodes. However, PIEZO1 was enriched with ion transport and also to 3 nodes (protein-containing complex assembly (p=2.9E-18), protein-containing complex subunit organisation (p=1.1E-21) and cellular component assembly (p=4.4E-18)), nodes that ontologically identified for ribonucleoprotein complex biogenesis and cellular component assembly.

include black circles to identify the GO functions to which PIEZO1 is mapped, and a black arrow to identify the ion transport GO node to which ORAI1 and PIEZO1 are both mapped.
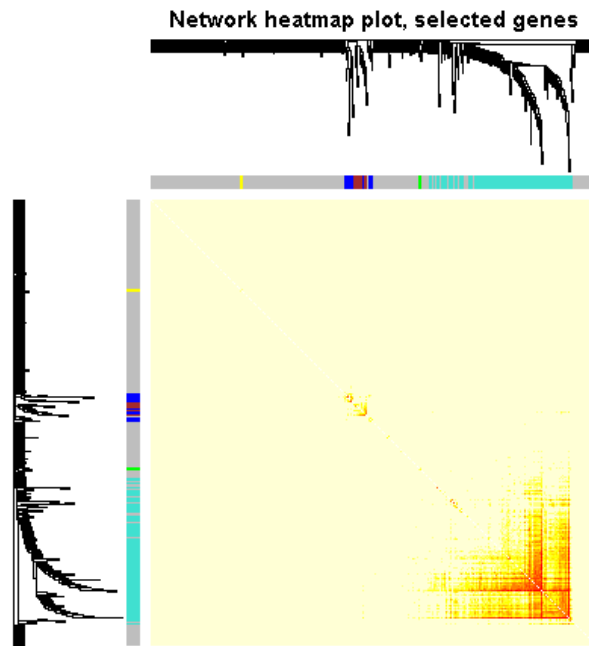
Figure 5.12. Network heatmap plot of modules and the eigengene correlation. The modules are denoted denoted by colour. High co-expression interconnectedness of genes is denoted by saturated yellow and red colours.
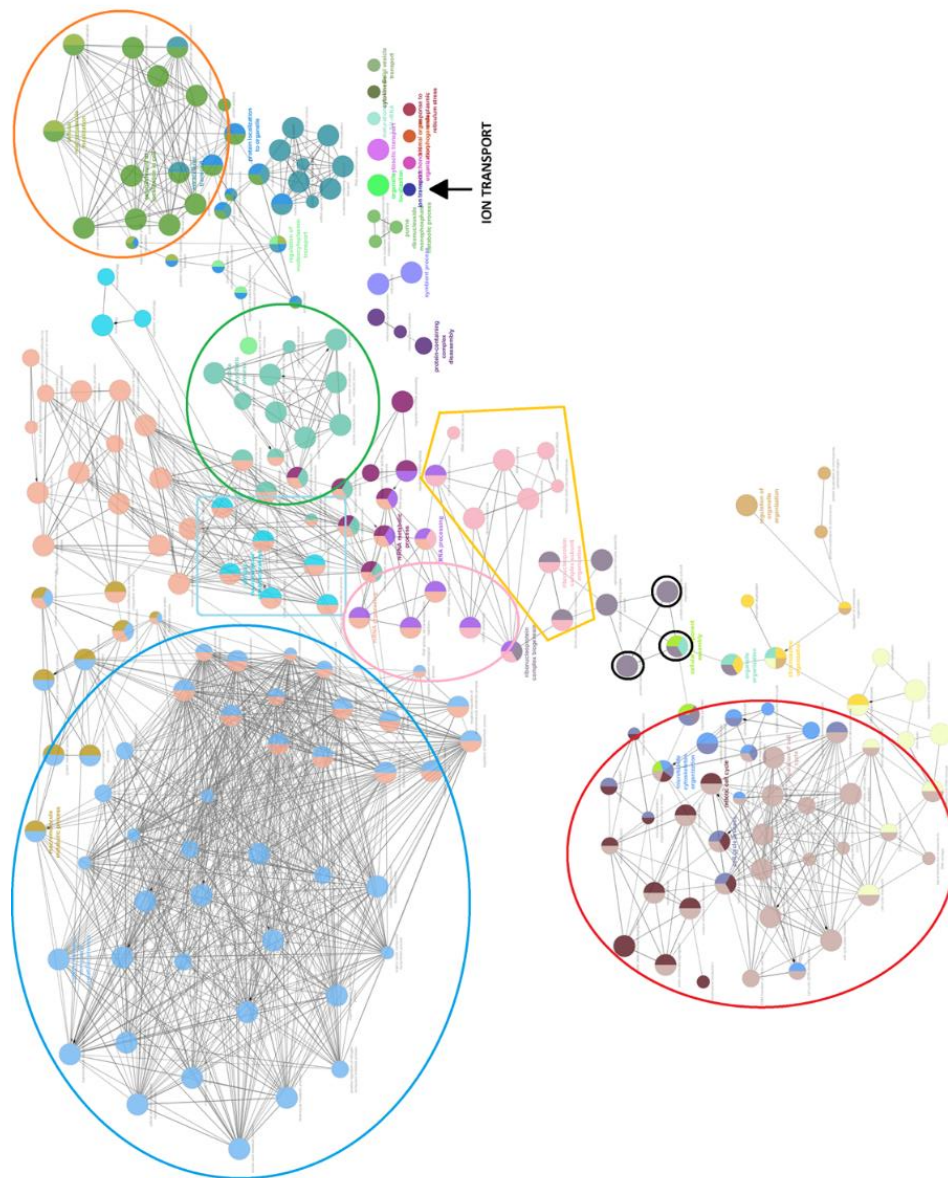
Figure 5.13. Network diagram visualising the biological functions of the genes clustered to the turquoise module. Gene nodules are coloured according to their ontological functions and edges denote interconnectedness. The ontological functions are crudely summarised using circles to aid interpretation: blue = cellular nitrogen compound metabolic processes; turquoise = cellular macromolecule catabolic processes; Green = peptide biosynthesis process; Orange = cellular macromolecular localization and ribonucleoprotein complex subunit organisation; Pink = RNA processing; Red = cell cycle process and regulation. Further annotations

5.7.2.2. Gene co-expression with clinicopathological traits

Analysis was carried out to explore whether gene clusters correlate with different clinicopathological traits.

Correlation of the gene clusters with relevant clinical traits is generated within the WGCNA package as a module-trait relationship heatmap, which is presented in Figure 5.14. Yellow did not cluster to any clinical trait. The turquoise module was the largest and correlated significantly to the most traits, with lymphatic invasion (pearsons correlation coefficient 0.33, p=0.04), sex (pearsons correlation coefficient 0.36, p=0.01) and polyps (pearsons correlation coefficient 0.45, p=0.003) (Figure 5.14). The blue module correlated with venous invasion (p=0.32, p=0.04). Stage, residual tumour, number of positive lymph nodes, the overall survival time and progression-free survival time did not correlate with any gene modules. The green module correlated with polyps (pearsons correlation coefficient 0.48, p=0.001) and lymphatic invasion (0.33, p=0.04).

The WGCNA output also looks at correlation of individual genes as well as gene modules with each clinical trait. Both PIEZO1 and ORAI1 negatively correlated with lymphatic invasion (PIEZO1 gene significance -0.38, p=0.014; ORAI1 gene significance -0.33, p=0.04).

5.7.2.3. Conclusion

The WGCNA analysis has reported an association of PIEZO1 in ribonucleoprotein complex function, but no association of ORAI1 with any particular cellular function. In addition, there is also a negative correlation of ORAI1 and PIEZO1 expression with lymphatic invasion.
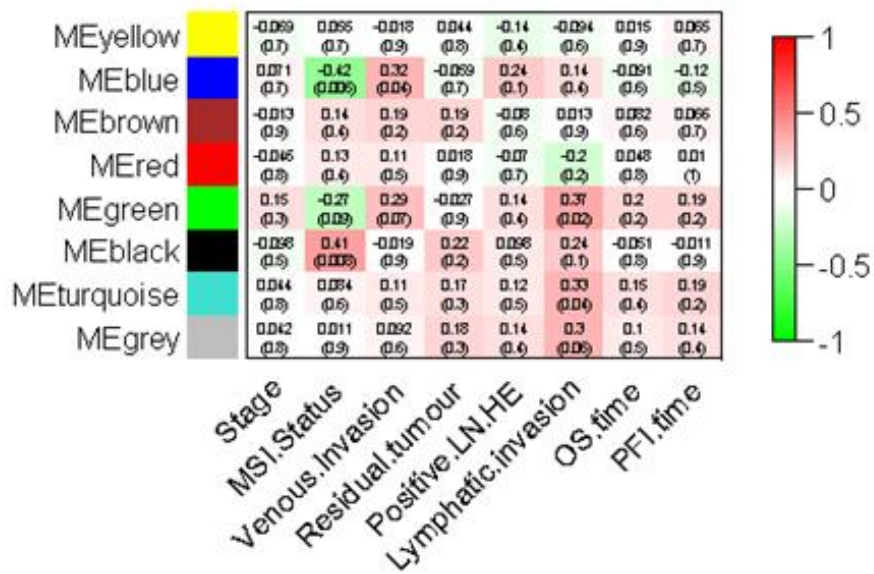
Figure 5.14. Module-trait map presenting the correlations of clinical traits with each module. Correlations are presented in numerical format with p values in brackets and also in colour.

5.8. Association with the molecular characteristics of colorectal cancer

Data analysis so far has demonstrated that the calcium signalling receptors ORAI1 and PIEZO1 are differentially overexpressed in cancer. However, there is downregulation of the cellular machinery involved in the molecular signalling processes that have been described for these channels. Furthermore, gene set enrichment has demonstrated downregulation of calcium channel signalling processes in cancer tissue.

It can be hypothesized that differential upregulation may be caused by an oncogenic process. This was explored further.

5.8.1. Copy number variation

Copy number variations (CNV) are structural variations that alter the number of copies of regions of DNA, either by deletion or duplication. The 2012 TCGA paper analysed data from 190 fully sequenced colorectal cancer samples. Therefore, given the negative enrichment of calcium ion channel signalling in Section 5.3, ORAI1 and PIEZO1 expression data was matched with CNV data for each of these 190 patient samples. There was no relationship between copy number status and level of expression for ORAI1 and PIEZO1 (Figure 5.15).

5.8.2. ORAI1 and PIEZO1 and colorectal-specific oncogenic processes

Further analysis was carried out to determine whether ORAI1 and PIEZO1 expression was affected by chromosomal instability as well as known oncogenic signalling pathways, oncogenic proteins and mutations described in colorectal cancer. The original landmark TCGA paper for colorectal cancer published in 2012 reported a number of important genomic alterations that affected the oncogenic signalling in the tumours(The Cancer Genome Atlas et al., 2012). These included samples with a hypermutated profile versus a non-hypermutated profile, defined by the authors by somatic mutation analysis via exome capture DNA sequencing as samples with mutation rates over 12 per 10^6 bases as hypermutated and those with less than 8.24 per 10^6 bases as non-hypermutated. They also defined somatic recurrently mutated genes by MutSig analysis in genes pertinent to colorectal tumourigenesis, such as p53, WNT and PI3K, K-RAS and PTEN.
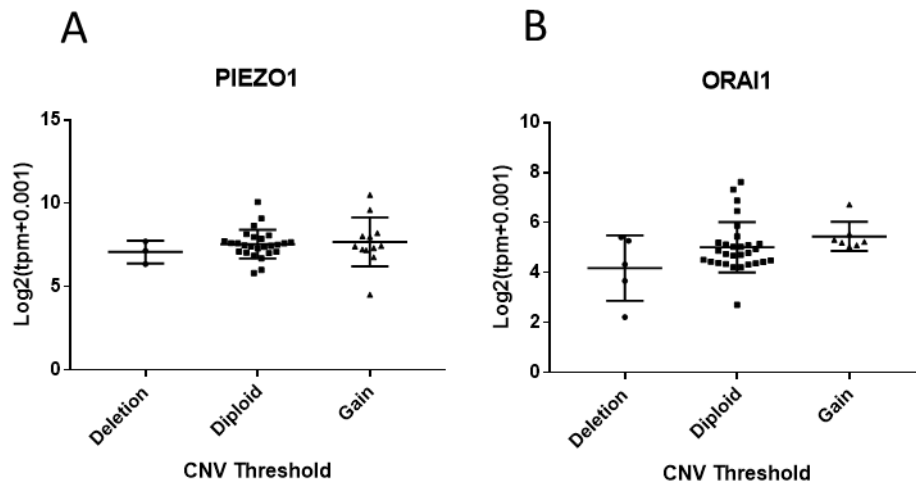
Figure 5.15. Dot plots presenting counts for copy number variation data. A. PIEZO1; B. ORAI1.

There was no difference in expression data between hypermutated and non-hypermutated samples, WNT, TGFB, RTK, PI3K, p53 and APC mutations, nor for PTEN, K-RAS or ERBB2 status, for either ORAI1 (Figure 5.16) or PIEZO1 (Figure 5.17). However, expression was higher where the IGF2 receptor was amplified for both ORAI1 (wildtype 3.98±0.06, amplification 4.26±0.01, p=0.0215) (Figure 5.18A) and PIEZO1 (wildtype 5.28±0.06, amplification 5.6±0.12, p=0.0258) (Figure 5.18B).

5.8.4. Conclusion

In conclusion, PIEZO1 and ORAI1 differential upregulation do not appear to be due to chromosomal instability as there is no association with CNV or the hypermutated CIMP genotypic signature. In addition, their expression profiles do not appear to correlate with the established oncogenic mutational signatures that have been described as pathognomonic for colorectal tumourigenesis and oncogenic signalling. However, they do correlate with IGF2 R upregulation.

5.9. Chapter Conclusion and closing points

Analysis of the tumour transcriptome in this chapter has made a number of novel discoveries about calcium channel expression in CRC. It has revealed differential expression patterns of TRP, PIEZO and CRAC channels in CRC relative to the normal colon. Of the panel of TRP, ORAI and PIEZO channels, relatively few are differentially expressed and only 4 channels are upregulated. Differential upregulation of ORAI1 has been previously reported, but downregulation of STIM1 is novel, as many studies have reported STIM1 to be overexpressed in cancer studies(Wang et al., 2014). These findings in themselves will drive further work to define the functional dynamics of CRC calcium channel signalling. For instance, TRPM4 has previously been shown to negatively impact on store operated calcium entry in androgen-insensitive prostate cancer cells through the transduction of sodium current (Holzmann et al., 2015a), so negative enrichment of TRPM4 with positive enrichment of ORAI1 may represent channel remodelling to drive CRAC channel signalling in colorectal cancer.
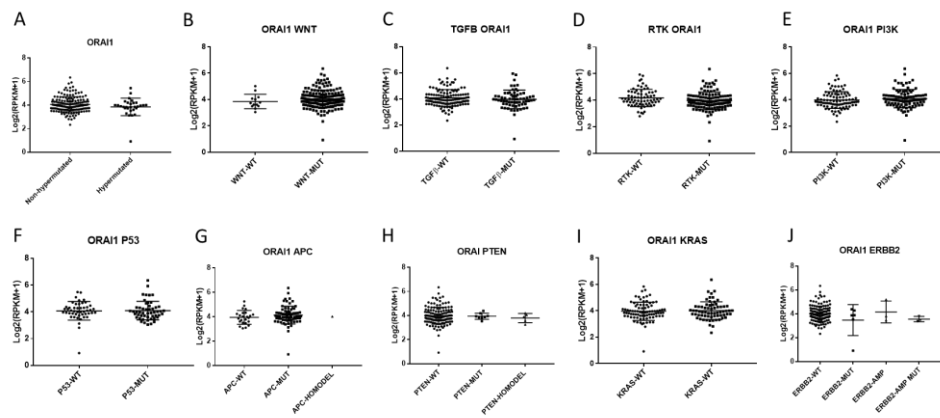
Figure 5.16. Graphs plotting expression data of ORAI1 by oncogenic alterations. A. Hypermutated status; B. Mutated WNT signalling; C. Mutated TGFβ signalling; D. Mutated RTK signalling; E. Mutated PI3K signalling; F. Mutated p53 status; G. Mutated APC signalling; H. Mutated PTEN signalling; I. Mutated KRAS signalling; J. Mutated ERBB2 signalling.
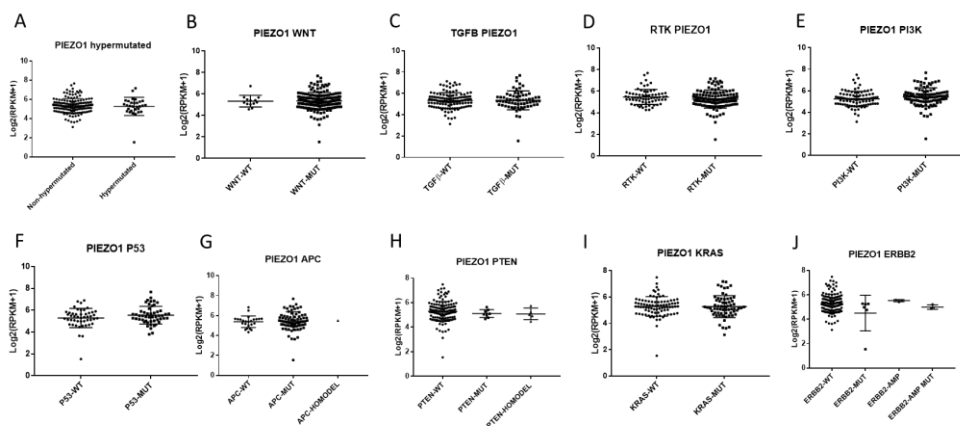
Figure 5.17. Graphs plotting expression data of PIEZO1 by oncogenic alterations. A. Hypermutated status; B. Mutated WNT signalling; C. Mutated TGFβ signalling; D. Mutated RTK signalling; E. Mutated PI3K signalling; F. Mutated p53 status; G. Mutated APC signalling; H. Mutated PTEN signalling; I. Mutated KRAS signalling; J. Mutated ERBB2 signalling.
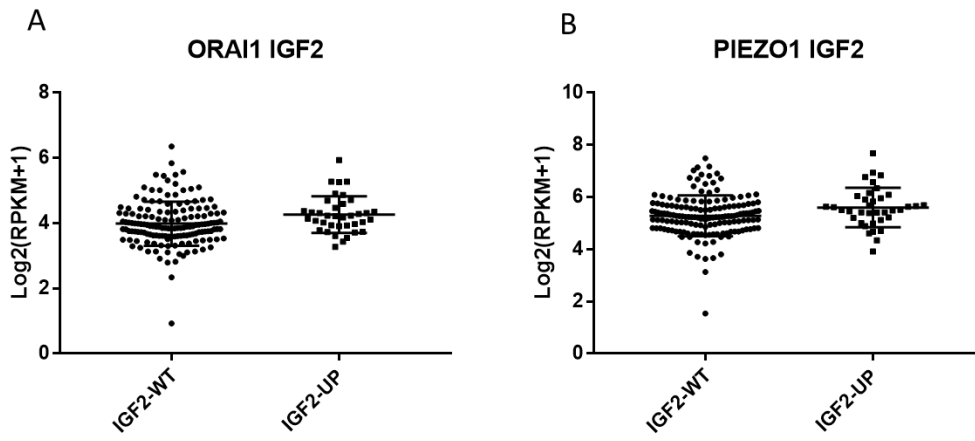
Figure 5.18. Graphs plotting expression data by wild type and upregulation of IGF2R. A. ORAI1; B. PIEZO1.

Interestingly, functional enrichment analysis of the differentially expressed genes has revealed that calcium channel signalling processes and ion transport are differentially downregulated in cancer. Further scrutiny of these genes finds that the majority of the genes in these classes are differentially under-expressed. These GO terms are standardised and have been mapped to processes by the Gene Ontology Consortium, and it should be borne in mind that interpretation of these terms is limited by their inherent lack of specificity to different tissues and potential tissue-specific signalling. Considering the tissue-specific differences in events such as cellular proliferation and cell cycle arrest in different cancers and tissues, it will not include every gene involved and may even include ones that are functionally irrelevant to cancer. This data indicates that ORAI1 and PIEZO1 are remodelled in some way in colorectal tumours, with both differential overexpression and their strong differential correlation in cancer. The literature base supports roles for PIEZO1 and ORAI1 in cancer cell proliferation, migration and invasion of human cancer cells, and GO analysis is not going to be able to wholly depict this. Therefore, as novel as the GSEA results are, it is reasonable to study associations with these channels beyond the scope of GO and GSEA.

Integration of mutational profiling from the TCGA 2012 paper has revealed that PIEZO1 and ORAI1 are not overexpressed due to chromosomal gain either(The Cancer Genome Atlas et al., 2012), suggesting that upregulation of the channel is being functionally driven through molecular signalling. Furthermore, PIEZO1 and ORAI1 do not appear to be driven by oncogenic processes pivotal for colorectal tumourigenesis such as Wnt signalling, K-RAS activated mutations and PI3K mutations. However, expression does appear to correlate with IGF2R amplification. IGF2R is a tyrosine kinase receptor and its amplification was described in the TCGA 2012 analysis, and has subsequently proved to be important in colorectal tumour proliferation and is a potentially druggable target(Zhong et al., 2016). This finding can drive further work to characterise the role that ORAI1 and PIEZO1 play in colorectal cancer *in vitro* as it is possible that they play an important role in the downstream signalling process of IGF2R.

This work has also revealed an inverse relationship between the differential expression of both ORAI1 and PIEZO1 with lymphatic invasion. This suggests that higher levels of channel expression are protective against lymphatic invasion, but without any impact on survival. WGCNA analysis also corroborates an inverse

relationship between PIEZO1 and ORAI1 expression and lymphatic invasion. This work also revealed that lower ORAI1 and PIEZO1 levels are associated with poor prognosis in patients with venous invasion. These are novel findings. One can hypothesize that molecular processes involved in the processes of lymphatic invasion may negatively regulate PIEZO1 and ORAI1 expression and function. One possibility is the process of epithelial-mesenchymal transition (EMT), a reversible process in which polarised epithelial cells undergo molecular changes into a mesenchymal phenotype that increases cellular migratory and invasive properties as well as resistance to apoptosis. However, this contradicts findings from other cancer studies, as ORAI1 and STIM1 has been shown to be overexpressed in the process of EMT initiation in breast cancer cell lines(Hu et al., 2011). Furthermore, mRNA levels of E-cadherin, vimentin, slug, snail and twist did not differ between patients with and without lymphatic invasion. This could be initially explored *in vitro* by inducing EMT in CRC cells and confirming this with qRT-PCR and western blot analysis of EMT markers and looking at the effects on PIEZO1 and ORAI1 expression. Bioinformatics analysis also revealed that there is no relationship between expression levels and disease stage, suggesting that channel signalling is stable and necessary for tumour signalling rather than driving progression.

Steps were taken to ensure that the data was of a decent standard prior to analysis. However, one factor that could potentially skew the accuracy of the results was infiltration of stromal and immune cells that are invariably included within the processed and sequenced tissue blocks. These are inherent to any real tumour and have been found to have autocrine and paracrine cross-talk with the cancer(Choi et al., 2015), so there is an argument for not filtering these out of analyses.

Chapter 6. General Discussion and Future Direction

In summary, this thesis provides evidentiary support for the hypotheses outlined in Chapter 1 that ORAI1 and PIEZO1 are expressed and functional in colorectal cancer.

This work has found that ORAI1 and PIEZO1 are expressed in both human colon cancer cell lines and solid colon tumours, with qRT-PCR analysis of human colon cancer as well as RNASeq analysis of both human colon cancers and normal colon samples analysed as part of the TGCA project. Furthermore, TCGA analysis has found that both of these channels are differentially overexpressed in colon tumours relative to the normal colon. Differential expression of ORAI1 has been reported previously in colorectal cancer, with higher expression in HT-29 compared to the normal colon epithelial cell lines NCM460 and NCM356(Sobradillo et al., 2014). This has also been shown in studies of cancer cell lines and human tissues from other cancer types, including oesophageal squamous cell carcinoma (SCC)(Zhu et al., 2014) and glioblastoma multiforme(Motiani et al., 2013a). Differential overexpression of PIEZO1 has been reported in breast cancer cell line relative to the benign mammary line MCF10A(Li et al., 2015a) and glioma cells relative to the normal glia cells (Chen et al., 2018b). However, such differential expression has not been reported in CRC. Differential study of both tumour and normal tissue is a useful approach in cancer research to explore tumour-specific function. Furthermore, the incorporation of genomic profiling data for colorectal tumours carried out in TCGA also allowed us to determine that there were no genetic amplifications or alterations in the CNV underlying this expression. This data suggests that both ORAI1 and PIEZO1 are functionally upregulated and serves a specific purpose in the tumour tissue. This tumour-specific upregulation also fits with the *in vitro* findings of this thesis that both PIEZO1 and ORAI1 appear to play a functional role in tumour cell function.

This work supports the hypothesis that both ORAI1 and PIEZO1 play a role in the viability, migration and invasion of colorectal cancer cells, using our novel CRAC channel inhibitor JPIII and PIEZO1 siRNA transfection. This is consistent with

findings from other cancer studies, using both siRNA and CRAC channel inhibitors. SFK96365 has previously been shown to inhibit viability of CRC(Sobradillo et al., 2014) and multiple myeloma (Wang et al., 2018) cell lines. YM58483 also inhibited cell viability in malignant melanoma lines(Umemura et al., 2014). Both ORAI1 and STIM1 siRNA knockdown inhibited migration and invasion in cell line studies both *in vitro* and *in vivo* in breast cancer (Yang et al., 2009) and malignant melanoma (Umemura et al., 2014). Similarly, SFK96365 treatment inhibited migration in breast cancer cell lines (Yang et al., 2009). Our novel CRAC channel inhibitor, JPIII, inhibits CRAC channel activity in endothelial cells. This is consistent with existing literature regarding CRAC channel function and inhibition in endothelial cells. ORAI1 has previously been reported to be important in CRAC channel signalling, as Abdullaev and colleagues reported significantly reduced CRAC current following ORAI1 and STIM1 siRNA transfection(Abdullaev et al., 2008). JPIII also had a functional effect on endothelial cell viability, migration and invasion. This is also consistent with existing literature. Abdullaev *et al* reported reduced cell viability using the trypan blue exclusion assay in HUVECs following ORAI1 siRNA transfection, with altered cell cycling and increasing numbers of cells in S and G2M phases(Abdullaev et al., 2008). Furthermore, our laboratory has previously reported reduced HUVEC Boyden chamber migration and *in vitro* HUVEC endothelial tube formation following ORAI1 siRNA transfection(Li et al., 2011a). Functional effects of small compound CRAC channel inhibition on endothelial cell function have also previously been reported. Treatment of HUVEC cells with JPIII's parent compound S66 inhibited cell viability, endothelial tube formation and *in vivo* angiogenesis using the chick chorioallantoic membrane assay(Li et al., 2011a). There is emerging evidence in the literature that CRAC channel signalling is an important signalling mechanism in tumour endothelial cell function. Lodola and colleagues found that the compounds BTP2/YM58483 and carboxyamidotriazole (CAI) inhibited SOCE and the viability and *in vitro* tube formation of breast cancer-derived endothelial colony forming cells(Lodola et al., 2017). Therefore, it is reasonable to hypothesize that CRAC channel inhibition may have an anti-angiogenic function *in vivo*.

The next step to take this work forwards would be testing these channels using *in vivo* models. JPIII only dissolves in 100% DMSO, however this preparation has previously been used successfully *in vivo* in our laboratory in C57Bl/6 mice using mini-osmotic pumps implanted in a subcutaneous pocket. PIEZO1 could be studied *in vivo* using a number of different approaches. Our laboratory has previously

published on the role of PIEZO1 in endothelial cell function and embryonic neovascularisation using a mouse strain genetically reared to generate endothelial cell (EC)-specific PIEZO1 mutation. This used murine strains that were bred heterozygotes for PIEZO1 as well as a model that was cross-bred to create a Cre recombinase-inducible PIEZO1 EC deletion(Li et al., 2014). Establishing such genetic models in a nude mouse strain would allow the study of the effect of PIEZO1 on tumour angiogenesis, using both Cre-inducible PIEZO1 depletion prior to tumour cell implantation, as well as implanting tumour cells into a heterozygotic EC-specific model alongside PIEZO1-wild type and mock-induced control mice. At the end of the study the tumour vasculature can be studied using studies such as immunohistochemistry for endothelial markers such as CD31/PECAM-1(Albelda, 1991) and CD34 and measuring tumour micro-vessel density (MVD)(Kather et al., 2015). These techniques can be used to study the effect of both JPIII treatment or EC-specific PIEZO1 knockdown on tumour angiogenesis to be studied. Genetic manipulation of cancer cell lines *in vitro* to alter ORAI1 and PIEZO1 gene expression could produce either gene knock-out or stable gene overexpression (or knock-in). The technology for this is becoming more readily accessible and less expensive, an important example being CRISPR/Cas-9. There are some foreseeable issues with using this to modify gene expression prior to *in vivo* study. In this thesis PIEZO1 siRNA transfection was seen to halt cancer cell growth and viability, therefore stable knockouts could make it impossible to upscale sufficient cells for implantation. However, CRISPR/Cas9 can also be used to generate inducible models using doxycycline-inducible Cas9 lentiviral vectors that can be induced both *in vitro* and *in vivo(Kim et al., 2018)*, which could be the best way forward.

TCGA analysis found that PIEZO1 and ORAI1 expression are both positively associated with IGF2R amplification. which is a promising lead into discovering the molecular role of PIEZO1 and ORAI1 signalling in colorectal cancer, and will lead further laboratory study. The IGF2R channel gene is amplified in CRC(The Cancer Genome Atlas Network et al., 2012) and has since been reported as being necessary for CRC cell proliferation(Zavorka et al., 2016). Given the *in vitro* effects of targeting these channels in this thesis, it is reasonable to hypothesize that IGF2R may be driving PIEZO1 and ORAI1 function and expression.

Bioinformatics analysis has revealed a strong correlation between ORAI1 and PIEZO1 expression in CRC, with a correlation coefficient of 0.9, which did not exist in the normal colon tissue. It is possible that tumour-specific molecular processes

may drive channel activity and may be upregulating expression and driving their function. Considering the fact that targeting PIEZO1 and ORAI1 both generate the same functional effects (reduced proliferation, migration and invasion) and given the fact that the two channels correlate so strongly, it is possible that these channels co-express and co-function with one another. However, *in vitro* molecular studies to date are not clear regarding this. McHugh found that PIEZO1 mediates integrinβ1 activation via R-Ras store depletion(McHugh et al., 2010), thereby activating CRAC channel signalling downstream of PIEZO1. However, more recently the SERCA2 channel responsible for ER calcium re-uptake has been reported to negatively gate the PIEZO1 channel, with increased PIEZO1 current where SERCA2 is knocked down(Zhang et al., 2017). This may be a mechanism for regulating the amount of PIEZO1-mediated calcium entry. This definitely warrants further study.

Previous studies in other cancers have found that higher expression of CRAC channel machinery is associated with a poor prognostic outcome and survival, such as ORAI1 expression in NSCLC(Zhan, 2015). Furthermore, ORAI1 upregulation has previously been described in advanced colorectal cancer. Differential ORAI1 protein expression has been found to be higher in advanced colorectal cancer(Deng, 2016, Gui et al., 2016), as a greater proportion of patients with T4 disease had higher ORAI1 protein expression than those without(Deng, 2016). Analysis of the TCGA transcriptome has not demonstrated any upregulation across disease stages. This result should be interpreted within the limitations of not possessing proteomic data to substantiate expression profiles, as correlation between mRNA expression and protein levels has been shown to be poor(Kosti et al., 2016). However, this analysis has generated some important questions that will drive further research.

In considering *in vivo* testing in murine models and patients, there are some potential concerns regarding systemic administration of CRAC channel inhibitors. These receptors are constitutively expressed in all tissues, and there are concerns that disruption of the signalling processes in certain tissues will have pathological effects on host function. One important example of this is the effect on immune cells. This became more of a concern when *in vivo* studies of inducible ORAI1-knockout mice were reported to demonstrate defective immune responses, including impaired mast cell signalling, cytokine secretion and degranulation(Vig et al., 2008) as well as defective B cell-driven cytokine production and skin and hair abnormalities(Gwack et al., 2008). This is also a reasonable concern as licensed

immunosuppressant drugs such as cyclosporin A generate potent immunosuppressive effects by inhibiting calcineurin(Foor et al., 1992), a downstream activator target of CRAC channel signalling(Zhu et al., 2018). Immunosuppression is an absolute contraindication in the presence of active cancer as it propagates tumour dissemination. ORAI1 channel knockout has also been associated with potentially dangerous side effects. Platelets of ORAI1 knockout mice have been shown to have defective CRAC channel signalling and impaired activation and thrombus formation(Braun et al., 2009). There is evidence that the immune effects are not as potent with CRAC channel inhibition as those seen in the knockout mice. Gaida and colleagues found that monoclonal ORAI1 treatment did suppress IL2 production but did not impact on IgM or IgG production in cynomolgus monkeys whereas cyclosporin A predictably did(Gaida et al., 2015). There is little evidence in the literature beyond this regarding the immune effects of CRAC channel inhibition. JPIII has been used *in vivo* in our laboratory in C57Bl/6 mice through mini-osmotic pumps, and there has been no difference in cytokine expression profiles found in the serum of these mice and no side effects have been reported. However, this still remains an area for further work and consideration, particularly prior to using it in cancer.

There are a number of limitations to take into account when interpreting the data in this thesis. Firstly, the molecular work is limited to 2 cancer cell lines, which may not be wholly representative of human CRC or the tumour heterogeneity. However, there are other limitations in using cell lines. They are a convenient model for study, particularly where we want to determine the effect of gene knockout on tumourigenesis. However it should be borne in mind that cell lines are less representative of solid human tumours, as they lack the 3D architecture of solid tumours, something that is preserved in using *in vivo* patient derived xenografts (PDX) in immunodeficient mice (Sulaiman and Wang, 2017). Furthermore, they are not as homogeneous as they were once thought to be, as genetic drift has been highlighted significantly greater genetic variation than expected in a study undertaking sequencing of MCF7 cell lines from 27 laboratories worldwide showing significant genetic drift that resulted in 75% of 321 original anti-cancer drug effects reproducible across the different strains (Ben-David et al., 2018). However, the data derived from the *in vitro* cell line study supports carrying this work forward into murine *in vivo* studies. Furthermore, the interpretation is limited by the limited

scope of assays used. Further work *in vitro* could expand this, including a time course of JPIII treatment and PIEZO1 siRNA knockdown characterising activation of cell proliferation pathways, cell cycle studies in synchronised cells, autophagy processes and cell death assays. Furthermore, this work did not undertake protein expression of ORAI1 and PIEZO1 using western blotting. In the absence of decent antibodies for these protein in our laboratory, other techniques can be used to look at both gene and protein expression, using so-called next generation sequencing techniques including microarray analysis or RNASeq for gene expression, and proteomics applications such as MALDI-TOF(Aslam et al., 2017).

Further work

To study the impact of PIEZO1 and ORAI1 on molecular signalling further, cell lines should be generated with both loss and gain of function using technology such as CRISPR/Cas9. These can be used for the molecular studies detailed above *in vitro* as well as *in vivo* murine xenograft studies. In addition, PDX models can be used for studying JPIII inhibition in future studies.

Chapter 7. References

ABDULLAEV, I. F., BISAILLON, J. M., POTIER, M., GONZALEZ, J. C., MOTIANI, R. K. & TREBAK, M. 2008. Stim1 and Orai1 mediate CRAC currents and store-operated calcium entry important for endothelial cell proliferation. *Circ Res,* 103**,** 1289-99.

AKIYAMA, Y., SATO, H., YAMADA, T., NAGASAKI, H., TSUCHIYA, A., ABE, R. & YUASA, Y. 1997. Germ-Line Mutation of the hMSH6/GTBP Gene in an Atypical Hereditary Nonpolyposis Colorectal Cancer Kindred. *Cancer Research,* 57**,** 3920-3923.

ALBELDA, S., MULLER, WA., BUCK, CA., NEWMAN, PJ. 1991. Molecular and cellular properties of PECAM-1 (endoCAM/CD31): a novel vascular cell-cell adhesion molecule. *The Journal of Cell Biology,* 114**,** 1059-1068.

ANDOLFO, I., ALPER, S. L., DE FRANCESCHI, L., AURIEMMA, C., RUSSO, R., DE FALCO, L., VALLEFUOCO, F., ESPOSITO, M. R., VANDORPE, D. H., SHMUKLER, B. E., NARAYAN, R., MONTANARO, D., D'ARMIENTO, M., VETRO, A., LIMONGELLI, I., ZUFFARDI, O., GLADER, B. E., SCHRIER, S. L., BRUGNARA, C., STEWART, G. W., DELAUNAY, J. & IOLASCON, A. 2013. Multiple clinical forms of dehydrated hereditary stomatocytosis arise from mutations in PIEZO1. *Blood,* 121**,** 3925-35, s1-12.

ASLAM, B., BASIT, M., NISAR, M. A., KHURSHID, M. & RASOOL, M. H. 2017. Proteomics: Technologies and Their Applications. *Journal of Chromatographic Science,* 55**,** 182-196.

ATKIN, W., DADSWELL, E., WOOLDRAGE, K., KRALJ-HANS, I., VON WAGNER, C., EDWARDS, R., YAO, G., KAY, C., BURLING, D., FAIZ, O., TEARE, J., LILFORD, R. J., MORTON, D., WARDLE, J. & HALLIGAN, S. 2013. Computed tomographic colonography versus colonoscopy for investigation of patients with symptoms suggestive of colorectal cancer (SIGGAR): a multicentre randomised trial. *Lancet,* 381**,** 1194-202.

ATKIN, W., WOOLDRAGE, K., BRENNER, A., MARTIN, J., SHAH, U., PERERA, S., LUCAS, F., BROWN, J. P., KRALJ-HANS, I., GRELIAK, P., PACK, K., WOOD, J., THOMSON, A., VEITCH, A., DUFFY, S. W. & CROSS, A. J. 2017. Adenoma surveillance and colorectal cancer incidence: a retrospective, multicentre, cohort study. *The Lancet Oncology,* 18**,** 823-834.

AZIMI, I., BONG, A. H., POO, G. X. H., ARMITAGE, K., LOK, D., ROBERTS-THOMSON, S. J. & MONTEITH, G. R. 2018. Pharmacological inhibition of store-operated calcium entry in MDA-MB-468 basal A breast cancer cells: consequences on calcium signalling, cell migration and proliferation. *Cellular and Molecular Life Sciences,* 75**,** 4525-4537.

AZIMI, I., MILEVSKIY, M. J. G., CHALMERS, S. B., YAPA, K. T. D. S., ROBITAILLE, M., HENRY, C., BAILLIE, G. J., THOMPSON, E. W., ROBERTS-THOMSON, S. J. & MONTEITH, G. R. 2019. ORAI1 and ORAI3 in Breast Cancer Molecular Subtypes and the Identification of ORAI3 as a Hypoxia Sensitive Gene and a Regulator of Hypoxia Responses. *Cancers,* 11**,** 208.

BABU, A., RAO, V. G., SU, H. & GULATI, J. 1993. Critical minimum length of the central helix in troponin C for the Ca2+ switch in muscular contraction. *J Biol Chem,* 268**,** 19232-8.

BAE, C., GNANASAMBANDAM, R., NICOLAI, C., SACHS, F. & GOTTLIEB, P. A. 2013. Xerocytosis is caused by mutations that alter the kinetics of the mechanosensitive channel PIEZO1. *Proc Natl Acad Sci U S A,* 110**,** E1162-8.

BAE, C., GNANASAMBANDAM, R, NICOLAI, C, SACHS, F, GOTTLIEB, PA. 2013. Xerocytosis is caused by mutations that alter the kinetics of the mechanosensitive channel PIEZO1. *Proceedings of the National Academy of Sciences of the United States of America,* 110**,** E1162-E1168.

BAE C, S. F., GOTTLIEB PA. 2011. The mechanosensitive ion channel Piezo1 is inhibited by the peptide GsMTx4. *Biochemistry,* 50**,** 6295-6300.

BAE, C. S., F.; GOTTLIEB, PA. 2011. The Mechanosensitive Ion Channel Piezo1 Is Inhibited by the Peptide GsMTx4. *Biochemistry,* 50**,** 6295-6300.

BAEK, M. W., CHO, H. S., KIM, S. H., KIM, W. J. & JUNG, J. Y. 2017. Ascorbic Acid Induces Necrosis in Human Laryngeal Squamous Cell Carcinoma via ROS, PKC, and Calcium Signaling. *J Cell Physiol,* 232**,** 417-425.

BARYSHNIKOV, S. G., PULINA, M. V., ZULIAN, A., LINDE, C. I. & GOLOVINA, V. A. 2009. Orai1, a critical component of store-operated Ca2+ entry, is functionally associated with Na+/Ca2+ exchanger and plasma membrane Ca2+ pump in proliferating human arterial myocytes. *Am J Physiol Cell Physiol,* 297**,** C1103-12.

BECK, A., FLEIG, A., PENNER, R. & PEINELT, C. 2014. Regulation of endogenous and heterologous Ca2+ release-activated Ca2+ currents by pH. *Cell Calcium,* 56**,** 235-243.

BEN-DAVID, U., SIRANOSIAN, B., HA, G., TANG, H., OREN, Y., HINOHARA, K., STRATHDEE, C. A., DEMPSTER, J., LYONS, N. J., BURNS, R., NAG, A., KUGENER, G., CIMINI, B., TSVETKOV, P., MARUVKA, Y. E., O'ROURKE, R., GARRITY, A., TUBELLI, A. A., BANDOPADHAYAY, P., TSHERNIAK, A., VAZQUEZ, F., WONG, B., BIRGER, C., GHANDI, M., THORNER, A. R., BITTKER, J. A., MEYERSON, M., GETZ, G., BEROUKHIM, R. & GOLUB, T. R. 2018. Genetic and transcriptional evolution alters cancer cell line drug response. *Nature,* 560**,** 325-330.

BENJAMINI, Y. & HOCHBERG, Y. 1995. Controlling the False Discovery Rate: A Practical and Powerful Approach to Multiple Testing. *Journal of the Royal Statistical Society. Series B (Methodological),* 57**,** 289-300.

BENVENUTI, S., SARTORE-BIANCHI, A., DI NICOLANTONIO, F., ZANON, C., MORONI, M., VERONESE, S., SIENA, S. & BARDELLI, A. 2007. Oncogenic Activation of the RAS/RAF Signaling Pathway Impairs the Response of Metastatic Colorectal Cancers to Anti–Epidermal Growth Factor Receptor Antibody Therapies. *Cancer Research,* 67**,** 2643-2648.

BERSTEIN, G., BLANK, J. L., SMRCKA, A. V., HIGASHIJIMA, T., STERNWEIS, P. C., EXTON, J. H. & ROSS, E. M. 1992. Reconstitution of agonist-stimulated phosphatidylinositol 4,5-bisphosphate hydrolysis using purified m1 muscarinic receptor, Gq/11, and phospholipase C-beta 1. *J Biol Chem,* 267**,** 8081-8.

BISAILLON, J. M., MOTIANI, R. K., GONZALEZ-COBOS, J. C., POTIER, M., HALLIGAN, K. E., ALZAWAHRA, W. F., BARROSO, M., SINGER, H. A., JOURD'HEUIL, D. & TREBAK, M. 2010. Essential role for STIM1/Orai1-mediated calcium influx in PDGF-induced smooth muscle migration. *Am J Physiol Cell Physiol,* 298**,** C993-1005.

BISGAARD, M. L., FENGER, K., BULOW, S., NIEBUHR, E. & MOHR, J. 1994. Familial adenomatous polyposis (FAP): frequency, penetrance, and mutation rate. *Hum Mutat,* 3**,** 121-5.

BITTREMIEUX, M., LA ROVERE, R. M., SCHUERMANS, M., LUYTEN, T., MIKOSHIBA, K., VANGHELUWE, P., PARYS, J. B. & BULTYNCK, G. 2018. Extracellular and ER-stored Ca2+ contribute to BIRD-2-induced cell death in diffuse large B-cell lymphoma cells. *Cell Death Discovery,* 4**,** 101.

BOOTMAN, M. D., CHEHAB, T., BULTYNCK, G., PARYS, J. B. & RIETDORF, K. 2018. The regulation of autophagy by calcium signals: Do we have a consensus? *Cell Calcium,* 70**,** 32-46.

BOUDJADI, S., CARRIER, J. C., GROULX, J. F. & BEAULIEU, J. F. 2016. Integrin alpha1beta1 expression is controlled by c-MYC in colorectal cancer cells. *Oncogene,* 35**,** 1671-8.

BOURNE, G. W., TRIFARÓ, J. M. 1982. The gadolinium ion: A potent blocker of calcium channels and catecholamine release from cultured chromaffin cells. *Neuroscience,* 7**,** 1615-1622.

BRAUN, A., VARGA-SZABO, D., KLEINSCHNITZ, C., PLEINES, I., BENDER, M., AUSTINAT, M., BÖSL, M., STOLL, G. & NIESWANDT, B. 2009. Orai1 (CRACM1) is the platelet SOC channel and essential for pathological thrombus formation. *Blood,* 113**,** 2056-2063.

BRAY, F., FERLAY, J., SOERJOMATARAM, I., SIEGEL, R. L., TORRE, L. A. & JEMAL, A. 2018. Global cancer statistics 2018: GLOBOCAN estimates of incidence and mortality worldwide for 36 cancers in 185 countries. *CA: A Cancer Journal for Clinicians,* 68**,** 394-424.

BRINI, M., DE GIORGI, F., MURGIA, M., MARSAULT, R., MASSIMINO, M. L., CANTINI, M., RIZZUTO, R. & POZZAN, T. 1997. Subcellular analysis of Ca2+ homeostasis in primary cultures of skeletal muscle myotubes. *Mol Biol Cell,* 8**,** 129-43.

BRISAC, C., TÉOULÉ, F., AUTRET, A., PELLETIER, I., COLBÈRE-GARAPIN, F., BRENNER, C., LEMAIRE, C. & BLONDEL, B. 2010. Calcium Flux between the Endoplasmic Reticulum and Mitochondrion Contributes to Poliovirus-Induced Apoptosis. *Journal of Virology,* 84**,** 12226-12235.

BUTTON, D. & EIDSATH, A. 1996. Aequorin targeted to the endoplasmic reticulum reveals heterogeneity in luminal Ca++ concentration and reports agonist- or IP3-induced release of Ca++. *Mol Biol Cell,* 7**,** 419-34.

CAIRNS, S. R., SCHOLEFIELD, J. H., STEELE, R. J., DUNLOP, M. G., THOMAS, H. J., EVANS, G. D., EADEN, J. A., RUTTER, M. D., ATKIN, W. P., SAUNDERS, B. P., LUCASSEN, A., JENKINS, P., FAIRCLOUGH, P. D. & WOODHOUSE, C. R. 2010. Guidelines for colorectal cancer screening and surveillance in moderate and high risk groups (update from 2002). *Gut,* 59**,** 666-89.

CANAVAN, C., ABRAMS, K. R. & MAYBERRY, J. 2006. Meta-analysis: colorectal and small bowel cancer risk in patients with Crohn's disease. *Aliment Pharmacol Ther,* 23**,** 1097-104.

CANCER GENOME ATLAS RESEARCH NETWORK 2011. Integrated genomic analyses of ovarian carcinoma. *Nature,* 474**,** 609-15.

CANCER RESEARCH UK. 2019a. *Bowel cancer diagnosis and treatment statistics* [Online]. Available: https://www.cancerresearchuk.org/health-professional/cancer-statistics/statistics-by-cancer-type/bowel-cancer/diagnosis-and-treatment [Accessed 05/05/2019].

CANCER RESEARCH UK. 2019b. *Bowel cancer survival statistics* [Online]. Available: https://www.cancerresearchuk.org/health-professional/cancer-statistics/statistics-by-cancer-type/bowel-cancer/survival#heading-Two [Accessed 05/05/2019].

CASPARI, R., OLSCHWANG, S., FRIEDL, W., MANDL, M., BOISSON, C., BÖKER, T., AUGUSTIN, A., KADMON, M., MÖSLEIN, G., THOMAS, G. & PROPPING, P. 1995. Familial adenomatous polyposis: desmoid tumours and lack of ophthalmic lesions (CHRPE) associated with APC mutations beyond codon 1444. *Human Molecular Genetics,* 4**,** 337-340.

CASTANO-MILLA, C., CHAPARRO, M. & GISBERT, J. P. 2014. Systematic review with meta-analysis: the declining risk of colorectal cancer in ulcerative colitis. *Aliment Pharmacol Ther,* 39**,** 645-59.

CHAUDHARI, S., LI, W., WANG, Y., JIANG, H., MA, Y., DAVIS, M. E., ZUCKERMAN, J. E. & MA, R. 2017. Store-operated calcium entry suppressed the TGF-beta1/Smad3 signaling pathway in glomerular mesangial cells. *Am J Physiol Renal Physiol,* 313**,** F729-f739.

CHAUVET, S., JARVIS, L., CHEVALLET, M., SHRESTHA, N., GROSCHNER, K. & BOURON, A. 2016. Pharmacological Characterization of the Native Store-Operated Calcium Channels of Cortical Neurons from Embryonic Mouse Brain. *Front Pharmacol,* 7**,** 486.

CHEN, G., PANICKER, S., LAU, K. Y., APPARSUNDARAM, S., PATEL, V. A., CHEN, S. L., SOTO, R., JUNG, J. K., RAVINDRAN, P., OKUHARA, D., BOHNERT, G., CHE, Q., RAO, P. E., ALLARD, J. D., BADI, L., BITTER, H. M., NUNN, P. A., NARULA, S. K. & DEMARTINO, J. A. 2013. Characterization of a novel CRAC inhibitor that potently blocks human T cell activation and effector functions. *Mol Immunol,* 54**,** 355-67.

CHEN, J. & SANDERSON, M. J. 2017. Store-operated calcium entry is required for sustained contraction and Ca(2+) oscillations of airway smooth muscle. *J Physiol,* 595**,** 3203-3218.

CHEN, Q., KANG, J. & FU, C. 2018a. The independence of and associations among apoptosis, autophagy, and necrosis. *Signal Transduction and Targeted Therapy,* 3**,** 18.

CHEN, X., WANGGOU, S., BODALIA, A., ZHU, M., DONG, W., FAN, J. J., YIN, W. C., MIN, H.-K., HU, M., DRAGHICI, D., DOU, W., LI, F., COUTINHO, F. J., WHETSTONE, H., KUSHIDA, M. M., DIRKS, P. B., SONG, Y., HUI, C.-C., SUN, Y., WANG, L.-Y., LI, X. & HUANG, X. 2018b. A Feedforward Mechanism Mediated by Mechanosensitive Ion Channel PIEZO1 and Tissue Mechanics Promotes Glioma Aggression. *Neuron,* 100**,** 799-815.e7.

CHEN, Y. F., CHIU, W. T., CHEN, Y. T., LIN, P. Y., HUANG, H. J., CHOU, C. Y., CHANG, H. C., TANG, M. J. & SHEN, M. R. 2011. Calcium store sensor stromal-interaction molecule 1-dependent signaling plays an important role in cervical cancer growth, migration, and angiogenesis. *Proc Natl Acad Sci U S A,* 108**,** 15225-30.

CHEUNG, K. H., SHINEMAN, D., MULLER, M., CARDENAS, C., MEI, L., YANG, J., TOMITA, T., IWATSUBO, T., LEE, V. M. & FOSKETT, J. K. 2008. Mechanism of Ca2+ disruption in Alzheimer's disease by presenilin regulation of InsP3 receptor channel gating. *Neuron,* 58**,** 871-83.

CHOI, H., SHENG, J., GAO, D., LI, F., DURRANS, A., RYU, S., LEE, SHARRELL B., NARULA, N., RAFII, S., ELEMENTO, O., ALTORKI, NASSER K., WONG, STEPHEN T. C. & MITTAL, V. 2015. Transcriptome Analysis of Individual Stromal Cell Populations Identifies Stroma-Tumor Crosstalk in Mouse Lung Cancer Model. *Cell Reports,* 10**,** 1187-1201.

CLARKE, D. M., LOO, T. W., INESI, G. & MACLENNAN, D. H. 1989. Location of high affinity Ca2+-binding sites within the predicted transmembrane domain of the sarcoplasmic reticulum Ca2+-ATPase. *Nature,* 339**,** 476-8.

COLORECTAL CANCER COLLABORATIVE GROUP 2000. Palliative chemotherapy for advanced colorectal cancer: systematic review and meta-analysis. *BMJ,* 321**,** 531-535.

CORIAT, R., NICCO, C., CHEREAU, C., MIR, O., ALEXANDRE, J., ROPERT, S., WEILL, B., CHAUSSADE, S., GOLDWASSER, F. & BATTEUX, F. 2012. Sorafenib-induced hepatocellular carcinoma cell death depends on reactive oxygen species production in vitro and in vivo. *Mol Cancer Ther,* 11**,** 2284-93.

COSTE, B., MATHUR, J., SCHMIDT, M., EARLEY, T. J., RANADE, S., PETRUS, M. J., DUBIN, A. E. & PATAPOUTIAN, A. 2010a. Piezo1 and Piezo2 are essential components of distinct mechanically-activated cation channels. *Science (New York, N.Y.),* 330**,** 55-60.

COSTE, B., MATHUR, J., SCHMIDT, M., EARLEY, T. J., RANADE, S., PETRUS, M. J., DUBIN, A. E. & PATAPOUTIAN, A. 2010b. Piezo1 and Piezo2 are essential components of distinct mechanically activated cation channels. *Science,* 330**,** 55-60.

COSTE, B., XIAO, B., SANTOS, J. S., SYEDA, R., GRANDL, J., SPENCER, K. S., KIM, S. E., SCHMIDT, M., MATHUR, J., DUBIN, A. E., MONTAL, M. & PATAPOUTIAN, A. 2012. Piezo proteins are pore-forming subunits of mechanically activated channels. *Nature,* 483**,** 176-81.

CREMOLINI, C., LOUPAKIS, F., ANTONIOTTI, C., LUPI, C., SENSI, E., LONARDI, S., MEZI, S., TOMASELLO, G., RONZONI, M., ZANIBONI, A., TONINI, G., CARLOMAGNO, C., ALLEGRINI, G., CHIARA, S., D'AMICO, M., GRANETTO, C., CAZZANIGA, M., BONI, L., FONTANINI, G. & FALCONE, A. 2015a. FOLFOXIRI plus bevacizumab versus FOLFIRI plus bevacizumab as first-line treatment of patients with metastatic colorectal cancer: updated overall survival and molecular subgroup analyses of the open-label, phase 3 TRIBE study. *Lancet Oncol,* 16**,** 1306-15.

CREMOLINI, C., LOUPAKIS, F., ANTONIOTTI, C., LUPI, C., SENSI, E., LONARDI, S., MEZI, S., TOMASELLO, G., RONZONI, M., ZANIBONI, A., TONINI, G., CARLOMAGNO, C., ALLEGRINI, G., CHIARA, S., D'AMICO, M., GRANETTO, C., CAZZANIGA, M., BONI, L., FONTANINI, G. & FALCONE, A. 2015b. FOLFOXIRI plus bevacizumab versus FOLFIRI plus bevacizumab as first-line treatment of patients with metastatic colorectal cancer: updated overall survival and molecular subgroup analyses of the open-label, phase 3 TRIBE study. *The Lancet Oncology,* 16**,** 1306-1315.

CSORDAS, G., MADESH, M., ANTONSSON, B. & HAJNOCZKY, G. 2002. tcBid promotes Ca(2+) signal propagation to the mitochondria: control of Ca(2+) permeation through the outer mitochondrial membrane. *Embo j,* 21**,** 2198-206.

DATKHAEVA, I., ARBOLEDA, V. A., SENARATNE, T. N., NIKPOUR, G., MEYERSON, C., GENG, Y., AFSHAR, Y., SCIBETTA, E., GOLDSTEIN, J., QUINTERO-RIVERA, F., CRANDALL, B. F., GRODY, W. W., DEIGNAN, J. & JANZEN, C. 2018. Identification of novel PIEZO1 variants using prenatal exome sequencing and correlation to ultrasound and autopsy findings of recurrent hydrops fetalis. *American Journal of Medical Genetics Part A,* 176**,** 2829-2834.

DE JONG, A. E., MORREAU, H., VAN PUIJENBROEK, M., EILERS, P. H. C., WIJNEN, J., NAGENGAST, F. M., GRIFFIOEN, G., CATS, A., MENKO, F. H., KLEIBEUKER, J. H. & VASEN, H. F. A. 2004. The role of mismatch repair gene defects in the development of adenomas in patients with HNPCC. *Gastroenterology,* 126**,** 42-48.

DELA PAZ, N. G. & FRANGOS, J. A. 2018. Yoda1-induced phosphorylation of Akt and ERK1/2 does not require Piezo1 activation. *Biochemical and biophysical research communications,* 497**,** 220-225.

DENG, W., ET AL., 2016. Orai1, a Direct Target of microRNA-519, Promotes Progression of Colorectal Cancer via Akt/GSK3beta Signaling Pathway. *Dig Dis Sci*, 1-8.

DI GREGORIO, E., ORSI, L., GODANI, M., VAULA, G., JENSEN, S., SALMON, E., FERRARI, G., SQUADRONE, S., ABETE, M. C., CAGNOLI, C., BRUSSINO, A. & BRUSCO, A. 2010. Two Italian families with ITPR1 gene deletion presenting a broader phenotype of SCA15. *Cerebellum,* 9, 115-23.

DI SABATINO, A., ROVEDATTI, L., KAUR, R., SPENCER, J. P., BROWN, J. T., MORISSET, V. D., BIANCHERI, P., LEAKEY, N. A., WILDE, J. I., SCOTT, L., CORAZZA, G. R., LEE, K., SENGUPTA, N., KNOWLES, C. H., GUNTHORPE, M. J., MCLEAN, P. G., MACDONALD, T. T. & KRUIDENIER, L. 2009. Targeting gut T cell Ca2+ release-activated Ca2+ channels inhibits T cell cytokine production and T-box transcription factor T-bet in inflammatory bowel disease. *J Immunol,* 183, 3454-62.

DIEP, C. B., KLEIVI, K., RIBEIRO, F. R., TEIXEIRA, M. R., LINDGJAERDE, O. C. & LOTHE, R. A. 2006. The order of genetic events associated with colorectal cancer progression inferred from meta-analysis of copy number changes. *Genes Chromosomes Cancer,* 45, 31-41.

DONG, Z., SHANMUGHAPRIYA, S., TOMAR, D., SIDDIQUI, N., LYNCH, S., NEMANI, N., BREVES, S. L., ZHANG, X., TRIPATHI, A., PALANIAPPAN, P., RIITANO, M. F., WORTH, A. M., SEELAM, A., CARVALHO, E., SUBBIAH, R., JAÑA, F., SOBOLOFF, J., PENG, Y., CHEUNG, J. Y., JOSEPH, S. K., CAPLAN, J., RAJAN, S., STATHOPULOS, P. B. & MADESH, M. 2017. Mitochondrial Ca2+ Uniporter Is a Mitochondrial Luminal Redox Sensor that Augments MCU Channel Activity. *Molecular Cell,* 65, 1014-1028.e7.

DONNARD, E., ASPRINO, P. F., CORREA, B. R., BETTONI, F., KOYAMA, F. C., NAVARRO, F. C., PEREZ, R. O., MARIADASON, J., SIEBER, O. M., STRAUSBERG, R. L., SIMPSON, A. J., JARDIM, D. L., REIS, L. F., PARMIGIANI, R. B., GALANTE, P. A. & CAMARGO, A. A. 2014. Mutational analysis of genes coding for cell surface proteins in colorectal cancer cell lines reveal novel altered pathways, druggable mutations and mutated epitopes for targeted therapy. *Oncotarget,* 5, 9199-213.

DRUMM, B. T., REMBETSKI, B. E., COBINE, C. A., BAKER, S. A., SERGEANT, G. P., HOLLYWOOD, M. A., THORNBURY, K. D. & SANDERS, K. M. 2018. Ca(2+) signalling in mouse urethral smooth muscle in situ: role of Ca(2+) stores and Ca(2+) influx mechanisms. *J Physiol,* 596, 1433-1466.

DUBOIS, C., VANDEN ABEELE, F., LEHEN'KYI, V., GKIKA, D., GUARMIT, B., LEPAGE, G., SLOMIANNY, C., BOROWIEC, A. S., BIDAUX, G., BENAHMED, M., SHUBA, Y. & PREVARSKAYA, N. 2014. Remodeling of channel-forming ORAI proteins determines an oncogenic switch in prostate cancer. *Cancer Cell,* 26, 19-32.

DUGOURD, C., GERVAIS, M., CORVOL, P. & MONNOT, C. 2003. Akt Is a Major Downstream Target of PI3-Kinase Involved in Angiotensin II–Induced Proliferation. *Hypertension,* 41, 882-890.

EBASHI, S. & LIPMANN, F. 1962. ADENOSINE TRIPHOSPHATE-LINKED CONCENTRATION OF CALCIUM IONS IN A PARTICULATE FRACTION OF RABBIT MUSCLE. *The Journal of cell biology,* 14, 389-400.

EISENHOFFER, G. T., LOFTUS, P. D., YOSHIGI, M., OTSUNA, H., CHIEN, C. B., MORCOS, P. A. & ROSENBLATT, J. 2012. Crowding induces live cell extrusion to maintain homeostatic cell numbers in epithelia. *Nature,* 484, 546-9.

ELMORE, S. 2007. Apoptosis: a review of programmed cell death. *Toxicologic pathology,* 35, 495-516.

ENNS, A., GASSMANN, P., SCHLUTER, K., KORB, T., SPIEGEL, H. U., SENNINGER, N. & HAIER, J. 2004. Integrins can directly mediate metastatic tumor cell adhesion within the liver sinusoids. *J Gastrointest Surg,* 8**,** 1049-59; discussion 1060.

ERISMAN, M. D., ROTHBERG, P. G., DIEHL, R. E., MORSE, C. C., SPANDORFER, J. M. & ASTRIN, S. M. 1985. Deregulation of c-myc gene expression in human colon carcinoma is not accompanied by amplification or rearrangement of the gene. *Molecular and cellular biology,* 5**,** 1969-1976.

EVANS, E. L., CUTHBERTSON, K., ENDESH, N., RODE, B., BLYTHE, N. M., HYMAN, A. J., HALL, S. J., GAUNT, H. J., LUDLOW, M. J., FOSTER, R. & BEECH, D. J. 2018. Yoda1 analogue (Dooku1) which antagonizes Yoda1-evoked activation of Piezo1 and aortic relaxation. *Br J Pharmacol,* 175**,** 1744-1759.

FALASCA, M., RAIMONDI, C. & MAFFUCCI, T. 2011. Boyden Chamber. *In:* WELLS, C. M. & PARSONS, M. (eds.) *Cell Migration: Developmental Methods and Protocols.* Totowa, NJ: Humana Press.

FALASCA, M., RAIMONDI, C, MAFFUCI, T. 2011. Boyden Chamber *In:* WELLS, C., PARSONS, M. (ed.) *Cell MigrationCell Migration. Methods in Molecular Biology (Methods and Protocols).* Humana Press

FAUCHERRE, A., KISSA, K., NARGEOT, J., MANGONI, M. E. & JOPLING, C. 2014. Piezo1 plays a role in erythrocyte volume homeostasis. *Haematologica,* 99**,** 70-75.

FERLAY, J., ERVIK, M., LAM, F., COLOMBET, M., MER,Y L., PIÑEROS, M., ZNAOR, A., SOERJOMATARAM, I., BRAY, F. . 2018. *Global Cancer Observatory: Cancer Today* [Online]. Lyon, France: International Agency for Research on Cancer. Available: Available from: https://gco.iarc.fr/today [Accessed 18/04/2018 2019].

FESKE, S., GWACK, Y., PRAKRIYA, M., SRIKANTH, S., PUPPEL, S. H., TANASA, B., HOGAN, P. G., LEWIS, R. S., DALY, M. & RAO, A. 2006. A mutation in Orai1 causes immune deficiency by abrogating CRAC channel function. *Nature,* 441**,** 179-85.

FLIS, S., SPLAWINSKI, J. 2009. Inhibitory Effects of 5-Fluorouracil and Oxaliplatin on Human Colorectal Cancer Cell Survival Are Synergistically Enhanced by Sulindac Sulfide. *Anticancer Research,* 29**,** 435-441.

FLOURAKIS, M., LEHEN'KYI, V., BECK, B., RAPHAEL, M., VANDENBERGHE, M., ABEELE, F. V., ROUDBARAKI, M., LEPAGE, G., MAUROY, B., ROMANIN, C., SHUBA, Y., SKRYMA, R. & PREVARSKAYA, N. 2010. Orai1 contributes to the establishment of an apoptosis-resistant phenotype in prostate cancer cells. *Cell Death Dis,* 1**,** e75.

FODDE, R., KUIPERS, J., ROSENBERG, C., SMITS, R., KIELMAN, M., GASPAR, C., VAN ES, J. H., BREUKEL, C., WIEGANT, J., GILES, R. H. & CLEVERS, H. 2001. Mutations in the APC tumour suppressor gene cause chromosomal instability. *Nat Cell Biol,* 3**,** 433-8.

FOO, C. C., POON, S. H. T., CHIU, R. H. Y., LAM, W. Y., CHEUNG, L. C. & LAW, W. L. 2019. Is bridge to surgery stenting a safe alternative to emergency surgery in malignant colonic obstruction: a meta-analysis of randomized control trials. *Surg Endosc,* 33**,** 293-302.

FOOR, F., PARENT, S. A., MORIN, N., DAHL, A. M., RAMADAN, N., CHREBET, G., BOSTIAN, K. A. & NIELSEN, J. B. 1992. Calcineurin mediates inhibition by FK506 and cyclosporin of recovery from alpha-factor arrest in yeast. *Nature,* 360**,** 682-4.

GAIDA, K., SALIMI-MOOSAVI, H., SUBRAMANIAN, R., ALMON, V., KNIZE, A., ZHANG, M., LIN, F. F., NGUYEN, H. Q., ZHOU, L., SULLIVAN, J. K., WONG, M. & MCBRIDE, H. J. 2015. Inhibition of CRAC with a human anti-ORAI1

monoclonal antibody inhibits T-cell-derived cytokine production but fails to inhibit a T-cell-dependent antibody response in the cynomolgus monkey. *J Immunotoxicol,* 12**,** 164-73.

GERWECK, L. E. & SEETHARAMAN, K. 1996. Cellular pH gradient in tumor versus normal tissue: potential exploitation for the treatment of cancer. *Cancer Res,* 56**,** 1194-8.

GIANTONIO, B. J., CATALANO, P. J., MEROPOL, N. J., O'DWYER, P. J., MITCHELL, E. P., ALBERTS, S. R., SCHWARTZ, M. A. & BENSON, A. B. 2007. Bevacizumab in Combination With Oxaliplatin, Fluorouracil, and Leucovorin (FOLFOX4) for Previously Treated Metastatic Colorectal Cancer: Results From the Eastern Cooperative Oncology Group Study E3200. *Journal of Clinical Oncology,* 25**,** 1539-1544.

GOLDMAN, M., CRAFT, B., HASTIE, M., REPEČKA, K., KAMATH, A., MCDADE, F., ROGERS, D., BROOKS, A. N., ZHU, J. & HAUSSLER, D. 2019. The UCSC Xena platform for public and private cancer genomics data visualization and interpretation. *bioRxiv***,** 326470.

GONZALEZ-COBOS, J. C., ZHANG, X., ZHANG, W., RUHLE, B., MOTIANI, R. K., SCHINDL, R., MUIK, M., SPINELLI, A. M., BISAILLON, J. M., SHINDE, A. V., FAHRNER, M., SINGER, H. A., MATROUGUI, K., BARROSO, M., ROMANIN, C. & TREBAK, M. 2013. Store-independent Orai1/3 channels activated by intracrine leukotriene C4: role in neointimal hyperplasia. *Circ Res,* 112**,** 1013-25.

GRAHAM, T. A., WEAVER, C., MAO, F., KIMELMAN, D. & XU, W. 2000. Crystal Structure of a β-Catenin/Tcf Complex. *Cell,* 103**,** 885-896.

GROVER, S., KASTRINOS, F., STEYERBERG, E. W., COOK, E. F., DEWANWALA, A., BURBIDGE, L. A., WENSTRUP, R. J. & SYNGAL, S. 2012. Prevalence and phenotypes of APC and MUTYH mutations in patients with multiple colorectal adenomas. *JAMA,* 308**,** 485-492.

GRYNKIEWICZ, G., POENIE, M. & TSIEN, R. Y. 1985. A new generation of Ca2+ indicators with greatly improved fluorescence properties. *J Biol Chem,* 260**,** 3440-50.

GUDIPATY, S. A., LINDBLOM, J., LOFTUS, P. D., REDD, M. J., EDES, K., DAVEY, C. F., KRISHNEGOWDA, V. & ROSENBLATT, J. 2017. Mechanical stretch triggers rapid epithelial cell division through Piezo1. *Nature,* 543**,** 118-121.

GUI, L., WANG, Z., HAN, J., MA, H. & LI, Z. 2016. High Expression of Orai1 Enhances Cell Proliferation and is Associated with Poor Prognosis in Human Colorectal Cancer. *Clin Lab,* 62**,** 1689-1698.

GWACK, Y., SRIKANTH, S., OH-HORA, M., HOGAN, P. G., LAMPERTI, E. D., YAMASHITA, M., GELINAS, C., NEEMS, D. S., SASAKI, Y., FESKE, S., PRAKRIYA, M., RAJEWSKY, K. & RAO, A. 2008. Hair loss and defective T- and B-cell function in mice lacking ORAI1. *Mol Cell Biol,* 28**,** 5209-22.

HALLIGAN, S., WOOLDRAGE, K., DADSWELL, E., KRALJ-HANS, I., VON WAGNER, C., EDWARDS, R., YAO, G., KAY, C., BURLING, D., FAIZ, O., TEARE, J., LILFORD, R. J., MORTON, D., WARDLE, J. & ATKIN, W. 2013. Computed tomographic colonography versus barium enema for diagnosis of colorectal cancer or large polyps in symptomatic patients (SIGGAR): a multicentre randomised trial. *Lancet,* 381**,** 1185-93.

HAMADA, K., MIYATAKE, H., TERAUCHI, A. & MIKOSHIBA, K. 2017. IP3-mediated gating mechanism of the IP3 receptor revealed by mutagenesis and X-ray crystallography. *Proc Natl Acad Sci U S A,* 114**,** 4661-4666.

HANAHAN, D. & WEINBERG, ROBERT A. 2011. Hallmarks of Cancer: The Next Generation. *Cell,* 144**,** 646-674.

HARA, K., SHIGA, A., NOZAKI, H., MITSUI, J., TAKAHASHI, Y., ISHIGURO, H., YOMONO, H., KURISAKI, H., GOTO, J., IKEUCHI, T., TSUJI, S., NISHIZAWA, M. & ONODERA, O. 2008. Total deletion and a missense mutation of ITPR1 in Japanese SCA15 families. *Neurology,* 71**,** 547-51.

HOLTHAUZEN, L. M. F., CORRÊA, F. & FARAH, C. S. 2004. Ca2+-induced Rolling of Tropomyosin in Muscle Thin Filaments: THE α- AND β-BAND HYPOTHESIS REVISITED. *Journal of Biological Chemistry,* 279**,** 15204-15213.

HOLZMANN, C., KAPPEL, S., KILCH, T., JOCHUM, M. M., URBAN, S. K., JUNG, V., STOCKLE, M., ROTHER, K., GREINER, M. & PEINELT, C. 2015a. Transient receptor potential melastatin 4 channel contributes to migration of androgen-insensitive prostate cancer cells. *Oncotarget,* 6**,** 41783-93.

HOLZMANN, C., KILCH, T., KAPPEL, S., DORR, K., JUNG, V., STOCKLE, M., BOGESKI, I. & PEINELT, C. 2015b. Differential Redox Regulation of Ca(2)(+) Signaling and Viability in Normal and Malignant Prostate Cells. *Biophys J,* 109**,** 1410-9.

HOTH, M. & PENNER, R. 1992. Depletion of intracellular calcium stores activates a calcium current in mast cells. *Nature,* 355**,** 353-6.

HOTH, M. & PENNER, R. 1993. Calcium release-activated calcium current in rat mast cells. *The Journal of physiology,* 465**,** 359-386.

HOU, X., PEDI, L., DIVER, M. M. & LONG, S. B. 2012. Crystal structure of the calcium release-activated calcium channel Orai. *Science,* 338**,** 1308-13.

HOYER-HANSEN, M. B., L.; SZYNIAROWSKI, P.; CAMPANELLA, M.; SZABADKAI, G.; FARKAS, T.; BIANCHI, K.; FEHRENBACHER, N.; ELLING, F.; RIZZUTO, R.; MATHIASEN, IS.; JAATTELA, M. 2007. Control of macroautophagy by calcium, calmodulin-dependent kinase kinase-beta, and Bcl-2. *Mol. Cell***,** 193-205.

HU, J., QIN, K., ZHANG, Y., GONG, J., LI, N., LV, D., XIANG, R. & TAN, X. 2011. Downregulation of transcription factor Oct4 induces an epithelial-to-mesenchymal transition via enhancement of Ca2+ influx in breast cancer cells. *Biochemical and Biophysical Research Communications,* 411**,** 786-791.

HUANG, X., STERN, D. F. & ZHAO, H. 2016. Transcriptional Profiles from Paired Normal Samples Offer Complementary Information on Cancer Patient Survival – Evidence from TCGA Pan-Cancer Data. *Scientific Reports,* 6**,** 20567.

HUANG, Z., CHENG, S.-L. & SLATOPOLSKY, E. 2001. Sustained Activation of the Extracellular Signal-regulated Kinase Pathway Is Required for Extracellular Calcium Stimulation of Human Osteoblast Proliferation. *Journal of Biological Chemistry,* 276**,** 21351-21358.

HURWITZ, H., FEHRENBACHER, L., NOVOTNY, W., CARTWRIGHT, T., HAINSWORTH, J., HEIM, W., BERLIN, J., BARON, A., GRIFFING, S., HOLMGREN, E., FERRARA, N., FYFE, G., ROGERS, B., ROSS, R. & KABBINAVAR, F. 2004. Bevacizumab plus irinotecan, fluorouracil, and leucovorin for metastatic colorectal cancer. *N Engl J Med,* 350**,** 2335-42.

INTERNATIONAL AGENCY FOR RESEARCH ON CANCER. 2019. *Cancer Today* [Online]. Available: http://gco.iarc.fr/today/home [Accessed 01.10.2019 2019].

JENKINS, M. A., BAGLIETTO, L., DOWTY, J. G., VAN VLIET, C. M., SMITH, L., MEAD, L. J., MACRAE, F. A., ST JOHN, D. J., JASS, J. R., GILES, G. G., HOPPER, J. L. & SOUTHEY, M. C. 2006. Cancer risks for mismatch repair gene mutation carriers: a population-based early onset case-family study. *Clin Gastroenterol Hepatol,* 4**,** 489-98.

JIANG, L., ZHAO, Y, CHEN, W. 2017. The Function of the Novel Mechanical Activated Ion Channel Piezo1 in the Human Osteosarcoma Cells. *Medical Science Monitor : International Medical Journal of Experimental and Clinical Research,* 23**,** 5070-5082.

JING, Z., SUI, X., YAO, J., XIE, J., JIANG, L., ZHOU, Y., PAN, H. & HAN, W. 2016. SKF-96365 activates cytoprotective autophagy to delay apoptosis in colorectal cancer cells through inhibition of the calcium/CaMKIIγ/AKT-mediated pathway. *Cancer letters,* 372**,** 226-238.

KAR, P., SAMANTA, K., KRAMER, H., MORRIS, O., BAKOWSKI, D. & PAREKH, A. B. 2014. Dynamic assembly of a membrane signaling complex enables selective activation of NFAT by Orai1. *Curr Biol,* 24**,** 1361-1368.

KASSAMBARA, A., KOSINSKI, M., BIECEK, P., FABIAN, S. 2019. survminer: Drawing Survival Curves using 'ggplot2'.

KATHER, J. N., MARX, A., REYES-ALDASORO, C. C., SCHAD, L. R., ZÖLLNER, F. G. & WEIS, C.-A. 2015. Continuous representation of tumor microvessel density and detection of angiogenic hotspots in histological whole-slide images. *Oncotarget,* 6**,** 19163-19176.

KHAW-ON, P., POMPIMON, W. & BANJERDPONGCHAI, R. 2019. Goniothalamin Induces Necroptosis and Anoikis in Human Invasive Breast Cancer MDA-MB-231 Cells. *International journal of molecular sciences,* 20**,** 3953.

KIM, J. H., ET AL 2014. Orai1 and STIM1 are critical for cell migration and proliferation of clear cell renal cell carcinoma. *Biochem Biophys Res Commun,* 448**,** 76-82.

KIM, J. H., LKHAGVADORJ, S., LEE, M. R., HWANG, K. H., CHUNG, H. C., JUNG, J. H., CHA, S. K. & EOM, M. 2014. Orai1 and STIM1 are critical for cell migration and proliferation of clear cell renal cell carcinoma. *Biochem Biophys Res Commun,* 448**,** 76-82.

KIM, K. J., LI, B., WINER, J., ARMANINI, M., GILLETT, N., PHILLIPS, H. S. & FERRARA, N. 1993. Inhibition of vascular endothelial growth factor-induced angiogenesis suppresses tumour growth in vivo. *Nature,* 362**,** 841-4.

KIM, S. E., COSTE, B., CHADHA, A., COOK, B. & PATAPOUTIAN, A. 2012. The role of Drosophila Piezo in mechanical nociception. *Nature,* 483**,** 209-12.

KIM, W., LEE, S., KIM, H. S., SONG, M., CHA, Y. H., KIM, Y.-H., SHIN, J., LEE, E.-S., JOO, Y., SONG, J. J., CHOI, E. J., CHOI, J. W., LEE, J., KANG, M., YOOK, J. I., LEE, M. G., KIM, Y.-S., PAIK, S. & KIM, H. H. 2018. Targeting mutant KRAS with CRISPR-Cas9 controls tumor growth. *Genome research,* 28**,** 374-382.

KNUDSEN, A. L., BULOW, S., TOMLINSON, I., MOSLEIN, G., HEINIMANN, K. & CHRISTENSEN, I. J. 2010. Attenuated familial adenomatous polyposis: results from an international collaborative study. *Colorectal Dis,* 12**,** e243-9.

KONDRATSKA, K., KONDRATSKYI, A., YASSINE, M., LEMONNIER, L., LEPAGE, G., MORABITO, A., SKRYMA, R. & PREVARSKAYA, N. 2014. Orai1 and STIM1 mediate SOCE and contribute to apoptotic resistance of pancreatic adenocarcinoma. *Biochim Biophys Acta,* 1843**,** 2263-9.

KOSTI, I., JAIN, N., ARAN, D., BUTTE, A. J. & SIROTA, M. 2016. Cross-tissue Analysis of Gene and Protein Expression in Normal and Cancer Tissues. *Scientific reports,* 6**,** 24799-24799.

KOSUGI, C., KODA, K., ISHIBASHI, K., YOSHIMATSU, K., TANAKA, S., KATO, R., KATO, H., OYA, M., NARUSHIMA, K., MORI, M., SHUTO, K. & ISHIDA, H. 2018. Safety of mFOLFOX6/XELOX as adjuvant chemotherapy after curative resection of stage III colon cancer: phase II clinical study (The FACOS study). *International Journal of Colorectal Disease,* 33**,** 809-817.

KOZIN, S. V., SHKARIN, P. & GERWECK, L. E. 2001. The cell transmembrane pH gradient in tumors enhances cytotoxicity of specific weak acid chemotherapeutics. *Cancer Res,* 61**,** 4740-3.

KRAMER, K., VAN ACKER, S. A., GRIMBERGEN, J. A., VAN DEN BERG, D. J., VAN DER VIJGH, W. J. & BAST, A. 1995. Effect of dimethyl sulfoxide (DMSO) on the electrocardiogram (ECG) in freely moving male Balb/c mice. *Gen Pharmacol,* 26**,** 1403-7.

KYLLÖNEN, L. E. 1987. Obstruction and perforation complicating colorectal carcinoma. An epidemiologic and clinical study with special reference to incidence and survival. *Acta chirurgica Scandinavica,* 153**,** 607-614.

LAKEN, S. J., PETERSEN, G. M., GRUBER, S. B., ODDOUX, C., OSTRER, H., GIARDIELLO, F. M., HAMILTON, S. R., HAMPEL, H., MARKOWITZ, A., KLIMSTRA, D., JHANWAR, S., WINAWER, S., OFFIT, K., LUCE, M. C., KINZLER, K. W. & VOGELSTEIN, B. 1997. Familial colorectal cancer in Ashkenazim due to a hypermutable tract in APC. *Nature Genetics,* 17**,** 79-83.

LANGFELDER, P. & HORVATH, S. 2008. WGCNA: an R package for weighted correlation network analysis. *BMC Bioinformatics,* 9**,** 559.

LAUDICELLA, M., WALSH, B., BURNS, E. & SMITH, P. C. 2016. Cost of care for cancer patients in England: evidence from population-based patient-level data. *British journal of cancer,* 114**,** 1286-1292.

LEACH, F. S., NICOLAIDES, N. C., PAPADOPOULOS, N., LIU, B., JEN, J., PARSONS, R., PELTOMÄKI, P., SISTONEN, P., AALTONEN, L. A., NYSTRÖM-LAHTI, M., GUAN, X. Y., ZHANG, J., MELTZER, P. S., YU, J.-W., KAO, F.-T., CHEN, D. J., CEROSALETTI, K. M., FOURNIER, R. E. K., TODD, S., LEWIS, T., LEACH, R. J., NAYLOR, S. L., WEISSENBACH, J., MECKLIN, J.-P., JÄRVINEN, H., PETERSEN, G. M., HAMILTON, S. R., GREEN, J., JASS, J., WATSON, P., LYNCH, H. T., TRENT, J. M., DE LA CHAPELLE, A., KINZLER, K. W. & VOGELSTEIN, B. 1993. Mutations of a mutS homolog in hereditary nonpolyposis colorectal cancer. *Cell,* 75**,** 1215-1225.

LEE, C. H., PARK, D., WU, D., RHEE, S. G. & SIMON, M. I. 1992. Members of the Gq alpha subunit gene family activate phospholipase C beta isozymes. *Journal of Biological Chemistry,* 267**,** 16044-7.

LEWIS, A., GRANDL, J. 2015. Mechanical sensitivity of Piezo1 ion channels can be tuned by cellular membrane tension. *eLife,* 4.

LI, C., REZANIA, S., KAMMERER, S., SOKOLOWSKI, A., DEVANEY, T., GORISCHEK, A., JAHN, S., HACKL, H., GROSCHNER, K., WINDPASSINGER, C., MALLE, E., BAUERNHOFER, T. & SCHREIBMAYER, W. 2015a. Piezo1 forms mechanosensitive ion channels in the human MCF-7 breast cancer cell line. *Scientific Reports,* 5**,** 8364.

LI, J., BRUNS, A.-F., HOU, B., RODE, B., WEBSTER, P. J., BAILEY, M. A., APPLEBY, H. L., MOSS, N. K., RITCHIE, J. E., YULDASHEVA, N. Y., TUMOVA, S., QUINNEY, M., MCKEOWN, L., TAYLOR, H., PRASAD, K. R., BURKE, D., O'REGAN, D., PORTER, K. E., FOSTER, R., KEARNEY, M. T. & BEECH, D. J. 2015b. Orai3 Surface Accumulation and Calcium Entry Evoked by Vascular Endothelial Growth Factor. *Arteriosclerosis, Thrombosis, and Vascular Biology,* 35**,** 1987-1994.

LI, J., CUBBON, R. M., WILSON, L. A., AMER, M. S., MCKEOWN, L., HOU, B., MAJEED, Y., TUMOVA, S., SEYMOUR, V. A., TAYLOR, H., STACEY, M., O'REGAN, D., FOSTER, R., PORTER, K. E., KEARNEY, M. T. & BEECH, D. J. 2011a. Orai1 and CRAC channel dependence of VEGF-activated Ca2+ entry and endothelial tube formation. *Circ Res,* 108**,** 1190-8.

LI, J., CUBBON, RM., WILSON, LA., AMER, MS., MCKEOWN, L., HOU, B., MAJEED, Y., TUMOVA, S.,SEYMOUR, VAL., TAYLOR, H., STACEY, M., O'REGAN, D.,FOSTER, R.,PORTER, KE., KEARNEY, MT., BEECH, DJ. 2011. Orai1 and CRAC Channel Dependence of VEGF-Activated Ca(2+)-Entry and Endothelial Tube Formation. *Circulation research,* 108**,** 1190-1198.

LI, J., HOU, B., TUMOVA, S., MURAKI, K., BRUNS, A., LUDLOW, M., SEDO, A., HYMAN, A., MCKEOWN, L., YOUNG, R., YULDASHEVA, N., MAJEED, Y., WILSON, L., RODE, B., BAILEY, M., KIM, H., FU, Z., CARTER, D., BILTON, J., IMRIE, H., AJUH, P., DEAR, T., CUBBON, R., KEARNEY, M., PRASAD, R., EVANS, P., AINSCOUGH, J. & BEECH, D. 2014. Piezo1 integration of vascular architecture with physiological force. *Nature,* 515**,** 279-282.

LI, J., MCKEOWN, L., OJELABI, O., STACEY, M., FOSTER, R., O'REGAN, D., PORTER, K. E. & BEECH, D. J. 2011b. Nanomolar potency and selectivity of a Ca(2)(+) release-activated Ca(2)(+) channel inhibitor against store-operated Ca(2)(+) entry and migration of vascular smooth muscle cells. *Br J Pharmacol,* 164**,** 382-93.

LIOU, J., FIVAZ, M., INOUE, T. & MEYER, T. 2007. Live-cell imaging reveals sequential oligomerization and local plasma membrane targeting of stromal interaction molecule 1 after Ca(2+) store depletion. *Proceedings of the National Academy of Sciences of the United States of America,* 104**,** 9301-9306.

LIOUDYNO, M. I., KOZAK, J. A., PENNA, A., SAFRINA, O., ZHANG, S. L., SEN, D., ROOS, J., STAUDERMAN, K. A. & CAHALAN, M. D. 2008. Orai1 and STIM1 move to the immunological synapse and are up-regulated during T cell activation. *Proc Natl Acad Sci U S A,* 105**,** 2011-6.

LIS, A., PEINELT, C., BECK, A., PARVEZ, S., MONTEILH-ZOLLER, M., FLEIG, A. & PENNER, R. 2007. CRACM1, CRACM2, and CRACM3 are store-operated Ca2+ channels with distinct functional properties. *Curr Biol,* 17**,** 794-800.

LIU, G., HONISCH, S., SCHMIDT, S., ALKAHTANI, S., ALKAHTANE, A. A., STOURNARAS, C. & LANG, F. 2015. Up-regulation of Orai1 expression and store operated Ca(2+) entry following activation of membrane androgen receptors in MCF-7 breast tumor cells. *BMC Cancer,* 15**,** 995.

LIU, H., HUGHES, J. D., ROLLINS, S., CHEN, B. & PERKINS, E. 2011. Calcium entry via ORAI1 regulates glioblastoma cell proliferation and apoptosis. *Exp Mol Pathol,* 91**,** 753-60.

LIU, J., LICHTENBERG, T., HOADLEY, K. A., POISSON, L. M., LAZAR, A. J., CHERNIACK, A. D., KOVATICH, A. J., BENZ, C. C., LEVINE, D. A., LEE, A. V., OMBERG, L., WOLF, D. M., SHRIVER, C. D., THORSSON, V., CAESAR-JOHNSON, S. J., DEMCHOK, J. A., FELAU, I., KASAPI, M., FERGUSON, M. L., HUTTER, C. M., SOFIA, H. J., TARNUZZER, R., WANG, Z., YANG, L., ZENKLUSEN, J. C., ZHANG, J., CHUDAMANI, S., LIU, J., LOLLA, L., NARESH, R., PIHL, T., SUN, Q., WAN, Y., WU, Y., CHO, J., DEFREITAS, T., FRAZER, S., GEHLENBORG, N., GETZ, G., HEIMAN, D. I., KIM, J., LAWRENCE, M. S., LIN, P., MEIER, S., NOBLE, M. S., SAKSENA, G., VOET, D., ZHANG, H., BERNARD, B., CHAMBWE, N., DHANKANI, V., KNIJNENBURG, T., KRAMER, R., LEINONEN, K., LIU, Y., MILLER, M., REYNOLDS, S., SHMULEVICH, I., THORSSON, V., ZHANG, W., AKBANI, R., BROOM, B. M., HEGDE, A. M., JU, Z., KANCHI, R. S., KORKUT, A., LI, J., LIANG, H., LING, S., LIU, W., LU, Y., MILLS, G. B., NG, K.-S., RAO, A., RYAN, M., WANG, J., WEINSTEIN, J. N., ZHANG, J., ABESHOUSE, A., ARMENIA, J., CHAKRAVARTY, D., CHATILA, W. K., DE BRUIJN, I., GAO, J., GROSS, B. E., HEINS, Z. J., KUNDRA, R., LA, K., LADANYI, M., LUNA, A., NISSAN, M. G., OCHOA, A., PHILLIPS, S. M., REZNIK, E., SANCHEZ-VEGA, F., SANDER, C., SCHULTZ, N., SHERIDAN, R.,

SUMER, S. O., SUN, Y., et al. 2018. An Integrated TCGA Pan-Cancer Clinical Data Resource to Drive High-Quality Survival Outcome Analytics. *Cell,* 173**,** 400-416.e11.

LIU, X., BERRY, C. T., RUTHEL, G., MADARA, J. J., MACGILLIVRAY, K., GRAY, C. M., MADGE, L. A., MCCORKELL, K. A., BEITING, D. P., HERSHBERG, U., MAY, M. J. & FREEDMAN, B. D. 2016. T cell receptor-induced NF-kappaB signaling and transcriptional activation are regulated by STIM1- and Orai1-mediated calcium entry. *J Biol Chem*.

LOCATELLI, S. L., CAREDDU, G., MAGAGNOLI, M., DI TRANI, M., MORELLO, L., VISWANADHA, S., VAKKALANKA, S. K. V., CASTAGNA, L., SANTORO, A. & CARLO-STELLA, C. 2017. The Novel Calcium Release-Activated Calcium (CRAC) Channel Inhibitor RP4010 Exerts Potent Antitumor Effects in NOD/SCID/IL2Rg$^{-/-}$ Mice with Diffuse Large B Cell Lymphoma (DLBCL) Cell Line Xenografts. *Blood,* 130**,** 4101-4101.

LODOLA, F., LAFORENZA, U., CATTANEO, F., RUFFINATTI, F. A., POLETTO, V., MASSA, M., TANCREDI, R., ZUCCOLO, E., KHDAR, D. A., RICCARDI, A., BIGGIOGERA, M., ROSTI, V., GUERRA, G. & MOCCIA, F. 2017. VEGF-induced intracellular Ca(2+) oscillations are down-regulated and do not stimulate angiogenesis in breast cancer-derived endothelial colony forming cells. *Oncotarget,* 8**,** 95223-95246.

LOGAN, R. F., PATNICK, J., NICKERSON, C., COLEMAN, L., RUTTER, M. D. & VON WAGNER, C. 2012a. Outcomes of the Bowel Cancer Screening Programme (BCSP) in England after the first 1 million tests. *Gut,* 61**,** 1439-46.

LOGAN, R. F. A., PATNICK, J., NICKERSON, C., COLEMAN, L., RUTTER, M. D. & VON WAGNER, C. 2012b. Outcomes of the Bowel Cancer Screening Programme (BCSP) in England after the first 1 million tests. *Gut,* 61**,** 1439-1446.

LOWRY, O. H., ROSEBROUGH, N. J., FARR, A. L. & RANDALL, R. J. 1951. Protein measurement with the Folin phenol reagent. *J Biol Chem,* 193**,** 265-75.

LUKACS, V., MATHUR, J., MAO, R., BAYRAK-TOYDEMIR, P., PROCTER, M., CAHALAN, S. M., KIM, H. J., BANDELL, M., LONGO, N., DAY, R. W., STEVENSON, D. A., PATAPOUTIAN, A. & KROCK, B. L. 2015. Impaired PIEZO1 function in patients with a novel autosomal recessive congenital lymphatic dysplasia. *Nature Communications,* 6**,** 8329.

LYTTON, J., WESTLIN, M., HANLEY, MR. 1991. Thapsigargin Inhibits the Sarcoplasmic or Endoplasmic Reticulum Ca-ATPase Family of Calcium Pumps. *Journal of Biological Chemistry,* 266**,** 17067-17071.

MARSHALL, J. 2011. Transwell((R)) invasion assays. *Methods Mol Biol,* 769**,** 97-110.

MARSHALL, T. W., LLOYD, I. E., DELALANDE, J. M., NATHKE, I. & ROSENBLATT, J. 2011. The tumor suppressor adenomatous polyposis coli controls the direction in which a cell extrudes from an epithelium. *Mol Biol Cell,* 22**,** 3962-70.

MARTIN-LOPEZ, J. E., BELTRAN-CALVO, C., RODRIGUEZ-LOPEZ, R. & MOLINA-LOPEZ, T. 2014. Comparison of the accuracy of CT colonography and colonoscopy in the diagnosis of colorectal cancer. *Colorectal Dis,* 16**,** O82-9.

MCHUGH, B. J., BUTTERY, R., LAD, Y., BANKS, S., HASLETT, C. & SETHI, T. 2010. Integrin activation by Fam38A uses a novel mechanism of R-Ras targeting to the endoplasmic reticulum. *J Cell Sci,* 123**,** 51-61.

MCHUGH, B. J., MURDOCH, A., HASLETT, C. & SETHI, T. 2012. Loss of the Integrin-Activating Transmembrane Protein Fam38A (Piezo1) Promotes a Switch to a Reduced Integrin-Dependent Mode of Cell Migration. *PLoS ONE,* 7**,** e40346.

MCKENZIE, A. T., KATSYV, I., SONG, W.-M., WANG, M. & ZHANG, B. 2016. DGCA: A comprehensive R package for Differential Gene Correlation Analysis. *BMC systems biology,* 10**,** 106-106.

MCNALLY, B. A., SOMASUNDARAM, A., JAIRAMAN, A., YAMASHITA, M. & PRAKRIYA, M. 2013. The C- and N-terminal STIM1 binding sites on Orai1 are required for both trapping and gating CRAC channels. *J Physiol,* 591**,** 2833-50.

MCNALLY, B. A., SOMASUNDARAM, A., YAMASHITA, M. & PRAKRIYA, M. 2012. Gated regulation of CRAC channel ion selectivity by STIM1. *Nature,* 482**,** 241-5.

MHAIDAT, N. M., BOUKLIHACENE, M. & THORNE, R. F. 2014. 5-Fluorouracil-induced apoptosis in colorectal cancer cells is caspase-9-dependent and mediated by activation of protein kinase C-delta. *Oncol Lett,* 8**,** 699-704.

MIGNEN, O., THOMPSON, J. L. & SHUTTLEWORTH, T. J. 2008a. Both Orai1 and Orai3 are essential components of the arachidonate-regulated Ca2+-selective (ARC) channels. *J Physiol,* 586**,** 185-95.

MIGNEN, O., THOMPSON, J. L. & SHUTTLEWORTH, T. J. 2008b. Orai1 subunit stoichiometry of the mammalian CRAC channel pore. *J Physiol,* 586**,** 419-25.

MIGNEN, O., THOMPSON, J. L. & SHUTTLEWORTH, T. J. 2009. The molecular architecture of the arachidonate-regulated Ca2+-selective ARC channel is a pentameric assembly of Orai1 and Orai3 subunits. *J Physiol,* 587**,** 4181-97.

MIYAKI, M., KONISHI, M., KIKUCHI-YANOSHITA, R., ENOMOTO, M., IGARI, T., TANAKA, K., MURAOKA, M., TAKAHASHI, H., AMADA, Y., FUKAYAMA, M. & ET AL. 1994. Characteristics of somatic mutation of the adenomatous polyposis coli gene in colorectal tumors. *Cancer Res,* 54**,** 3011-20.

MIYAMOTO, T., MOCHIZUKI, T., NAKAGOMI, H., KIRA, S., WATANABE, M., TAKAYAMA, Y., SUZUKI, Y., KOIZUMI, S., TAKEDA, M. & TOMINAGA, M. 2014. Functional role for Piezo1 in stretch-evoked Ca(2)(+) influx and ATP release in urothelial cell cultures. *J Biol Chem,* 289**,** 16565-75.

MIZUNO, H., CHO, Y.-Y., MA, W.-Y., BODE, A. M. & DONG, Z. 2006. Effects of MAP kinase inhibitors on epidermal growth factor-induced neoplastic transformation of human keratinocytes. *Molecular carcinogenesis,* 45**,** 1-9.

MONTERO, M., BRINI, M., MARSAULT, R., ALVAREZ, J., SITIA, R., POZZAN, T. & RIZZUTO, R. 1995. Monitoring dynamic changes in free Ca2+ concentration in the endoplasmic reticulum of intact cells. *Embo j,* 14**,** 5467-75.

MORI, Y., MATSUNAGA, M., ABE, T., FUKUSHIGE, S., MIURA, K., SUNAMURA, M., SHIIBA, K., SATO, M., NUKIWA, T. & HORII, A. 1999. Chromosome band 16q24 is frequently deleted in human gastric cancer. *Br J Cancer,* 80**,** 556-62.

MOTIANI, R. K., ABDULLAEV, I. F. & TREBAK, M. 2010. A novel native store-operated calcium channel encoded by Orai3: selective requirement of Orai3 versus Orai1 in estrogen receptor-positive versus estrogen receptor-negative breast cancer cells. *The Journal of biological chemistry,* 285**,** 19173-19183.

MOTIANI, R. K., HYZINSKI-GARCIA, M. C., ZHANG, X., HENKEL, M. M., ABDULLAEV, I. F., KUO, Y. H., MATROUGUI, K., MONGIN, A. A. & TREBAK, M. 2013a. STIM1 and Orai1 mediate CRAC channel activity and are essential for human glioblastoma invasion. *Pflugers Arch,* 465**,** 1249-60.

MOTIANI, R. K., ZHANG, X., HARMON, K. E., KELLER, R. S., MATROUGUI, K., BENNETT, J. A. & TREBAK, M. 2013b. Orai3 is an estrogen receptor alpha-regulated Ca(2)(+) channel that promotes tumorigenesis. *Faseb j,* 27**,** 63-75.

MOUTASIM, K. A., NYSTROM, M. L. & THOMAS, G. J. 2011. Cell migration and invasion assays. *Methods Mol Biol,* 731**,** 333-43.

MULDER, S. A., KRANSE, R., DAMHUIS, R. A., DE WILT, J. H. W., OUWENDIJK, R. J. T., KUIPERS, E. J. & VAN LEERDAM, M. E. 2011. Prevalence and prognosis of synchronous colorectal cancer: A Dutch population-based study. *Cancer Epidemiology,* 35**,** 442-447.

MULLINS, F. M., YEN, M. & LEWIS, R. S. 2016. Orai1 pore residues control CRAC channel inactivation independently of calmodulin. *J Gen Physiol,* 147**,** 137-52.

MUNEMITSU, S., ALBERT, I., SOUZA, B., RUBINFELD, B. & POLAKIS, P. 1995. Regulation of intracellular beta-catenin levels by the adenomatous polyposis coli (APC) tumor-suppressor protein. *Proc Natl Acad Sci U S A,* 92**,** 3046-50.

MUNSHI, A., HOBBS, M. & MEYN, R. E. 2005. Clonogenic Cell Survival Assay. *In:* BLUMENTHAL, R. D. (ed.) *Chemosensitivity: Volume 1 In Vitro Assays.* Totowa, NJ: Humana Press.

MUNSHI, A., HOBBS, M, MEYN, RE. 2005. Clonogenic Cell Survival Assay. *In:* BLUMENTHAL, R. (ed.) *Chemosensitivity Volume I: In Vitro Assays.* Humana Press.

NATIONAL INSTITUTE FOR HEALTH AND CARE EXCELLENCE 2015. Suspected cancer: recognition and referral.

NATIONAL INSTITUTE OF HEALTH AND CLINICAL EXCELLENCE 2014. Colorectal cancer: diagnosis and management.

NATIONAL INSTITUTE OF HEALTH AND CLINICAL EXCELLENCE 2017. Quantitative faecal immunochemical tests to guide referral for colorectal cancer in primary care. Diagnostic guidance DG30.

NETWORK, N. C. I. 2012a. The characteristics of individuals with colorectal cancer who die rapidly after their diagnosis NCIN Data Briefing.

NETWORK, T. C. G. A. 2012b. Comprehensive molecular portraits of human breast tumours. *Nature,* 490**,** 61-70.

NICHOLSON, B. D., SHINKINS, B., PATHIRAJA, I., ROBERTS, N. W., JAMES, T. J., MALLETT, S., PERERA, R., PRIMROSE, J. N. & MANT, D. 2015. Blood CEA levels for detecting recurrent colorectal cancer. *Cochrane Database of Systematic Reviews*.

NICOLAIDES, N. C., PAPADOPOULOS, N., LIU, B., WEI, Y. F., CARTER, K. C., RUBEN, S. M., ROSEN, C. A., HASELTINE, W. A., FLEISCHMANN, R. D., FRASER, C. M. & ET AL. 1994. Mutations of two PMS homologues in hereditary nonpolyposis colon cancer. *Nature,* 371**,** 75-80.

NIELSEN, M., HES, F. J., NAGENGAST, F. M., WEISS, M. M., MATHUS-VLIEGEN, E. M., MORREAU, H., BREUNING, M. H., WIJNEN, J. T., TOPS, C. M. & VASEN, H. F. 2007. Germline mutations in APC and MUTYH are responsible for the majority of families with attenuated familial adenomatous polyposis. *Clin Genet,* 71**,** 427-33.

NISHITANI, W. S., SAIF, T. A. & WANG, Y. 2011. Calcium Signaling in Live Cells on Elastic Gels under Mechanical Vibration at Subcellular Levels. *PLOS ONE,* 6**,** e26181.

NOEL, P. R. B., BARNETT, K. C., DAVIES, R. E., JOLLY, D. W., LEAHY, J. S., MAWDESLEY-THOMAS, L. E., SHILLAM, K. W. G., SQUIRES, P. F., STREET, A.

E., TUCKER, W. C. & WORDEN, A. N. 1975. The toxicity of dimethyl sulphoxide (DMSO) for the dog, pig, rat and rabbit. *Toxicology,* 3**,** 143-169.

OFFICE FOR NATIONAL STATISTICS. 2019. *Cancer survival in England: national estimates for patients followed up to 2017: 1-year, 5-year and 10-year net-survival estimates for adults diagnosed with cancer between 2012 and 2016 and followed up to 2017, and by stage at diagnosis.* [Online]. Available: https://www.ons.gov.uk/peoplepopulationandcommunity/healthandsocialcare/conditionsanddiseases/bulletins/cancersurvivalinengland/nationalestimatesforpatientsfollowedupto2017 [Accessed].

OFFICE OF NATIONAL STATISTICS 2016. Cancer survival by stage at diagnosis for England (experimental statistics): Adults diagnosed 2012, 2013 and 2014 and followed up to 2015. UK.

OHGA, K., KUROMITSU, S., TAKEZAWA, R., NUMAZAKI, M., ISHIKAWA, J., NAGASHIMA, S. & SHIMIZU, Y. 2008. YM-341619 suppresses the differentiation of spleen T cells into Th2 cells in vitro, eosinophilia, and airway hyperresponsiveness in rat allergic models. *Eur J Pharmacol,* 590**,** 409-16.

OKI, E., ODA, S., MAEHARA, Y. & SUGIMACHI, K. 1999. Mutated gene-specific phenotypes of dinucleotide repeat instability in human colorectal carcinoma cell lines deficient in DNA mismatch repair. *Oncogene,* 18**,** 2143-7.

ORMEROD, M. 2008. DNA Analysis. *Flow Cytometry - A Basic Introduction.*

ORRENIUS, S., GOGVADZE, V. & ZHIVOTOVSKY, B. 2015. Calcium and mitochondria in the regulation of cell death. *Biochemical and Biophysical Research Communications,* 460**,** 72-81.

PAPADOPOULOS, N., NICOLAIDES, N., WEI, Y., RUBEN, S., CARTER, K., ROSEN, C., HASELTINE, W., FLEISCHMANN, R., FRASER, C., ADAMS, M. & ET, A. 1994. Mutation of a mutL homolog in hereditary colon cancer. *Science,* 263**,** 1625-1629.

PAREKH, A., FLEIG, A, PENNER, R. 1997. The Store-Operated Calcium Current ICRAC: Nonlinear Activation by InsP3 and Dissociation from Calcium Release. *Cell,* 89**,** 973-980.

PAREKH, A. P. J., JW. 2005. Store-Operated Calcium Channels. *Physiological Reviews,* 85**,** 757-810.

PARKINS, C. S., CHADWICK, J. A. & CHAPLIN, D. J. 1996. Inhibition of intracellular pH control and relationship to cytotoxicity of chlorambucil and vinblastine. *Br J Cancer Suppl,* 27**,** S75-7.

PENG, L., BIAN, X. W., LI, D. K., XU, C., WANG, G. M., XIA, Q. Y. & XIONG, Q. 2015. Large-scale RNA-Seq Transcriptome Analysis of 4043 Cancers and 548 Normal Tissue Controls across 12 TCGA Cancer Types. *Scientific Reports,* 5**,** 13413.

PENG, S., GERASIMENKO, J. V., TSUGORKA, T., GRYSHCHENKO, O., SAMARASINGHE, S., PETERSEN, O. H. & GERASIMENKO, O. V. 2016. Calcium and adenosine triphosphate control of cellular pathology: asparaginase-induced pancreatitis elicited via protease-activated receptor 2. *Philos Trans R Soc Lond B Biol Sci,* 371.

PINTO, M. C. X., KIHARA, A. H., GOULART, V. A. M., TONELLI, F. M. P., GOMES, K. N., ULRICH, H. & RESENDE, R. R. 2015. Calcium signaling and cell proliferation. *Cellular Signalling,* 27**,** 2139-2149.

PINTUS, G., TADOLINI, B., POSADINO, A. M., SANNA, B., DEBIDDA, M., CARRU, C., DEIANA, L. & VENTURA, C. 2003. PKC/Raf/MEK/ERK signaling pathway

modulates native-LDL-induced E2F-1 gene expression and endothelial cell proliferation. *Cardiovascular Research,* 59**,** 934-944.

POLSTER, B. M., BASAÑEZ, G., ETXEBARRIA, A., HARDWICK, J. M. & NICHOLLS, D. G. 2005. Calpain I Induces Cleavage and Release of Apoptosis-inducing Factor from Isolated Mitochondria. *Journal of Biological Chemistry,* 280**,** 6447-6454.

POWELL, S. M., ZILZ, N., BEAZER-BARCLAY, Y., BRYAN, T. M., HAMILTON, S. R., THIBODEAU, S. N., VOGELSTEIN, B. & KINZLER, K. W. 1992. APC mutations occur early during colorectal tumorigenesis. *Nature,* 359**,** 235-237.

PUTKEY, J. A., SWEENEY, H. L. & CAMPBELL, S. T. 1989. Site-directed mutation of the trigger calcium-binding sites in cardiac troponin C. *J Biol Chem,* 264**,** 12370-8.

PUTNEY, J. 1986a. A model for receptor-regulated calcium entry *Cell Calcium,* 7**,** 1-12.

PUTNEY, J. W., JR. 1986b. A model for receptor-regulated calcium entry. *Cell Calcium,* 7**,** 1-12.

QUINTANA, A., RAJANIKANTH, V., FARBER-KATZ, S., GUDLUR, A., ZHANG, C., JING, J., ZHOU, Y., RAO, A. & HOGAN, P. G. 2015. TMEM110 regulates the maintenance and remodeling of mammalian ER-plasma membrane junctions competent for STIM-ORAI signaling. *Proc Natl Acad Sci U S A,* 112**,** E7083-92.

R CORE TEAM 2013. R: A language and environment for statistical computing. Vienna, Australia: R Foundation for Statistical Computing.

RAHMAN, S. & RAHMAN, T. 2017. Unveiling some FDA-approved drugs as inhibitors of the store-operated Ca2+ entry pathway. *Scientific Reports,* 7**,** 12881.

RANADE, S. S., WOO, S. H., DUBIN, A. E., MOSHOURAB, R. A., WETZEL, C., PETRUS, M., MATHUR, J., BEGAY, V., COSTE, B., MAINQUIST, J., WILSON, A. J., FRANCISCO, A. G., REDDY, K., QIU, Z., WOOD, J. N., LEWIN, G. R. & PATAPOUTIAN, A. 2014. Piezo2 is the major transducer of mechanical forces for touch sensation in mice. *Nature,* 516**,** 121-5.

REIMAND, J., ISSERLIN, R., VOISIN, V., KUCERA, M., TANNUS-LOPES, C., ROSTAMIANFAR, A., WADI, L., MEYER, M., WONG, J., XU, C., MERICO, D. & BADER, G. D. 2019. Pathway enrichment analysis and visualization of omics data using g:Profiler, GSEA, Cytoscape and EnrichmentMap. *Nature Protocols,* 14**,** 482-517.

RINGER, S. 1883. A further Contribution regarding the influence of the different Constituents of the Blood on the Contraction of the Heart. *The Journal of physiology,* 4**,** 29-42.3.

RIZZUTO, R., SIMPSON, A. W., BRINI, M. & POZZAN, T. 1992. Rapid changes of mitochondrial Ca2+ revealed by specifically targeted recombinant aequorin. *Nature,* 358**,** 325-7.

ROBINSON, M. D., MCCARTHY, D. J. & SMYTH, G. K. 2010. edgeR: a Bioconductor package for differential expression analysis of digital gene expression data. *Bioinformatics,* 26.

ROBINSON, M. D. & OSHLACK, A. 2010. A scaling normalization method for differential expression analysis of RNA-seq data. *Genome Biology,* 11**,** R25.

ROH, S. A., CHOI, E. Y., CHO, D. H., JANG, S. J., KIM, S. Y., KIM, Y. S. & KIM, J. C. 2010. Growth and invasion of sporadic colorectal adenocarcinomas in terms of genetic change. *Journal of Korean medical science,* 25**,** 353-360.

ROOS, J., DIGREGORIO, P. J., YEROMIN, A. V., OHLSEN, K., LIOUDYNO, M., ZHANG, S., SAFRINA, O., KOZAK, J. A., WAGNER, S. L., CAHALAN, M. D., VELICELEBI, G. & STAUDERMAN, K. A. 2005. STIM1, an essential and conserved

component of store-operated Ca2+ channel function. *J Cell Biol,* 169**,** 435-45.

ROSEN, L. B., GINTY, D. D., WEBER, M. J. & GREENBERG, M. E. 1994. Membrane depolarization and calcium influx stimulate MEK and MAP kinase via activation of Ras. *Neuron,* 12**,** 1207-21.

RUBINFELD, B., SOUZA, B., ALBERT, I., MULLER, O., CHAMBERLAIN, S., MASIARZ, F., MUNEMITSU, S. & POLAKIS, P. 1993. Association of the APC gene product with beta-catenin. *Science,* 262**,** 1731-1734.

SACHDEVA, R., FLEMING, T., SCHUMACHER, D., HOMBERG, S., STILZ, K., MOHR, F., WAGNER, A. H., TSVILOVSKYY, V., MATHAR, I. & FREICHEL, M. 2019. Methylglyoxal evokes acute Ca(2+) transients in distinct cell types and increases agonist-evoked Ca(2+) entry in endothelial cells via CRAC channels. *Cell Calcium,* 78**,** 66-75.

SALOVAARA, R., ROTH, S., LOUKOLA, A., LAUNONEN, V., SISTONEN, P., AVIZIENYTE, E., KRISTO, P., JÄRVINEN, H., SOUCHELNYTSKYI, S., SARLOMO-RIKALA, M. & AALTONEN, L. A. 2002. Frequent loss of SMAD4/DPC4 protein in colorectal cancers. *Gut,* 51**,** 56-59.

SCHLAPPACK, O. K., ZIMMERMANN, A. & HILL, R. P. 1991. Glucose starvation and acidosis: effect on experimental metastatic potential, DNA content and MTX resistance of murine tumour cells. *Br J Cancer,* 64**,** 663-70.

SCHMIDT, S., LIU, G., LIU, G., YANG, W., HONISCH, S., PANTELAKOS, S., STOURNARAS, C., HONIG, A. & LANG, F. 2014. Enhanced Orai1 and STIM1 expression as well as store operated Ca2+ entry in therapy resistant ovary carcinoma cells. *Oncotarget,* 5**,** 4799-810.

SCHMITTGEN, T. D. & LIVAK, K. J. 2008. Analyzing real-time PCR data by the comparative C(T) method. *Nat Protoc,* 3**,** 1101-8.

SCHNEIDER, C. A., RASBAND, W. S. & ELICEIRI, K. W. 2012. NIH Image to ImageJ: 25 years of image analysis. *Nat Methods,* 9**,** 671-5.

SCHOLEFIELD, J. H., MOSS, S., SUFI, F., MANGHAM, C. M. & HARDCASTLE, J. D. 2002. Effect of faecal occult blood screening on mortality from colorectal cancer: results from a randomised controlled trial. *Gut,* 50**,** 840-844.

SEPULVEDA, A. R., HAMILTON, S. R., ALLEGRA, C. J., GRODY, W., CUSHMAN-VOKOUN, A. M., FUNKHOUSER, W. K., KOPETZ, S. E., LIEU, C., LINDOR, N. M., MINSKY, B. D., MONZON, F. A., SARGENT, D. J., SINGH, V. M., WILLIS, J., CLARK, J., COLASACCO, C., RUMBLE, R. B., TEMPLE-SMOLKIN, R., VENTURA, C. B. & NOWAK, J. A. 2017. Molecular Biomarkers for the Evaluation of Colorectal Cancer: Guideline From the American Society for Clinical Pathology, College of American Pathologists, Association for Molecular Pathology, and the American Society of Clinical Oncology. *Journal of Clinical Oncology,* 35**,** 1453-1486.

SHANKLEMAN, J., MASSAT, N. J., KHAGRAM, L., ARIYANAYAGAM, S., GARNER, A., KHATOON, S., RAINBOW, S., RANGREZ, S., COLORADO, Z., HU, W., PARMAR, D. & DUFFY, S. W. 2014. Evaluation of a service intervention to improve awareness and uptake of bowel cancer screening in ethnically-diverse areas. *Br J Cancer,* 111**,** 1440-7.

SHIVAPURKAR, N., HUANG, L., RUGGERI, B., SWALSKY, P. A., BAKKER, A., FINKELSTEIN, S., FROST, A. & SILVERBERG, S. 1997. K-ras and p53 mutations in aberrant crypt foci and colonic tumors from colon cancer patients. *Cancer Lett,* 115**,** 39-46.

SLATTUM, G., GU, Y., SABBADINI, R. & ROSENBLATT, J. 2014. Autophagy in oncogenic K-Ras promotes basal extrusion of epithelial cells by degrading S1P. *Curr Biol,* 24**,** 19-28.

SLAUGHTER, D. P., SOUTHWICK, H. W. & SMEJKAL, W. 1953. "Field cancerization" in oral stratified squamous epithelium. Clinical implications of multicentric origin. *Cancer,* 6**,** 963-968.

SMITH, A. J., STERN, H. S., PENNER, M., HAY, K., MITRI, A., BAPAT, B. V. & GALLINGER, S. 1994. Somatic APC and K-ras codon 12 mutations in aberrant crypt foci from human colons. *Cancer Res,* 54**,** 5527-30.

SMITH, K. J., JOHNSON, K. A., BRYAN, T. M., HILL, D. E., MARKOWITZ, S., WILLSON, J. K., PARASKEVA, C., PETERSEN, G. M., HAMILTON, S. R., VOGELSTEIN, B. & ET AL. 1993. The APC gene product in normal and tumor cells. *Proc Natl Acad Sci U S A,* 90**,** 2846-50.

SOBOLOFF, J., GLIGORIJEVIC, B. & ZAIDI, M. R. 2018. STIM1 (c)AMPs up melanogenesis. *The EMBO Journal,* 37**,** e99047.

SOBRADILLO, D., HERNÁNDEZ-MORALES, M., UBIERNA, D., MOYER, M. P., NÚÑEZ, L. & VILLALOBOS, C. 2014. A Reciprocal Shift in Transient Receptor Potential Channel 1 (TRPC1) and Stromal Interaction Molecule 2 (STIM2) Contributes to Ca2+ Remodeling and Cancer Hallmarks in Colorectal Carcinoma Cells. *Journal of Biological Chemistry,* 289**,** 28765-28782.

SORICH, M. J., WIESE, M. D., ROWLAND, A., KICHENADASSE, G., MCKINNON, R. A. & KARAPETIS, C. S. 2014. Extended RAS mutations and anti-EGFR monoclonal antibody survival benefit in metastatic colorectal cancer: a meta-analysis of randomized, controlled trials. *Annals of Oncology,* 26**,** 13-21.

SPASSOVA, M., HEWAVITHARANA, T., XU, W., SOBOLOFF, J., GILL, DL. 2006. A common mechanism underlies stretch activation and receptor activation of TRPC6 channels. *Proceedings of the National Academy of Sciences of the United States of America,* 103**,** 16586-16591.

SPIER, I., KERICK, M., DRICHEL, D., HORPAOPAN, S., ALTMULLER, J., LANER, A., HOLZAPFEL, S., PETERS, S., ADAM, R., ZHAO, B., BECKER, T., LIFTON, R. P., HOLINSKI-FEDER, E., PERNER, S., THIELE, H., NOTHEN, M. M., HOFFMANN, P., TIMMERMANN, B., SCHWEIGER, M. R. & ARETZ, S. 2016. Exome sequencing identifies potential novel candidate genes in patients with unexplained colorectal adenomatous polyposis. *Fam Cancer*.

SPINELLI, A. M., GONZALEZ-COBOS, J. C., ZHANG, X., MOTIANI, R. K., ROWAN, S., ZHANG, W., GARRETT, J., VINCENT, P. A., MATROUGUI, K., SINGER, H. A. & TREBAK, M. 2012. Airway smooth muscle STIM1 and Orai1 are upregulated in asthmatic mice and mediate PDGF-activated SOCE, CRAC currents, proliferation, and migration. *Pflugers Arch,* 464**,** 481-92.

SPURRIER, B., RAMALINGAM, S. & NISHIZUKA, S. 2008. Reverse-phase protein lysate microarrays for cell signaling analysis. *Nat Protoc,* 3**,** 1796-808.

STAUDERMAN, K. A. 2018. CRAC channels as targets for drug discovery and development. *Cell Calcium,* 74**,** 147-159.

SUBRAMANIAN, A., TAMAYO, P., MOOTHA, V. K., MUKHERJEE, S., EBERT, B. L., GILLETTE, M. A., PAULOVICH, A., POMEROY, S. L., GOLUB, T. R., LANDER, E. S. & MESIROV, J. P. 2005. Gene set enrichment analysis: A knowledge-based approach for interpreting genome-wide expression profiles. *Proceedings of the National Academy of Sciences,* 102**,** 15545-15550.

SUCHYNA, T., JOHNSON, JH., HAMER, K., LEYKAM, JF., GAGE, DA., CLEMO, HF., BAUMGARTEN, CM., SACHS, F. 2000. Identification of a Peptide Toxin from Grammostola spatulata Spider Venom That Blocks Cation-Selective Stretch-Activated Channels. *The Journal of General Physiology,* 115**,** 583-598.

SUCHYNA, T. M., TAPE, SE., KOEPPE II, RE., ANDERSEN, OS., SACHS, F., GOTTLIEB, PA. 2004. Bilayer-dependent inhibition of mechanosensitive channels by neuroactive peptide enantiomers. *Nature,* 430**,** 235.

SUGAWARA, T., HISATSUNE, C., LE, T. D., HASHIKAWA, T., HIRONO, M., HATTORI, M., NAGAO, S. & MIKOSHIBA, K. 2013. Type 1 Inositol Trisphosphate Receptor Regulates Cerebellar Circuits by Maintaining the Spine Morphology of Purkinje Cells in Adult Mice. *The Journal of Neuroscience,* 33**,** 12186-12196.

SULAIMAN, A. & WANG, L. 2017. Bridging the divide: preclinical research discrepancies between triple-negative breast cancer cell lines and patient tumors. *Oncotarget,* 8**,** 113269-113281.

SUN, J., LU, F., HE, H., SHEN, J., MESSINA, J., MATHEW, R., WANG, D., SARNAIK, A. A., CHANG, W. C., KIM, M., CHENG, H. & YANG, S. 2014. STIM1- and Orai1-mediated Ca(2+) oscillation orchestrates invadopodium formation and melanoma invasion. *J Cell Biol,* 207**,** 535-48.

SUZUKI, T., MURAKI, Y., HATANO, N., SUZUKI, H. & MURAKI, K. 2018. PIEZO1 Channel Is a Potential Regulator of Synovial Sarcoma Cell-Viability. *International journal of molecular sciences,* 19**,** 1452.

SYEDA, R., XU, J., DUBIN, A. E., COSTE, B., MATHUR, J., HUYNH, T., MATZEN, J., LAO, J., TULLY, D. C., ENGELS, I. H., PETRASSI, H. M., SCHUMACHER, A. M., MONTAL, M., BANDELL, M. & PATAPOUTIAN, A. 2015. Chemical activation of the mechanotransduction channel Piezo1. *Elife,* 4.

TAIEB, J., ZAANAN, A., LE MALICOT, K., JULIÉ, C., BLONS, H., MINEUR, L., BENNOUNA, J., TABERNERO, J., MINI, E., FOLPRECHT, G., VAN LAETHEM, J. L., LEPAGE, C., EMILE, J.-F. & LAURENT-PUIG, P. 2016. Prognostic Effect of BRAF and KRAS Mutations in Patients With Stage III Colon Cancer Treated With Leucovorin, Fluorouracil, and Oxaliplatin With or Without Cetuximab: A Post Hoc Analysis of the PETACC-8 TrialBRAF and KRAS Mutations in Stage III Colon CancerBRAF and KRAS Mutations in Stage III Colon Cancer. *JAMA Oncology,* 2**,** 643-653.

TAKAYAMA, T., KATSUKI, S., TAKAHASHI, Y., OHI, M., NOJIRI, S., SAKAMAKI, S., KATO, J., KOGAWA, K., MIYAKE, H. & NIITSU, Y. 1998. Aberrant crypt foci of the colon as precursors of adenoma and cancer. *N Engl J Med,* 339**,** 1277-84.

TAKAYAMA, T., OHI, M., HAYASHI, T., MIYANISHI, K., NOBUOKA, A., NAKAJIMA, T., SATOH, T., TAKIMOTO, R., KATO, J., SAKAMAKI, S. & NIITSU, Y. 2001. Analysis of K-ras, APC, and beta-catenin in aberrant crypt foci in sporadic adenoma, cancer, and familial adenomatous polyposis. *Gastroenterology,* 121**,** 599-611.

TAKEYAMA, Y., SATO, M., HORIO, M., HASE, T., YOSHIDA, K., YOKOYAMA, T., NAKASHIMA, H., HASHIMOTO, N., SEKIDO, Y., GAZDAR, A. F., MINNA, J. D., KONDO, M. & HASEGAWA, Y. 2010. Knockdown of ZEB1, a master epithelial-to-mesenchymal transition (EMT) gene, suppresses anchorage-independent cell growth of lung cancer cells. *Cancer Lett,* 296**,** 216-24.

TANG, B. D., XIA, X., LV, X. F., YU, B. X., YUAN, J. N., MAI, X. Y., SHANG, J. Y., ZHOU, J. G., LIANG, S. J. & PANG, R. P. 2017. Inhibition of Orai1-mediated Ca(2+) entry enhances chemosensitivity of HepG2 hepatocarcinoma cells to 5-fluorouracil. *J Cell Mol Med,* 21**,** 904-915.

TATE, J. G., BAMFORD, S., JUBB, H. C., SONDKA, Z., BEARE, D. M., BINDAL, N., BOUTSELAKIS, H., COLE, C. G., CREATORE, C., DAWSON, E., FISH, P., HARSHA, B., HATHAWAY, C., JUPE, S. C., KOK, C. Y., NOBLE, K., PONTING, L., RAMSHAW, C. C., RYE, C. E., SPEEDY, H. E., STEFANCSIK, R., THOMPSON, S. L., WANG, S., WARD, S., CAMPBELL, P. J. & FORBES, S. A.

2018. COSMIC: the Catalogue Of Somatic Mutations In Cancer. *Nucleic Acids Research***,** gky1015-gky1015.

TFELT-HANSEN, J., CHATTOPADHYAY, N., YANO, S., KANUPARTHI, D., ROONEY, P., SCHWARZ, P. & BROWN, E. M. 2004. Calcium-Sensing Receptor Induces Proliferation through p38 Mitogen-Activated Protein Kinase and Phosphatidylinositol 3-Kinase But Not Extracellularly Regulated Kinase in a Model of Humoral Hypercalcemia of Malignancy. *Endocrinology,* 145**,** 1211-1217.

THE CANCER GENOME ATLAS, N., MUZNY, D. M., BAINBRIDGE, M. N., CHANG, K., DINH, H. H., DRUMMOND, J. A., FOWLER, G., KOVAR, C. L., LEWIS, L. R., MORGAN, M. B., NEWSHAM, I. F., REID, J. G., SANTIBANEZ, J., SHINBROT, E., TREVINO, L. R., WU, Y.-Q., WANG, M., GUNARATNE, P., DONEHOWER, L. A., CREIGHTON, C. J., WHEELER, D. A., GIBBS, R. A., LAWRENCE, M. S., VOET, D., JING, R., CIBULSKIS, K., SIVACHENKO, A., STOJANOV, P., MCKENNA, A., LANDER, E. S., GABRIEL, S., GETZ, G., DING, L., FULTON, R. S., KOBOLDT, D. C., WYLIE, T., WALKER, J., DOOLING, D. J., FULTON, L., DELEHAUNTY, K. D., FRONICK, C. C., DEMETER, R., MARDIS, E. R., WILSON, R. K., CHU, A., CHUN, H.-J. E., MUNGALL, A. J., PLEASANCE, E., GORDON ROBERTSON, A., STOLL, D., BALASUNDARAM, M., BIROL, I., BUTTERFIELD, Y. S. N., CHUAH, E., COOPE, R. J. N., DHALLA, N., GUIN, R., HIRST, C., HIRST, M., HOLT, R. A., LEE, D., LI, H. I., MAYO, M., MOORE, R. A., SCHEIN, J. E., SLOBODAN, J. R., TAM, A., THIESSEN, N., VARHOL, R., ZENG, T., ZHAO, Y., JONES, S. J. M., MARRA, M. A., BASS, A. J., RAMOS, A. H., SAKSENA, G., CHERNIACK, A. D., SCHUMACHER, S. E., TABAK, B., CARTER, S. L., PHO, N. H., NGUYEN, H., ONOFRIO, R. C., CRENSHAW, A., ARDLIE, K., BEROUKHIM, R., WINCKLER, W., GETZ, G., MEYERSON, M., PROTOPOPOV, A., ZHANG, J., HADJIPANAYIS, A., LEE, E., XI, R., YANG, L., REN, X., ZHANG, H., SATHIAMOORTHY, N., SHUKLA, S., CHEN, P.-C., et al. 2012. Comprehensive molecular characterization of human colon and rectal cancer. *Nature,* 487**,** 330.

THE CANCER GENOME ATLAS NETWORK, MUZNY, D. M., BAINBRIDGE, M. N., CHANG, K., DINH, H. H., DRUMMOND, J. A., FOWLER, G., KOVAR, C. L., LEWIS, L. R., MORGAN, M. B., NEWSHAM, I. F., REID, J. G., SANTIBANEZ, J., SHINBROT, E., TREVINO, L. R., WU, Y.-Q., WANG, M., GUNARATNE, P., DONEHOWER, L. A., CREIGHTON, C. J., WHEELER, D. A., GIBBS, R. A., LAWRENCE, M. S., VOET, D., JING, R., CIBULSKIS, K., SIVACHENKO, A., STOJANOV, P., MCKENNA, A., LANDER, E. S., GABRIEL, S., GETZ, G., DING, L., FULTON, R. S., KOBOLDT, D. C., WYLIE, T., WALKER, J., DOOLING, D. J., FULTON, L., DELEHAUNTY, K. D., FRONICK, C. C., DEMETER, R., MARDIS, E. R., WILSON, R. K., CHU, A., CHUN, H.-J. E., MUNGALL, A. J., PLEASANCE, E., GORDON ROBERTSON, A., STOLL, D., BALASUNDARAM, M., BIROL, I., BUTTERFIELD, Y. S. N., CHUAH, E., COOPE, R. J. N., DHALLA, N., GUIN, R., HIRST, C., HIRST, M., HOLT, R. A., LEE, D., LI, H. I., MAYO, M., MOORE, R. A., SCHEIN, J. E., SLOBODAN, J. R., TAM, A., THIESSEN, N., VARHOL, R., ZENG, T., ZHAO, Y., JONES, S. J. M., MARRA, M. A., BASS, A. J., RAMOS, A. H., SAKSENA, G., CHERNIACK, A. D., SCHUMACHER, S. E., TABAK, B., CARTER, S. L., PHO, N. H., NGUYEN, H., ONOFRIO, R. C., CRENSHAW, A., ARDLIE, K., BEROUKHIM, R., WINCKLER, W., GETZ, G., MEYERSON, M., PROTOPOPOV, A., ZHANG, J., HADJIPANAYIS, A., LEE, E., XI, R., YANG, L., REN, X., ZHANG, H., SATHIAMOORTHY, N., SHUKLA, S., CHEN, P.-C., et al. 2012. Comprehensive molecular characterization of human colon and rectal cancer. *Nature,* 487**,** 330.

THE, L., WILSON, S. R. & BAUTISTA, D. M. 2013. ORAI1 Calcium Signaling Regulates the Release of the Atopic Dermatitis Cytokine TSLP. *Biophysical Journal,* 104**,** 40a.

THE NATIONAL INSTITUTE OF HEALTH. 2019. *TCGA Program Overview* [Online]. Available: https://cancergenome.nih.gov/abouttcga/overview [Accessed 02.01.2019 2019].

THEATRE, E., BOURS, V. & OURY, C. 2009. A P2X ion channel-triggered NF-kappaB pathway enhances TNF-alpha-induced IL-8 expression in airway epithelial cells. *Am J Respir Cell Mol Biol,* 41**,** 705-13.

THERMOFISHER SCIENTIFIC 2010. Indicators for Ca2+, Mg2+, Zn2+ and Other Metal Ions. *In:* THERMOFISHER SCIENTIFIC (ed.) *Molecular Probes™ Handbook A Guide to Fluorescent Probes and Labeling Technologies.* 11th edition ed.: ThermoFisher Scientific,.

THERNEAU, T. 2015. A Package for Survival Analysis in S.

THEWS, O., GASSNER, B., KELLEHER, D. K., SCHWERDT, G. & GEKLE, M. 2006. Impact of extracellular acidity on the activity of P-glycoprotein and the cytotoxicity of chemotherapeutic drugs. *Neoplasia (New York, N.Y.),* 8**,** 143-152.

THIAGALINGAM, S., LAKEN, S., WILLSON, J. K., MARKOWITZ, S. D., KINZLER, K. W., VOGELSTEIN, B. & LENGAUER, C. 2001. Mechanisms underlying losses of heterozygosity in human colorectal cancers. *Proc Natl Acad Sci U S A,* 98**,** 2698-702.

THOMPSON, J., MIGNEN, O. & SHUTTLEWORTH, T. J. 2010. The N-terminal domain of Orai3 determines selectivity for activation of the store-independent ARC channel by arachidonic acid. *Channels (Austin),* 4**,** 398-410.

TOMCZAK, K., CZERWIŃSKA, P. & WIZNEROWICZ, M. 2015. The Cancer Genome Atlas (TCGA): an immeasurable source of knowledge. *Contemporary oncology (Poznan, Poland),* 19**,** A68-A77.

TOURNIGAND, C., ANDRE, T., ACHILLE, E., LLEDO, G., FLESH, M., MERY-MIGNARD, D., QUINAUX, E., COUTEAU, C., BUYSE, M., GANEM, G., LANDI, B., COLIN, P., LOUVET, C. & DE GRAMONT, A. 2004. FOLFIRI followed by FOLFOX6 or the reverse sequence in advanced colorectal cancer: a randomized GERCOR study. *J Clin Oncol,* 22**,** 229-37.

TSUDA, H., CALLEN, D. F., FUKUTOMI, T., NAKAMURA, Y. & HIROHASHI, S. 1994. Allele loss on chromosome 16q24.2-qter occurs frequently in breast cancers irrespectively of differences in phenotype and extent of spread. *Cancer Res,* 54**,** 513-7.

UMEMURA, M., BALJINNYAM, E., FESKE, S., DE LORENZO, M. S., XIE, L. H., FENG, X., ODA, K., MAKINO, A., FUJITA, T., YOKOYAMA, U., IWATSUBO, M., CHEN, S., GOYDOS, J. S., ISHIKAWA, Y. & IWATSUBO, K. 2014. Store-operated Ca2+ entry (SOCE) regulates melanoma proliferation and cell migration. *PLoS One,* 9**,** e89292.

VANDENBERGHE, M., RAPHAEL, M., LEHEN'KYI, V., GORDIENKO, D., HASTIE, R., ODDOS, T., RAO, A., HOGAN, P. G., SKRYMA, R. & PREVARSKAYA, N. 2013. ORAI1 calcium channel orchestrates skin homeostasis. *Proc Natl Acad Sci U S A,* 110**,** E4839-48.

VAUPEL, P., KELLEHER, D. K. & HOCKEL, M. 2001. Oxygen status of malignant tumors: pathogenesis of hypoxia and significance for tumor therapy. *Semin Oncol,* 28**,** 29-35.

VIG, M., BECK, A., BILLINGSLEY, J. M., LIS, A., PARVEZ, S., PEINELT, C., KOOMOA, D. L., SOBOLOFF, J., GILL, D. L., FLEIG, A., KINET, J.-P. & PENNER, R. 2006a. CRACM1 Multimers Form the Ion-Selective Pore of the CRAC Channel. *Current Biology,* 16**,** 2073-2079.

VIG, M., DEHAVEN, W. I., BIRD, G. S., BILLINGSLEY, J. M., WANG, H., RAO, P. E., HUTCHINGS, A. B., JOUVIN, M. H., PUTNEY, J. W. & KINET, J. P. 2008. Defective mast cell effector functions in mice lacking the CRACM1 pore subunit of store-operated calcium release-activated calcium channels. *Nat Immunol,* 9**,** 89-96.

VIG, M., PEINELT, C., BECK, A., KOOMOA, D. L., RABAH, D., KOBLAN-HUBERSON, M., KRAFT, S., TURNER, H., FLEIG, A., PENNER, R. & KINET, J.-P. 2006b. CRACM1 Is a Plasma Membrane Protein Essential for Store-Operated Ca^{2+} Entry. *Science,* 312**,** 1220-1223.

VINGTDEUX, V. G., L.; ZHAO, H.; CHANDAKKAR, P.; WU, Q.; SIMON, JE.; JANLE, EM.; LOBO, J.; FERRUZZI, MG.; DAVIES, P.; MARAMBAUD, P. 2010. AMP-activated protein kinase signaling activation by resveratrol modulates amyloid-beta peptide metabolism. *J. Biol. Chem.,* 285**,** 9100-9113.

VOGELSTEIN, B., FEARON, E. R., HAMILTON, S. R., KERN, S. E., PREISINGER, A. C., LEPPERT, M., SMITS, A. M. M. & BOS, J. L. 1988. Genetic Alterations during Colorectal-Tumor Development. *New England Journal of Medicine,* 319**,** 525-532.

WANG, J. Y., SUN, J., HUANG, M. Y., WANG, Y. S., HOU, M. F., SUN, Y., HE, H., KRISHNA, N., CHIU, S. J., LIN, S., YANG, S. & CHANG, W. C. 2014. STIM1 overexpression promotes colorectal cancer progression, cell motility and COX-2 expression. *Oncogene,* 34**,** 4358.

WANG, S., CHENNAPUTTI, R, KAUR, H, IRING, A, WETTSCHURECK, N, OFFERMANNS, S 2016. Endothelial cation channel PIEZO1 controls blood pressure by mediating flow-induced ATP release. *Journal of Clinical Investigations,* 126**,** 4527-4536.

WANG, W., REN, Y., WANG, L., ZHAO, W., DONG, X., PAN, J., GAO, H. & TIAN, Y. 2018. Orai1 and Stim1 Mediate the Majority of Store-Operated Calcium Entry in Multiple Myeloma and Have Strong Implications for Adverse Prognosis. *Cell Physiol Biochem,* 48**,** 2273-2285.

WEBSTER, P. J., LITTLEJOHNS, A. T., GAUNT, H. J., YOUNG, R. S., RODE, B., RITCHIE, J. E., STEAD, L. F., HARRISON, S., DROOP, A., MARTIN, H. L., TOMLINSON, D. C., HYMAN, A. J., APPLEBY, H. L., BOXALL, S., BRUNS, A. F., LI, J., PRASAD, R. K., LODGE, J. P. A., BURKE, D. A. & BEECH, D. J. 2017. Upregulated WEE1 protects endothelial cells of colorectal cancer liver metastases. *Oncotarget,* 8**,** 42288-42299.

WESTWOOD, M., CORRO RAMOS, I., LANG, S., LUYENDIJK, M., ZAIM, R., STIRK, L., AL, M., ARMSTRONG, N. & KLEIJNEN, J. 2017. Faecal immunochemical tests to triage patients with lower abdominal symptoms for suspected colorectal cancer referrals in primary care: a systematic review and cost-effectiveness analysis. *Health Technol Assess,* 21**,** 1-234.

WILHELM, S. M., CARTER, C., TANG, L., WILKIE, D., MCNABOLA, A., RONG, H., CHEN, C., ZHANG, X., VINCENT, P., MCHUGH, M., CAO, Y., SHUJATH, J., GAWLAK, S., EVELEIGH, D., ROWLEY, B., LIU, L., ADNANE, L., LYNCH, M., AUCLAIR, D., TAYLOR, I., GEDRICH, R., VOZNESENSKY, A., RIEDL, B., POST, L. E., BOLLAG, G. & TRAIL, P. A. 2004. BAY 43-9006 Exhibits Broad Spectrum Oral Antitumor Activity and Targets the RAF/MEK/ERK Pathway and Receptor Tyrosine Kinases Involved in Tumor Progression and Angiogenesis. *Cancer Research,* 64**,** 7099-7109.

WITTRUP, A. & LIEBERMAN, J. 2015. Knocking down disease: a progress report on siRNA therapeutics. *Nature reviews. Genetics,* 16**,** 543-552.

WLODKOWIC, D., TELFORD, W., SKOMMER, J. & DARZYNKIEWICZ, Z. 2011. Apoptosis and beyond: cytometry in studies of programmed cell death. *Methods in cell biology,* 103**,** 55-98.

WORLD CANCER RESEARCH FUND INTERNATIONAL AND AMERICAN INSTITUTE FOR CANCER RESEARCH. 2016. *Continuous Update Project Report: Diet, Nutrition, Physical Activity and Colorectal Cancer 2016* [Online]. Available: Available at wcrf.org/colorectal-cancer-2017 [Accessed].

WU, J., GOYAL, R. & GRANDL, J. 2016. Localized force application reveals mechanically sensitive domains of Piezo1. *Nature Communications,* 7**,** 12939.

WU, L., KATZ, S, BROWN, GR 1994. Inositol 1,4,5-trisphosphate-, GTP-, arachidonic acid- and thapsigargin-mediated intracellular calcium movement in PANC-1 microsomes. *Cell Calcium,* 15**,** 228-240.

XU, L., WANG, R., ZIEGELBAUER, J., WU, W. W., SHEN, R.-F., JUHL, H., ZHANG, Y., PELOSOF, L. & ROSENBERG, A. S. 2017. Transcriptome analysis of human colorectal cancer biopsies reveals extensive expression correlations among genes related to cell proliferation, lipid metabolism, immune response and collagen catabolism. *Oncotarget,* 8**,** 74703-74719.

YAN, W.-F., WU, G., SUN, P.-C. & QIU, D. 2015. P53 mutations occur more commonly than KRAS mutations in colorectal adenoma. *International journal of clinical and experimental medicine,* 8**,** 1370-1375.

YANG, B., GWOZDZ, T., DUTKO-GWOZDZ, J. & BOLOTINA, V. M. 2012. Orai1 and Ca2+-independent phospholipase A2 are required for store-operated Icat-SOC current, Ca2+ entry, and proliferation of primary vascular smooth muscle cells. *Am J Physiol Cell Physiol,* 302**,** C748-56.

YANG, S., J.J. ZHANG, AND X.-Y. HUANG 2009. Orai1 and STIM1 Are Critical for Breast Tumor Cell Migration and Metastasis. *Cancer Cell,* 15**,** 124-134.

YANG, S., ZHANG, J. J. & HUANG, X. Y. 2009. Orai1 and STIM1 are critical for breast tumor cell migration and metastasis. *Cancer Cell,* 15**,** 124-34.

YOSHINO, T., ISHIKAWA, J., OHGA, K., MOROKATA, T., TAKEZAWA, R., MORIO, H., OKADA, Y., HONDA, K. & YAMADA, T. 2007. YM-58483, a selective CRAC channel inhibitor, prevents antigen-induced airway eosinophilia and late phase asthmatic responses via Th2 cytokine inhibition in animal models. *Eur J Pharmacol,* 560**,** 225-33.

YU, P., ZHOU, M., QU, J., FU, L., LI, X., CAI, R., JIN, B., TENG, Y., LIU, J., SHI, J. & ZHANG, J. 2018. The dynamic monitoring of CEA in response to chemotherapy and prognosis of mCRC patients. *BMC cancer,* 18**,** 1076-1076.

ZARYCHANSKI, R., SCHULZ, V. P., HOUSTON, B. L., MAKSIMOVA, Y., HOUSTON, D. S., SMITH, B., RINEHART, J. & GALLAGHER, P. G. 2012. Mutations in the mechanotransduction protein PIEZO1 are associated with hereditary xerocytosis. *Blood,* 120**,** 1908-15.

ZAVORKA, M. E., CONNELLY, C. M., GROSELY, R. & MACDONALD, R. G. 2016. Inhibition of insulin-like growth factor II (IGF-II)-dependent cell growth by multidentate pentamannosyl 6-phosphate-based ligands targeting the mannose 6-phosphate/IGF-II receptor. *Oncotarget,* 7**,** 62386-62410.

ZHAN, Z. Y., ET AL 2015. Over-expression of Orai1 mediates cell proliferation and associates with poor prognosis in human non-small cell lung carcinoma. *Int J Clin Exp Pathol,* 8**,** 5080-8.

ZHANG SL, Y. Z., ROOS J, KOZAK JA, DEERINCK TJ, ELLISMAN MH, STAUDERMAN KA, CAHALAN MD 2005. STIM1 is a calcium sensor that activates plasma membrane CRAC channels and maintains a high selectivity for calcium ions. *Nature* 437**,** 902-5.

ZHANG, T., CHI, S., JIANG, F., ZHAO, Q. & XIAO, B. 2017. A protein interaction mechanism for suppressing the mechanosensitive Piezo channels. *Nature communications,* 8**,** 1797-1797.

ZHANG, W., HALLIGAN, K. E., ZHANG, X., BISAILLON, J. M., GONZALEZ-COBOS, J. C., MOTIANI, R. K., HU, G., VINCENT, P. A., ZHOU, J., BARROSO, M., SINGER, H. A., MATROUGUI, K. & TREBAK, M. 2011. Orai1-mediated I (CRAC) is essential for neointima formation after vascular injury. *Circ Res,* 109**,** 534-42.

ZHAO, Q., ZHOU, H., CHI, S., WANG, Y., WANG, J., GENG, J., WU, K., LIU, W., ZHANG, T., DONG, M. Q., WANG, J., LI, X. & XIAO, B. 2018. Structure and mechanogating mechanism of the Piezo1 channel. *Nature,* 554**,** 487-492.

ZHONG, H., FAZENBAKER, C., CHEN, C., BREEN, S., HUANG, J., YAO, X., REN, P., YAO, Y., HERBST, R. & HOLLINGSWORTH, R. E. 2016. Overproduction of IGF-2 drives a subset of colorectal cancer cells, which specifically respond to an anti-IGF therapeutic antibody and combination therapies. *Oncogene,* 36**,** 797.

ZHU, H., ZHANG, H., JIN, F., FANG, M., HUANG, M., YANG, C. S., CHEN, T., FU, L. & PAN, Z. 2014. Elevated Orai1 expression mediates tumor-promoting intracellular Ca2+ oscillations in human esophageal squamous cell carcinoma. *Oncotarget,* 5**,** 3455-71.

ZHU, Z.-D., YU, T., LIU, H.-J., JIN, J. & HE, J. 2018. SOCE induced calcium overload regulates autophagy in acute pancreatitis via calcineurin activation. *Cell Death & Disease,* 9**,** 50.

ZUMBRUNN, J., KINOSHITA, K., HYMAN, A. A. & NÄTHKE, I. S. 2001. Binding of the adenomatous polyposis coli protein to microtubules increases microtubule stability and is regulated by GSK3β phosphorylation. *Current Biology,* 11**,** 44-49.